



88th Anniversary

For New Technology Network

NTN®

TECHNICAL REVIEW

No.
74

Special Issue;
Products for Industrial Machinery

November 2006



ISSN 0915-0528 OSAKA, JAPAN

The Eighty-Eighth Anniversary

1918-2006

Message on our 88th anniversary

Bearings are vital components for carrying the rotating loads of all types of machinery, from automobiles, aircraft, trains and other vehicles to construction machinery, machine tools and electronic equipment.

NTN was founded in 1918 dedicated to the manufacture of bearings, and we are now celebrating our 88th anniversary thanks to the continued support of numerous NTN product users. Throughout our history, we have taken on diverse challenges, including activities in overseas markets for many years and expansion of our business line into the development and manufacture of constant velocity joints. Now, we have grown into a global bearing manufacturer with bases in 19 countries worldwide.

In 1989, as an expression of our intention to make even more positive contributions to the world, we changed our corporate name from Toyo Bearing Mfg. Co. Ltd., the name we had used for many years, to NTN Corporation. We continue to remain focused on the new challenges that we face in the global market.



88th Anniversary

For New Technology Network

NTN®

www.ntn.co.jp



TECHNICAL REVIEW

No.74

Special Issue ● Products for
Industrial Machinery

CONTENTS

Preface	Kenji OKADA	1
Contribution	Trends in Recent Machine Tool Technologies Dr. Toshimichi MORIWAKI Professor Department of Mechanical Engineering KOBE University	2
● Special Issue for Machine Tool		
Development of a New Grease Lubrication System for Machine Tool Main Spindles Sun-Woo LEE and Masatsugu MORI		8
High-Speed Tapered Roller Bearing for Machine Tool Main Spindle Masatsugu MORI and Takuji KOBAYASHI		16
Minimum Quantity and Cooling Jet Lubricated Angular Contact Ball Bearings for Machine Tool Mineo KOYAMA		24
$d_{mn}170 \times 10^4$ Sealed High-Speed Angular Contact Bearing "New BNS Type" Futoshi KOSUGI		28
Development of Aerostatic Bearing Spindle for Precision Machine Tools Teruyoshi HORIUCHI, Kazuyuki AONO and Hiroaki HIYOSHI		34
Our Line of New products for Machine Tool		38
● Technical Papers Technical Articles New Products		
Atmospheric Control Method for JIS-SUJ2 Carbonitriding Processes Chikara OHKI		44
The Influence of Hydrogen on Tension-Compression and Rolling Contact Fatigue Properties of Bearing Steel Hiroshi HAMADA and Yukio MATSUBARA		54
Technical Trends in Bearings for Office Equipment Chikara KATAGIRI		62
Unit Products for Office Equipment Shoji ITOMI and Atsushi MOROOKA		68
Honing Sludge and Electro Furnace Dust Briquetter Shouzo GOTOH and Kanji NAKAMURA		74
Ultra-Clean Bearing for Clean Environments Ryouichi NAKAJIMA and Masaaki HONDA		80
Development of New RCT Bearing for Axleboxes and Insulated Bearing with Shields Ryutaro OKA		84
High Load Capacity Cylindrical Roller Bearings Takuya OZU		90
The Rust Guard Bearings of Highly Corrosion-resistant Bearings Takashi YAGI		96
"SSB" of Sliding Aseismic Isolation Unit Multi-ply Rubber Norio ITOH and Takuya ISHII		100
● Our Line of Award Winning Products		
"The Third Mono-Zukuri Products Creation Awards" Innovative Product Award Monodrive Two-Way Feeder Toshio OGUSU		104
"The Japanese Society of Tribologists 2005" Technical Award "Hybrid Bearphite" a Sintered Metal Sliding Bearing Inserted with Plastic Masaki EGAMI		108
Our Line of New Products		116

Introduction to this Special Feature Issue –

*NTN Products
for Industrial Machinery*

Kenji OKADA
Managing Director

The current trend in the Japanese economy can be characterized as a steady recovery led by domestic demand and supported by the active investments of Japanese manufacturers in manufacturing plants and facilities. These are fueled by the recovering business performance of Japanese enterprises and the strong personal consumption of consumers. However, at the same time, we face anxieties that threaten our everyday lifestyles, including unprecedented high petroleum prices and environmental pollution problems that are difficult to resolve. In short, we are experiencing an era that is increasing in complication.

In this age of dramatic change, **NTN** is now celebrating its 88th anniversary thanks to support from the users of **NTN** products. I would like to take this opportunity to express my deepest gratitude to them.

NTN took part in the 23rd Japan International Machine Tool Fair (JIMTOF2006), which ran from November 1 to 8, 2006. To mark this occasion, we issued the Japanese edition of this publication, the **NTN** Technical Review No. 74 (2006). This year's edition features topics about bearing products for industrial machinery, detailing how these products boast longer lifespans, lower running torques and compact sizes, which are merits that contribute to the realization of a society that promotes energy conservation and environmental protection. This publication describes **NTN**'s achievements in developing our latest technologies and novel products. The review begins with a contribution titled "Trends in Recent Machine Tool Technologies" by Kobe University Professor Toshimichi Moriwaki who is an international authority in the fields of production engineering and precision machining. Nine topics about **NTN** products for industrial machinery follow, including five topics about products for machine tools, three theses related to material and heat treatments, and two reports about **NTN** products that won awards in 2005—the Mono-Zukuri Component Grand Prize given for creation and manufacture of a novel product and the Engineering Award of the Japanese Society of Tribologists.

In recent years, the environmental consciousness of the public has been growing steadily, and, as a result, the responsibilities of manufacturers to achieve a harmonious balance with the global environment have also become greater. Given this reality, we must remain deeply committed to efforts for reducing CO₂ emissions to help control global warming and to efforts for realizing a recycling-oriented society.

In consideration of these issues, many **NTN** products directly and indirectly support energy conservation and environmental protection. These include our rolling bearings and constant velocity joints, as well as our hydrostatic bearings, repair devices and other products for precision machinery. Rolling bearings are essentially products that help reduce rolling friction, so they can be considered to be products that conserve energy. Our other energy-saving products include **NTN** constant velocity joints and rolling guideways, which boast much improved transmission efficiency and NVH characteristics (noise, vibration and riding comfort) through incorporation of rolling elements into their sliding sections, as well as products for precision equipment that feature non-contact bearings as supporting mechanisms.

Our commitments are not limited to energy-saving features for these fundamental products. We are fully committed to the development of new products in the fields of energy conservation and eco-friendly equipment that help reduce environmental impacts.

For 88 years since our foundation, in the belief that "quality is the source of **NTN** brand power," we have always conducted strict self-evaluations as we have developed novel products with the goal of "realizing quality that fulfills customer satisfaction." With the motto, "For New Technology Networks," our philosophy is to contribute to international society by using **NTN** engineering abilities to provide novel, high-quality products that are relevant to fulfilling ever-diversifying market needs. In keeping with this, we promise to continue our commitment to realizing the confidence and satisfaction of our customers.

FOR NEW TECHNOLOGY NETWORK

Trends in Recent Machine Tool Technologies



Dr. Toshimichi MORIWAKI

Professor Department of Mechanical Engineering KOBE University

Recent trends in the machine tool technologies are surveyed from the view points of high speed and high performance machine tools, combined multi-functional machine tools, ultraprecision machine tools and advanced and intelligent control technologies. The machine tools are bases of manufacturing industries and they are strategically important products for Japan. The views of the author towards the technical developments in both hardware and software are introduced together with the world wide trends in the relevant fields.

1. Introduction

At present, the machine tool industry worldwide is enjoying unprecedented demand, and the industry's output is apparently even failing to satisfy current demand. Japan's machine tool industry, in particular, has boasted the greatest share in the world since 1982, and its share has been exceptionally high in the last two years. In order for Japan's machine tool industry to maintain this share, I believe that the enterprises involved in it must remain committed not only to expansion and advancement of their product facilities, but also to steady research and development efforts. They must continue to add more value to their products in order to cope with future needs and maintain competitiveness compared to machine tool manufacturers in other nations.

In this paper, I intend to report on current topics about recent machine tools and trends in the research and development commitments of the Japanese machine tool industry, highlighting the efforts of The International Academy for Production Engineering (CIRP), an organization of which I am a member.

2. High-Speed, High-Efficiency Machine Tools

It is well known that demands are mounting for greater maximum main spindle speeds and feed speeds—in other words, that machine tools of higher speed and higher efficiency are much needed.¹⁾ Background information about high-speed machine tools and supporting technologies, and their resultant advantages are summarized in **Table 1**.

In this section, I will focus on the avoidance of chatter vibration, which is one outstanding advantage of high-speed, high-efficiency machine tools, as other engineering topics are discussed in papers by other researchers.

In the period of the 1960's and 1970's, there were research efforts worldwide on the chatter vibration of machine tools. As a result, the underlying principles behind so-called regenerative chatter vibration and forced chatter vibration were clarified, and basic solutions were proposed.

Unfortunately, however, examples of further systematic research efforts have been rare.

In recent years, avoidance of chatter vibration has been posing a new challenge in the machining of

Table 1 Background, supporting technologies and advantages of high-speed, high-efficient machine tools

High-speed, high-efficiency machine tools

(Background, supporting technologies)

- Need for highly efficient machining and decreased costs
- Development of high-speed main spindles and high-speed feed means (linear motors, etc.)
- Advances including the development of high-speed machining capable tools and progress in machining techniques

(Advantages)

- Decreased processing times (improved efficiency)
- Improved machining accuracy and better quality of finished surfaces
- Prevention of chatter vibration

hard-to-cut materials as well as in high-speed, high-efficiency machining of aluminum materials for aviation purposes. Generally, chatter vibration is avoided by reducing the depths of cuts and cutting speeds (low-speed stability), but it is possible to avoid chatter vibration by increasing spindle speed. This fact was already known from research done in the 1960's. Since high-speed spindles boasting this ability were not available in those days, however, this fact was regarded simply as a theoretical possibility. In the mathematical field, it was also difficult theoretically to handle chatter vibration in milling processes, including end milling. Notwithstanding, Prof. Y. Altintas et. al. obtained results for stability graphs such as the one shown in Fig. 1. This graph shows that chatter vibration does not occur in the region of depths cut below the stability lobes relative to spindle speeds on the horizontal axis. Though detailed discussion of this finding²⁾ is omitted in this paper, the underlying principle of chatter vibration can be understood from the expressions and diagrams given to the right of this graph. Variations in chip thickness are caused by differences between the roughness of the finished surface generated by the immediately previous revolution of the main spindle or by an immediately previous cutting edge and the roughness of the finished surface currently generated by the current cutting edge. This variation in chip thickness contributes to variation in the cutting force and contributes to continuing vibration. If we can run the main spindle at a higher speed that is equivalent to the vibration frequency, then the difference between the phase of vibration resulting from the immediately previous revolution and the phase of vibration deriving from the current revolution can be effectively controlled, thereby eliminating variations caused by

chip thickness. If such a condition is realized, chatter vibration will not occur even with greater cut depths.

Utilizing this principle, high-speed, high-efficiency cutting has been implemented for aircraft components made of aluminum and other materials. Given this, there has been mounting interest in the dynamic characteristics of a main spindle system that includes a main spindle, chuck and tools. As a result, the interrelation of bearings and other design factors with the dynamic characteristics of the main spindle and main spindle system has been clarified both theoretically and experimentally, and this achievement has been applied to the design of main spindles. Recently, various software packages are also being used frequently for analysis and design. The theoretical study of main spindle designs will become increasingly important.

3. Combined Multifunctional Machine Tools

In addition to high-speed, high-efficiency, cutting-capable machine tools, research on machine tools is currently focused on combined multifunctional machine tools, including 5-axis machining centers and combined multifunctional turning centers. The background and advantages of combined multifunctional machine tools are summarized in Table 2. Combined multifunctional machine tools can be roughly categorized into turning centers (TC) that have been developed from lathes and machining centers (MC) that started as milling machines.

A portion of the investigations into machining applications with combined machine tools based on lathes is illustrated in Fig. 2. In addition to machining of bores, outer circumferences and end faces, certain applications are executed for slope machining and

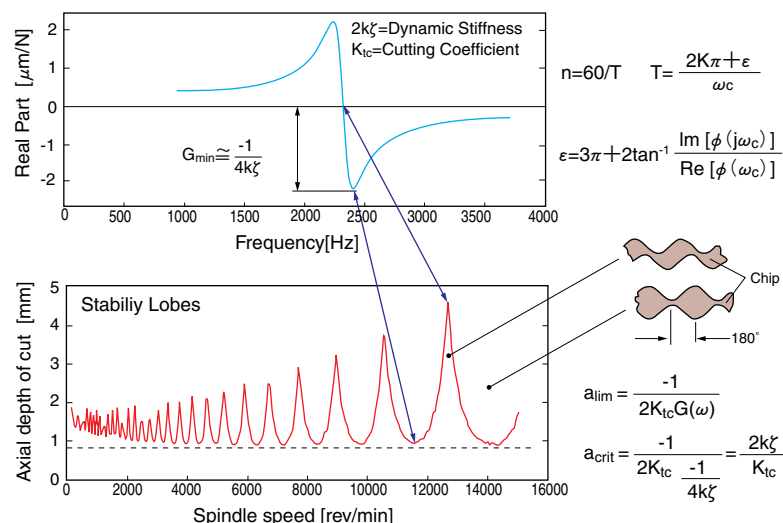


Fig. 1 Stability chart of regenerative chatter vibration (Y. Altintas)

hobbing. Recently, a main spindle mounted to an area equivalent to a turret is capable of not only auxiliary cutting processes, such as end milling, but also to more demanding milling processes. In addition, lathe-based machine tools that resemble milling machines have been developed. One example of such a combined machine tool is shown in Fig. 3 (Mori Seiki Co. NT5400DCG).

Table 2 Background, supporting technologies and advantages of combined multi-functional machine tools

<p>Simultaneous 5-axis control machining center (e.g.: three orthogonal axes and two rotational axes)</p> <p>Combined machining turning center (e.g.: lathe and 2nd main spindle, B axis, Y axis, etc.)</p>

(Background, supporting technologies)

- Need for high-precision, high-efficiency machining to make more advanced (complicated) parts and components
- Increased sophistication of supporting software (CAM)
- Development of high-precision, high-efficiency machine elements (e.g.: DD-motor driven tables, etc.)

(Advantages)

- Improved machining accuracy, reduction in machining time (one-chuck process)
- Machining of complicated shapes

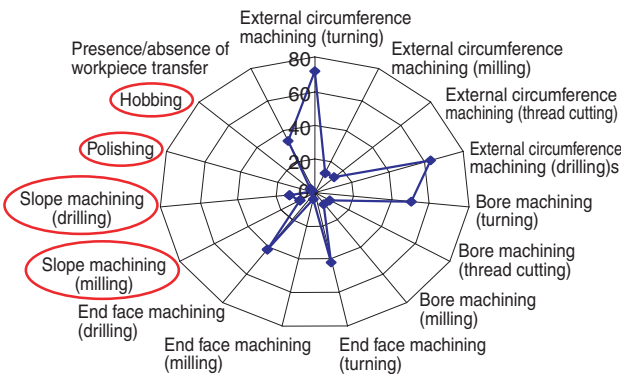


Fig. 2 Survey of machining examples by combined multi-axis machine tools based on turning machines

Many different 5-axis machining centers have been developed. In particular, in addition to orthogonal 3-axis vertical and horizontal machining centers, many simultaneous 5-axis control machining center products that have work tables with two additional axes for rotation and oscillation are used widely. Most recently, some machining centers have a work table driven by a DD motor and a high-speed, high-power rotary table capable of high-speed indexing, and they feature the functions of vertical turning centers. As mentioned above, deriving from either lathes or milling machines, combined multifunctional machining tools may evolve into novel machine tools that incorporate features of both turning centers and milling machines.

Combined multifunctional machine tools have advantages that include the following. They are capable of machining complex forms that require simultaneous control of five axes. Loss in machining accuracy from dismounting and remounting the workpiece is prevented because once a workpiece has been mounted to the chuck, all machining processes are executed without need for rechucking the workpiece. As the needs for function-intensive parts and components increase, advanced combined multifunctional machine tools are capable of machining these workpieces at higher precision and higher efficiency. As superior machine tools, the demand for combined multifunctional machine tools will increase further in the future. To meet this demand, the researchers and engineers in this field must develop the hardware that helps realize sophisticated functions as well as the supporting software (CAM) to enable advanced control techniques and application technology.

Incidentally, within the next 2 years, the STC-M (Scientific Technical Committee: Machines) of CIRP (The International Academy for Production Engineering) will issue a keynote paper that covers current and future trends in combined multifunctional machine tool technology.

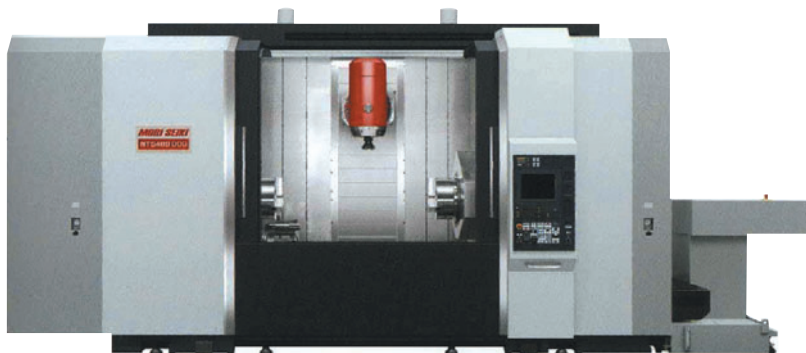


Fig. 3 An example of combined multi-axis machine tool (Mori Seiki Co. NT5400DCG)

4. Ultraprecision Machine Tools

Other than high speed and high efficiency, the most critical requirement for machine tools is high precision. Recently, various ultraprecision machine tools have been developed that are significantly more evolved than earlier high-precision machine tools. Previously, the industrial fields that required ultraprecision machine tools were limited and the market scale for ultraprecision machine tools was relatively small. In contrast, needs have been increasingly mounting for ultraprecision and micro-machined parts and components, such as dies for optical parts and components. In response to this trend, development is in progress for various ultraprecision machine tools.

The background for the needs for ultraprecision machine tools, supporting technologies for their realization and their advantages are summarized in **Table 3**. Progress in the component technologies for ultraprecision machinery, such as air hydrostatic bearings and guides, is remarkable. I believe that advances in hardware technologies for these mechanical elements are contributing to the higher

Table 3 Background, supporting technologies and advantages of ultraprecision machine tools

Ultraprecision machine tools (ultraprecision cutting/grinding machines)
<p>(Background, supporting technologies)</p> <ul style="list-style-type: none"> ● Growing needs for ultraprecision and micro-machined parts and components (Optical parts and components, dies, etc.) ● Sophistication of ultraprecision machine elements (main spindles, guideways, feed drive systems, etc.) ● High-precision control technologies
<p>(Advantages)</p> <ul style="list-style-type: none"> ● Development of new market segments through ultraprecision-machining and micro-machining (Satisfaction of needs) (Optical parts and components, micro parts, mechatronic parts, etc.)

Table 4 Trends in ultraprecision micro machining

<p>1. Form accuracy, finished surface roughness:</p> <ul style="list-style-type: none"> ● Microns→nanometers
<p>2. Form (in the case of optical parts)</p> <ul style="list-style-type: none"> ● Spherical surfaces→aspherical surfaces→nonaxisymmetric surfaces→free-curved surfaces
<p>3. Workpiece materials</p> <ul style="list-style-type: none"> ● Soft metals (aluminum, copper, etc.) ● Hard metals (nickel, hardened steel, etc.) ● Resin materials, anisotropic materials (lithium niobate, fluorite, etc.) ● Brittle materials (tungsten carbide, ceramic materials, etc.) ● Other materials (plastics, etc.)

value of Japanese machine tools.

In the field of ultraprecision-machining and micro-machining, typically for the machining of optical parts and components, the requirements for form accuracy and finished surface roughness have always been demanding, and the forms of machined parts and components have become increasingly complicated as summarized in **Table 4**. Also, the process for preparing optical lenses has changed from injection molding with plastic materials to a hot-pressing process with glass. To cope with this trend, an increasingly larger number of dies are being made of materials that are extremely difficult to machine, such as tungsten carbide and ceramics, and these dies must undergo many machining processes including grinding and polishing. These techniques in die machining processes and glass press-forming processes are contributing positively to the manufacture of the lenses on camera cell phones and digital cameras, which are both increasingly common.

Looking more closely at the lenses used in these types of digital equipment, machining processes that are more demanding are necessary to realize their unique optical arrangements. For example, this is needed to create a combination of a Fresnel lens and an aspherical lens, which enhances the optical characteristics of the related optical systems. At the same time, laser printers and other optical equipment that utilize lasers need more sophisticated optical elements that involve nonaxisymmetric or free-curved surfaces. Therefore, needs are growing increasingly for more advanced ultraprecision machining techniques. To this end, I believe that the importance of ultraprecision machine tools needed for ultraprecision-machining and micro-machining will be further highlighted because they are indispensable in machining highly sophisticated parts and components with high added value.

One example of a 3-axis FTS (Fast Tool Servo)³⁾ device, which is capable of forming a free-curved surface with ultra high precision and higher efficiency, is illustrated schematically in **Fig. 4**. This device, as shown in the diagram, machines a workpiece fixed on a running ultraprecision rotary table while shifting in the radial direction a tool that has its cutting depth in three axial directions controlled at high-speeds and high-response frequencies. If the axial infeed is controlled while the tool is fed in a radial direction, then theoretically any intended shape could be formed on the surface of the workpiece.

In reality, however, it is impossible to form a step square to the cutting direction of a machine tool even at the maximum possible response frequency and response speed of the tool. Therefore, by

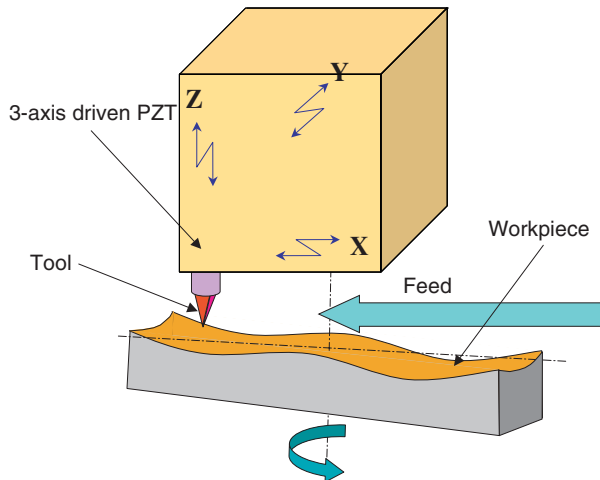


Fig. 4 Schematic illustration of ultraprecision cutting by 3-axis FTS

simultaneously controlling the tool along three axes, the freedom of the machined forms can be increased and the trajectory of motion of the tool being controlled can be simplified. Use of such FTS helps greatly reduce the necessary cutting time on free-curved surfaces.

5. Advanced and Intelligent Control

The increasing sophistication of machine tools is supported by progress in not only hardware but also in software. The background, supporting technologies and advantages of advanced and intelligent control technologies are summarized in Table 5. Recently, many advanced (intelligent) control techniques are available that reflect an understanding of machine tool characteristics and machining processes. For

example, let us think of a control technique for controlling thermal deformation, which is the most critical factor adversely affecting the machining accuracy of machine tools. A much advanced control technique is now commercially used in which the magnitude of the current thermal deformation is estimated in real-time based on information about the machine tool and temperatures at various spots on the tool.⁴⁾ Using this information, the motion of the machine tool is controlled so that higher machining accuracy is ensured under any operating condition.

It is also possible to simulate the motion of the machine tool in real-time based on information about the motion control applied to the machine tool. Utilizing this idea, Okuma Co. has developed an anti-crush system that predicts events such as the crushing of a tool with a chuck and stops the machine as necessary by simulating the motion somewhat in advance of the actual motion of the machine tool. The schematic diagram for this system is illustrated in Fig. 5.

Table 5 Background, supporting technologies and advantages of advanced and intelligent control technologies

Advanced and intelligent control
(Background, supporting technologies)
<ul style="list-style-type: none"> • Need for low-cost controllers with advanced functions • High-speed, high-precision interpolation systems • Real-time thermal deformation compensation • Anti-crush systems that also utilizes simulations • More advances in computer and IT technologies
(Advantages)
<ul style="list-style-type: none"> • Greater added value for machine tools • Evolution of knowledge into established technologies

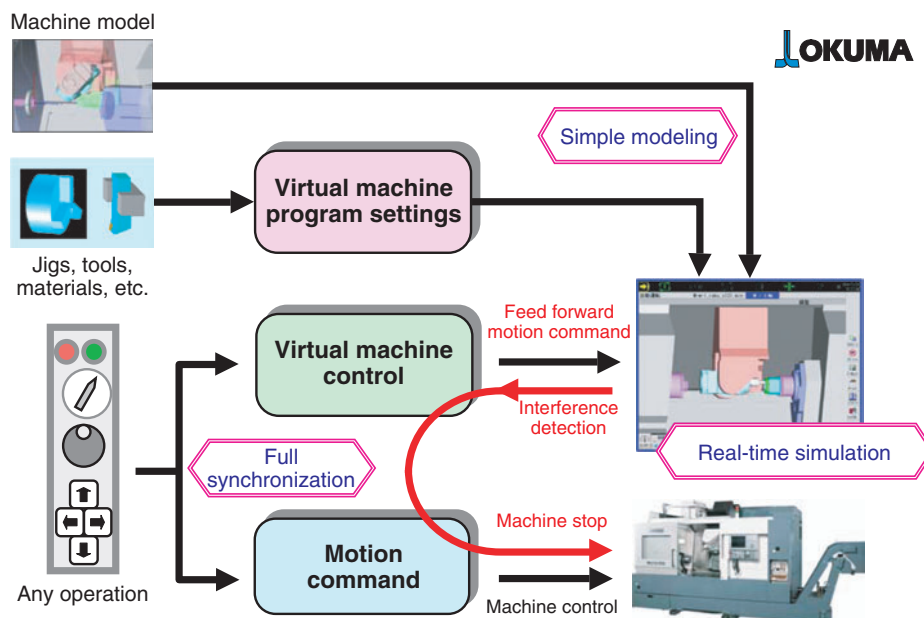


Fig. 5 Conceptual diagram of anti-crush system (Okuma Co.)

In an effort to further advance this idea, under the title of Virtual Machine Tools, the previously mentioned STC-M in CIRP is currently attempting to perform complete simulations that cover machining processes, dynamic characteristics and control characteristics for machine tools.

This simulation scheme is, for example, capable of complete computer simulation of a machine and its processes, allowing it to determine how various components of a machine tool will react when a motion command is given to the machine. It can also determine how the tool and workpiece will interact with each other to machine the workpiece and how the resultant cutting force will affect the machine and tool. The architecture of one example of such a simulation scheme, the virtual CNC system, ⁵⁾ is schematically shown in Fig. 6.

In order to make virtual machine tools become a reality, further research and study efforts need to be made on many issues, including machining processes, and the dynamics and motion characteristics of machine tools. I want to point out that such research and studies are steadily making progress to this end.

6. Conclusion

Based on my own experience, I have described several examples of recent trends in machine tool technologies. The machine tool industry constitutes the backbone of Japan's machinery industry, and for this reason, endeavors to achieve higher speed, higher efficiency and ultraprecision will continue with increasing commitment. In concluding this paper, I want to express my wish that the staff members of NTN continue their efforts so that NTN technologies and products lead their counterparts in the global

machine tool industry in the ever-demanding challenge to achieve the ultra-high-speed and ultra-high-precision required of the main spindle bearings that are critical components of many machine tools.

References

- 1) Y. Kakino: Latest Trend of Main Spindle for NC Machine Tool
- 2) Y. Altintas, M. Weck: Chatter Stability of Metal Cutting and Grinding, *Annals of the CIRP*, 53/2 (2004) p619.
- 3) Wada et. al.: Development of Three-axis Fast Tool Servo for Ultraprecision Machining, *Proc. 6th Int. Conf. of euspen* (2006) p115.
- 4) H. Senda et al.: Main spindle thermal deformation estimation with the goal of mass production (2nd report), *Japan Society of Mechanical Engineers Journal Series C*, 71-709 (2005), p. 2813. (In Japanese)
- 5) K. Erkorkmaz et. al. : Virtual Computer Numerical Control system, *Annals of the CIRP*, 55/1 (2006) p399.

About the author

Toshimichi Moriwaki, Dr. of Engineering
Professor, Kobe University Faculty of Engineering

1966 Graduates Kyoto University Faculty of Engineering, Department of Precision Engineering
 1968 Receives Masters degree from Kyoto University Graduate School of Engineering, Department of Precision Engineering
 1974 Becomes Assistant Professor of Kobe University Faculty of Engineering
 1975 Becomes Assistant Professor of McMaster University (Canada)
 1985 Becomes Professor of Kobe University Faculty of Engineering (2000~2004 Dean of Faculty of Engineering)

Specialties: production systems, machine tools, ergonomic engineering
 Select prizes and awards (not all listed)
 International Academy for Production Engineering (CIRP) F.W. Taylor medal 1977
 Machine Tool Engineering Foundation Encouragement Prizes 1991, 1994, 1995, 1998, 2001
 Iue Cultural Prize (Science and Technology Division) (Iue Memorial Foundation) 1998
 Japan Society for Precision Engineering Prize 2002, 2003
 Hyogo Prefecture Science Prize (Hyogo Prefecture) 2004

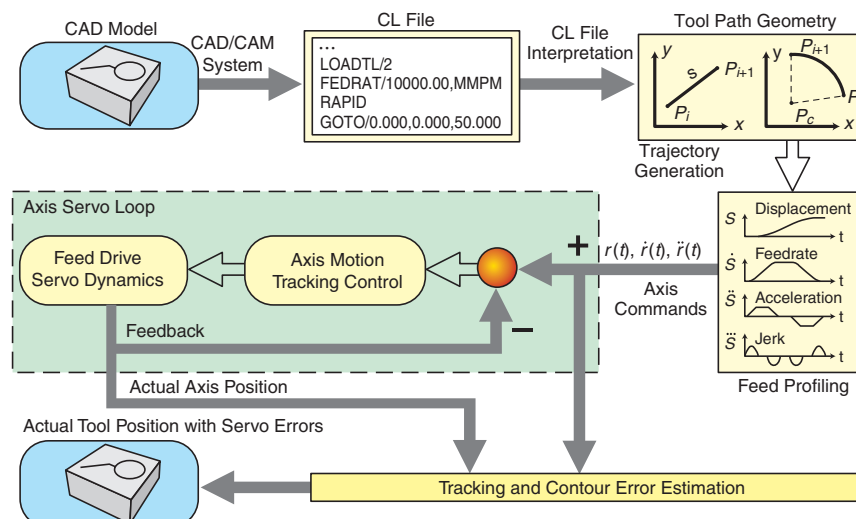


Fig. 6 System architecture of virtual CNC ⁴⁾

Development of a New Grease Lubrication System for Machine Tool Main Spindles

Sun-Woo LEE*
Masatsugu MORI*



NTN has developed a new grease lubrication system for machine tools main spindles which features heat-induced base oil delivery from a grease chamber installed next to the bearing. The lubrication system does not require any external additional lubrication device. Experimental result demonstrates high-speed rotation of an angular contact ball bearing with a 100 mm bore diameter, that has a 1.8 million $d_{m\Omega}$ value for definite position preloading and 2.0 million $d_{m\Omega}$ value for constant pressure preloading. NTN's new grease lubrication system can thus be an alternative to the air-oil lubrication technique while keeping the maintenance-free advantage of the conventional grease lubrication method, in addition, it will support higher performance machine tools as well as improve customer's work environment and reduce environmental burden.

1. Introduction

The use of higher speed main spindles has been increased used on machine tools, including machining centers, in order to achieve better machining efficiency and machining accuracy. To cope with the challenges associated with high-speed machine tool main spindles, NTN has been developing and improving various main spindle bearings and currently markets these bearings under the “**ULTAGE Series**” brand name.¹⁾ In recent years, people around the globe have been becoming increasingly concerned about the environment, so manufacturers worldwide must remain committed to eco-friendly technologies. In response to the technological challenges related to this, NTN has been developing unique bearing products through investigations into bearing lubrication techniques. The resultant bearing product lines include “eco-friendly jet lubrication angular contact ball bearings,”²⁾ “eco-friendly air-oil lubricated angular contact ball bearings (HSL type)”¹⁾ and “grease lubricated sealed angular contact ball bearings (BNS type).”¹⁾ Grease lubrication systems, in particular, have smaller impacts on the environment and can be maintenance-free. As a result, demand is

growing for grease lubrication systems for machine tool main spindles.

One typical example of the authors' achievement is that the above-mentioned “grease lubricated sealed angular contact ball bearing (BNS type)” has achieved a bearing life of more than 20,000 hours at a running speed equivalent to $d_{m\Omega}$ of 1.4 million.

The authors developed a “new grease lubrication system for machine tool main spindles” that is capable of greater bearing speed and longer bearing life with grease lubrication that does not need maintenance. This novel grease lubrication system is comprised of a conventional internal design but has a grease chamber in the front side of the bearing from which only the base oil in the grease is extracted to lubricate the bearing. This novel grease lubrication system was incorporated into an angular contact ball bearing with a bore diameter of 100 mm, making the bearing capable of high-speed operation and a long bearing life. The $d_{m\Omega}$ value reached 2 million with constant pressure preloading and 1.8 million with definite position preloading. In this paper, the authors report the achievements of their research into a novel grease lubrication system that is completely maintenance-free.

*Elemental Technological R&D Center

2. Structure of the New Grease Lubrication System

To achieve high speed and long life with a bearing by using grease lubrication, it is necessary to not only provide a sufficient amount of lubricant for a bearing while running at a high speed but also to maintain the supply of grease base oil from a limited amount of prefilled grease. With the authors' newly developed grease lubrication system, the base oil in the grease is actively separated while the bearing is running, and this separated base oil is steadily supplied to the raceway surface of the bearing. The bearing structure of the authors' new grease lubrication system is illustrated schematically in Fig. 1. As a part of the outer ring spacer, a cavity is formed in front of the bearing and the grease prefills this space. At the same time, this provides a shouldered surface near the contact point between the rolling elements and the outer ring raceway. In addition, a thin axial flow path is formed between the shouldered surface and the end point of the grease chamber, thus connecting the grease chamber to the raceway surface.

For this structure, the authors considered a base oil delivery mechanism that works as follows. The running bearing generates heat, causing the temperature of the grease in the grease chamber to increase and the base oil in the grease to separate from the thickener. As the temperature increases, the pressure in the grease chamber also increases, causing the base oil from the above-mentioned axial flow path to flow through the clearance on the shouldered surface, resulting in delivery to the outer ring raceway surface. As a result, the bearing is actively lubricated by the base oil delivered to the outer ring raceway surface.

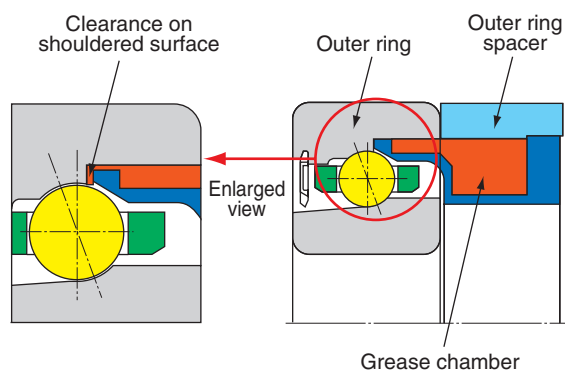


Fig. 1 Schematic construction of new lubrication system

3. Experiment Using a Model Test Rig

To investigate the characteristics of base oil delivery from the grease chamber and verify the base oil delivery mechanism described in Sec. 2, the authors used a model in which this base oil delivery mechanism was applied to an angular contact ball bearing with a 100 mm bore diameter. The findings from the experiment are provided below.

3.1 Model test rig and test method

The authors' model test rig for base oil delivery is schematically illustrated in Fig. 2. The appearance of the test rig is shown in Photo 1. The radial clearance in Fig. 2 is indicated on a radius basis. The properties of the two types of grease developed for machine tool main spindle bearings that were used are summarized in Table 1. Grease was filled into the grease chamber via four grease prefilling holes provided on the outer circumferential surface until the entire space of the grease chamber was filled. The amount of prefilled grease was approximately 47 g.

The following characteristics were tested since they were considered to affect base oil delivery:

- Temperature-dependent variation in the grease chamber
- Size of radial clearance at the end point
- Type of grease used

Table 1 Grease properties

Characteristic	Grease	
	Grease-A	Grease-B
Thickener	Urea	Urea
Base oil	PAO	PAO
	Polyol ester	Diester
		Polyol ester
Amount of thickener wt%	11.2	11.7
Base oil kinematic viscosity mm ² /s ² 40°C	40.6	40.6
Worked penetration, 60 strokes 60W 25°C	243	280
Spreading consistency	230	260

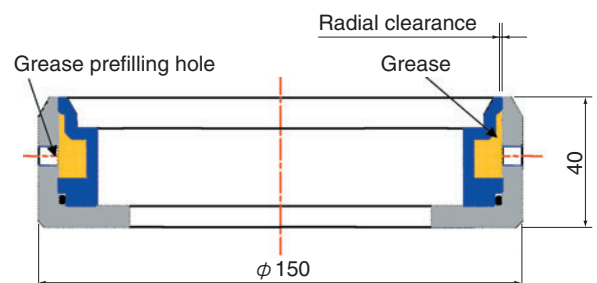


Fig. 2 Sketch of model test rig for base oil delivery

3.1.1 Variation in the amount of base oil delivery depending on the heat cycle

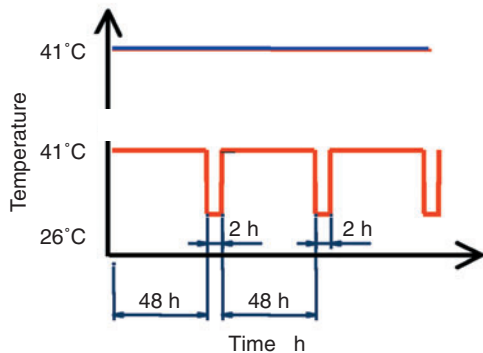
Grease-A in **Table 1** was used to investigate the base oil delivery due to heat increase. The amount of base oil delivery in a model test rig subjected to repeated temperature increase and decrease (hereinafter referred to as the “heat cycle”) was compared with a model test rig in which the temperature was increased and then maintained that increased. The temperature was automatically controlled by a constant temperature chamber and the pattern of the heat cycle was as illustrated in **Fig. 3(a)**. The temperature variation in each heat cycle (15°C) was equivalent to the difference between the temperature in the grease chamber when the bearing was running (41°C) and when the bearing was at a standstill (room temperature: 26°C).

The results of the amounts of base oil delivery relative to the radial clearance of 0.15 mm are summarized in **Fig. 3(b)**. The model test rig (**Photo 1**) was set so that the flow path composed of the radial

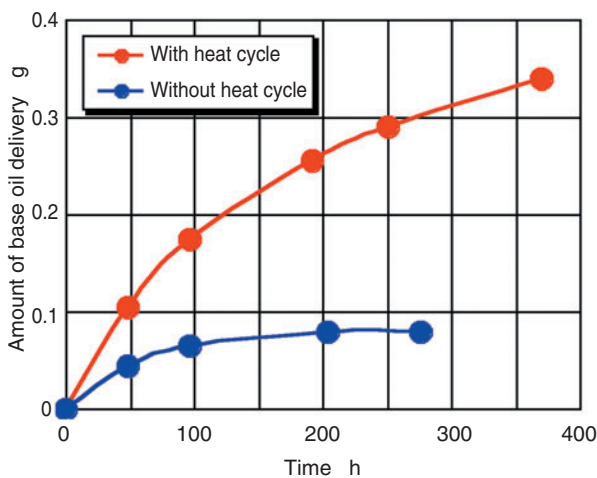
clearance was situated vertically, and the oil content delivered to the clearance end point was removed with a piece of blotting paper once every 50 to 100 hours. The increases in the weight of the pieces of blotting paper were totaled and the resultant sum was taken as the amount of oil delivery.

Immediately after grease prefilling, delivery of not only the base oil but also of the grease itself was observed. This portion was wiped away and was not included in the amount of delivery. The state of base oil delivery at the end point of clearance is shown in **Photo 2**. When the model test rig was not subject to the heat cycle, no delivery was observed after 100 hours elapsed though a minor delivery occurred at the initial stage of testing. In contrast, when the model test rig was subject to the heat cycle, the delivery continued and the amount of delivered base oil was proportional to the time elapsed. In other words, when the heat cycle is applied to the grease chamber, the base oil in the grease is repeatedly separated from the grease and delivered through the clearance to function as a lubricant.

Next, the effect of temperature differences in each heat cycle on the amount of base oil delivery was studied using the combination of Grease-A and a radial clearance of 0.15 mm. For comparison, the test was performed with temperature differences in each heat cycle of 15°C and 3°C. The heat cycle pattern used for this test is shown in **Fig. 4(a)**, and the result



(a) Heat cycle pattern



(b) Base oil delivery versus elapsed time

Fig. 3 Base oil delivery with/without heat cycle



Photo 1 Model test rig for base oil delivery

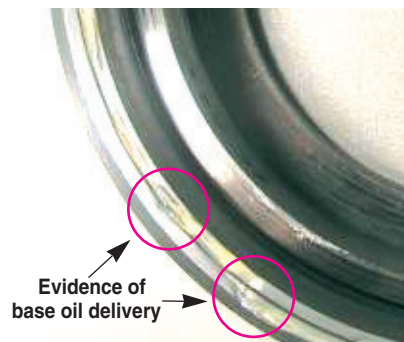


Photo 2 Delivered base oil

of this test is graphically plotted in Fig. 4(b). The amount of base oil delivery is greater with a greater temperature difference in each heat cycle. However, base oil delivery is still possible with a temperature difference of about 3°C.

Thus, the minimum temperature difference necessary for base oil delivery through a clearance seems to be 3°C. Assuming that a machine tool main spindle is continuously run for an extended period virtually without stoppage, the authors' lubrication system can be applied even though, for example, only periodic temperature variation due to control over the jacket cooling temperature is available.

3.1.2 Size of radial clearance and associated amount of base oil delivery

The authors studied the interrelation between the size of radial clearance at the end point through which the base oil is delivered and the amount of base oil delivery. The sizes of the radial clearances adopted were 0.05 mm, 0.15 mm, 0.2 mm and 0.45 mm. The differences in temperature in the heat cycles, relative to the temperatures on the outer rings of the running

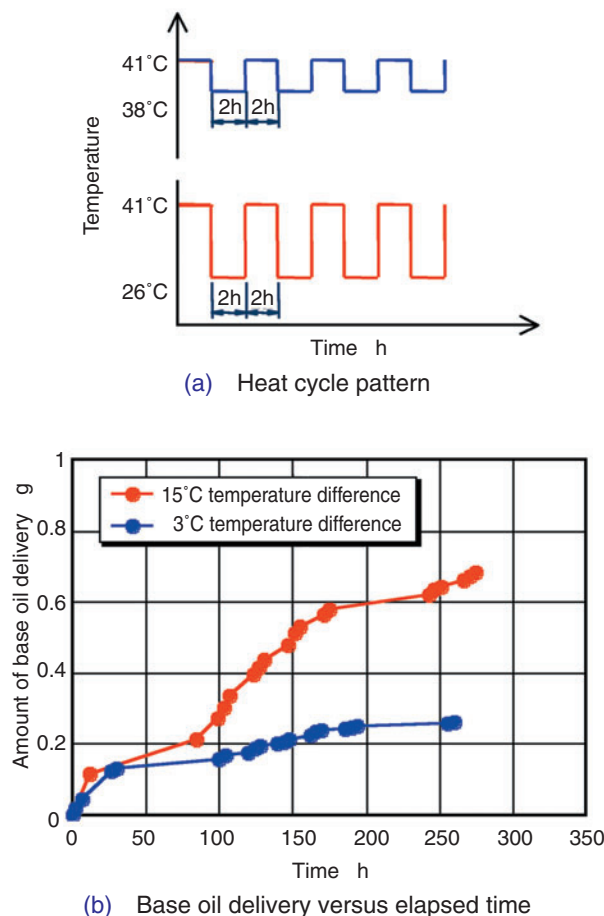


Fig. 4. Relation between temperature difference and base oil delivery

bearings (41°C) were 3°C (between 41°C and 38°C) and 15°C (between 41°C and 26°C). The heat cycle patterns shown in Fig. 4(a) are the same as mentioned previously. After 250 test hours, the measured amounts of base oil delivery were graphically plotted in Fig. 5. Grease-B was used in this test and the properties, are summarized in Table 1.

The absolute value of the amount of base oil delivery with a temperature difference of 3°C differs from that with a temperature difference of 15°C. Nevertheless, under each of these different temperature conditions, a smaller radial bearing clearance led to a greater amount of base oil delivery.

3.1.3 Effects of different grease types on the amount of base oil delivery

The authors studied the effect of the type of grease prefilled in the grease chamber on the amount of base oil delivery by using the two types of greases summarized in Table 1. The temperature difference in each adopted heat cycle was 15°C, and the size of the radial clearance used was 0.05 mm. The heat cycle pattern adopted was the same as that described

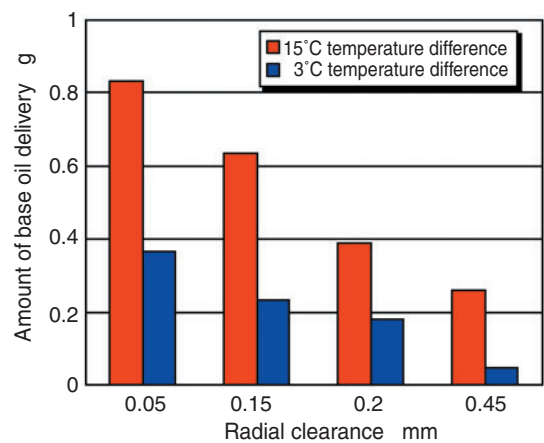


Fig. 5 Base oil delivery versus radial gap

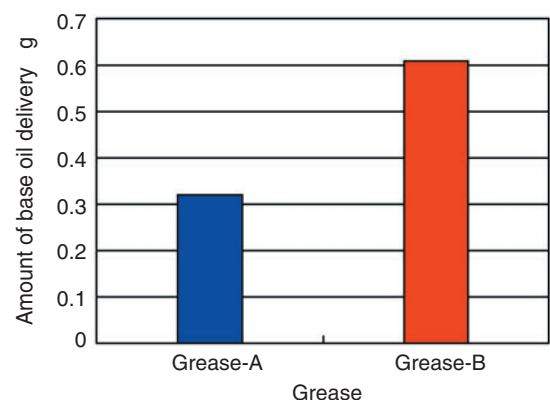


Fig. 6 Base oil delivery versus grease property

previously and illustrated in Fig.3(a). After 250 test hours, the measured amounts of base oil delivered are graphically plotted in Fig. 6.

It can be understood that the amount of base oil delivery varies greatly depending on the type of grease used. Compared with Grease-A, the amount of base oil delivery with Grease-B was approximately 2 times more than Grease-A. In other words, compared with Grease-A, Grease-B is more prone to base oil separation. The choice of a grease that is prone to base oil separation is one important consideration for the authors' new grease lubrication system.

3.2 Base oil delivery mechanism

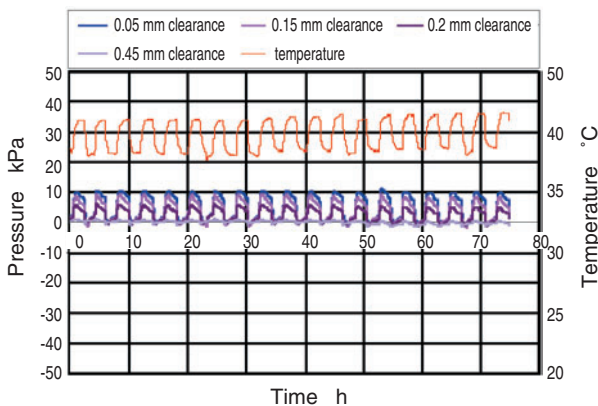
As mentioned above, the factors that allow the authors' novel grease lubrication system to be capable of base oil delivery include the heat cycle, optimized radial clearance and the choice of grease. The authors studied how these factors affect base oil delivery by measuring the pressure in the grease chamber in the base oil delivery mechanism. For the test, the base oil delivery model illustrated in Fig. 2

was used, the pressure in the grease chamber was measured with a distortion gage pressure sensor and the grease temperature was determined with a thermocouple. The sizes of radial clearances adopted were 0.05 mm, 0.15 mm, 0.2 mm and 0.45 mm. Grease-B was prefilled in the grease chamber.

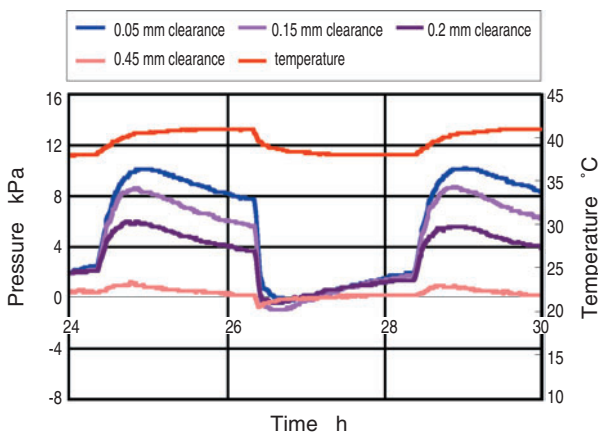
The results of the grease chamber pressure measurements are summarized in Fig. 7(a). In addition, the temperature readings in the grease chamber obtained at the same time using the model with a radial clearance of 0.05 mm are also indicated. In the heat cycle pattern adopted, the lowest temperature was 38°C and the highest temperature was 41°C (temperature difference of 3°C), and the cycle was repeated once every 2 hours. The pressure in the grease chamber kept at 38°C at the start of the test was taken as 0 kPa. Fig. 7(b) is a partial view of the measurement record shown in Fig. 7(a), with the time axis enlarged.

From these diagrams, the following observations, which fulfill expectations, can be made about the grease chamber. First, the pressure increases as the temperature increases and the pressure drops as the temperature drops. Second, the pressure during temperature increase also correlates to the size of the radial clearance at the end point of the grease chamber. The pressure was greatest when the clearance was the smallest at 0.05 mm and decreased with greater clearance. Furthermore, the maximum pressure relative to the clearance of 0.05 mm is approximately 10 kPa. The authors think that the pressure in the grease chamber readily increases with the smaller radial clearance due to better sealing of the interior of the grease chamber. They also conclude that the grease in the grease chamber expands as the temperature increases, causing the base oil and thickener in the grease to separate. Since the fluidity of the separated base oil is higher than the thickener, as the pressure in the grease chamber increases, the separated base oil is pushed out through the clearance. It appears that when delivery of the separated base oil through the clearance begins, the pressure in the grease chamber gradually decreases as shown in Fig. 7(b).

Next, when the temperature of the grease drops, the grease begins to shrink, and as a result, the pressure in the grease chamber drops. While the pressure is dropping, the rate of base oil delivery from the clearance gradually decreases and a portion of the delivered base oil is drawn back into the clearance. Then, the interior of the grease chamber seems to be sealed due to the surface tension of the oil. This theory is further supported by the fact that the minimum pressure value is somewhat negative. The



(a) Pressure change history in grease chamber



(b) Detailed pressure change

Fig. 7 Pressure change history in grease chamber

authors believe that slight increases in the pressure that follow are due to the gradual shrinking of the model itself. This pattern is further repeated when the temperature increases and decreases again due to the repeated heat cycle.

Thus, existence of the base oil delivery mechanism described above has been confirmed.

4. Spindle Test

The authors applied their new grease lubrication system to an angular contact ball bearing that carries a spindle and executed a running test, simulating operation with a machine tool. The bearing used was an angular ball contact bearing with a 100 mm bore diameter. The technical data for the bearing is summarized in **Table 2**, and a cross-sectional view of the bearing is shown in **Fig. 8**.

Incidentally, the lubricant feed rate adjustment function provided by the “radial clearance (see **Fig. 2**)” in Sec. 3. “Experiment Using a Model Test Rig” is borne by the “shouldered surface clearance (see **Fig. 1**)” with actual bearings such as those used in the authors’ spindle test.

Table 2 Bearing specifications for spindle test

Tested bearing	$\phi 100 \times \phi 150 \times 24 \text{ mm}$
Contact angle	20°
Rolling element material	Si_3N_4
Cage material	Laminated phenol resin
Prefilled grease in bearing	Prefilled Grease-A, 6 g

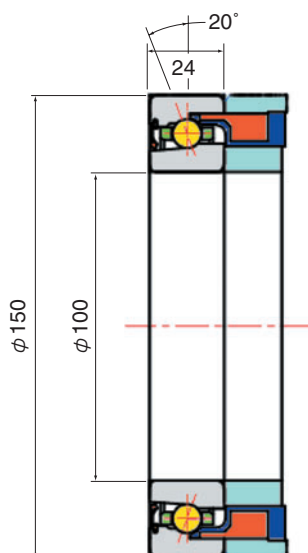
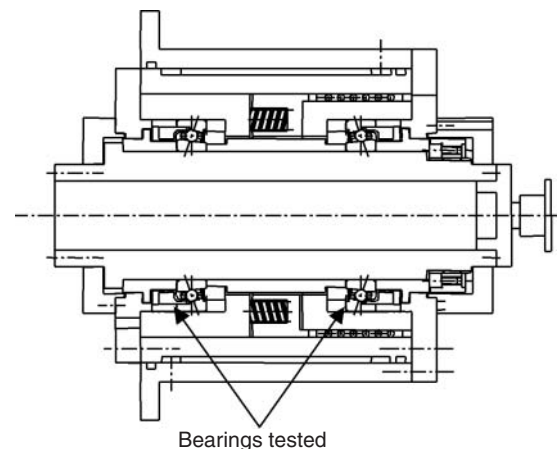


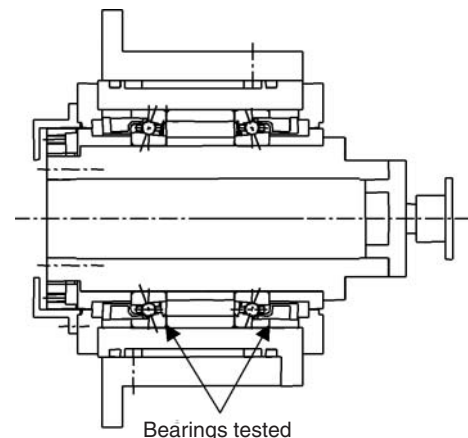
Fig. 8 Section view of test bearing

4.1 Temperature increase confirmation test

To investigate the operating characteristics of the authors’ new grease lubrication system, they measured the temperature increase on both constant pressure preloaded bearings and definite position preloaded bearings. A critical requirement in order for the grease lubrication system to be used industrially is the prevention of a significant increase in bearing temperature. **Fig. 9(a)** and **9(b)** illustrate spindle test rigs for both preloading systems. In each test rig, two bearings being tested were arranged in a back-to-back duplex configuration (DB set). The test conditions used are summarized in **Table 3**. Among the test conditions, the axial load value was determined by considering the maximum allowable load for the contact surface pressure of the rolling elements. For the definite position preloading test, the preload was set to the minimum level necessary for practical machine tool operation (0 initial clearance on mounted bearing).



(a) Schematic construction of test spindle supported with constant pressure preloaded bearings



(b) Schematic construction of test spindle supported with definite position preloaded bearings

Fig. 9 Spindle test rig

The results of bearing temperature measurements with the constant pressure preloading system are graphically plotted in Fig. 10(a), and the results with the definite pressure preloading system are provided in Fig. 10(b). With the definite preloading system that keeps the axial load to the bearings at a near-constant level, the test rig was run at $d_{m\Omega}$ of 2 million (15000 min^{-1}). As a result, the authors confirmed that the

Table. 3 Temperature rise test conditions

Item	Details	
Grease chamber technical data	Shouldered surface clearance	0.08 mm
	Prefilled grease in bearing	47 g Grease-A prefilled
	Heat cycle	None
Bearing preloading	Constant pressure preloading test	2.2 kN
	Definite position preloading test	Clearance after mounting 0
Jacket cooling oil temperature	Room temperature $\pm 1^\circ\text{C}$	

temperature on the bearings at various running speeds were stable and the spindle can operate without any problems.

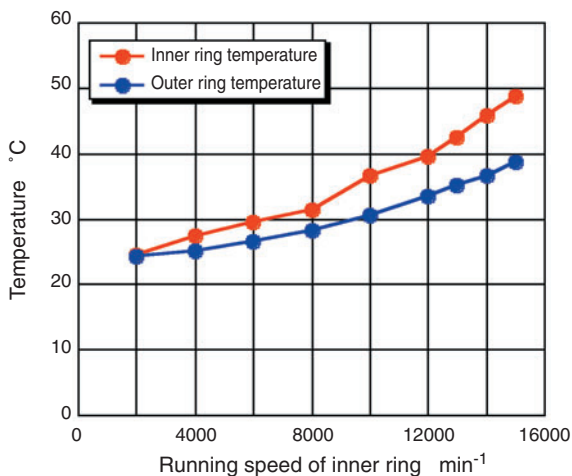
At the same time, as can be understood from Fig. 10, with the definite position preloading system, the temperatures on the inner ring and outer ring at $d_{m\Omega}$ of 1.8 million (14000 min^{-1}) were 46°C and 37°C , respectively, which are roughly the same as in the case of the constant pressure preloading system that runs at the same speed. However, with the definite position preloading system at $d_{m\Omega}$ of 2 million (15000 min^{-1}), the temperatures on the inner ring and outer ring were 53°C and 43°C , respectively. These values are higher than those of the constant pressure preloading system. Since the running bearings were overloaded (preloading) under this situation, the authors judged that the bearings were not capable of operating normally under these conditions.

Assuming that the limiting speed at a particular bearing temperature in the definite position preloading system is the same as the bearing speed of the same bearing with the constant pressure preloading system, and based on the test result described above, the limiting speed of the definite preloading system matches $d_{m\Omega}$ of 1.8 million (14000 min^{-1}).

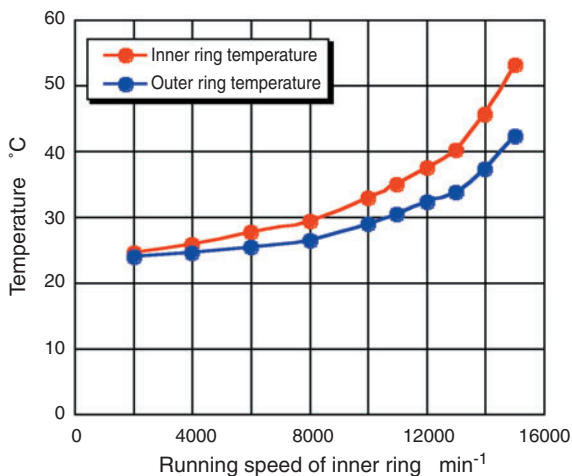
Thus, by using the authors' new grease lubrication system, it is possible to operate machine tool spindles at higher speed ranges than had been previously possible with air-oil lubrication systems.

4.2 Endurance test

The durability of bearings lubricated with the authors' new grease lubrication system was evaluated. Durability tests were performed with both a definite position preloading system and a constant pressure preloading system. The test rigs used are illustrated in Figs. 9(a) and 9(b). The constitution of the grease chamber and the operating conditions used are summarized in Table 4. The bearing speed of both the constant pressure preloading system and the definite position preloading system were at $d_{m\Omega}$ of 2 million (15000 min^{-1}) to emphasize the running speed. With the definite position preloading system, overloading would occur as judged from the results obtained in the previous Sec. 4.1. Therefore, the initial clearance of the bearing was adjusted so that an appropriate preload (axial load 2.2 kN) was attained at the speed of 2 million $d_{m\Omega}$ (15000 min^{-1}). In the adopted heat cycle pattern, as illustrated in Fig. 11(a), each repeated cycle consists of 50 hours of operation and 1 hour of rest. The temperature difference in each cycle was approximately 15°C . With the definite position preloading system, the spindle was also tested in both vertical and horizontal positions to



(a) Constant pressure preloading



(b) Definite position preloading

Fig. 10 Temperature rise versus rotational speed

examine the effect of the attitude of the main spindle on the bearing life.

The test results are graphically illustrated in Fig. 11(b). The endurance test results of bearings lubricated with the authors' new grease lubrication system are presented along with the results for a conventional grease lubricated angular contact ball bearing with seals on both sides that was tested under the same conditions. When operated at d_{mN} of 2 million, the conventional grease lubricated bearing seized after approximately 500 hours had elapsed.

It is clear that the authors' new grease lubrication system is effective at providing a sufficient amount of lubricant and an uninterrupted lubricant supply. A certain bearing lubricated with the authors' new

lubrication system has successfully achieved 18000 hours of continuous operation and is still running.

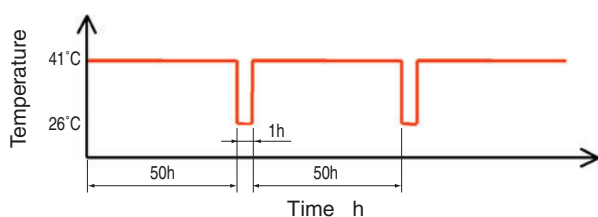
Incidentally, the endurance test results reported here are all obtained from bearings lubricated with Grease-A. Currently, a bearing endurance test is in progress with the definite position preloading system using Grease-B. The bearings being tested in both horizontal and vertical attitudes have already achieved 2000 operating hours and are still operating smoothly.

5. Conclusion

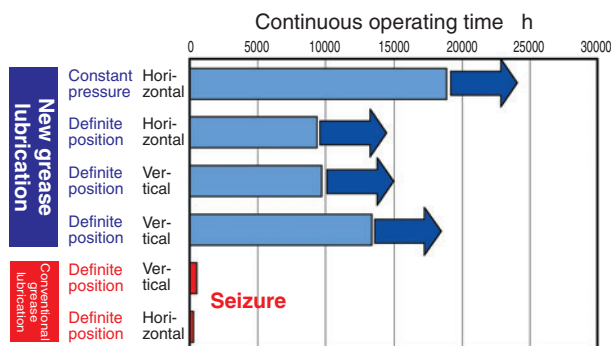
To cope with the mounting needs for higher-speed machine tool main spindles, the authors have developed a unique grease lubrication system that allows the bearings being lubricated to be completely maintenance-free. By using this lubrication system that features heat cycle-driven base oil delivery from the grease chamber, an angular contact ball bearing with a 100 mm bore diameter can run at d_{mN} of 1.8 million with a definite position preloading system and at d_{mN} of 2 million with a constant pressure preloading system. In summary, the authors' new grease lubrication system is a unique lubrication scheme that helps achieve better machine tool performance and mitigate environmental impacts because it possesses a completely maintenance-free operation of the grease lubrication system and is also capable of higher speed operation not possible with any conventional grease lubrication system.

Table. 4 Endurance test conditions

Item		Details		
Grease chamber technical data	Shouldered surface clearance	0.08 mm		
	Prefilled grease in bearing	Grease-A		
	Amount of prefilled grease	47 g		
Operating conditions	Definite position preloading	Spindle attitude and number of spindles tested	Vertical (2 units), horizontal (1 unit)	
		Preload	Initial clearance that coincides with 2.2 kN axial load when the bearing is running at d_{mN} 2 million	
		Running speed	d_{mN} 2 million	
	Constant pressure preloading	Spindle attitude and number of spindles tested	Horizontal (1 unit)	
		Preload	2.2 kN	
		Running speed	d_{mN} 2 million	
Jacket cooling oil temperature		Room temperature $\pm 1^\circ\text{C}$		



(a) Heat cycle pattern



(b) Bearing endurance of new and conventional grease lubrication system

Fig. 11 Endurance test results

References

- 1) NTN Precision Rolling Bearings, Cat. No. 2260/E
- 2) Y. Akamatsu, M. Mori: Development of Eco-friendly Oil Jet Lubricated Angular Contact Ball Bearings for Machine Tool, NTN Technical Review No. 72 (2004) pp. 6-10.

Photos of authors



Sun-Woo LEE

Elemental Technological R&D Center



Masatsugu MORI

Elemental Technological R&D Center

High-Speed Tapered Roller Bearing for Machine Tool Main Spindles

Masatsugu MORI*
Takuji KOBAYASHI*



Tapered roller bearings feature high stiffness and are used to support the main spindles of machine tools, but require new geometrical and air-oil lubrication systems to overcome their difficulty in high-speed operation. Power loss minimization of the bearings are attained by fully lubricating the rib-roller end contacts as well as by reducing lubricant supply to the roller-race contacts to enable high-speed rotation. The mechanism is specified by a ribbed cup, multiple nozzle holes penetrating the rib for air-oil supply and a resin cage riding on outer-ring spacers. Based on this concept NTN has experimentally produced an air-oil lubricated 100 mm bore tapered roller bearing which successfully operates with a maximum d_{mN} value of 1.25 million which is beyond previously reported records within the category of air-oil lubrication.

1. Introduction

High-speed running performance and rigidity, which are generally required for machine tool main spindles, are factors that greatly depend on the performance of the bearings that support the main spindles. The types of main spindle bearings used include rolling bearings, dynamic pressure and hydrostatic bearings lubricated by oil and air, and magnetic bearings. Rolling bearings are often used for this purpose because they feature an excellent total balance of all the important considerations, including maintainability and cost-effectiveness. When rolling bearings are incorporated into machine tools such as machining centers that are required to run at higher speeds, four rows of high-speed angular contact ball bearings are provided on the main spindle front side. In this arrangement, high-speed operation is possible with a definite position preloading system. However, the rigidity of this configuration is not always high enough, as the main spindles in combined multifunctional machine tools, such as lathe main spindles, need higher rigidity. Therefore, the front-side bearing arrangement on combined multifunctional machine tools is often

comprised of a double row cylindrical roller bearing and an axial load carrying angular contact ball bearing.

However, with this spindle-bearing configuration, the contact angle of the axial load carrying angular contact ball bearing exceeds 30° and slipping occurs on the bearing due to a gyro-moment when it runs at a higher speed. Thus, the high speed running performance of this configuration is not satisfactory.

Modern machine tools are required to have enhanced machining efficiency which can be achieved by using tapered roller bearings which feature very high rigidity in both radial and axial directions. Due to their greater rigidity, tapered roller bearings are employed on certain large lathes and turning centers. However, since they do not excel in the high-speed running performance required of recent machine tools, they are used less frequently. Therefore, NTN attempted to develop a unique tapered roller bearing that not only features the high rigidity associated with tapered roller bearings but also boasts a high-speed performance that is better than a combination of a double row cylindrical roller bearing and an axial load carrying angular contact ball bearing.

*Elemental Technological R&D Center

There have been efforts to develop high-speed tapered roller bearings for machine tool main spindles, and an example¹⁾ has been reported in which 1.25 million $d_{m\Omega}$ was achieved with a tapered roller bearing equivalent to the 32020 model. In this example, however, a forced circulation lubrication system was employed with a lubricating oil flow rate that exceeds 4 liters per minute. Unfortunately, this example is not practical as a replacement for a grease- or air-oil-lubricated combination of a double row cylindrical roller bearing and an axial load carrying angular contact ball bearing because of a greater lubrication cost and a greater power loss from the entire bearing system that includes this lubricating oil circulation system. The authors have conducted research, prototyping and experiments on high-speed application with an air-oil lubricated tapered roller bearing and have achieved an unprecedented 1.25 million $d_{m\Omega}$. This paper reports on this achievement.

2. Requirements for Higher Bearing Speed

A challenge that must be addressed to achieve higher speed with a rolling bearing is limiting the temperature increase that results from higher bearing speed. If the temperature on a rolling bearing is excessively high, the preload varies greatly due to thermal expansion, and this in turn further promotes temperature increase. This problem is particularly apparent with definite position preloading systems, which are often used on bearing systems that must have very high rigidity.

Arrangements for inhibiting temperature increases on a rolling bearing include a forced circulation lubrication system and a jet lubrication system in which a large amount of lubricant is fed to a rolling bearing to remove heat from the bearing in an amount greater than the heat generated on the bearing that results from the viscosity of the lubricating oil. However, the authors did not employ either of these arrangements. In the case of air-oil lubrication systems in which small amounts of lubricating oil are fed to the rolling bearing with compressed air, the key to high-speed operation is minimization of the heat occurring from the running rolling bearing.

Now, let us consider the heat generating factor, that is, the torque generation factor for the tapered roller bearing illustrated in Fig. 1. On a tapered roller bearing, the generatrix of the rollers intersects the prolonged line from the inner-outer ring raceway at a point on the rotation axis. Therefore, sliding friction from spinning between rollers and raceway does not occur.²⁾ Also, since the mode of roller-bearing ring contact is linear contact, differential sliding does not

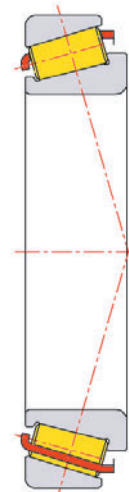


Fig. 1 Section view of standard tapered roller bearing

take place and the elastic hysteresis loss is usually small.³⁾ Given this, typical factors to be considered for a high-speed tapered roller bearing include:

- 1) **EHL (elasto-hydrostatic lubrication) rolling viscous friction between rollers and the bearing ring**
- 2) **Sliding friction between the roller large-end face and the rib face**
- 3) **Sliding friction between the rollers and cage pockets**
- 4) **Stirring friction with oil and air in the bearing**

First, the EHL (elasto-hydrostatic lubrication) rolling viscous friction between rollers and the bearing ring in 1) can be determined with the following expression⁴⁾:

$$f_{EHL} = \phi_{s, EHL} \phi_l \frac{29.2R(GU)^{0.648} W^{0.246}}{\alpha} l \dots\dots\dots(1)$$

where, $\phi_{s, EHL}$ is an EHL starvation coefficient that represents the degree that the amount of oil is insufficient, and can take a value in the range from 0 to 1; ϕ_l represents a correction coefficient derived from shearing heat generation occurring at the EHL inlet and is determined based on the load, bearing speed and lubricating oil physical properties; α is the viscosity-pressure coefficient of the lubricating oil used; l stands for the contact length of the rollers; G , U and W are non-dimensional material, velocity and load parameters, respectively, and are uniquely determined by the geometrical shape and running speed of the bearing, the load, and the physical properties of the lubricating oil. Therefore, if the geometrical shape of the bearing, operating conditions and the lubricating oil are given, the rolling viscous friction can be decreased by gradually decreasing $\phi_{s, EHL}$ to zero by allowing starvation to occur whenever possible by

decreasing the oil fed between the rollers and bearing ring while maintaining the EHL oil film. Consequently, at the same time, the shearing heat generation at the inlet decreases and ϕ_i becomes smaller.

Next, let us consider the sliding friction occurring between the roller large-end face and the rib face mentioned in 2) above. The contact surface pressure at this area is low, and the fluid lubrication mode occurring there is an equivalent viscosity-rigid body or changing viscosity-elastic body (EHL) mode.⁵⁾ Thus, the authors executed numerical analysis in the equivalent viscosity-rigid body mode in order to evaluate quantitatively the effect of starvation on the frictional resistance between the roller large-end face and rib face.

More specifically, the authors determined the reaction force on the oil film and the pressure center position from the oil film pressure distribution, which was obtained by solving the Reynolds equation for the two-dimensional flow on a polar coordinate system in accordance with a relaxation method. They repeated calculation with the Newton-Raphson formula until the conditional expression, where the reaction force on the oil film was equal to the applied load and the pressure center position passed the roller center position, was satisfied. The cavitation boundary conditions applied to the Reynolds equation were the Reynolds conditions. From the floatation and skew angle on the roller large-end face finally obtained, the viscosity-friction torque on the rib can be calculated. Accordingly, in Fig. 2, which simulates the interference region in terms of fluid lubrication between the roller large-end face and inner-ring rib, the hatched area is the region subjected to fluid lubrication analysis for a case where no starvation is present ($\theta = \theta_{min}$). Assuming that the oil film pressure generation starts at

the angle θ , the rib starvation coefficient can be defined with the following expression:

$$\phi_{s, rib} = \frac{\theta - \theta_{min}}{\theta_{max} - \theta_{min}} \dots\dots\dots(2)$$

When this rib starvation coefficient is used and the rib viscosity-friction torques for all the 29 rollers are totaled, the result illustrated in Fig. 3 is obtained. Since most of the pressure occurs when θ is $\pi/2$ or lower, the authors assumed that $\phi_{s, rib}$ was less than 50%. From Fig. 3, it should be understood that when $\phi_{s, rib}$ is at 45%, the torque is approximately twice as great. This is because, despite the narrower pressure generation region (that is, frictional torque generation region), the rib needs to carry the same load, and as a result, the oil film thickness on the rib is smaller and the increase in the torque is greater than the effect of reduction in the pressure generation region. Assuming that in reality the starvation occurs not only in the circumferential direction but also in the radial direction, more increase in the torque can be expected.

In summary, to reduce the rolling viscosity resistance, it is necessary to minimize the amount of lubricating oil. On the other hand, to reduce the frictional resistance on the rib, it is necessary to provide a sufficient amount of lubricating oil. The authors believe that by reducing the amount of oil on the raceway surface, the torque resulting from 3) and 4) described above can also be reduced.

To determine the actual relation between amounts of air-oil lubrication and torques, the authors used the standard 32020 tapered roller bearing, which has specifications as summarized in Table 1, and measured the total torque and rib torque. As usual, lubricating oil was supplied from the back side (inner-ring smaller rib side) by using eccentric pump action.

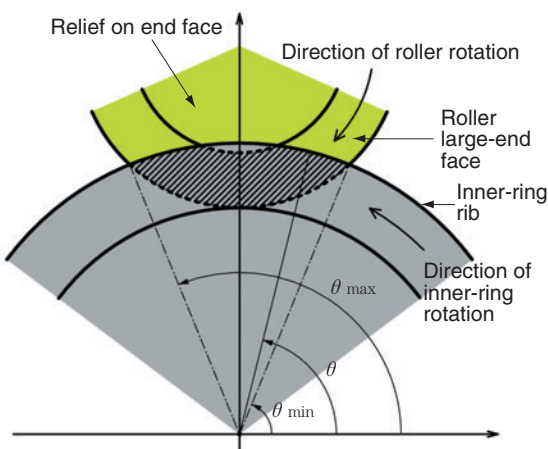


Fig. 2 Sketch of interaction between roller large end face and inner-ring rib

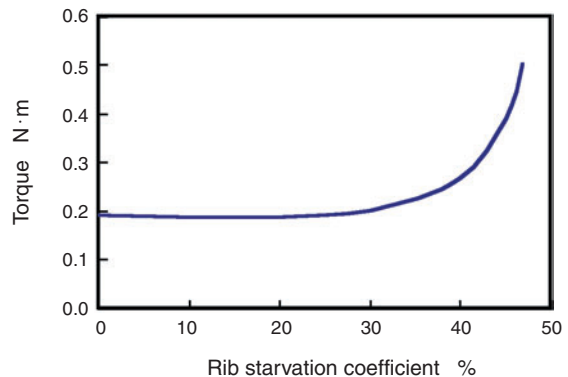


Fig. 3 Numerically evaluated viscous torque at inner-ring rib of standard tapered roller bearing 32020

The resultant measurements are graphically plotted in Fig. 4.

In Fig. 4 the difference between the total torque and rib torque equals the sum of 1), 3) and 4) described above. Since the effect of 4) is sufficiently small in the relatively low speed range of less than 4000 min⁻¹ and 1) is predominant over 3) with roller bearings,³⁾ the difference between the total torque and rib torque is essentially equivalent to 1), that is, the EHL rolling viscosity friction on the raceway surface. As can be understood from expression (1), when there is no effect of starvation and heat generation, the rolling viscosity resistance increases in proportion of the 0.65th power of the rotation speed. However, the total torque starts to decrease at around 300 min⁻¹ when the effect of heat generation seems to be minimal. This appears to be due to the significant effect of starvation.

Also, it will be understood that as the amount of oil is reduced, the effect of starvation is more apparent and the rolling viscosity resistance decreases. At the

Table 1 Specifications of torque test bearing and test conditions

Bearing	Description: 32020XUP4 Size: ID 100 x OD 150 x 32 mm total width Contact angle: 17° Rollers: 29 steel rollers Cage: Pressed steel cage, rolling element guide
Test conditions	Bearing load: 1 kN axial load Bearing lubrication: Air-oil Oil supply from both sides of bearing Nozzle dia. $\phi 1.2 \times 1$ (per side) ISO VG32 oil used Jacket cooling: None

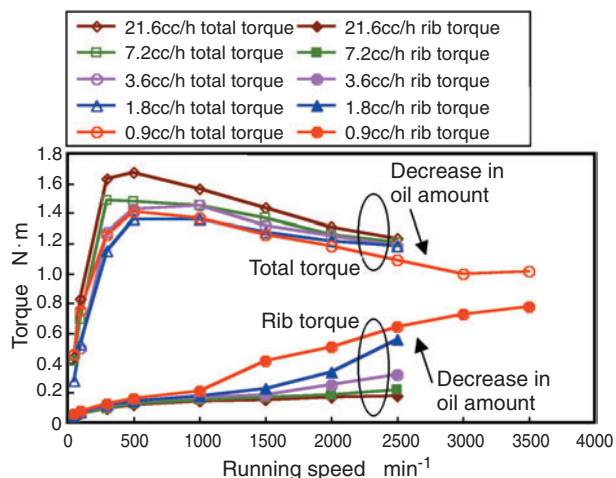


Fig. 4 Measured torque values of standard tapered roller bearing 32020

same time, because the rib is under fluid lubrication conditions, the rib torque is proportional to the bearing speed, and increases with a decreased amount of lubricating oil. This fact further supports the analysis results described above.

In summary, in order for a tapered roller bearing to be able to run at a higher speed, it is necessary to invent a mechanism that minimizes the supply of lubricating oil to the raceway surface while supplying plenty of lubricating oil to the rib.

3. Structure and Performance of the Authors' Bearing

3.1 Basic structure

Based on the approach described above, the authors developed and evaluated various prototype bearings with unique lubrication schemes and internal constructions. Consequently, the authors finally developed the unique tapered roller bearing with the construction illustrated in Fig. 5. Now, referring to Fig. 5, let us describe its features. First, the authors' tapered roller bearing lacks an ordinary inner-ring rib, and instead, the rib is situated on the outer-ring side. This arrangement prevents the lubricating oil from flying away due to the centrifugal force of the rotating inner-ring as well as resultant insufficiency in the amount of lubricating oil. At the same time, to effectively lubricate the rib, multiple direct-injection nozzles are provided on the rib surface that supply air-oil lubricating oil. Incidentally, the usual oil supply from the back side is not provided. Instead, the lubricating oil from the direct-injection nozzles is directed to the raceway surface through the spaces between the rollers. Because the pockets and rollers interfere with each other at higher speeds on roller guiding cages such as the standard type, the authors have adopted

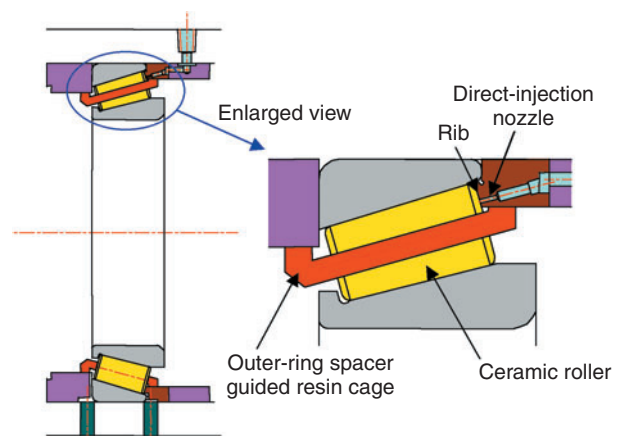


Fig. 5 Section view of developed tapered roller bearing

a guide arrangement on which the outer-ring rib guides the rollers. In addition, the authors have also adopted a lightweight oil-retaining phenol resin as the cage material. The rollers used are made of a lightweight ceramic material of a lower thermal expansion coefficient.

3.2 Test and bearing performance

The construction of the test spindle is illustrated in Fig. 6. The spindle was driven by an external inverter-regulated motor that was connected to the spindle by a coupling. Among the bearings used, only the authors' bearing was arranged in a two-row back-to-back duplex configuration. The boundary dimensions of the authors' bearing were the same as those of the 32020, with a bore diameter of 100 mm. Since the width of the pocket bars is greater with the authors' bearing than the pressed steel cages on standard bearings, the number of rollers on the authors' bearing is 23 which is less than standard bearings, which have 29. The housing incorporated an arrangement for jacket cooling. The preloading system used was a definite position preloading system with zero initial clearance. The major test conditions used are as summarized in Table 2.

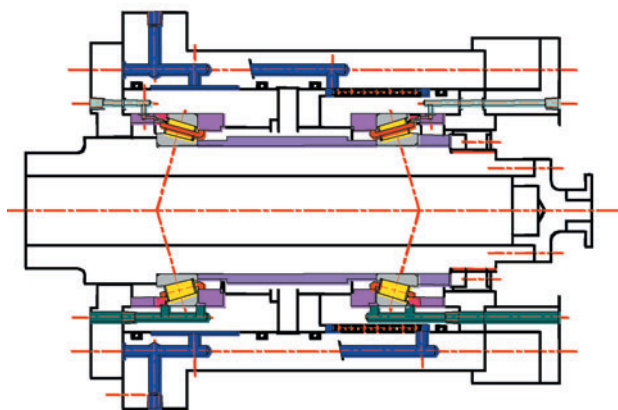


Fig. 6 Schematic construction of test spindle

Table 2 Specifications of spindle test bearing and test conditions

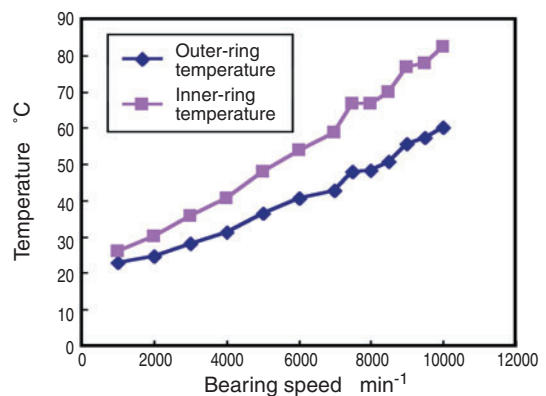
Bearing	Description: Equivalent to 32020XUP4 (modified rib construction) Size: ID 100 x OD 150 x 34 mm total width Contact angle: 17° Rollers: 23 Si3N4 rollers Cage: Phenol resin machined cage, outer-ring guide
Test conditions	Bearing clearance: Definite position preloading with a clearance of zero as assembled Bearing lubrication: Air-oil Oil supply only to the rib surface Nozzle dia. $\phi 0.6 \times 12$ (one bearing row) ISO VG32 oil used 0.01 cc/20 s oil feed rate (one bearing row) Jacket cooling oil temperature: Room temperature $\pm 1^\circ\text{C}$

In testing the authors' bearing, the temperatures and torques on the inner and outer rings relative to various spindle (inner ring) speeds were measured. For this purpose, the spindle running speed was set to each intended speed setting by controlling the inverter-regulated motor, and the temperatures and torques on the inner and outer rings were measured and recorded only when they became stable.

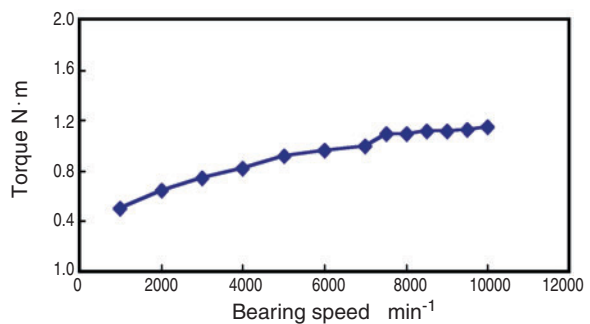
The torque was measured with a torque meter mounted to the spindle. Each torque measurement includes the torques on the two pieces of the authors' bearing and the windage on the rotating sections. The air-oil feed rate to each piece of the authors' bearing was 1.8 cc/h.

The measured temperatures on the inner and outer-rings are plotted in Fig. 7(a), and the obtained torques in Fig. 7(b). Note that the torque values in Fig. 7(b) are those converted for one bearing. As can be understood from these diagrams, the authors' bearing does not exhibit a rapid increase in temperature and torque up to an inner ring speed of 1000 min⁻¹, and can attain 1.25 million d_{mn} with air-oil lubrication.

In addition, the authors checked the running speed of the cage at various bearing speeds using a stroboscope. As a result, no slipping was found,



(a) Measured temperature of inner and outer ring



(b) Measured torque per bearing

Fig. 7 Test results of developed tapered roller bearing

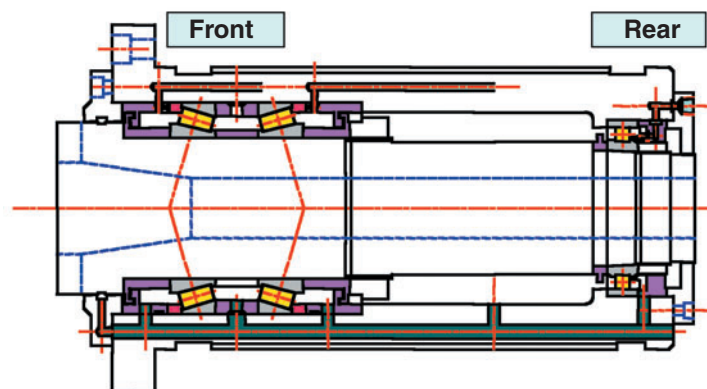
thereby it was confirmed that the rollers were rolling correctly. The authors also inspected the bearing elements that underwent the test and detected no damage such as discoloration and wear. Incidentally, the authors did not attempt to use a low viscosity lubricating oil for the purpose of preventing disruption of the oil film on the raceway surface that could result from a decrease in the amount of oil. Instead, they adopted ISO VG 32, a standard lubricating oil type commonly used for machine tools. However, the authors think that use of a lower-viscosity lubricating oil could further limit the increase in torque and temperature.

The authors also tested the standard 32020 bearing, and learned that even when a maximum bearing speed was attained by varying the viscosity and feed rate of lubricating oil, the bearing temperature dramatically increased at 6000 min^{-1} , and further operation was impossible.

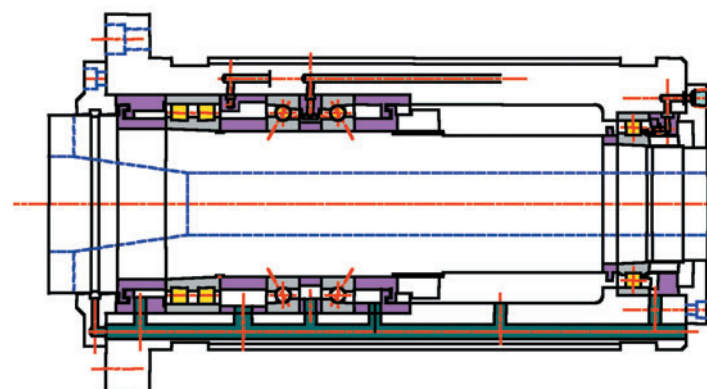
As previously mentioned in the first section of this report, the authors' bearing is expected to satisfy

requirements for not only high-speed performance but also rigidity. Therefore, the authors prepared two bearing arrangements, wherein one bearing arrangement was comprised of the authors' bearing type and the other bearing arrangement consisted of a double row cylindrical roller bearing (which was used as a front-side bearing on a conventional bearing arrangement for machine tool spindles) and an axial-load carrying angular contact ball bearing. Then, assuming that these bearing arrangements were each incorporated into a machine tool spindle, the authors calculated the deflections of the spindles that carried the loads, and compared the calculation results. The arrangement of the authors' bearing is illustrated in **Fig. 8(a)**, and the arrangement consisting of a double row cylindrical roller bearing and an axial-load carrying angular contact ball bearing is shown in **Fig. 8(b)**. The specifications for the authors' bearing are identical to those summarized in **Table 2**.

The double row cylindrical roller bearing used was a standard NN3020, the axial-load carrying angular



(a) Arrangement of developed tapered roller bearing

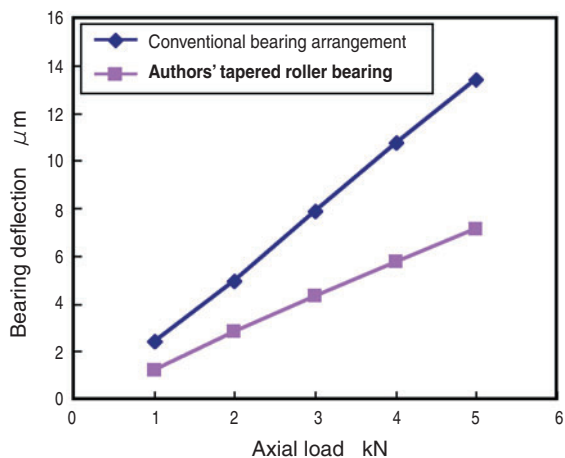


(b) Conventional bearing arrangement

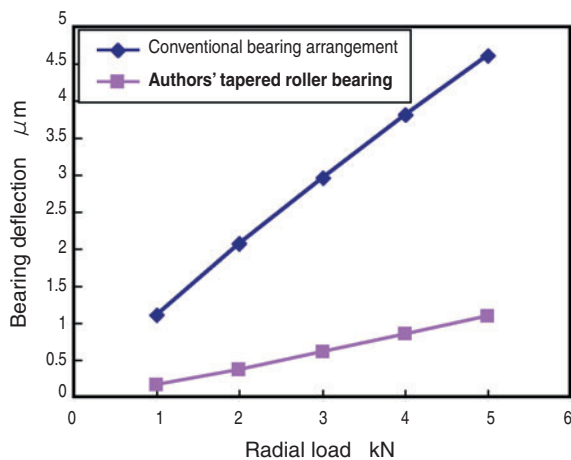
Fig. 8 Bearing arrangements for machine tool main spindle

contact ball bearing used was a standard HTA020ADB, and the bearing used on the rear side was the N1016 single row cylindrical roller bearing.

Deflections occurring on the front end of the spindle when pure axial loads and pure radial loads are applied to the front end are plotted in Figs. 9(a) and (b). For example, when an axial load of 4 kN is applied to the front end, the axial deflection on the authors' bearing is approximately 50% less than with the conventional bearing arrangement. When a radial load of 4kN is applied to the front end, the radial deflection on the authors' bearing is approximately 80% less than the conventional bearing arrangement even though the front side bearing span with the authors' tapered roller bearing is approximately 30% smaller than the conventional bearing arrangement. More specifically, it has been confirmed that the authors' bearing has high rigidity against both axial and radial loads.



(a) Calculated axial deflection



(b) Calculated radial deflection

Fig. 9 Comparison of spindle end deflections between developed bearing and conventional bearing arrangements

As mentioned in the first section of this report, the high-speed rotation performance of the axial-load carrying angular contact ball bearing within the conventional bearing arrangement shown in Fig. 8(b) is insufficient, and this bearing arrangement is capable of only 1 million d_{mN} with air-oil lubrication.

In contrast, in terms of both high-speed performance and rigidity, a spindle supported by the authors' tapered roller bearing excels over spindles supported by a conventional bearing arrangement that consists of a double row cylindrical roller bearing and an axial-load carrying angular contact ball bearing.

4. Conclusion

By using their unique tapered roller bearing that boasts greater rigidity for machine tool main spindles, the authors have invented a novel bearing construction and a novel air-oil lubrication mechanism to address the issue of unsatisfactory high-speed performance, which is a drawback of conventional tapered roller bearings. As a result of testing the authors' tapered roller bearing with an inner bore diameter of 100 mm, this bearing achieved unprecedentedly high d_{mN} of 1.25 million with air-oil lubrication. For bearings that support machine tool main spindles, higher running speed and greater rigidity are challenges to be addressed in achieving better surface finish quality for workpieces and improved machining efficiency. NTN will remain committed to addressing these technical challenges by pursuing further advances in its bearing technology.

References

- 1) T. Miki: Performance and Application of Ultra-High Speed HA-Type Tapered Roller Bearings, Mechanical Design 26, 10 (1982) pp. 109-114. (In Japanese)
- 2) N. Soda: Bearings, Iwanami Shoten (1964). (In Japanese)
- 3) H. Fujiwara, K. Fujii: Rolling bearing torque in oil bath lubrication, Japan Society for Precision Engineering Spring Conference Academic Lecture Proceedings (2002), p. 219. (In Japanese)
- 4) Zhou, R. S. and Hoeprich, M. R.: Torque of Tapered Roller Bearings, ASME J. of Tribology, 113, 3 (1991) 590-597.
- 5) Gadallah, N. and Dalmaz, G.: Hydrodynamic Lubrication of the Rib-Roller End Contact of a Tapered Roller Bearing, ASME J. of Tribology, 106, 2 (1984) 265-274.

Photos of authors



Masatsugu MORI
Elemental Technological
R&D Center



Takuji KOBAYASHI
Elemental Technological
R&D Center

Minimum Quantity and Cooling Jet Lubricated Angular Contact Ball Bearings for Machine Tool

Mineo KOYAMA*



Minimum Quantity and Cooling Jet (MQCJ) angular contact bearings feature a unique jet lubrication system. The design incorporates a special inner ring design, with a cooling groove combined with special geometry for directing lubricant to allow an optimally small amount of lubricant to reach the raceway, in order to minimize power losses from friction torque. It was developed in response to market demands for machine tool spindles with increased speed capability coupled with high rigidity. Its practical use has been demonstrated by having achieved a d_{mN} 3.6 million with fixed-position preloading. This technical review paper is intended as an overview of its development and design.

1. Introduction

Needs have been mounting for faster machine tool main spindles. This trend is even more apparent with the main spindles of machining centers for machining dies because of the desire to realize machine tools that are capable of providing higher quality finished surfaces of workpieces and to improve machining efficiency. To address these needs, attempts to develop higher speed main spindles by using air-oil lubrication and oil-mist lubrication have been undertaken. In 2004, NTN developed a novel jet lubrication mechanism that shoots lubricating oil to a scoop formed on the inner ring end face, realizing both high-speed operation at 5 million d_{mN} with a constant pressure preloading system for angular contact ball bearings and low power loss that is comparable to the power loss with air-oil lubrication. To satisfy market needs for higher bearing speed, we have recently developed angular contact ball bearings based on a fixed-position preloading system, and the newly developed bearings have realized high speed operation of 3.6 million d_{mN} while ensuring preloading at the initial stage of bearing operation. This report describes the features of these bearings, and the results of evaluation testing.

The author has named this novel jet lubrication system MQCJ (Minimum Quantity and Cooling Jet) lubrication.

2. Features of the MQCJ Lubrication Mechanism

2.1 Jet lubrication for the inner ring

The construction of an MQCJ-lubricated angular contact ball bearing is illustrated in Fig. 1. When the main spindle runs at a higher speed, the preload increases because of expansion on the inner ring due to centrifugal force as well as because of temperature differences across the inner ring and outer ring due to heat generation on the bearing. If jacket cooling is provided, the outer-ring side is actively cooled. However, because the inner-ring side is disadvantageous in terms of heat radiation compared to the outer-ring side, the temperature on the inner-ring side is higher than that on the outer-ring side, and the thermal expansion on the inner-ring side becomes greater. As a result, the preload on the bearing increases unavoidably. The author's lubrication mechanism is characterized in that lubricating oil is first shot to the scoop formed on the inner-ring end face to actively cool the inner ring in order to inhibit preload buildup.

2.2 Application of the minimum quantity of lubrication mechanism to the rolling contact surface

Conventional jet lubrication arrangements have the drawback that their power loss is greater due to

*Industrial Engineering Dept. Industrial Sales headquarters

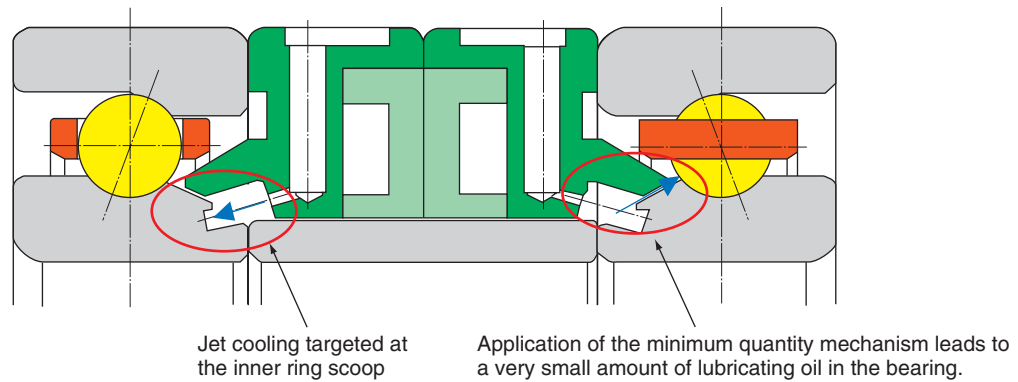


Fig. 1 Bearing and spacer design

greater stirring resistance when a bearing runs at a higher speed because a greater amount of lubricating oil flows inside the bearing. With the author’s lubricating system, the lubricating oil shot at the scoop deposits on the scoop inner surface, then centrifugal force and surface tension caused it to move to the conical surface on the inner-ring outer circumference, thereby only a minimal amount of lubricating oil is fed into the bearing.

Because the amount of lubricating oil entering the bearing is controlled by the gap between the conical surface and the outer ring spacer, most of the lubricating oil contributes to cooling the inner ring while a very limited amount of it flows through the bearing. Thus, the author’s bearing arrangement boasts lower power loss.

2.3 Bearing lubricating oil serves as jacket cooling oil

The author’s lubricating system is schematically illustrated in Fig. 2. In many air-oil lubrication and oil-mist lubrication systems for machine tool main spindles, the bearing is lubricated by a lubricating oil supply system and the jacket is cooled by a cooling oil supply system. In contrast, with the author’s

lubrication mechanism, one common oil supply system feeds oil to both the bearing section and the jacket cooling section, and the used oil is recovered by a scavenge pump. Since the jacket cooling oil also serves as the bearing lubricating oil, the necessary accessory equipment can be of simpler construction.

3. Test Result

The test conditions used are summarized in Table 1, while the construction of the test rig is illustrated in Fig. 3. Because of dimensional limitations, only the front side bearing (lower section) in the test rig incorporated the MQCJ lubrication mechanism (the rear side is provided with air-oil lubrication). The measurements of temperature increase on the outer ring at varied lubricating oil feed rates are graphically plotted in Fig. 4, and the resultant power losses are given in Fig. 5. When the spindle was arranged vertically and the as-mounted preload was set to 0 N (zero axial clearance), the author’s bearing was capable of stable operation at 3.6 million $d_{m\Omega}$ and higher, the outer ring temperature was lower than 50°C and the resultant power loss was not greater than 8 kW.

The outer ring temperature increases measured at initial preloads of 0 N and 150 N are plotted in Fig. 6. Though the temperature increase with the initial preload of 150 N is somewhat significant compared to that with the preload of 0 N, when the $d_{m\Omega}$ exceeded 3.6 million, the outer ring temperature was less than 50°C. Therefore, the author’s bearing arrangement seems to be capable of practical use. The measurements of temperature increases on the outer rings of vertically and horizontally arranged spindles are illustrated in

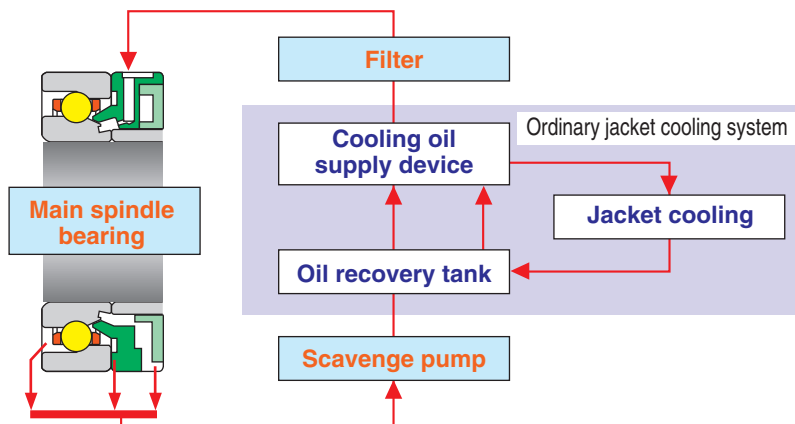


Fig. 2 MQCJ lubrication system

Fig. 7. Regardless of the spindle attitude, the temperature increase profiles are virtually same, so the author's bearing arrangement can be used for practical applications in both vertical and horizontal arrangements.

Table 1 Test condition

Test bearing	ID 70 x OD 110 x 20 mm width
Contact angle	20°
Preload system	Definite position preloading
Initial preload	0, 150 N
Spindle attitude	Vertical, horizontal
Lubricating oil/cooling oil	ISO VG1.5
Rate of oil feed to bearing	0.8, 1.5, 3.0 L/min
Jacket cooling	Only for the motor section
Jacket cooling oil temperature	20°C
Bearing ring material	Special cemented steel
Rolling element material	Ceramic Si ₃ N ₄
Cage material	Phenol resin

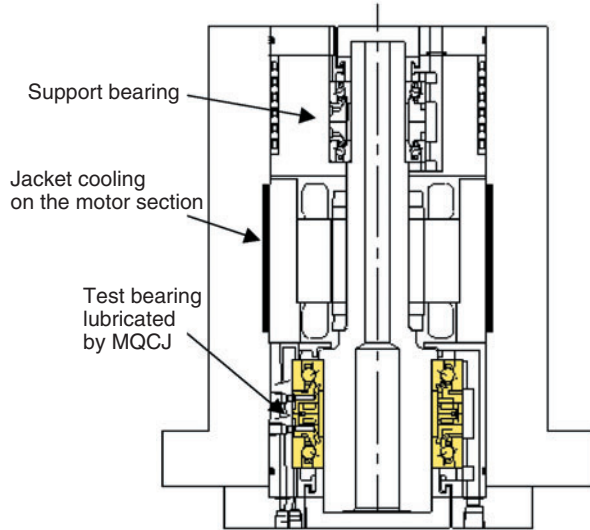


Fig. 3 Schematic construction of test spindle

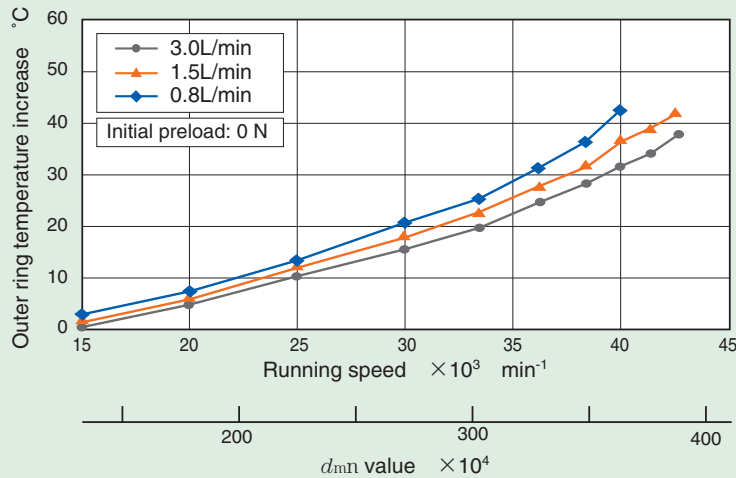


Fig. 4 Affect of amount of lubricant on outer race temperature

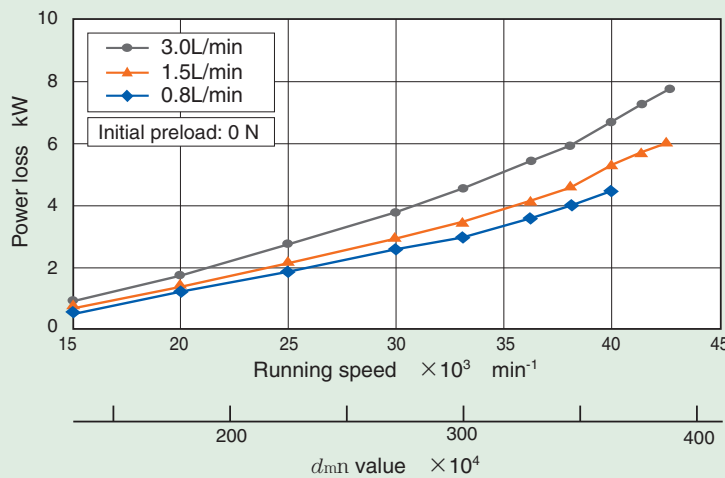


Fig. 5 Affect of amount of lubricant on power loss

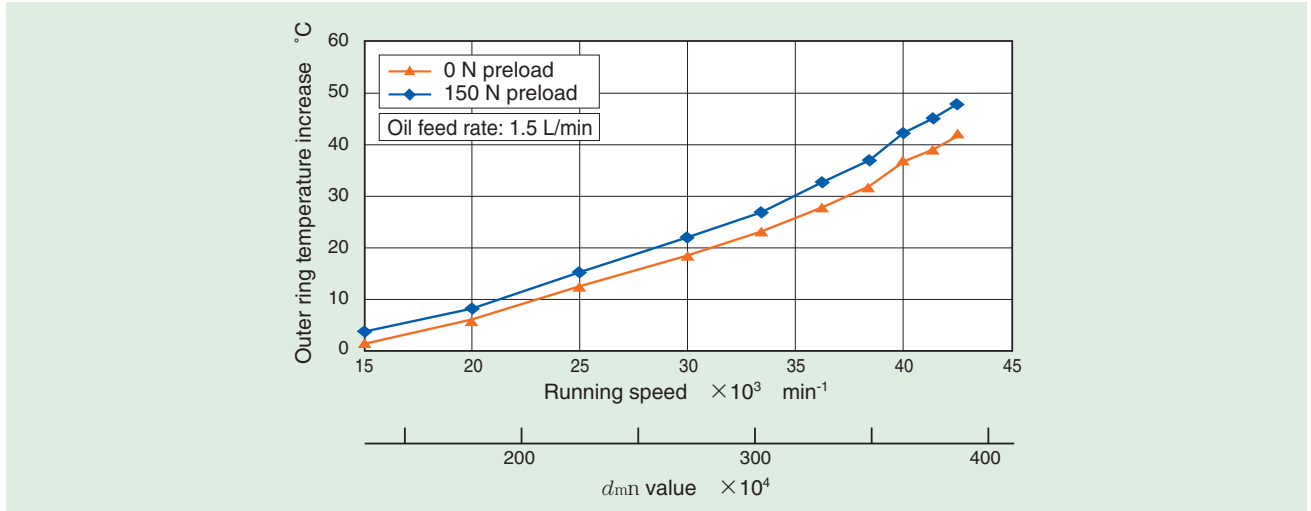


Fig. 6 Initial preload after mounted with DB set on outer race temperature

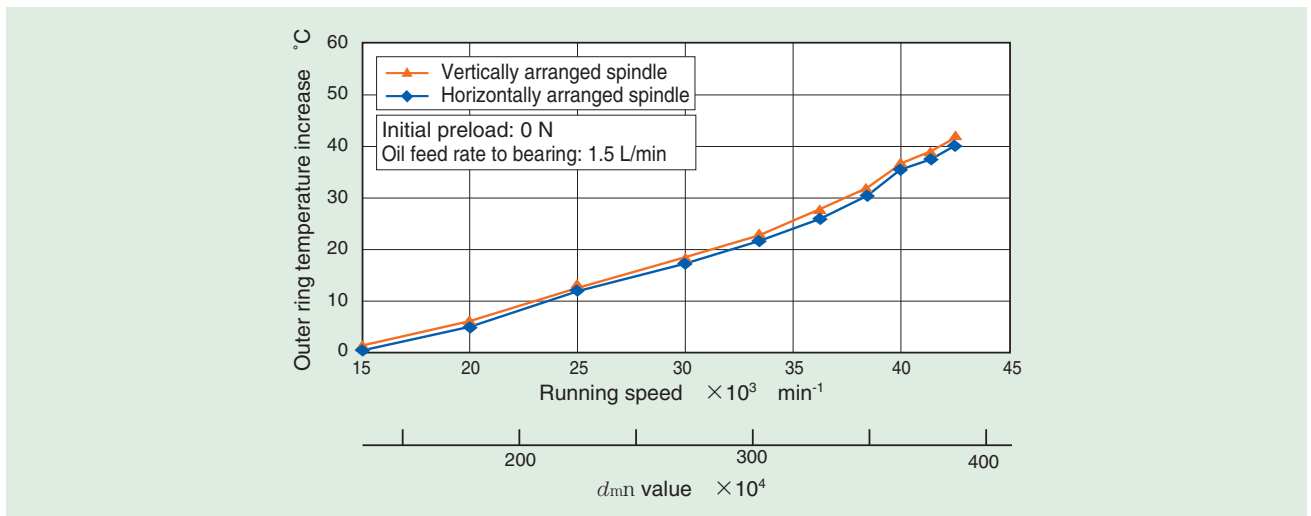


Fig. 7 Main spindle orientation on outer race temperature

4. Conclusion

The author has demonstrated that a combination of an angular contact ball bearing and a definite position preloading system is capable of high-speed operation at 3.6 million d_{mN} by adopting MQCJ lubrication. The author believes that this novel technique will greatly contribute to higher speed, greater rigidity and higher precision with machine tool main spindle bearings.

References

- 1) Y. Akamatsu, M. Mori: Development of Eco-friendly Oil Jet Lubricated Angular Contact Ball Bearings for Machine Tool, NTN Technical Review No. 72 (2004) p. 6.

Photo of author



Mineo KOYAMA

Industrial Engineering Dept.
Industrial Sales headquarters

$d_{mN}170 \times 10^4$ Sealed High-Speed Angular Contact Bearing “New BNS Type”

Futoshi KOSUGI*



The limiting d_{mN} value of the BNS type sealed high-speed angular contact bearing is $d_{mN} 140 \times 10^4$.

A new limiting speed of $d_{mN} 170 \times 10^4$ (the world's highest speed level) was enabled by optimized internal design and a new grease. New grease improves the running-in operation for main spindle bearings. It corresponds to the small machining center and tapping machine by making it to the series up to the small diameter size of $\phi 20$ mm bore.

1. Introduction

Four years have already passed since the ULTAGE Series of products were presented at JIMTOF 2002. The main purpose for developing the ULTAGE Series was to provide bearing products that can handle higher speeds and advanced functions in machine tool main spindles. The need for higher main spindle speeds has posed new challenges for bearings that support machine tool main spindles. That is, higher main spindle speeds have led to higher bearing speeds, and main spindle bearings must handle the increased heat generation that results from the adoption of built-in spindle motors capable of rapid acceleration and deceleration. Main spindle bearings must also accommodate shorter bearing lengths in order to help increase critical bearing speeds. Greater centrifugal force, higher ambient temperatures, and shorter bearing spans have led to increased internal bearing preloads, making operating conditions for main spindle bearings much more demanding. To address this problem, NTN has developed and marketed the ULTAGE Series of standard angular contact ball bearings (HSE type) that are capable of high-speed operation under high bearing stress conditions.

The ULTAGE Series consists of 12 product types capable of meeting various customer needs for higher speeds and difficult environmental considerations. It includes an eco-friendly bearing product line and a

sealed angular contact ball bearing product line.

This report describes NTN's product development efforts for the “New BNS Type” sealed angular contact ball bearing product, which is capable of the world's highest d_{mN} limiting speed, at 170×10^4 , with a definite position preloading system. Based on the conventional BNS type, this product has been developed through optimization of the internal design, introduction of the new SE-1 grease and employment of a special carburized steel for the inner and outer rings.

2. Development of the "New BNS Type" Sealed Super High-Speed Angular Contact Ball Bearing Featuring the World's Highest d_{mN} of 170×10^4

2.1 Highlights of development

For machine tool main spindle bearings, higher speed and greater stiffness are required to shorten machining time, while inhibition of excessive temperature increases and higher running accuracy are also needed to improve machining accuracy. Furthermore, reduction in the amount of lubricating oil and employment of grease lubrication are necessary to ensure eco-friendliness. Among these requirements, the most outstanding market need is the adoption of a grease lubrication system because of its friendliness to the environment and ease of

*Industrial Engineering Dept. Industrial Sales headquarters

handling. In this context, the ULTAGE Series grease-lubricated, sealed angular contact ball bearing products are highly favored in the market.

However, demand is strong for higher speeds in excess of the 140×10^4 d_{mn} limit of conventional grease-lubricated, sealed angular contact ball bearings. The proposed arrangements for coping with this trend are a starvation lubrication unit that is intended to extend lubrication life, as well as a grease lubrication system for bearing spacers (NTN’s new grease lubrication system).

The most critical performance characteristic associated with employment of grease lubrication is long-term durability, and a bearing life of longer than 20,000 hours is usually required. To achieve long-term durability for grease-lubricated main spindle bearings, it is necessary to inhibit excessive heat increases with the bearings, retain the grease and supply the base oil around the rolling surface. It is also necessary to maintain the durability of the bearings against heat buildup from built-in motors situated near the bearings. In addition, the reduction of main spindle costs is also an important consideration.

To address these challenges and satisfy the need for super high speed, the author has developed the New BNS Type, which is capable of the world’s fastest level of running speed. This new product line retains the bore diameters, single outside diameters and widths of conventional grease-lubricated, sealed angular contact ball bearings. The New BNS Type bearing products allow high-speed main spindles, which previously needed oil lubrication arrangements including air-oil lubrication, to be actively lubricated with grease. This advantage can help decrease costs for main spindles. Compared with the conventional

BNS type bearings, the New BNS Type products feature an improved internal design optimized for higher speed, thereby achieving stable operation at the world’s highest d_{mn} , 170×10^4 , a 20% increase over conventional BNS type products. Furthermore, temperature increases on main spindles are limited to the same level as conventional BNS type bearings.

The author believes that adoption of the new grease leads to simplification of bearing running-in operation and inhibition of adverse effects from heat generated by built-in motors. Thus, the author’s new bearing product line can withstand long periods of operation, in excess of 20,000 hours.

The New BNS Type product series will also include bearings with bore diameters measuring 20 to 100 mm so that the products can be used on small-sized machining centers and tapping centers.

2.2 Optimized design

Beginning with the conventional grease-lubricated BNS type, the author first redesigned the internal structure to achieve a higher bearing speed while maintaining a grease-lubrication arrangement. The author reached a design with an optimal combination of diameter, number of balls, groove curvature, and other factors. This combination helped prevent heat buildup in the bearing, inhibit increases in internal bearing pressure and minimize loss in bearing rigidity (Fig. 1). In addition, the author adopted grease pockets identical to those used on conventional BNS type products so that grease is kept nearest to the rolling elements running at higher speeds in order to optimize the lubricating performance of the grease (Fig. 2).

Furthermore, since hoop stress can pose a problem

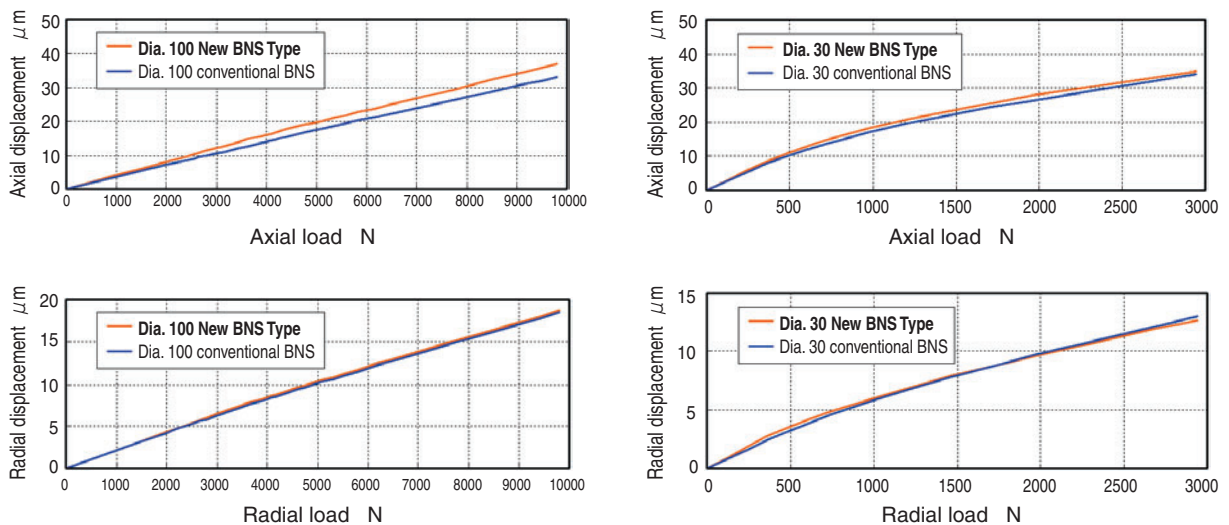


Fig. 1 Rigidity graph

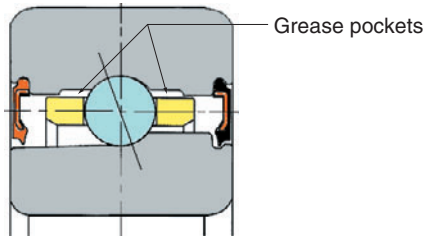


Fig. 2 New design

when a bearing is used at a higher speed range, the bearing ring of the author's bearing is made of a special carburized steel that has an optimized alloy composition.

In bearing performance test, the newly developed bearing was run at a maximum speed of $190 \times 10^4 d_{mN}$ ($150 \times 10^4 dn$), exceeding the target of the development effort of $170 \times 10^4 d_{mN}$ ($135 \times 10^4 dn$). Thus, the author proved that the newly developed bearing design features limited temperature increase in comparison with the conventional BNS type (Fig. 3).

Note that, at same d_{mN} values, the temperature

increase in the 100 mm bore diameter bearings differ from those of the 30 mm bore diameter bearings. This is because of the difference in the construction of the test rigs (Fig. 4).

2.3 Grease life (lubrication life)

One important consideration in determining the lubrication specifications for a main spindle bearing is grease life (lubrication life). The useful life of any grease greatly varies depending on its operating environment. The typical factors that greatly affect grease life include the operating temperature, bearing load (preload) and ingress of foreign matter (chips, etc.).

Unlike the main spindles used on the test rigs, main spindles used on real machine tools feature better sealing performance in order to avoid ingress of coolant during machining operation. This means that heat buildup tends to occur inside machine tool main spindles.

In addition, main spindles that are more compact mean smaller bearing-to-bearing distances, which hinders heat dissipation. Poor heat dissipation causes

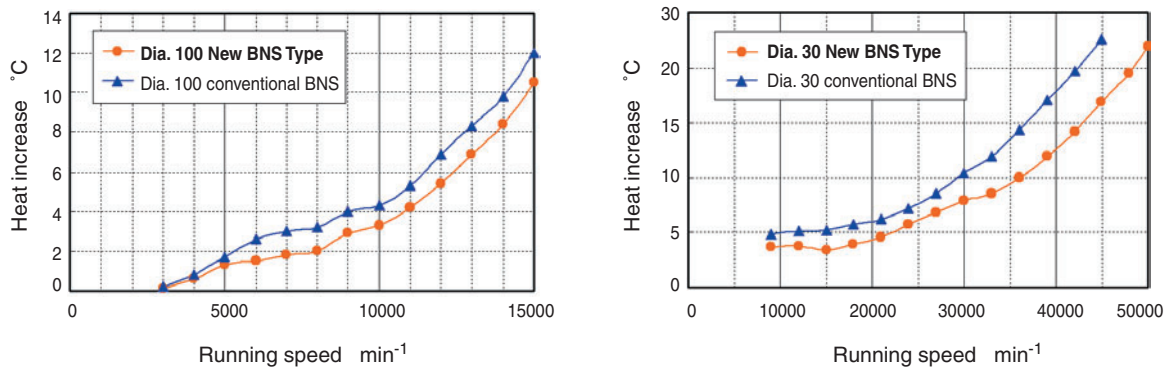


Fig. 3 Temperature rise test results

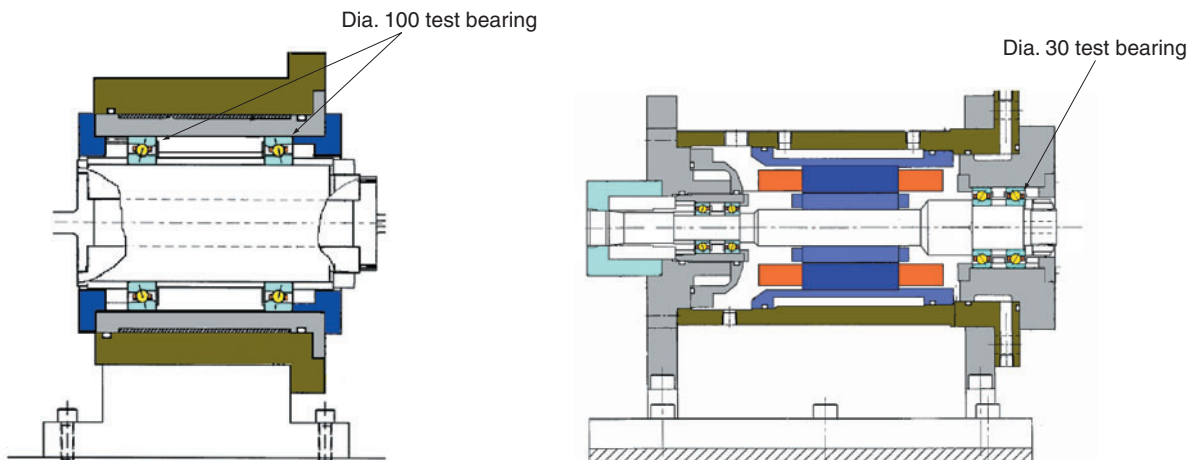


Fig. 4 Test machine

accelerated heat buildup in main spindles. Furthermore, when a machining load works on a main spindle, heat buildup is further promoted, leading to shorter grease life. This trend is more apparent with machine tool main spindle bearings that lack the provision of jacket cooling.

Provision of a cooling arrangement on a main spindle such as jacket cooling greatly affects the temperature profile of a given machine tool main spindle, and significantly influences the useful life of the grease used on the bearings on that main spindle.

The newly developed bearing employs a novel grease. In developing this grease, a test rig arrangement was developed that incorporated a main spindle configuration without jacket cooling to simulate operation on real machine tool. Thus, the author attempted to obtain more reliable grease endurance data.

Note that the main role of the seals on a sealed bearing is to retain grease, and due to the limitations of their function, these seals are not intended to prevent coolant ingress.

Ingress of foreign matter (chips, etc.) into main spindles on actual machine tools rarely occurs. However, coolant entering a bearing on a main spindle bearing can cause the consistency of grease in it to vary, possibly allowing the grease to flow out or to become hardened. If this situation occurs, the grease will fail to develop its designed performance and the bearing will no longer run smoothly. Therefore, this situation must be actively avoided.

2.4 Development of the new SE-1 grease

The conventional BNS type is lubricated with

prefilled MP-1 (urea-based thickener and synthetic oil) as a standard grease. This grease had been performing well in high-speed electric motors and in the CRC grease high-temperature life test conducted according to ASTM D 3336, exhibiting longer life. For this reason, this grease was applied to the BNS type. In addition, it has been performing very well as a grease for machine tool main spindles.

Immediately after adoption by the author, the MP-1 was subjected to a durability test with an angular contact ball bearing. It exhibited a high degree of lubrication performance as it withstood 20,000 hours of operation at $140 \times 10^4 d_{mn}$ (bore diameter $100 \times 11000 \text{ min}^{-1}$, with jacket cooling) (Fig. 5).

The downside, however, is that the viscosity of the base oil in MP-1 is relatively high ($40.6 \text{ mm}^2/\text{s}$ at 40°C) compared with general-purpose greases for main spindle bearings that are commonly used by machine tool manufacturers (Fig. 6). When jacket cooling is not provided, the outer ring temperature sometimes (though rarely) exceeds 60°C during the running-in period. In other words, MP-1 needs improvement to achieve easy running-in operation.

As previously mentioned, the durability test was executed at a high-speed condition of $140 \times 10^4 d_{mn}$, and therefore, jacket cooling was provided. However, there has been demand for main spindles that perform reliably even when no jacket cooling is provided. A portion of the data from durability test is given in Fig. 7.

SE-1 grease has been developed to address two challenges: easy running-in operation and durability without jacket cooling.

Employing diurea as a thickener of excellent shear

Bearing type	Attitude	10000h		20000h	
		BNS	Vertical	Discontinued	
Horizontal	Discontinued				

Test conditions

BNS type
5S-2LA-BNS020LLB

- Grease: MP-1
- Running speed: $1,1000 \text{ min}^{-1}$
- Preload: 0 N as mounted (definite position preloading)
- Jacket cooling: Yes

Fig. 5 Durability test results of BNS type

Grease brand	General purpose grease for main spindle bearing	MP-1	SE-1
Thickener	Barium complex soap	Urea-based	Urea-based
Base oil	Ester oil	Synthetic oil	Ester oil
Base oil viscosity ($40^\circ\text{C mm}^2/\text{S}$)	20	40.6	22
Operating temperature ($^\circ\text{C}$) range (for reference)	$-60 \sim +130$	$-40 \sim +150$	$-50 \sim +120$

Fig. 6 Grease properties

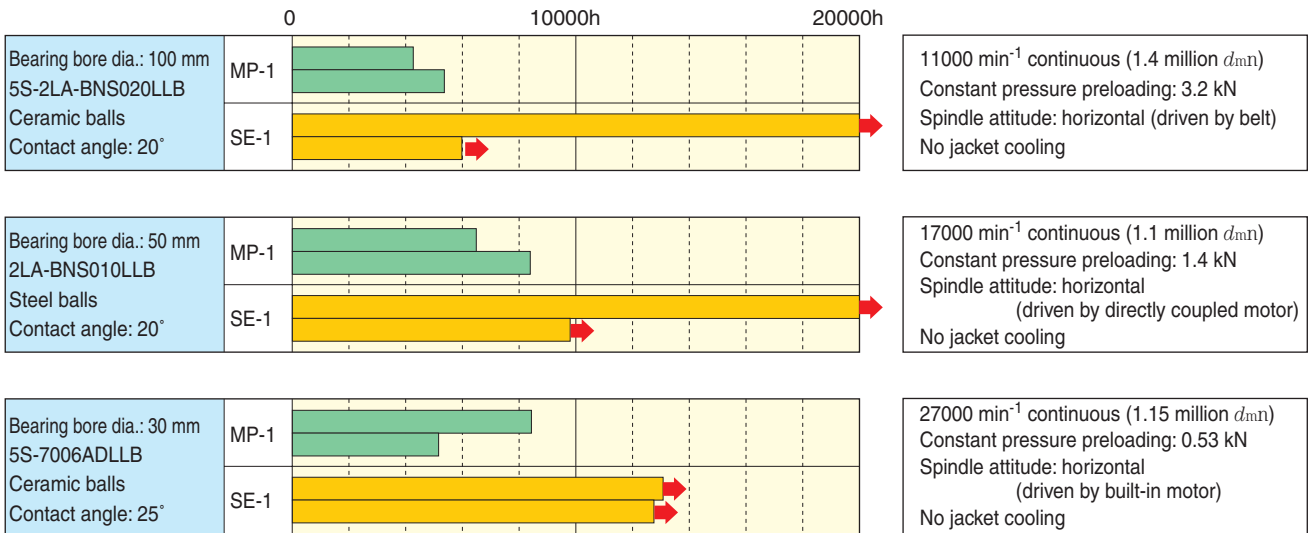


Fig. 7 Durability test results (no jacket cooling)

<Test conditions>
 5S-2LA-BNS010LLBDB
 0-20000 min⁻¹
 Preload as mounted: 98 N
 Jacket cooling: No

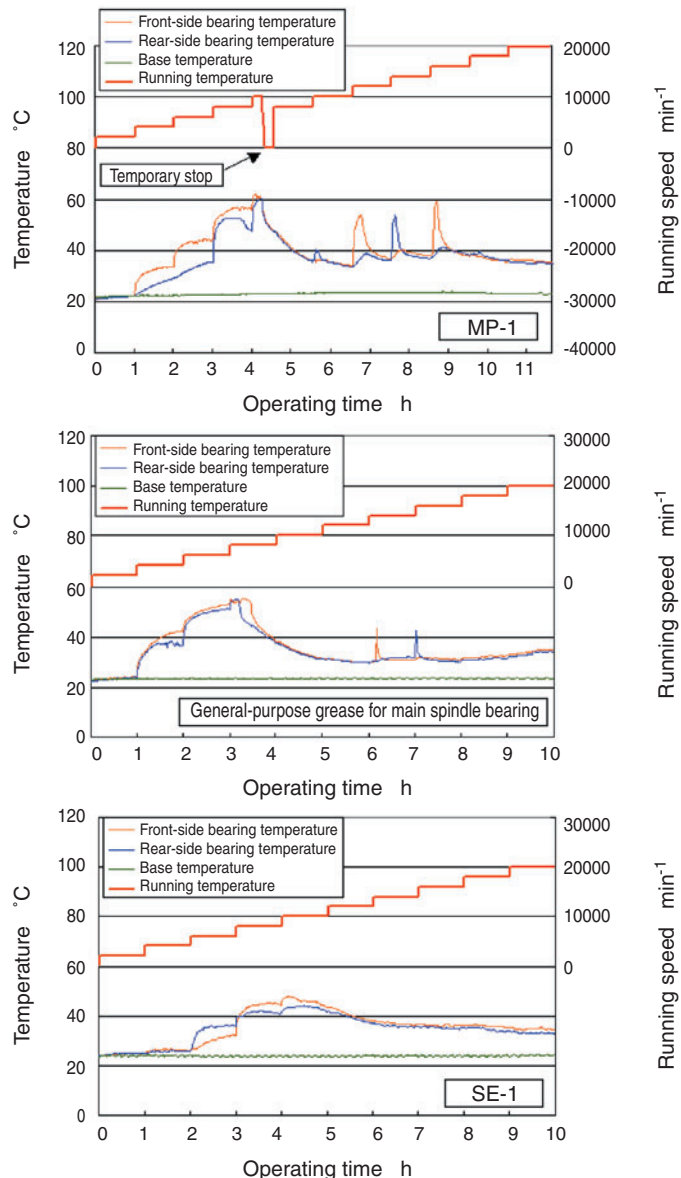


Fig. 8 Running in operation

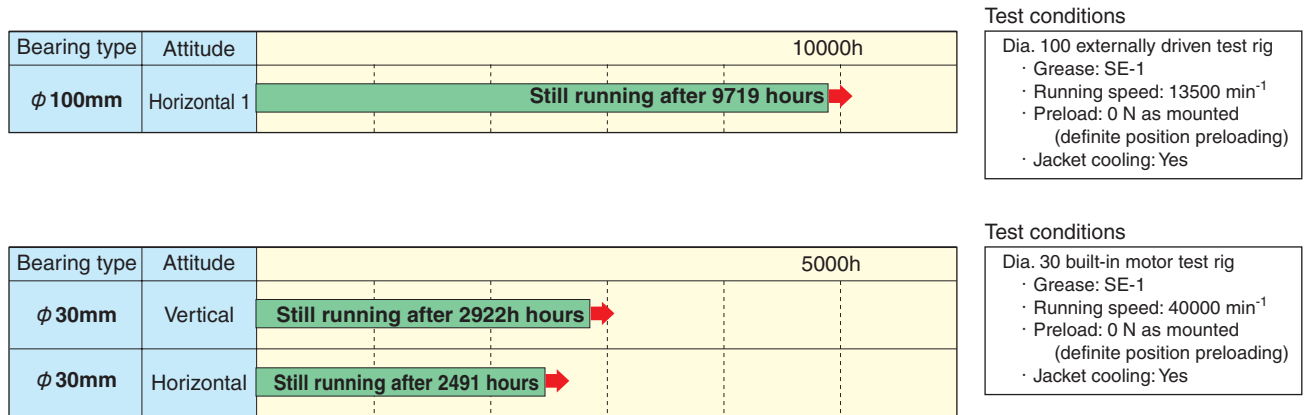


Fig. 9 Durability test results

stability, SE-1 is capable of lubrication in a wide speed range, from very low speeds to higher speeds. The base oil used in SE-1 is an ester oil that excels in heat resistance and oxidation stability, helping extend grease life.

The viscosity of the base oil is 22 mm²/s (40°C), which contributes to achieving easy running-in operation (Fig. 8).

Currently, the author is performing high-speed durability testing with the newly developed bearing type that is configured in a back-to-back duplex arrangement (DB arrangement), with each of the paired bearings being prefilled with SE-1 (Fig. 9). The running speed is 13,500 min⁻¹ for the 100 mm bore diameter bearing and 40,000 min⁻¹ for the 30 mm bore diameter bearing. The main spindle speed corresponding with $170 \times 10^4 d_{mn}$ falls in a sufficiently

high-speed range and requires the provision of jacket cooling. Therefore, the author’s durability test rigs incorporate jacket cooling. During testing, the bearing temperatures have been stable.

3. Conclusion

The process for developing the New BNS Type bearing has been described above. The most important considerations in developing a high-speed lubrication arrangement are how to inhibit heat increase in the bearing and how to feed lubricant to the rolling surface.

The author is now conducting a durability test at $170 \times 10^4 d_{mn}$, and will remain committed to the development of a grease that is capable of much greater bearing speed.

Photo of author

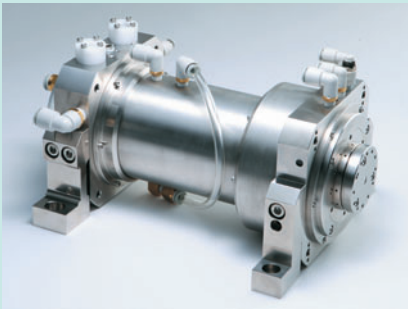


Futoshi KOSUGI

Industrial Engineering Dept.
Industrial Sales headquarters

Development of Aerostatic Bearing Spindle for Precision Machine Tools

Teruyoshi HORIUCHI*
Kazuyuki AONO*
Hiroaki HIYOSHI*



The main reasons for aerostatic bearing spindles in precision machining are the increase in stiffness and reduction of thermal displacement of the work. To meet such demands, NTN has developed a new aerostatic bearing spindle for precision machining by reviewing the bearing design, cooling mechanism, and material selection. The results of the performance evaluation test of the prototype air bearing spindle are described here.

1. Introduction

As the demand for personal digital equipment, including mobile phones and DVD recorders, has increased, there has been a growing need to improve productivity the machining precision dies for aspheric lenses and other precision components. Ultra-precision machine tools for machining very small precision dies for these components often employ precision aerostatic spindles that incorporate hydrostatic air bearings. To improve the productivity of these machine tools, their aerostatic bearing spindles must be capable of both higher running speed and greater precision.

NTN has long been providing high-precision aerostatic bearings that are used on original recording devices for optical disks, as well as on magnetic disk inspection devices. By further advancing our aerostatic bearing spindle technology, we have successfully developed a high-speed, high-precision aerostatic bearing product for precision machine tools.

2. Challenges for Aerostatic Bearing Spindles for Machine Tools

Generally, an aerostatic bearing spindle is comprised of two journal bearings that support the rotary shaft in the radial direction, a pair of thrust bearings that support the rotary shaft in the axial

direction, a driving AC servomotor, and a rotary encoder for detecting the running speed of the spindle, as illustrated in **Fig. 1**. The rotary shaft is supported by the bearings without contacting them by using the pressure of an air layer that is several micrometers thick. The motor and the rotary encoder are also non-contact types. Since the rotary shaft is supported without contacting fixed members, the frictional resistance on the rotary shaft is limited, allowing the rotary motion of the rotary shaft to be controlled very accurately.

In addition to the fundamental structure described above, as with any other aerostatic bearing spindle for precision machine tools, the spindle needs to incorporate a bearing arrangement for high spindle rigidity, a high-torque motor that provides the torque necessary for the intended machining operation, and a vacuum chuck mechanism to hold workpieces in position with vacuum force. Also, measures against thermal deformation resulting from heat generation on the motor and bearings will be necessary in the form of a cooling mechanism. Furthermore, since the environments where the aerostatic bearing spindles for precision machine tools are situated differ from the environments in which aerostatic bearing spindles for inspecting devices are used, a sealing mechanism must be provided for the former in order to prevent ingress of chips and coolant mist.

*Product Engineering Department Precision Equipment Division

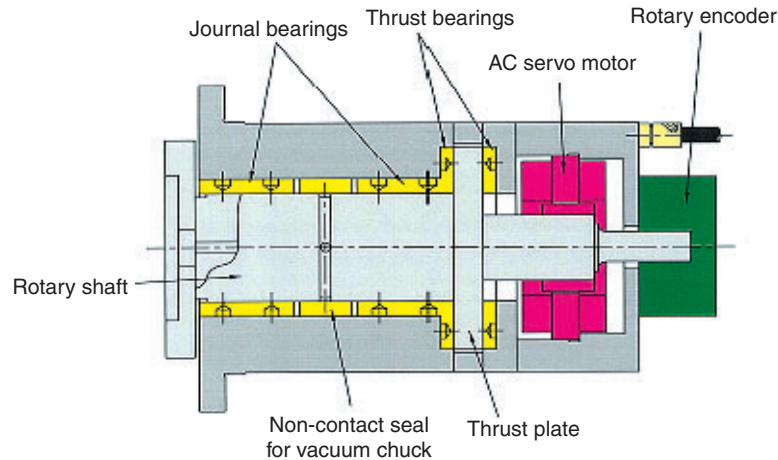


Fig. 1 Structure of air spindle

3. Specifications of Prototype Spindle

The specifications (target values) for NTN's prototype aerostatic bearing spindle for machine tools are summarized in **Table 1**.

Previously, the maximum running speed with this type of spindle was approximately 10,000 r/min. In contrast, the maximum targeted running speed with NTN's spindle is 20,000 r/min. To ensure good machining accuracy, it has been determined that it should have an NRRO (non-repetitive run-out) comparable to that of an aerostatic spindle for inspection devices and the axial displacement of the chuck face during steady running of the spindle should be limited to 1 μm or smaller.

Table 1 Specifications

Max. running speed		20,000 r/min
Air feed pressure to bearing		0.49 MPa
Radial rigidity		45 N/ μm
Axial rigidity		227 N/ μm
NRRO	Radial	0.010 μm or less
	Axial	0.010 μm or less
Displacement on chuck face		1 μm or less during steady running

4. Structure of the Aerostatic Spindle for Machine Tools

1) Realization of greater rigidity and higher accuracy

The structure of the authors' aerostatic bearing spindle is illustrated in **Fig. 2**. A total of four journal bearings are placed in the front and rear sides of the thrust bearings to enhance the rigidity of the aerostatic bearing spindle. Furthermore, seeking higher accuracy, the layout for the air feed holes on the

journal bearings have been optimized in order to inhibit high order vibration that would otherwise occur due to the interaction between the form errors on the rotary shaft and the layout of the air feed holes, as well as to improve the dynamic rigidity of the bearings.

2) Realization of higher torque

To attain both a higher torque on the driving section and a smaller spindle outside diameter, two motors are coupled in tandem, thereby the authors' aerostatic bearing spindle features a torque twice as high compared to ordinary aerostatic bearing spindle designs.

3) Control of chips and coolant

For the vacuum chuck mechanism that secures workpieces, to prevent the coolant entering the chuck from reaching the bearing section, the suction holes are situated further apart from the bearings compared to conventional aerostatic bearing spindle arrangements. To avoid ingress of chips and coolant into the bearings, a non-contact air-seal has been incorporated and a narrow gap is provided between the rotary shaft and the fixed section (housing), thereby compressed air is allowed to gush out through this gap to prevent chips and coolant from reaching the bearings.

4) Control of heat buildup

Aerostatic bearings are known to generate less heat. However, when any aerostatic bearing is run at a higher speed, the heat buildup resulting from the shearing of gaseous matter in the bearing clearance cannot be ignored. In addition, the magnitude of heat generated from the motor arrangement of NTN's prototype spindle was expected to be greater than that of similar conventional arrangements. To solve this

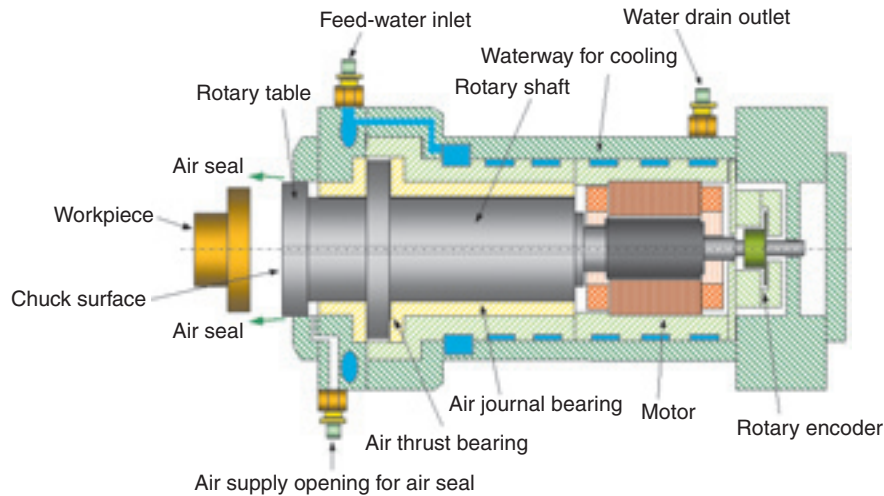


Fig. 2 Structure of the air spindle which we developed

problem, the housing on the motor and bearing sections is water-cooled and the associated components are composed of materials with low thermal-expansion in order to inhibit their thermal deformation and the displacement of the chuck face. Furthermore, air feed holes are provided in the bore sides of the motor stators for feeding compressed air to cool the motors.

For evaluation of the control measure against thermal deformation, the aerostatic bearing spindle was started from a standstill in a room temperature environment and allowed to run constantly at 20,000 r/min, and displacement in the position of the workpiece was measured. This measurement result is graphically plotted in Fig. 4. Immediately after the start of operation, the shaft developed an elongation of

5. Spindle Evaluation Test

A dummy workpiece simulating an actual workpiece was mounted to the prototype spindle, and then the spindle was subjected to an accuracy evaluation test. Run-outs were measured at the locations shown in Fig. 3 with a capacitance type non-contact displacement gage. Jitter (variation in rotation frequency) was determined by measuring variation in the frequency of Z-phase signal (1 pulse/revolution) of the rotary encoder with a pulse jitter counter. The measurement result for non-repetitive run-out (NRRO) is summarized in Table 2 and that for jitter (variation in rotation frequency) is given in Table 3. As can be understood from the data in these tables, NTN's aerostatic bearing spindle performed very well from low speed to the maximum speed.

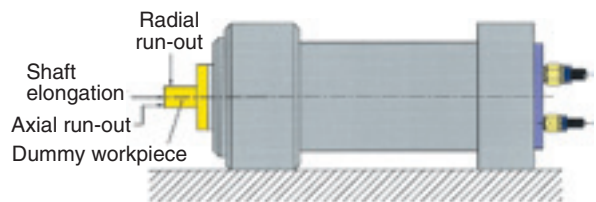


Fig. 3 A measurement position

Table 2 A measurement result of NRRO

Running speed r/min	NRRO, nm Radial	NRRO, nm Axial
1000	3.75	3.75
5000	3.75	3.75
10000	3.75	3.75
15000	3.75	3.75
20000	3.75	6.25

Table 3 A measurement result of jitter (A dummy)

Running speed (r/min)	Jitter (nsec)					Accuracy (%)
500	213.0	180.1	190.9	205.5	195.0	0.00018
1800	82.1	72.7	68.5	84.3	67.6	0.00025
5400	33.5	28.2	27.9	31.8	26.5	0.00031
10000	20.8	21.2	17.4	21.2	18.8	0.00035
15000	14.1	12.2	11.5	13.6	14.3	0.00036
20000	9.3	10.3	10.9	10.8	10.2	0.00036

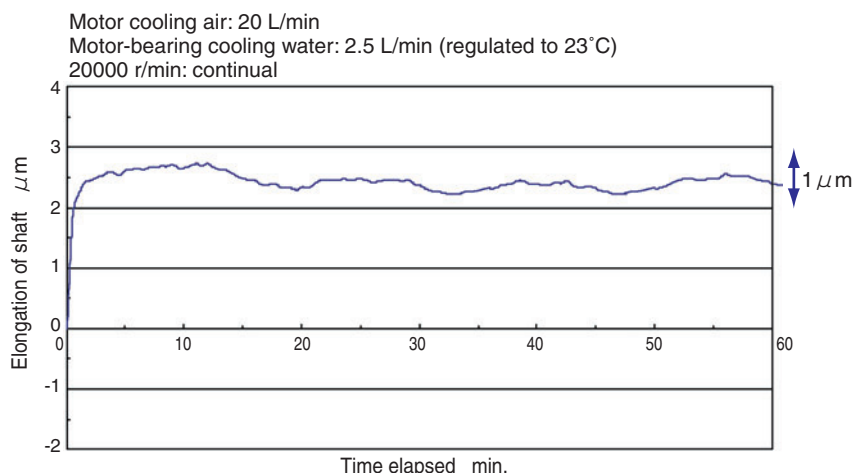


Fig. 4 The measurement of a work position)

approximately $2.5 \mu\text{m}$ (to the left in Fig. 3). After an elapse of 5 to 10 minutes, the displacement of the workpiece was approximately $0.6 \mu\text{m}$.

6. Machining Test

For a test cut, NTN's aerostatic bearing spindle was temporarily installed on a super-high-precision turning center, and the end face of a workpiece was surface-machined, and then the resultant surface roughness was evaluated. The authors proved that their aerostatic bearing spindle can help achieve nanometer-class surface roughness.

Table 4 Precision of cut side

Machining conditions	Mean surface roughness (Ra)	Mean surface roughness on one cross-section (Ra)
1000 r/min – A	3.127 nm	1.675 nm
2000r/min – A	2.672 nm	0.819 nm
20000r/min – B	2.386 nm	2.671 nm

A : Feed rate 2.0 mm/min

B : Feed rate 4.0 mm/min

7. Conclusion

NTN has successfully developed an aerostatic bearing spindle for machine tools that features a higher-torque motor arrangement, coolant mist control and thermal deformation control, and have demonstrated its usefulness through an evaluation test on the spindle proper and a machining test with a machine tool that incorporated NTN's aerostatic bearing spindle.

Aerostatic bearings are capable of super high-precision running at a nanometer order, and NTN has been employing these types of bearings in inspecting devices and semiconductor device manufacturing systems that are used in clean environments. NTN believes that their newly developed aerostatic bearing spindle has helped expand the applicability of aerostatic bearings to the field of machine tools, which is a new field for NTN. NTN will make further efforts to achieve higher precision and higher speed to perfect their newly developed spindle product and satisfy the requirements for further improved machining accuracy and productivity in preparation for commercialization.

Photos of authors



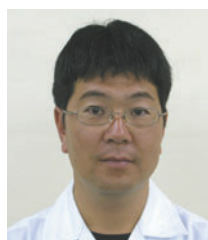
Teruyoshi HORIUCHI

Product Engineering Department
Precision Equipment Division



Kazuyuki AONO

Product Engineering Department
Precision Equipment Division



Hiroaki HIYOSHI

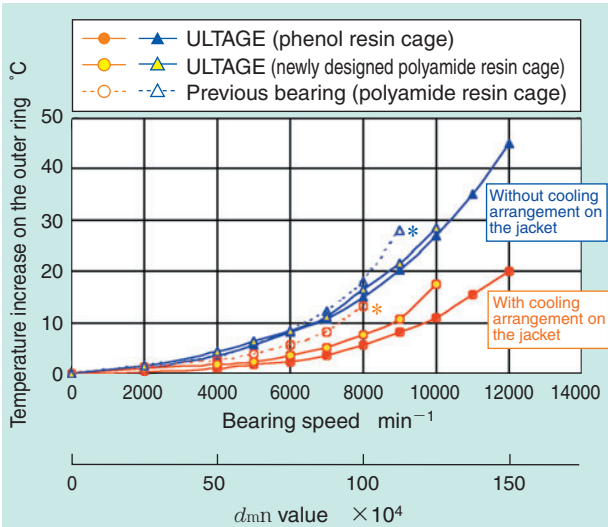
Product Engineering Department
Precision Equipment Division

79U/70U Type Standard Angular Contact Ball Bearings

Standard series features high-speed performance, long bearing life, and high rigidity, which are among the best in the world

Features

- **High-speed**
Maximum d_{mn} value with air-oil lubrication is 1.5 million
Maximum d_{mn} value with grease lubrication is 0.95 million
- **Longer life: 10% increase in bearing life**
- **Maximum allowable axial load: 2~3 times greater**



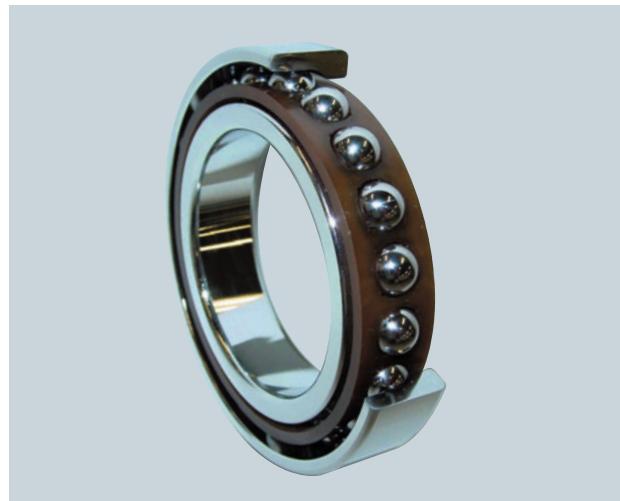
[Test conditions]

Bearing description	[ULTAGE] 7020UCDB [Previous bearing] 7020CDB [φ100mm × φ150mm × 24mm × two rows] [Contact angle 15°]
Preload as mounted	150 N (definite position preloading system)
Lubrication system	Air-oil lubrication
Air supply rate	40 NL/min
Oil supply rate	0.03 mL/5 min/shot
Oil grade	ISO VG32
Cooling arrangement on the jacket	Available

Fig. 1 High-speed test (air-oil lubrication)

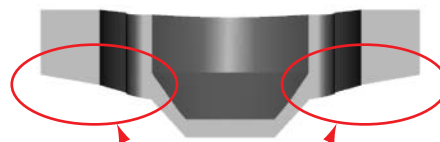
Applications

- Machine tool main spindles, precision machinery, etc.



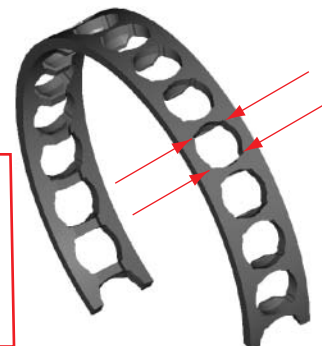
Structure

New design for molded resin cage



<Tapered bore form>
 Air-oil lubrication: Helps to circulate and redistribute lubricating oil
 Grease lubrication: Helps with prefilling of grease

Fig. 2 (a) New resin cage (section of the ball pocket)



<Relieving on four corners of each ball pocket>
 Air-oil lubrication: promotion of discharge of lubricating oil
 Grease lubrication: improved grease retention

Fig. 2 (b) New resin cage (appearance)

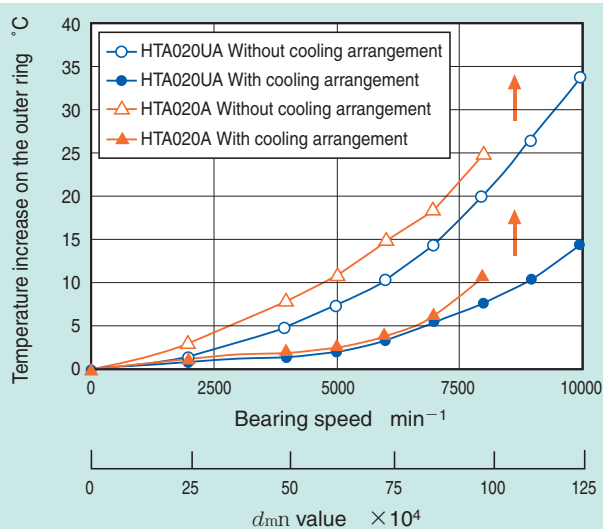
HTA U Type Axial Load Carrying Angular Contact Ball Bearings

Designed to have the highest speed, load capacity, and rigidity among thrust carrying angular contact ball bearings worldwide

Features

- **High-speed**

Maximum d_{mn} value of 1.25 million with air-oil lubrication
(25% improvement over previous NTN design)
Maximum d_{mn} value of 1 million with grease lubrication
(60% improvement over previous NTN design)



【Test conditions】

Bearing [$\alpha:30^\circ$]	HTA020UADB HTA020ADB ($\phi 100 \times \phi 150 \times 22.5$ mm \times two rows)
Bearing speed	$\sim 10000 \text{ min}^{-1}$
Preload as mounted	880N
Lubrication system	Air-oil lubrication
Oil supply rate	0.03 mL/shot 5 min oil shot intervals
Air supply rate	40NL/min
Cooling arrangement on the jacket	Available

Fig. 1 Results of high-speed test (air-oil lubrication) ($\alpha:30^\circ$)

Applications

- Machine tool main spindles, etc.



Structure

- Adoption of internal design that inhibits temperature increases at high-speeds
- Improved design of inner and outer rings for better oil discharge with oil-lubrication systems
- Improved design of contact areas between polyamide resin molded cage and rolling elements for improved lubrication efficiency for both grease and air-oil lubrication

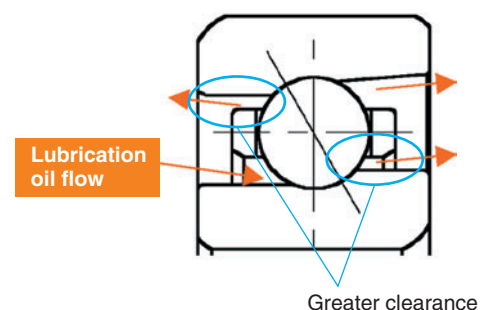


Fig. 2 Flow of lubricating oil

Super High-Speed, Long-Life Double Row Cylindrical Roller Bearing

A precision double row cylindrical roller bearing that boasts the highest speed in the world, while maintaining high load carrying capacity and high rigidity compared to previous design

Features

● High-speed

- Maximum d_{mn} value of 1.75 million with air-oil lubrication (50% improvement over previous NTN design)
- Maximum d_{mn} value of 1 million with grease lubrication (20% improvement over previous NTN design)

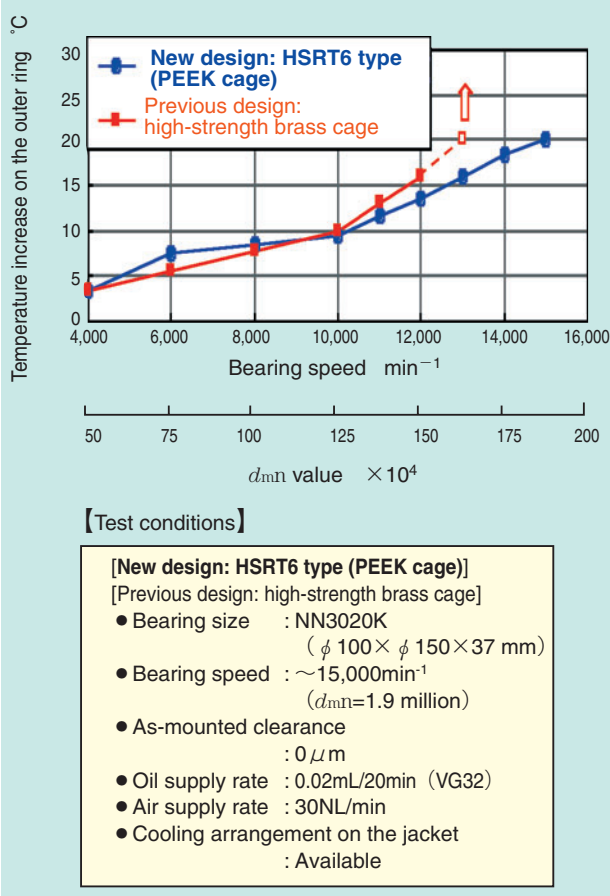


Fig. 1 Temperature rise test results (air-oil lubrication)



Structure

- Optimized internal structure design with much improved cage

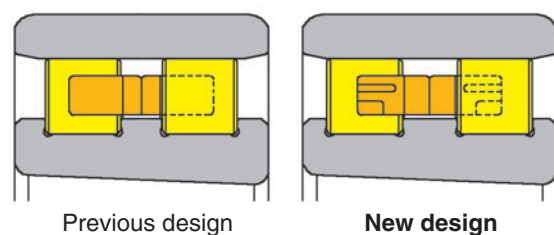


Fig. 2 Conventional design and new design (HSRT6 Type)

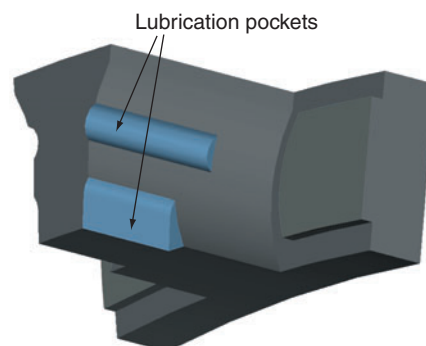


Fig. 3 Drawing of the retainer

Applications

- Machine tool main spindles, etc.

Next-Generation Deep-Groove Ball Bearing for High-Speed Servo Motors

New design of high speed deep-groove ball bearings with prefilled grease



Sealed deep-groove ball bearings
62XX and 63XX series

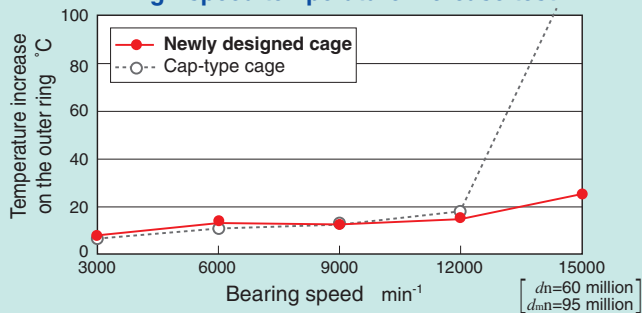
Capable of $d_{mn} 95 \times 10^4$

Newly designed resin cage for high-speed with long-life grease

Structure

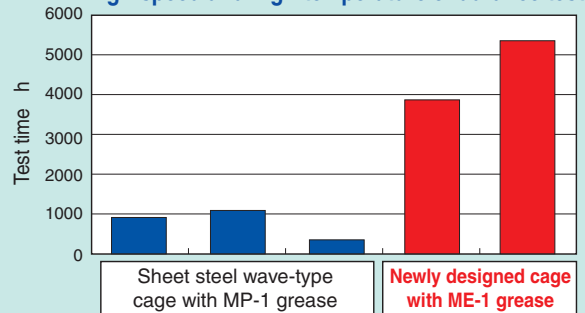
- **Optimized design that ensures reliable lubrication**
Newly designed resin cage for high-speed with long-life grease
- **Maintenance-free**
No grease refilling needed
No cleaning needed
More than three times as durable

High-speed temperature increase test



Bearing description	6308 dual-side non-contact seal ($\phi 40\text{mm} \times \phi 90\text{mm} \times 23\text{mm}$)
Grease	ME-1 grease common to both cage designs

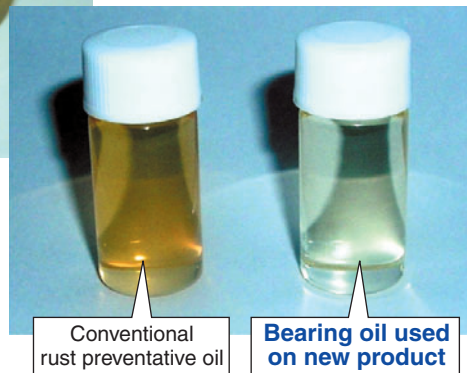
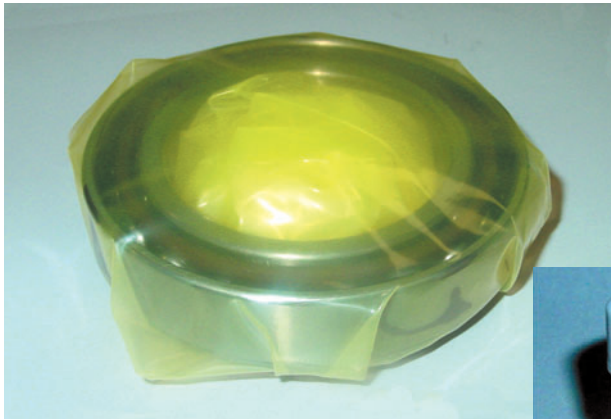
High-speed and high-temperature endurance test



Bearing description	6209 dual-side non-contact seal ($\phi 45\text{mm} \times \phi 85\text{mm} \times 19\text{mm}$)
Bearing speed	Blue: $n = 11,111\text{min}^{-1}$, red: $n = 13,333\text{min}^{-1}$
Bearing temperature	130°C (on outer circumference of the bearing)

“Ecologically Packaged Precision Bearing” that is Easy on People and the Environment

This bearing can be mounted immediately after unpacking with no need to remove the rust preventative oil



Features

"Ecological bearing that is easy on people and the environment"

- No rinsing is needed to remove the rust preventative oil, therefore reducing labor time.
- No need to manage the cleanliness of the washing device and cleaning oil
- No need to manage waste cleaning oil

Structure

- The bearing surface is coated with spindle oil that contains an additive featuring excellent rust preventative characteristics
- The bearings are shipped specially packed in a volatile corrosion inhibitor film
- Guaranteed rustproofing for one year

Bearings that can use this oil

- Precision angular contact ball bearings with 50 to 100 mm bore diameters (oil-lubricated type)

Applications

- Machine tool main spindles, etc.

Super High-Speed AT Spindle

Hydrostatic air bearing spindle that can be mounted to a machining center main spindle



Features

- Attachment type can be mounted to a machining center main spindle (no special machine tool is needed)
- Hydrostatic air bearing helps achieve a super high speed of 150,000 rpm and high-accuracy running
- High-accuracy, high-rigidity chucking is possible with "a chuck that is shrink-fitted to the shaft"
- Low-vibration, quiet, and long-life

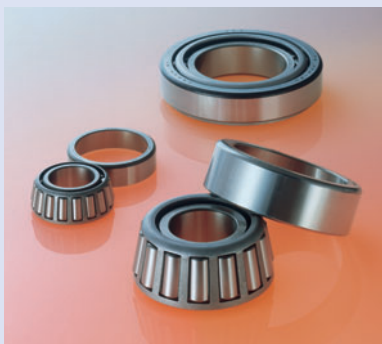
Specifications

Maximum speed	150,000 min ⁻¹	Motor	Rating: 0.6 kW 3-phase induction motor: 200 VAC Water-cooled: 1-2 L/min
Load capacity	Axial : 40 N		Applicable tool diameter
	Radial : 20 N		
Static rigidity	Axial : 1.8 N / μ m	Tool grip system	Heat-shrink method (dia. 6 mm)
	Radial : 1.0 N / μ m	Bearing air supply pressure	0.49 MPa
Spindle mass	5 kg (not including shank)	Bearing air consumption	90 L/min (A.N.R.)

*The data for radial load capacity and rigidity were taken at a point 14 mm away from the spindle end.

Atmospheric Control Method for JIS-SUJ2 Carbonitriding Processes

Chikara OHKI*



NTN has been investigating the mechanism of nitrogen penetration into JIS-SUJ2 bearing steel during carbonitriding processes. In the course of carbonitriding experiments under various conditions and Electron Probe Micro Analysis (EPMA) analysis, the influences of carbon activity and base gas components on nitrogen penetration behavior were examined. As a result, the nitrogen penetration content of steel increased with an increase in undecomposed NH_3 partial pressure and with a decrease in carbon activity, and H_2 partial pressure.

Assuming that the penetration mechanism of nitrogen is similar to that of carbon, a calculation method was developed in order to estimate nitrogen concentration distribution profiles. It was confirmed that the nitrogen concentration distribution profiles predicted by NTN's method agreed well with the experiment results under various conditions. Hence, a development of a new atmosphere control method for JIS-SUJ2 carbonitriding processes was achieved.

1. Introduction

Carbonitriding processes are heat treatment techniques that are often used to improve the fatigue strength of steel materials. There are many applications for using carbonitriding techniques on bearing steels. In particular, it has been verified that carbonitriding bearing steel materials contribute to longer bearing life under contaminated lubrication conditions.¹⁾

The carbon penetration mechanism that takes place during carburizing is understood. In contrast, although there has been active research on the nitrogen penetration mechanism in carbonitriding processes,²⁾ there has been little research on nitrogen penetration in carbonitriding processes for high carbon steels (including bearing steel). To address this, NTN has systematically performed a series of carbonitriding experiments for JIS-SUJ2 bearing steel in an attempt to clarify the nitrogen penetration mechanism.^{3) 4)}

2. Test Methods

2.1 Experimental furnace and furnace atmosphere measuring method

For the series of experiments performed, a batch-type heat treatment furnace (capacity 120 L) was used. During carbonitriding processes, the atmosphere was analyzed by the equipment summarized in [Table 1](#). The furnace itself is schematically illustrated in [Fig. 1](#) and the base gas feeder is shown in [Fig. 2](#).

2.2 Material tested and method for measuring nitrogen concentration

The material used for the test was a JIS-SUJ2 high carbon chromium bearing steel. The chemical components of the material are summarized in [Table 2](#). The test pieces were ring-shaped with dimensions of 30 ID x 38 OD x 10 T (mm).

Nitrogen concentration distributions of the test

*Elemental Technological R&D Center

Table 1 Equipment used for atmospheric measurement

Equipment	Measurement	Measurement technique
IR gas concentration analyzer	CO/CO ₂ concentration	Non-dispersion IR absorption
Mirror-surface cooling dew-point recorder	H ₂ O concentration	Optical dew point
Zirconia sensor	O ₂ concentration	Zirconia oxygen partial pressure analyzer
Thermal conductivity gas analyzer	H ₂ concentration	Thermal conductivity
Thermal conductivity detector	Undecomposed NH ₃ concentration	Gas chromatograph (carrier: helium)

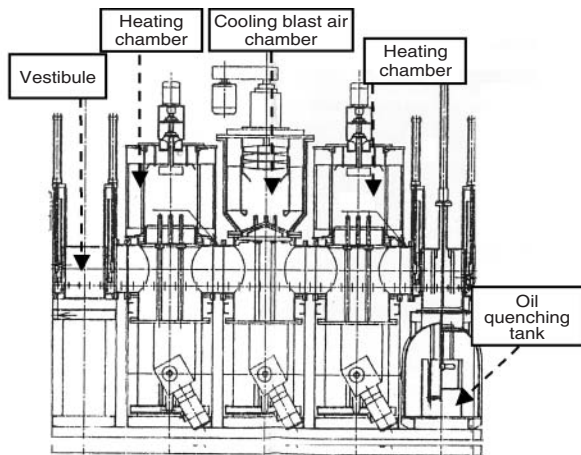


Fig. 1 Heat treatment furnace

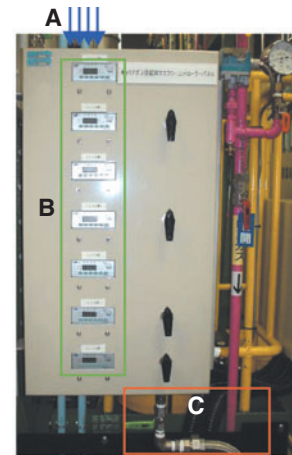


Fig. 2 Base gas feeder

(A: Supply from pure gas tank, B: mass flow controller, C: gas mixer)

pieces were determined by electron beam analysis (2 μm spot diameter, 2 μm intervals between measuring points) with an Electron Probe Micro Analyzer (EPMA). The test pieces were placed in the center of the experimental furnace for carbonitriding prior to this measurement. A sample piece was cut, as illustrated in **Fig. 3**, from each test piece that underwent carbonitriding (after quenching). Then, the nitrogen concentration distribution on each sample piece was measured on the cut surface, beginning at the midpoint at the outer diameter and proceeding toward the bore.

To determine the amount of nitrogen penetration of each test piece, the nitrogen concentration distribution obtained from analysis were integrated in the direction to where the nitrogen concentration approached zero (**Fig. 4**). The total amount of nitrogen penetration was converted into a weight, assuming that the specific gravity of the original material was $7.85 \times 10^{-3} \text{ g/mm}^3$.

2.3 Definition of carbon activity

One very important factor that can influence the atmosphere for carbonitriding is the carbon activity, which determines carbon penetration. The author employed the Boudouard reaction for calculating carbon activity. The equilibrium reaction is defined by expressions (1), (2) and (3) below:

Table 2 Chemical composition of JIS-SUJ2 used (wt%)

C	Si	Mn	P	S	Ni	Cr	Mo	Cu
0.99	0.26	0.44	0.012	0.006	0.08	1.46	0.03	0.15

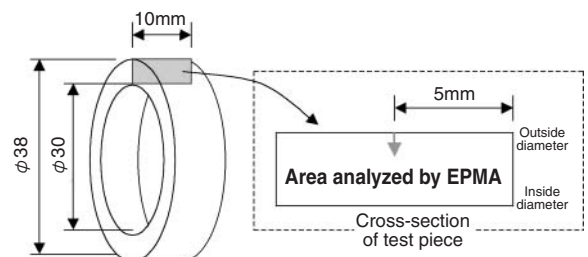
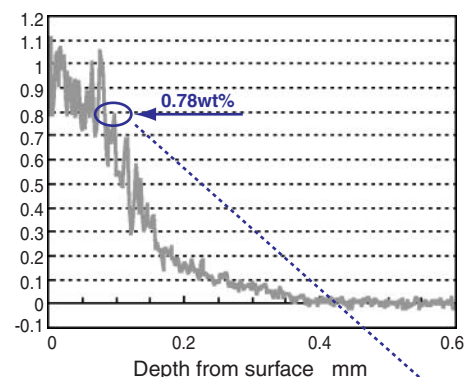


Fig. 3 Test specimen dimensions and scanning position



$$\text{Amount of nitrogen penetration (g/mm}^2\text{)} = \dots + 7.85 \times 10^{-3} \text{ (g/mm}^3\text{)} \times 0.002 \text{ (mm)} \times 0.78 \text{ (wt\%)} \div 100 + \dots$$

Fig. 4 Definition of nitrogen penetration content

$\langle C \rangle + CO_2 \rightleftharpoons 2CO$Boudouard reaction

$$a_c = \frac{P_{CO}^2}{K_1 \cdot P_{CO_2}} \dots\dots\dots (1)$$

$$K_1 = \exp\left(\frac{-\Delta G_T^0}{RT}\right) \dots\dots\dots (2)$$

$$\Delta G_T^0 = 172500 - 175.6 \cdot T \dots\dots\dots (3)$$

where a_c = carbon activity; K_1 = equilibrium constant; R = gas constant (8.31441 J/(mol·K)); T = absolute temperature (°K); ΔG^{**} = standard free energy of formation;⁵⁾ P_{CO} = CO partial pressure and P_{CO_2} = CO₂ partial pressure (atm).

Because of the definition of carbon activity, $a_c > 1$ is not possible. However, as shown by expression (1), a calculated value of a_c can be greater than 1 in certain situations, and a carbonitriding process can take place.⁶⁾ To investigate the effect of such an atmosphere, expression (1) was redefined as (1'), and this expression was used as a parameter for the experiment.

$$a_c^* = \frac{P_{CO}^2}{K_1 \cdot P_{CO_2}} \dots\dots\dots (1')$$

where, when $a_c^* \leq 1$, $a_c^* = a_c$ (carbon activity), and when $a_c^* > 1$, a_c^* is a variant expressed by expression (1').

2.4 Experimental Parameters

2.4.1 Effects of partial pressure of undecomposed NH₃ and carbon activity on carbonitriding processes

Within every set of parameters in these experiments, temperature was maintained at 850°C and furnace pressure was held at 1.03 atm (1 atm = 1.013 x 10⁵ Pa). At the same time, the total surface area of the test pieces was the same. Four types of test parameters were varied: the carbon activity a_c^* , carbonitriding process duration, base gas flow rates and partial pressure of undecomposed NH₃. The a_c^* was held at one of six levels ranging between 0.78 and 1.08 and the carbonitriding process duration varied from 1,800 to 18,000 seconds. The base gas flow rate ranged from 6 to 20 L/min and the undecomposed NH₃ varied from 0.36 to 3.4 x 10⁻³ atm. Incidentally, the base gas feeder shown in Fig. 2 was not used for these experiments. Instead, the base gas used was an ordinary endothermic modified gas derived from propane.

2.4.2 Effects of base gas component partial pressures on carbonitriding processes

For this series of experiments, the heating

temperature was maintained at 850°C, the process duration was set at 9,000 seconds, and the furnace pressure was kept at 1.03 atm. At the same time, the total surface area of the respective test pieces was the same.

The flow rates of each component in the base gas and the partial pressure of undecomposed NH₃ are listed in Table 3. The H₂ flow rate was set to a range from 1.15 to 6.9 L/min, N₂ flow rate from 0 to 9.2 L/min and the CO flow rate from 1.15 to 4.6 L/min. The flow rates of these gases were adjusted so that the total flow rate of the mixture of gases was 11.5 L/min in each set of conditions. This adjustment was achieved with the base gas feeder shown in Fig. 2. Two levels of partial pressure of undecomposed NH₃ were used: 0.0010 atm and 0.0021 atm.

Table 3 Conditions for experiments to investigate the influence of base gas components

Undecomposed NH ₃ volumetric partial pressure	H ₂ flow rate (L/min) ¹⁾	N ₂ flow rate (L/min) ¹⁾	CO flow rate (L/min) ¹⁾	Total (L/min) ¹⁾
0.0010	6.9	3.45	1.15	11.5
0.0010	6.9	2.30	2.3	11.5
0.0021	6.9	2.30	2.3	11.5
0.0010	6.9	0	4.6	11.5
0.0021	6.9	0	4.6	11.5
0.0010	1.15	9.2	1.15	11.5
0.0021	1.15	9.2	1.15	11.5
0.0010	1.15	8.05	2.3	11.5
0.0021	1.15	8.05	2.3	11.5
0.0010	1.15	5.75	4.6	11.5
0.0021	1.15	5.75	4.6	11.5
0.0010	3.45	5.75	2.3	11.5
0.0021	3.45	5.75	2.3	11.5
0.0010	3.45	6.9	1.15	11.5
0.0021	3.45	6.9	1.15	11.5
0.0010	3.45	3.45	4.6	11.5
0.0021	3.45	3.45	4.6	11.5

1) Converted to values under ordinary temperature and atmospheric pressure

3. Results of Experiments

The actual measurements of nitrogen concentration are non-continuous, and their reliability is low due to the effects of deposits and measurement errors. Thus, it would be inappropriate to use the measurements to predict a general trend. Therefore, the results of the experiments were adjusted by the amount of nitrogen penetration, allowing the effects of deposits and measurement errors to be averaged and errors in the data to be minimized.

3.1 Effects of NH₃ on amounts of nitrogen penetration

To clarify the effect of base gas flow rates on the relationship between NH₃ addition flow rates and nitrogen penetration amounts, nitrogen penetration amounts were measured in a series of experiments performed with $a_c^* = 1.03$ and a carbonitriding process time of 9,000 seconds.

Figs. 5 through 7 plot the results of these experiments.

It was learned that there is strong relationship between the partial pressure of undecomposed NH₃ and nitrogen penetration amounts, regardless of the base gas flow rate.

The relationship between carbonitriding process duration, partial pressure of undecomposed NH₃ and nitrogen penetration amounts is graphically illustrated in Fig. 8. The profile shown in Fig. 8 is an approximation of the actual measurement values, and the black dots represent actual measurement values. It was learned that with a partial pressure of undecomposed NH₃ of 0.002 atm or higher, the nitrogen penetration amount is nearly maximized and the maximum amount of nitrogen penetration increases as the process duration is lengthened.

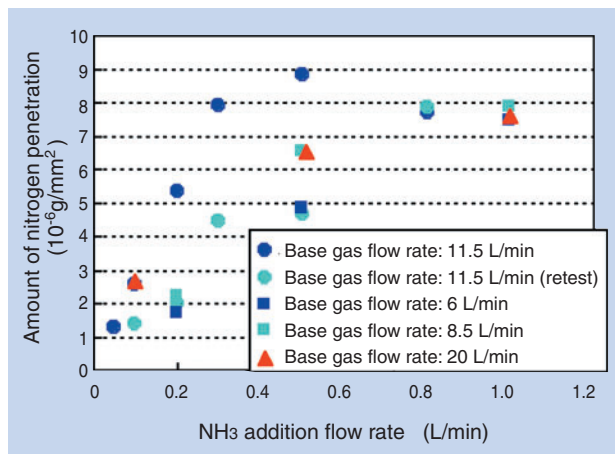


Fig. 5 Relationship between the flow rate of NH₃ and nitrogen penetration content

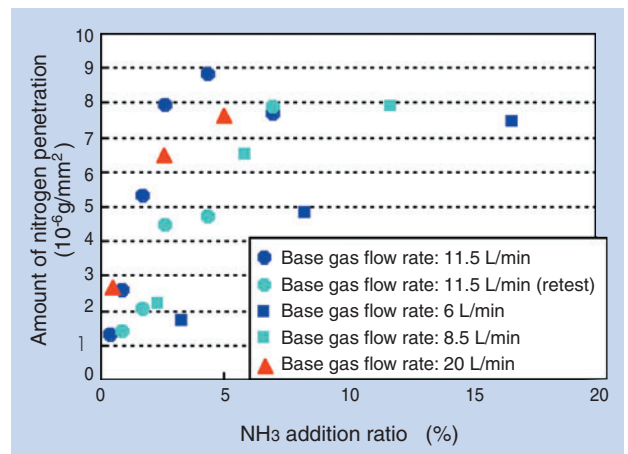


Fig. 6 Relationship between the addition ratio of NH₃ and nitrogen penetration content

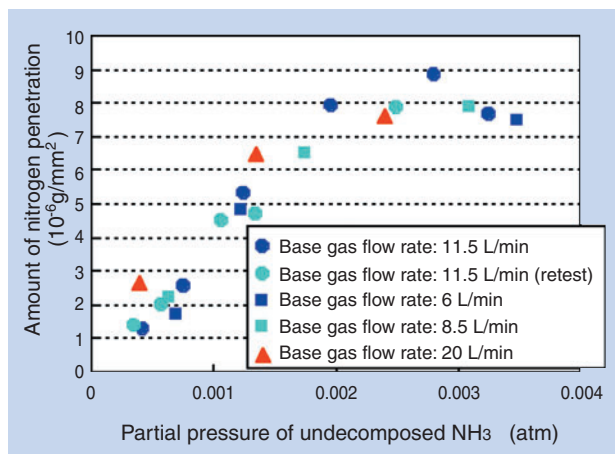


Fig. 7 Relationship between partial pressure of undecomposed NH₃ and nitrogen penetration content

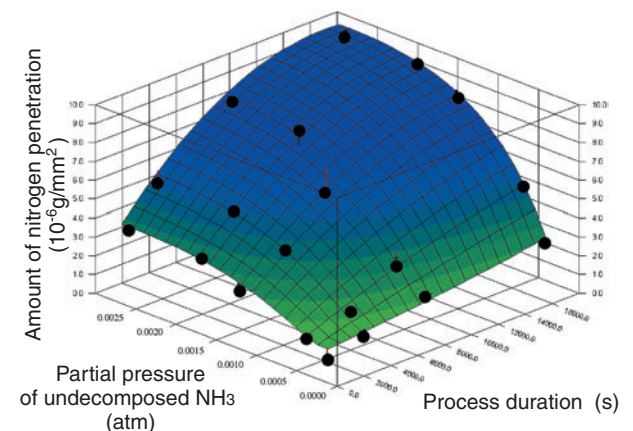


Fig. 8 Relationship among duration times and undecomposed NH₃, and nitrogen penetration content

3.2 Effects of carbon activities on nitrogen penetration amounts

To clarify the effects of carbon activities on nitrogen penetration amounts, a series of experiments was performed with various a_{c^*} values. In these experiments, the process duration was set to 9,000 seconds and the base gas flow rate was maintained at 11.5 L/min. The results are graphically plotted in Fig. 9. It is apparent that at the same partial pressure of undecomposed NH_3 , the smaller a_{c^*} is, the greater the nitrogen penetration amount becomes.

In the scope of this series of experiments, when the partial pressure of undecomposed NH_3 was 0.002 atm or greater, the surface nitrogen concentration exhibited a saturation value at every a_{c^*} value. The relationship between carbon activity and saturation values of the surface nitrogen concentrations is shown in Fig. 10. When a_{c^*} falls in a range between 0.89 and 1.08, the saturation values of surface nitrogen concentration can be linearly approximated with expression (4).

$$[A_{SN}] = -1.0549 \cdot a_{c^*} + 1.8771 \dots \dots \dots (4)$$

where, A_{SN} is the saturation value (wt%) of surface nitrogen concentration.

3.3 Effects of base gas component partial pressures on nitrogen penetration amounts

Multiple regression analysis was performed by taking the nitrogen penetration amounts obtained from experiments summarized in Table 3 as target variables, and using partial pressures of CO , N_2 , undecomposed NH_3 and H_2 as variables. As a result, it was learned that CO and N_2 partial pressures do not significantly affect nitrogen penetration amounts and that nitrogen penetration amounts are governed by both NH_3 partial pressures and H_2 partial pressures (1% significance, degree of freedom dual adjustment contribution ratio of 0.953).

The relationship between H_2 partial pressures, partial pressures of undecomposed NH_3 and nitrogen penetration amounts are illustrated in Fig. 11. The spaces between the plotted results of the experiments are approximated with a curved plane to see a visual overview of the results of the experiments. From Fig. 11, it is apparent that the nitrogen penetration amount tends to increase as the partial pressure of undecomposed NH_3 increases and the H_2 partial pressure decreases.

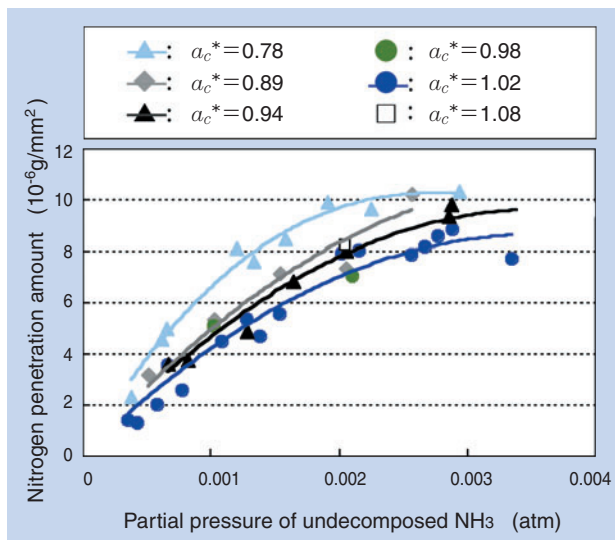


Fig. 9 Relationship among undecomposed NH_3 and nitrogen penetration content, and carbon activity a_{c^*}

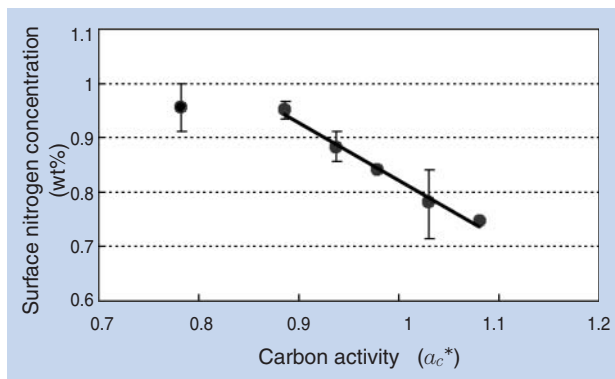


Fig. 10 Relationship between carbon activity a_{c^*} and the surface nitrogen concentration

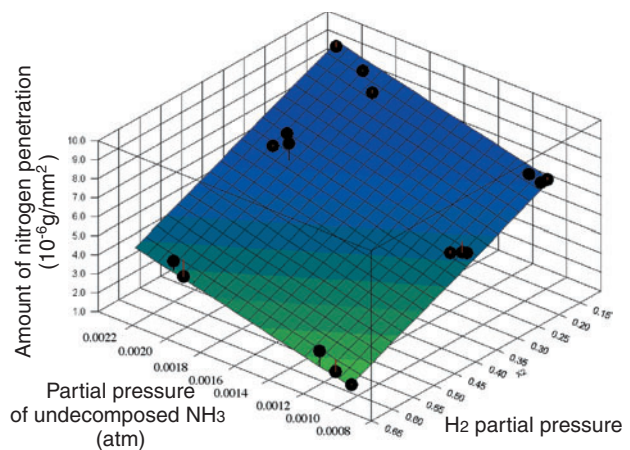


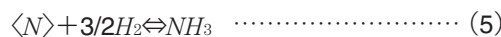
Fig. 11 Relationship between partial pressures of undecomposed NH_3 and H_2 , and nitrogen penetration content

4. Nitrogen Penetration Mechanism, and Prediction of Nitrogen Concentration Distribution

From these findings, it is apparent that regarding nitrogen penetration during carbonitriding of JIS-SUJ2 high-carbon chromium bearing steel, the following three factors are critical: 1) partial pressure of undecomposed NH₃ in the furnace, 2) *a_c** in the atmosphere (carbon activity), and 3) H₂ partial pressure in the furnace. Based on these findings, the nitrogen penetration mechanism and the method for predicting nitrogen concentration are discussed below.

4.1 Hypothesis of the nitrogen penetration mechanism

Let us assume that the nitrogen penetration in carbonitriding of JIS-SUJ2 proceeds according to the equilibrium reaction defined in expression (5). Expression (6) represents the equilibrium constant *K_X* for expression (5).



$$a_N^* = \frac{P_{NH_3}}{K_X \cdot P_{H_2}^{\frac{3}{2}}} \dots\dots\dots (6)$$

where, *a_N** is “an unknown quantity equivalent to the nitrogen activity” in equilibrium between atmospheric gas and steel, and the unit of partial pressure is atm. For convenience, the equilibrium constant *K_X* in expression (6) is allowed to remain an unknown quantity.

In a carbonitriding process, even if the carbon potential, carburizing duration and process temperature remain unchanged, the carburized depth can vary depending on variation in the atmospheric components according to Neumann et al.⁷⁾ They expressed the cause of this phenomenon with a carbon penetration velocity formula (expression (7)) that uses a carbon transfer coefficient *β*.

$$q = \beta (C_G - C_s) \dots\dots\dots (7)$$

where, *q* = carbon penetration velocity (g/mm²s); *β* = carbon transfer coefficient (g/mm²s); *C_G* = final carbon concentration (wt%); *C_S* = carbon concentration on the material’s outermost surface (wt%).

Being equivalent to the carbon potential, *C_G* can be expressed as a product of the carbon activity *a_c* and a carbon solubility limit concentration *A_S*. Therefore, expression (7) can be rewritten as expression (7’) below.

$$q = \beta (a_c \cdot A_s - C_s) \dots\dots\dots (7')$$

If the manner of the nitrogen penetration mechanism is assumed to be identical to that of the carbon penetration mechanism, then, by referring to expression (7), the nitrogen penetration velocity can be described by expression (8) below.

$$q_N = \beta_N (N_G - N_s) \dots\dots\dots (8)$$

where, *q_N* = nitrogen penetration velocity (g/mm²s); *β_N* = nitrogen transfer coefficient (g/mm²s); *N_G* = final nitrogen concentration (wt%); *N_S* = nitrogen concentration on the material’s outermost surface (wt%).

Then, expression (8) is rewritten as expression (8’) below by replacing *N_G* in expression (8) with *a_N**·*A_{SN}*.

$$q_N = \beta_N (a_N^* \cdot A_{SN} - N_s) \dots\dots\dots (8')$$

where, *A_{SN}* is the saturation value of nitrogen concentration (wt%).

When expression (6) is substituted in expression (8’), then the nitrogen penetration velocity is defined by expression (9).

$$q_N = \beta_N \left(\frac{P_{NH_3}}{K_X \cdot P_{H_2}^{\frac{3}{2}}} \cdot A_{SN} - N_s \right) \dots\dots\dots (9)$$

In expression (9), the variables that can be investigated by measuring the atmosphere for carbonitriding processes are NH₃ partial pressure and H₂ partial pressure. Since *N_S* is determined based on the actual measurements of nitrogen concentration distribution, there are three unknown quantities in expression (9): *β_N*, *K_X*, and *A_{SN}*. (*N_S* can also be determined through calculation involving *β_N*, *K_X*, *A_{SN}* and the diffusion coefficient *D*.)

4.2 Hypothesis about nitrogen concentration distribution in steel

Suppose that the nitrogen concentration distribution profile is compatible with the Gaussian error function as in the case of the carbon concentration profile, then the nitrogen concentration distribution profile can be expressed by the expression (10).

$$N = N_s \cdot \left\{ 1 - erf \left(\frac{X}{2\sqrt{D \cdot t_t}} \right) \right\} \dots\dots\dots (10)$$

where, *N* = nitrogen concentration at a position *X* (wt%); *N_S* = nitrogen concentration on the material’s outermost surface (wt%); *X* = distance from the surface of the material being processed (mm); *D* = diffusion coefficient (mm²/s); and *t_t* = process duration (s). The unknown quantity in expression (10) is the diffusion coefficient *D* because the diffusion coefficient is dependent on nitrogen concentration. Next, let us assume that the diffusion coefficient is approximated

in the form of expression (11).

$$D=A\exp(B \cdot N) \dots\dots\dots (11)$$

where, *A* and *B* are unknown quantities and *N* is nitrogen concentration (wt%).

The value obtained by multiplying the specific gravity of the material by a value calculated by integrating expression (10) in the depth direction is the nitrogen penetration amount in the process duration *t_i*. At the same time, the value obtained by integrating expression (9) with the process duration (s) is the nitrogen penetration amount. Therefore, expression (12) can be derived from expressions (9) and (10).

$$\int_0^{t_i} q_N dt = Q = \rho \int_0^{\delta} N dx = \rho \int_0^{\delta} N_s \cdot \left\{ 1 - \operatorname{erf} \left(\frac{X}{2\sqrt{D \cdot t_i}} \right) \right\} dx \dots (12)$$

where, *Q* = nitrogen penetration amount (g/mm²) at process duration *t_i* (s); *ρ* = specific gravity of iron (7.85 x 10⁻³ g/mm³); *δ* = minimum depth where the nitrogen concentration is virtually zero (mm).

Accordingly, if *β*, *K_X*, *A_{SN}* and all the unknown quantities for *A* and *B* are determined from the results of a series of experiments, then it is possible to predict the nitrogen concentration distribution based on the assumptions described above.

4.3 Calculation of unknown quantities based on the results of the experiments

4.3.1 Calculation of *β*

Unlike the multistep carbon penetration, the reaction formula modeling nitrogen penetration into a steel material is believed to be simply expression (5).

Judging from the results of a series of experiments, nitrogen penetration amounts are not influenced by CO partial pressure and are slightly affected by N₂ partial pressure. Therefore, it was assumed that the nitrogen transfer coefficient *β_N* would remain unchanged.

When the partial pressure of undecomposed NH₃, partial pressure of H₂ and *a_c^{*}* remain unchanged,

$$\frac{P_{NH_3}}{K_X \cdot P_{H_2}^{\frac{3}{2}}} \cdot A_{SN} \text{ in expression (9) takes a constant}$$

value. Therefore, from the actual measurements of nitrogen concentration distribution, the nitrogen penetration velocity *q_N* (g/mm²s) and surface nitrogen concentration *N_S* (wt%) can be determined, thereby *β_N* can be calculated.

4.3.2 Calculation of *A_{SN}*

In expression (8'), which describes nitrogen penetration velocity, the saturation value *A_{SN}* of nitrogen concentration should be defined as the

concentration on a substrate. However, it is impossible to accurately determine the nitrogen concentration on the substrate. Therefore, the surface nitrogen concentration is considered to be the “mean nitrogen concentration of the deposited substances and substrate.”

From the results of the experiment illustrated in Fig. 10, in the range of 0.9 < *a_c^{*}* < 1.1, the *a_c^{*}* in the atmosphere is linearly proportional to the saturation values of surface nitrogen concentration. The saturation value of nitrogen concentration *A_{SN}* is determined based on this fact.

4.3.3 Calculation of *K_X*, *A* and *B*

The unknown quantity *K_X* can be calculated by substituting the nitrogen transfer coefficient *β_N*, the saturation value of nitrogen concentration *a_c^{*}* and the nitrogen concentration *N_S* on the outermost surface in expression (9). They are determined from actual measurements of the nitrogen concentration distribution.

The diffusion coefficient was calculated on a reverse analysis basis (trial and error) by altering unknown quantities *A* and *B* in expression (11) to solve the diffusion formula through numerical analysis. The diffusion coefficient should coincide with the actual measurements of nitrogen concentration distribution obtained through EPMA analysis.

4.3.4 Summary of unknown quantity calculations

The unknown quantities obtained from the results of the author’s experiments are listed in Table 4. When these unknown quantities are substituted in expressions (9) and (12), expression (13) is obtained. By using expression (13), prediction of nitrogen concentration distribution is possible. For example, when a small time difference *D_t* is fixed, and because the surface nitrogen concentration *N_S* at *t_i* = 0_S is 0,

Table 4 Calculated unknown quantities

Type of unknown quantity		
Nitrogen transfer coefficient: <i>β_N</i>		1.7 × 10 ⁻⁷
Saturation value of nitrogen concentration: <i>A_{SN}</i>		(1.8771 - 1.0549 · <i>a_c[*]</i>) / 100
Equilibrium constant: <i>K_X</i>		0.006
Diffusion coefficient: <i>D</i>	<i>A</i>	6.5 × 10 ⁻⁷
	<i>B</i>	149

$$\int_0^{t_i} 1.7 \times 10^{-7} \cdot \left(\frac{P_{NH_3}}{0.006 \cdot P_{H_2}^{\frac{3}{2}}} \cdot \frac{(1.8771 - 1.0549 \cdot a_c^*)}{100} - N_s \right) dt = \rho \int_0^{\delta} N_s \cdot \left\{ 1 - \operatorname{erf} \left(\frac{X}{2\sqrt{6.5 \times 10^{-7} \exp(149 \cdot N) \cdot t_i}} \right) \right\} dx \dots (13)$$

expression (13) may be used in several calculations to determine the surface nitrogen concentration and nitrogen concentration distribution.

Note, however, that prediction of nitrogen concentration distribution with expression (13) is possible only until the time that the surface nitrogen concentration on the steel material being processed reaches saturation. In reality, once having reached saturation, surface nitrogen concentration will increase little, if any.

Therefore, after the nitrogen concentration on the outermost surface of the steel has reached saturation, it is necessary to maintain the surface nitrogen concentration at a constant level. Then, solve the diffusion formula through numerical calculations in order to predict the nitrogen concentration distribution.

4.4 Verification by comparison of predicted values of nitrogen concentration distribution and values obtained through experiments

By comparing the actual measurements from experiments with predicted nitrogen concentration distribution values, NTN has proved the validity of the nitrogen penetration mechanism and nitrogen concentration distribution prediction method described above. For this verification, the results of experiments with the test conditions summarized in Table 5 were adopted.

The actual measurements and predicted values for nitrogen concentration distribution are graphically plotted in Fig. 12. NTN has learned that the predicted nitrogen concentration distribution values match actual measurements well with various partial pressures of undecomposed NH₃, carbon activity a_c^* values, H₂ partial pressure values and process duration values. Thus, it is believed that the assumed values and determined unknown quantities related to nitrogen penetration in this paper are valid.

Table 5 Experimental conditions

Test conditions	Gas component partial pressure (atm) ¹⁾		a_c^*	Process duration (s)
	Undecomposed NH ₃	H ₂		
1)	0.0016	0.354	1.03	9,000
2)	0.0020	0.622	0.97	9,000
3)	0.0016	0.356	0.94	9,000
4)	0.0010	0.332	0.88	4,500

1) Converted to values under ordinary temperature and atmospheric pressure

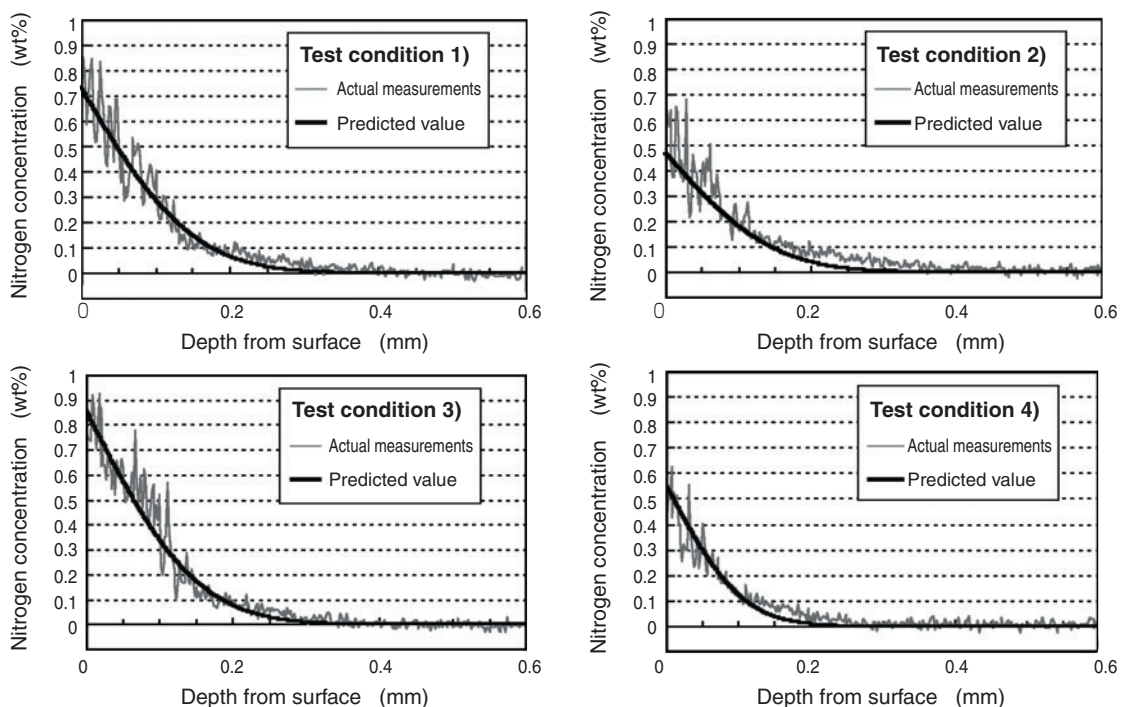


Fig. 12 Nitrogen concentration distribution profile of experimental numbers 1)~4)

5. Conclusion

NTN has performed a systematic series of experiments for carbonitriding with JIS-SUJ2 high carbon chromium bearing steel in an attempt to clarify the nitrogen penetration mechanism associated with this material. Also, assuming that the nitrogen penetration mechanism is similar to the carbon penetration mechanism, NTN has established a method for predicting nitrogen concentration distribution based on a series of experiments. The findings are summarized as follows:

- 1) **The nitrogen penetration amount increases directly with an increases in the partial pressure of undecomposed NH₃.**
- 2) **The nitrogen penetration amount increases directly with decreases in both carbon activity a_c^* and H₂ partial pressure.**
- 3) **NTN has established a method for predicting the nitrogen concentration distribution of JIS-SUJ2 material. This method reflects considerations for the partial pressure of undecomposed NH₃, the carbon activity a_c^* , H₂ partial pressure and the diffusion coefficient that is dependent on nitrogen concentration.**
- 4) **NTN confirmed that, for various carbonitriding atmospheres, the predicted steel nitrogen concentration distribution (using NTN's method for determining nitrogen concentration distribution) closely matches actual data obtained through EPMA analysis.**

References

- 1) N. Tsushima: SAE Technical Paper Series (1986) 860725 (in Japanese)
- 2) S. Narita and K. Yokose: "Effects of the nitriding potential caused by surface nitrogen concentration on various types of carbonitrided case hardening steel," Japan Society for Heat Treatment 61st Lecture Series Preliminary draft (2005) 5 (in Japanese)
- 3) C. Ohki, M. Kawakita: "Effects of carbon activity from the carbonitriding process on high-carbon steel," Japan Society for Heat Treatment 62nd Lecture Series Preliminary draft (2006) 5 (in Japanese)
- 4) C. Ohki, M. Kawakita: "Effects of base gas partial pressure from the carbonitriding process on high-carbon steel," Japan Society for Heat Treatment 62nd Lecture Series Preliminary draft (2006) 17 (in Japanese)
- 5) Editorial Committee of the Society of Chemical Engineers Japan: Chemical Engineering Handbook, Maruzen (1950) 64 (in Japanese)
- 6) R. Collin, S. Gunnarson, and D. Thulin: "Influence of Reaction Rate on Gas Carburizing of Steel in a CO-H₂-CO₂-H₂O-CH₄-N₂ Atmosphere," Journal of The Iron and Steel Institute, (1972), 777
- 7) F. Neumann and U. Wyss: "Thermodynamische Grundlagen zum indirekten Messen des C-Pegels," H.T.M., vol.49, No.4, (1994) 255 (in German)

Photo of author

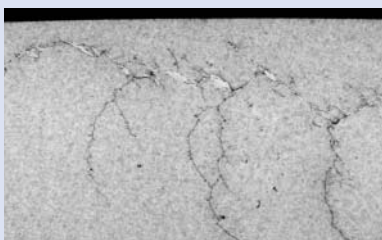


Chikara OHKI

Elemental Technological
R&D Center

The Influence of Hydrogen on Tension-Compression and Rolling Contact Fatigue Properties of Bearing Steel

Hiroshi HAMADA*
Yukio MATSUBARA**



In this report, the fatigue properties of JIS-SUJ2 bearing steel were investigated under various hydrogen pre-charging conditions. The results demonstrated that the fatigue strength substantially decreased by the influence of hydrogen and that the decrease of the fatigue strength was in direct correlation with the diffusible hydrogen content. Additionally, double-roller rolling-sliding contact fatigue tests were conducted to investigate the influence of

hydrogen on surface crack initiation life and microstructural change beneath contact surfaces. As a result, surface cracking occurred much earlier as compared to the calculated life. The crack initiation life decreased as the amount of the diffusible hydrogen increased. Unusual microstructural changes were distinctly observed when a relatively high concentration of the diffusible hydrogen had penetrated. In contrast, a relatively low amount of diffusible hydrogen did not always cause unusual microstructural changes, although only marginal difference was seen in the surface crack initiation life for varying levels of diffusible hydrogen content above 0 ppm.

1. Introduction

In certain bearing applications with automotive auxiliary equipment, it has been known that premature flaking accompanied by unusual microstructural changes can occur under rolling surfaces, and that one typical cause of this problem appears to be hydrogen embrittlement.¹⁾ In addition, though a very rare occurrence, premature flaking sometimes occurs in actual applications, and the cause is difficult to determine. Currently, many researchers believe that hydrogen-induced failures accompany microstructural changes. However, assuming that microstructural changes result only from the penetration of a large amount of hydrogen, then there is the possibility that hydrogen can induce premature flaking without accompanying microstructural change.

The effects of hydrogen on the fatigue characteristics of bearing steel were evaluated using an ultrasonic fatigue test. High-speed load application during this test inhibits dissipation of hydrogen. This paper reports the results of this test.

In addition, this paper also reports the results of the

investigations into the effects of hydrogen on surface crack initiation life and microstructural change behavior using the double-roller rolling-sliding test.

2. Test Methods

2.1 Material

The chemical composition of JIS-SUJ2 bearing steel, which was the material analyzed, is summarized in **Table 1**. The material was subjected to a standard quenching/tempering process under the heat treatment conditions summarized in **Table 2**, and was finished to the specified test piece dimensions through a grinding process. The surface hardness after heat treatment was HV747 and the residual γ content, determined through an X-ray diffraction method, was 9.3%. These values mean that the test pieces feature standard heat treatment quality.

2.2 Ultrasonic fatigue test method

The ultrasonic fatigue test executed was an axial load fatigue test (stress ratio: $R = -1$) in which each test piece was brought into a resonant state by

*Elemental Technological R&D Center

**New Product Development Dept. New Product Development R&D Center

Table 1 Chemical compositions of JIS-SUJ2 bearing steel

C	Si	Mn	P	S	Ni	Cr	Mo	O
0.97	0.20	0.38	0.005	0.005	0.08	1.35	0.03	5

Table 2 Heat treatment conditions

Quenching	Tempering
840°C×45min	180°C×120min

ultrasonic vibration (20 kHz), causing the repeated generation of stress. Further, the fatigue strength of the test piece could be determined in a shorter time span relative to conventional fatigue test methods. This test method is characterized by the fact that the hydrogen-charged steel test piece is fatigued before the hydrogen dissipates. Thus, the effect of penetrated hydrogen can be reliably evaluated.

A typical ultrasonic fatigue test machine is schematically illustrated in Fig. 1. The ultrasonic fatigue test machine used for the test was Model USF-2000 from Shimadzu Corporation. The entire test system is comprised of a personal computer that controls the test machine, an amplifier, a piezo oscillator, an amplitude magnifying horn, and other parts.

The shape and dimensions of the test piece for the ultrasonic fatigue test are provided in Fig. 2. This test piece is known as a circular tapered dumbbell test piece. It consists of round columns with a uniform cross-section from both ends to the shoulder while the side face of the narrower section between these round columns is curved.

Since the test piece lacks a smooth flat section, moderate stress concentration occurs on it with a

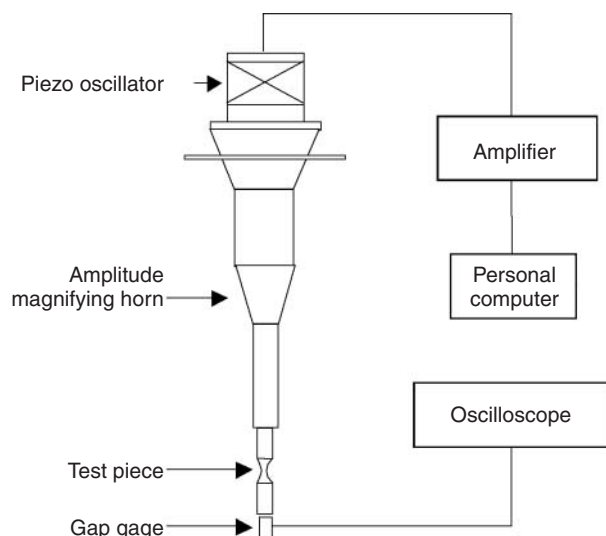


Fig. 1 Schematic of ultrasonic fatigue test machine

stress concentration coefficient of approximately 1.03.²⁾ The test piece is designed so that it resonates at 20 kHz. The thread on one end is to allow it to be installed on the test rig.

When the test piece resonates, the stress amplitude maximizes at the smallest diameter portion at the middle of the narrower section. The maximum stress amplitude S can be determined by measuring the displacement amplitude, a , at the free end of the test piece with a gap sensor and substituting the obtained measurement in expression (1).³⁾ E is Young's modulus, $c = (E/\rho)^{1/2}$ where ρ is density) is longitudinal wave velocity, and $\omega (= 2\pi f$ where f is resonance frequency) is angular frequency. l , b and β in expression (1) can be represented by expressions (2), (3) and (4), respectively, where $R (= 6 \text{ mm})$, $H (= 2 \text{ mm})$ and $g (= 10 \text{ mm})$ are the maximum radius, minimum radius and half-chord length of the test piece, respectively.

$$S = a \cdot E \cdot \beta \cdot \cos\left(\frac{\omega \cdot l}{c}\right) \cdot \cosh \beta g \cdot \left(\frac{1}{\cosh \beta g}\right) \dots (1)$$

$$l = \frac{c}{\omega} \tan^{-1} \left[\frac{c}{\omega} (\beta \coth \beta g - b \tanh \beta g) \right] \dots (2)$$

$$b = \frac{1}{g} \cosh^{-1} \left(\frac{R}{H} \right) \dots (3)$$

$$\beta = \sqrt{b^2 - \left(\frac{\omega}{c}\right)^2} \dots (4)$$

The test procedure is schematically illustrated in Fig. 3(a). The surface of the test piece can be roughened as a result of the hydrogen pre-charging (described later in Sec. 2.3). This roughness can cause stress concentrations that may lead to surface initiated failures. To prevent this problem, immediately after hydrogen pre-charging, the surface of the narrower section of the test piece was polished with emery papers (starting with #500 and ending with #2000) and buffed with diamond paste ($1 \mu\text{m}$). The

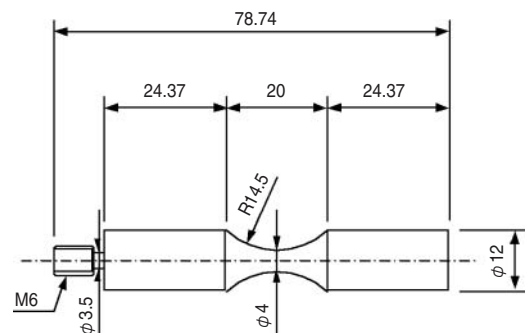


Fig. 2 Geometry and dimensions of ultrasonic fatigue test specimen

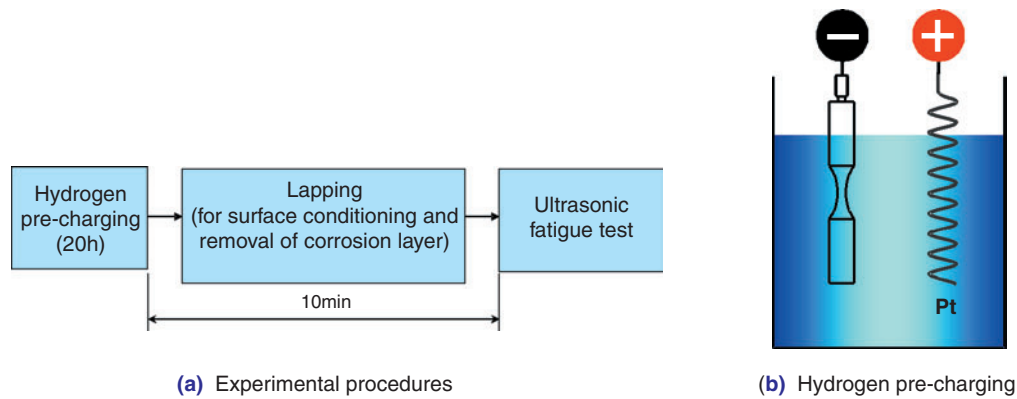


Fig. 3 Experimental procedures of ultrasonic fatigue testing and schematic of hydrogen pre-charging

test sequence began by fixing the threaded portion of the test piece to the end of the horn and then verifying that the test piece resonated in the frequency range of $20 \text{ kHz} \pm 30 \text{ Hz}$.

The test sequence was performed within 10 minutes to avoid dissipation of the penetrated hydrogen, and the time span after hydrogen pre-charging to the beginning of the test was fixed to 10 minutes.

The conditions of the ultrasonic fatigue test are summarized in **Table 3**. When a load is continually applied during an ultrasonic fatigue test, heat buildup occurs on the test piece due to the internal friction that results from high-speed vibration. To avoid this problem in the test, an intermittent load application scheme was adopted⁴⁾ in which a cycle consisting of a 0.11-second loading period and a 1.10-second non-loading period was repeated. If a crack occurs in a ductile material, its resonant frequency will decrease greatly when the crack develops to a certain size. The test rig was designed to stop each test run using this change. Since the test pieces were all made of a brittle material, certain test pieces fractured completely into two pieces. On the other hand, if a test piece did not develop a fracture after 10^8 load application repetitions, that test run was aborted.

Table 3 Conditions of ultrasonic fatigue test

Loading frequency	20 kHz	
Loading cycle	Intermittent loading	Loading: 0.11 sec.
		Non-loading: 1.10 sec.
Stress ratio	$R = -1$ (fully bidirectional)	
Test atmosphere	Room temperature atmosphere	

2.3 Method of hydrogen pre-charging of ultrasonic fatigue test pieces

The hydrogen pre-charging method is schematically illustrated in **Fig. 3(b)**. Cathode hydrogen pre-charging is a hydrogen pre-charging technique in which the test piece is used as the cathode and the aqueous solution of the electrolyte is electrolyzed. During this process a portion of the hydrogen atoms occurring on the surface of the test piece are introduced into the test piece. This technique helps achieve safe and easy hydrogen penetration into the specimen. With this technique, it is possible to control the hydrogen penetration content relatively easily by controlling the applied current density.

The hydrogen pre-charging conditions are summarized in **Table 4**. The electrolyte solution used was prepared by diluting sulfuric acid with thiourea, which serves as a hydrogen rebonding inhibiting additive. Five levels of current density in a range of $0.1\text{--}0.5 \text{ mA/cm}^2$ were used as listed in **Table 4**. The hydrogen pre-charging duration was fixed to 20 hours. The hydrogen diffusion coefficient with the JIS-SUJ2 steel at an ordinary temperature is $3.8 \times 10^{-11} \text{ m}^2/\text{s}$.⁵⁾ If the hydrogen diffusion coefficient takes this value, then the relative concentration distribution of diffusible hydrogen in the minimum diameter section ($\phi 4$) on the ultrasonic fatigue test piece can become nearly uniform within 20 hours.

Table 4 Hydrogen pre-charging conditions prior to ultrasonic fatigue test

Electrolyte	H_2SO_4 (0.05 mol/L) + $\text{CH}_4\text{N}_2\text{S}$ (1.4 g/L) (thiourea)
Pre-charging current density (mA/cm^2)	0.1, 0.2, 0.3, 0.4, 0.5
Pre-charging duration (h)	20

2.4 Double-roller rolling-sliding test method

The concept of the double-roller rolling-sliding test is schematically illustrated in Fig. 4. To provide 2% relative sliding at the contact point between the two rollers, the driving roller and the following roller were each driven with an independent motor.

The test piece and test conditions are summarized in Table 5.

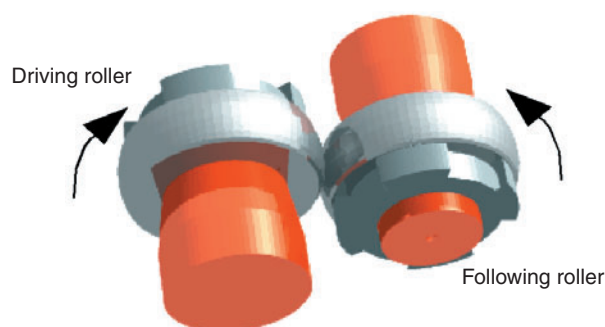


Fig. 4 Schematic of double-roller rolling-sliding test

Table 5 Conditions of rolling-sliding test

Driving roller	$\phi 40\text{mm} \times L12\text{mm}$, Sub-curvature R60mm, $R_a=0.02\mu\text{m}$	
Following roller	$\phi 40\text{mm} \times L12\text{mm}$, Sub-curvature R60mm, $R_a=0.02\mu\text{m}$	
Running speed (min^{-1})	Driving roller	3060
	Following roller	3000
Max. contact bearing pressure (GPa)	2.1	
Contact oval form	2a \times 2b	1.375mm \times 0.669mm
Sliding ratio (%)	2	
Lubricating oil	VG22	
Lubrication system	Lubrication with felt pad	
Oil film parameter (Λ)	18	
Test atmosphere	Room temperature atmosphere	

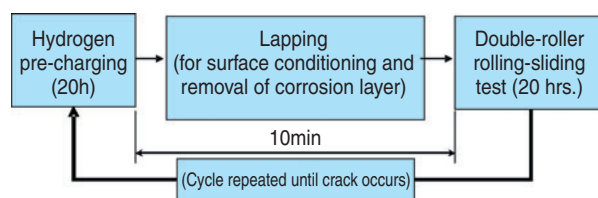


Fig. 5 Experimental procedures of double-roller rolling-sliding test

Table 6 Hydrogen pre-charging conditions for rolling-sliding test

Electrolyte	H_2SO_4 (0.05 mol/L) + $\text{CH}_4\text{N}_2\text{S}$ (1.4 g/L) (thiourea)
Pre-charging current density (mA/cm^2)	0.3, 0.5, 1.0
Pre-charging duration (h)	20

The test procedure is schematically illustrated in Fig. 5. Either the driving roller or the following roller was subjected to cathode hydrogen pre-charging similar to that described previously in Sec. 2.3. The hydrogen pre-charging conditions are summarized in Fig. 6. The pre-charging duration was set to 20 hours. In this pre-charging duration, the hydrogen concentration distribution does not become uniform through the interior of the test piece. However, the surface of the test piece will have near-uniform hydrogen concentration distribution. Prior to the rolling-sliding test after hydrogen pre-charging, the surface of the test piece was polished with emery papers (starting with #500 and ending with #2000) and buffed with diamond paste ($1\mu\text{m}$) to remove a thin corrosion film and avoid the effect of surface roughness. In the rolling-sliding test, the rollers were allowed to turn continuously for 20 hours. Taking the above-mentioned process as one cycle, the cycle (consisting of hydrogen pre-charging and rolling of the rollers) was repeated until surface cracking occurred.

2.5 Thermal desorption analysis method

The thermal desorption analysis was executed to investigate the interrelation between the hydrogen pre-charging current density and the resultant diffusible hydrogen content. The data for the test piece and the analysis conditions are summarized in Table 7. The hydrogen pre-charging conditions for the test piece including the electrolyte solution and pre-charging duration (20 h) were identical to those summarized in Tables 4 and 6. Since the test piece was a slender form, the relative hydrogen concentration distribution inside the test piece became sufficiently uniform after 20 hours of pre-charging.⁵⁾ Gas chromatography was used for the analysis. The analysis was started exactly 10 minutes after completion of hydrogen pre-charging in accordance with the test conditions of the ultrasonic fatigue test and double-roller rolling-sliding test.

Table 7 Conditions of thermal desorption analysis of hydrogen

Analyzer		Gas chromatograph
Carrier gas	Type	Ar
	Flow rate (mL/min)	20
Test piece size (mm^3)		27 \times 1 \times 1
Heat increase rate ($^{\circ}\text{C}/\text{min}$)		3
Temperature range for analysis ($^{\circ}\text{C}$)		Room temperature to 360

3. Test Results and Discussion

3.1 Ultrasonic fatigue test results

3.1.1 SN characteristics

The results of the ultrasonic fatigue test are plotted graphically in Fig. 6. Compared to the results obtained without hydrogen pre-charging, the fatigue strength with hydrogen pre-charging was much lower. In addition, fatigue strength decreased with greater current densities. As shown in Fig. 7, the mode of fracture was a fish-eye fracture initiated at a non-metal inclusion or other impurities within each test piece regardless of whether or not they were subjected to hydrogen pre-charging. Thus, no macro-scale difference in fracture mode was found.

3.1.2 Relationship between fatigue strength and diffusible hydrogen content

The relationship between the temperature and the hydrogen release rate were obtained from the thermal desorption analysis of hydrogen. The results are shown graphically in Fig. 8. The amount of hydrogen released was greater with greater hydrogen pre-charging current densities, peaking at around 80°C. The hydrogen released at temperatures up to 200°C

was defined as diffusible hydrogen and the amount of such hydrogen is plotted in Fig. 8.

Based on the results shown in Figs. 6 and 8, the effects of diffusible hydrogen on fatigue strength of JIS-SUJ2 steel were evaluated considering the following two points.

First, because scattering was present in fatigue test data, a statistical approach for handling the data was needed. Second, because premature flaking would accidentally occur on JIS-SUJ2 steel accidentally in real machines, it appeared reasonable to make the above-mentioned evaluation based on the characteristics of this material at around the fatigue limit rather than based on the high loading characteristics of this material, the latter being the evaluation practice in conventional rolling fatigued tests. Furthermore, the fatigue characteristics that can be reflected in machine designs appear to be fatigue strength-related characteristics rather than life-related characteristics. In this context, based on the JSMS-SD-6-02 SN curve regression method⁶⁾ of the Society of Materials Science, Japan, the fatigue test data was applied to a continuously-decreasing one-sided logarithmic curve model. In this way, the 50% fatigue strength curve and the 10% fatigue strength curve were determined. The curve in Fig. 9 is the 50% fatigue strength curve. The evaluation criterion was 10% fatigue strength after 10⁷ load application cycles.

$$\sigma = 10^{-A} \log_{10} N + B + D \quad (A, B, D : \text{constants}) \quad \dots \dots \dots (5)$$

The relationship between the amount of diffusible hydrogen and the 10% fatigue strength after 10⁷ load application cycles is illustrated in Fig. 10. Since there is a good linear relation between these two factors, it could be understood that the loss in fatigue strength is governed by the diffusible hydrogen content.

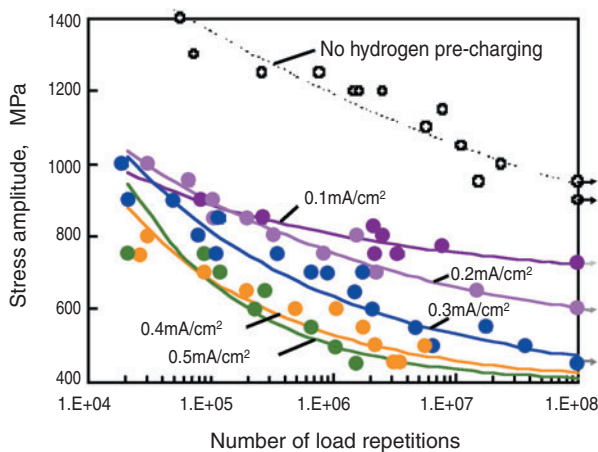


Fig. 6 Results of ultrasonic fatigue testing

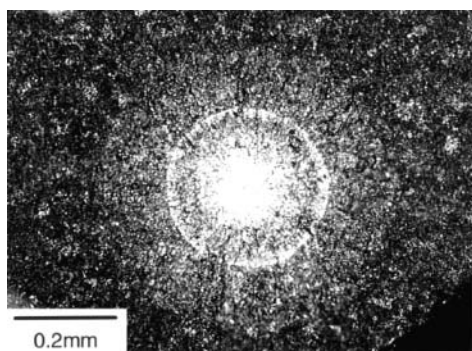


Fig. 7 Photograph of fracture center

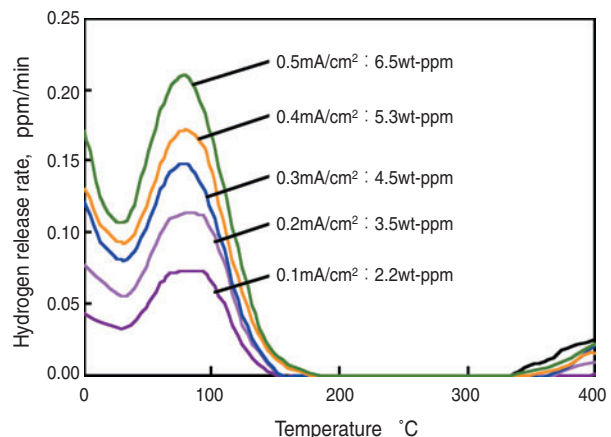


Fig. 8 Results of thermal desorption analysis of hydrogen

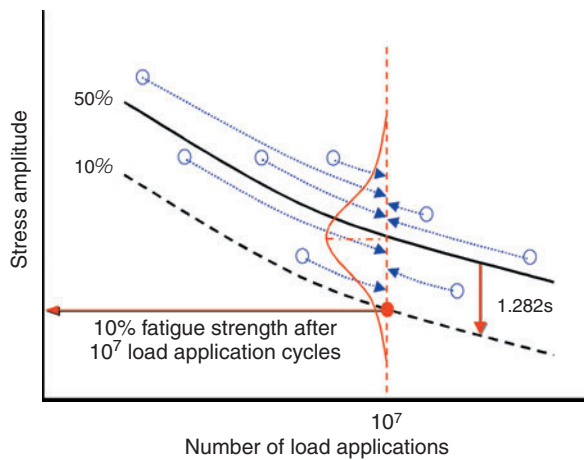


Fig. 9 Estimation of 10% fatigue strength at 10^7 cycles

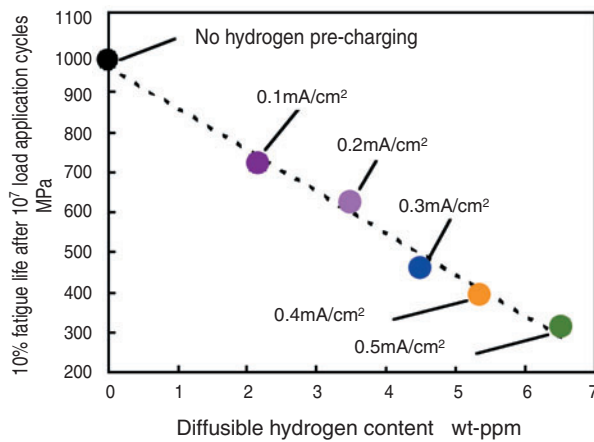


Fig. 10 Relationship between diffusible hydrogen concentration and 10% fatigue strength at 10^7 cycles

3.2 Results of roller rolling-sliding test

3.2.1 Crack initiation life

The relationship between the hydrogen pre-charging current densities and the number of rolling test runs before occurrence of surface cracking in the double-roller rolling-sliding test is illustrated in Fig. 11. Because the calculated life under the conditions of this

test was 36,511 hours (approx. 4 years)^{7),8)} cracking must not occur during the effective bearing life. However, as shown in Fig. 11, in the result of each test run that underwent hydrogen pre-charging, surface cracking occurred before 80 hours had elapsed, which is much shorter than the calculated life. The accumulated test duration (the number of load application cycles) before the occurrence of cracking was shorter with greater current densities, that is, with greater amounts of penetrated hydrogen.

3.2.2 Relationship between microstructural changes and diffusible hydrogen contents

Photos of surface cracks and their circumferential cross sections are shown in Fig. 12. Fig. 12(a) shows the test result from a current density of 1.0 mA/cm² and Fig. 12(b) shows the test result from a current density of 0.3 mA/cm². In the case of Fig. 12(a), what is distinctive about 12(a), that is not observed in 12(b) were observed under the rolling surface. In contrast, in the case of Fig. 12(b), no distinctive microstructural changes were observed. Judging from these results, it appears that distinctive microstructural changes occur with greater amounts of penetrated hydrogen, but they do not always occur with lower amounts of penetrated hydrogen.

3.2.3 Correlation between the results of the ultrasonic fatigue tests and the results of the double-roller rolling-sliding test

As previously described in the introduction, with the bearing products on the market, though a very rare occurrence, surface-initiated flaking sometimes occurs on the contact surface without apparent damage. The cause of this problem could be tensile stress that is repeatedly applied circumferentially to the rolling contact surface. This tensile stress is greater with a greater rolling friction coefficient. It could be easily imagined that, under such conditions, premature flaking would tend to occur if diffusible hydrogen penetrates the material and the fatigue strength of the material deteriorates. Therefore, an investigation was conducted to determine the effect of the SN

Current density (mA/cm ²)	Roller subjected to hydrogen pre-charging	Number of test repetitions (accumulated test duration)			
		1 (20h)	2 (40h)	3 (60h)	4 (80h)
0.3	Driving side				✕
	Following side				✕
0.5	Driving side			✕	
	Following side			✕	
1.0	Driving side		✕		
	Following side	✕			

Fig. 11 Relationship between the current density for hydrogen pre-charging and the number of repetitions to failure

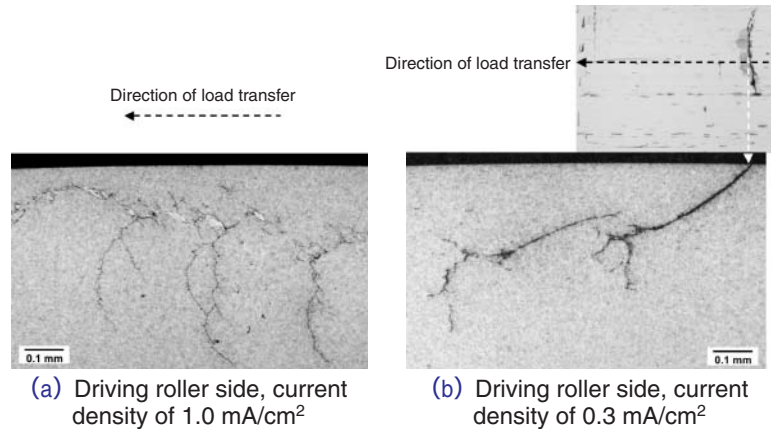


Fig. 12 Photographs of surface cracks and their circumferential cross sections

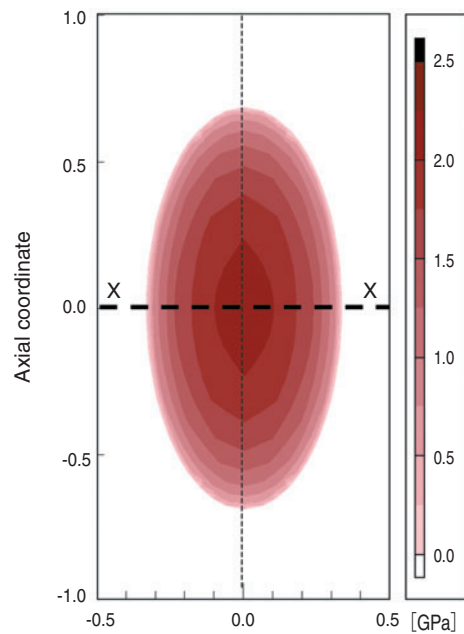
characteristics of penetration of diffusible hydrogen on the possibility of premature flaking. This effect was examined by repeatedly applying circumferential tensile stress to the rolling surface in a double-roller test using an ultrasonic fatigue test.

The dynamics of contact between the rollers were calculated under the loading conditions of the double-roller test. The calculation results are illustrated in **Figs. 13(a)** and **13(b)**. Contact pressure distribution is provided in **Fig. 13(a)**, while **Fig. 13(b)** shows circumferential tensile stress distribution on the rolling surface along the X-X line where the tensile stress maximizes on the edge of the contact ellipsoid. When the rolling friction coefficient is 0, the maximum tensile stress of both contact edges is 214 MPa. When the rolling friction coefficient is 0.1, the maximum tensile stress of one contact edge becomes 531 MPa.

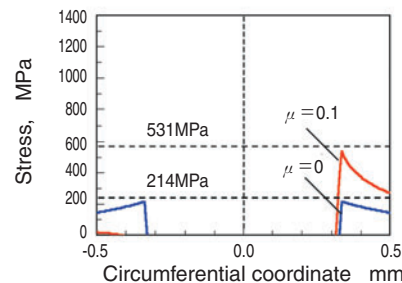
From the results of the ultrasonic fatigue test, as shown in **Fig. 14**, the 10% fatigue strength after 10^7 load application cycles is 981 MPa when there is no diffusible hydrogen penetration. This strength is sufficiently greater than the results shown in **Fig. 13(b)**. In contrast, the 10% fatigue strength dropped to 460 MPa when diffusible hydrogen penetrated the material, as in the result of the ultrasonic fatigue test with a hydrogen pre-charging current density of 0.3 mA/cm² (4.5 wt-ppm). Consequently, if hydrogen penetrates the material, cracks can occur at a tensile stress less than those shown in **Fig. 13(b)**.

As summarized above, if for any reason the rolling friction coefficient becomes greater and a large amount of diffusible hydrogen penetrates the material at the same time, there is a higher possibility of crack occurrence on the rolling surface, which can lead to premature flaking. However, to verify this assumption, it will be necessary to prove that diffusible hydrogen penetrates the material in an amount sufficient enough to lower the fatigue strength of the material in the rolling contact mode. Detailed research efforts for

quantitative verification of the effects of hydrogen on rolling fatigue were made from the 1950's to the 1970's. Grunberg et al. proposed a theory that the loss in rolling life of a steel material due to ingress of water is caused by hydrogen derived from the water.⁹⁾
¹¹⁾ This theory was supported by Scharzberg et al.^{12),13)}



(a) Contact pressure distribution between two rollers



(b) Distribution of circumferential tensile stress working on the contact surface along the X-X line

Fig. 13 Distribution of circumferential tensile stress at contact surface along X-X line

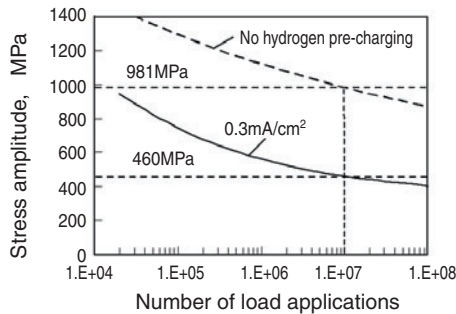


Fig. 14 10% fatigue strength curves

Incidentally, Swets et al. suggested that hydrogen occurring from decomposed lubricating oil penetrates steel materials and causes the rolling fatigue life of the materials to become shorter.¹⁴⁾ Additionally, Kino et al. reported that hydrogen content in a steel material increases after a rolling fatigue test and the increase in hydrogen content varies depending on the type of lubricating oil used.¹⁵⁾ Based on this knowledge about water ingress and decomposed lubricating oil, further investigation is needed to determine quantitatively whether diffusible hydrogen penetrates the steel material in an amount sufficient enough to lower its fatigue strength in the rolling contact mode.

4. Conclusion

The authors have evaluated the effects of hydrogen on the fatigue characteristics of JIS-SUJ2 bearing steel by using an ultrasonic fatigue test that is capable of high-speed loading on the material in order to inhibit dissipation of hydrogen during the test. In addition, through a double-roller rolling-sliding test, the authors investigated the effects of hydrogen on the surface crack life of the material and microstructural changes in the material. As a result, the authors have confirmed the following:

- 1) In the ultrasonic fatigue test, the fatigue strength of the material significantly decreased due to the penetrated hydrogen, and there is an apparent relation between the amount of penetrated hydrogen and the fatigue strength values after 10^7 load application cycles on the material.
- 2) In the double-roller rolling-sliding test after hydrogen pre-charging, premature flaking occurs due to the effect of penetrated hydrogen. A greater penetrated hydrogen content will cause distinctive microstructural changes in the material, while a smaller penetrated hydrogen content may not always lead to the occurrence of distinctive microstructural changes in the material.

Incidentally, the problem of loss in the effective service life of bearings available in the market, which results from penetrated hydrogen, has been addressed through various improvements in lubricants, bearing materials and surface modification techniques. NTN bearing products improved in these ways have already been made available to the market.

References

- 1) K. Tamada and H. Tanaka, *Wear*, 199 (1996) 245-252
- 2) R. E. Peterson, *Stress Concentration Factors*, John Wiley & Sons, New York, (1974) 51p
- 3) K. Salama and R. K. Lamerand, *Proceedings of the 1st International Conference on fatigue and Corrosion Fatigue up to Ultrasonic Frequencies* (1981) 109-118
- 4) H. Ishii, K. Yamanaka and K. Tohgo, *Material Science Research International, Special Technical Publication -1*, (2001) 59-63
- 5) Y. Matsubara and H. Hamada, *Journal of ASTM International*, 3 (2006) , Online ISSN: 1546-962X.
- 6) JSMS Committee on Fatigue of Materials, *JSMS Committee on Reliability Engineering: Standard Evaluation Method of Fatigue Reliability for Metallic Materials—Standard Regression Method of S-N Curves (JSMS-SD-6-02)*, Society of Materials Science, Japan (2002) (in Japanese)
- 7) J. J. Coy, D. P. Townsend and E. V. Zaretsky, *Analysis of Dynamic Capacity of Low-Contact-Ratio Spur Gears using Lundberg-Palmgren Theory*, NASA TN D-8029, (1975)
- 8) J. J. Coy and E. V. Zaretsky, *Life Analysis of Helical Gear Sets using Lundberg-Palmgren Theory*, NASA TN D-8045, (1975)
- 9) L. Grunberg, *Proc. Phys. Soc. (London)* , B66 (1953) 153-161
- 10) L. Grunberg and D. Scott, *J. Inst. Petrol.*, 44 (1958) 406-410
- 11) L. Grunberg, D. T. Jamieson and D. Scott, *Phil. Mag.*, 8 (1963) 1553-1568
- 12) P. Schatzberg and I. M. Felsen, *Wear*, 12 (1968) 331-342
- 13) P. Schatzberg, *J. Lub. Tech.*, 231 (1971) 231-235
- 14) D. E. Swets and R. C. Frank, *Trans. AIME*, 221 (1961) 1082-1083
- 15) N. Kino and K. Otani, *JSAE Review*, 24 (2003) 289-294

Photos of authors



Hiroshi HAMADA

Elemental Technological
R&D Center

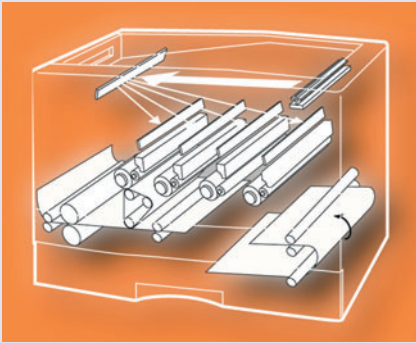


Yukio MATSUBARA

New Product Development Dept.
New Product Development R&D Center

Technical Trends in Bearings for Office Equipment

Chikara KATAGIRI*



Recently, the demand for digital color PPC's (Plain Paper Copiers) and MFP's (Multi Function Printers) has been increasing alongside personal computers, digital cameras and the internet. During this time, NTN has been aggressively working to develop technologies and products for this ever increasing digital media market. This report discusses the required function of photosensitive drums and fuser rollers for the latest PPC's and MFP's, as well as bearing technologies for these applications.

1. Introduction

Electrophotography began as a monochromatic analog technology. Then, in 1983, Carlson (USA) proposed color xerography, and in the 1990's, digital electrophotography became a technology that was more commonly used. As more and more people have begun using personal computers and the Internet, electrophotographic equipment, including digital plain paper copiers (PPC) and laser beam printers (LBP) have become increasingly used as imaging devices for diverse applications worldwide.

The requirements for bearings used in digital copying machines and printers have become more demanding. This paper describes the most recent requirements for these bearings and the technologies used to satisfy these requirements.

2. Structure of Color Copying Machines and Color LBPs

The structure of a typical color copying machine or color LBP is illustrated schematically in **Fig. 1**. Many rolling bearings are used in color copying machines and color LBPs. Recently, thin deep groove ball bearings, such as those shown in **Photo 1**, have been used more frequently in photosensitive sections and fusing sections of these devices. Featuring smaller cross-sectional areas, thin deep groove ball bearings contribute to the compact design of mechanisms in color copying machines and color LBPs and also help provide extra space around the bearings.

Basic process of color copying machines and color LBPs

- 1) **Image exposure:** The image being copied or printed is formed as a latent image on the photosensitive drum.
- 2) **Developing:** The toner is allowed to be attracted to the latent image on the photosensitive drum to make the image visible.
- 3) **Transfer:** The toner powder on the photosensitive drum is transferred to a sheet of copy paper.
- 4) **Fusing (fixing):** The toner powder is fixed to the copy paper by heat and pressure.

*Industrial Engineering Dept. Industrial Sales headquarters

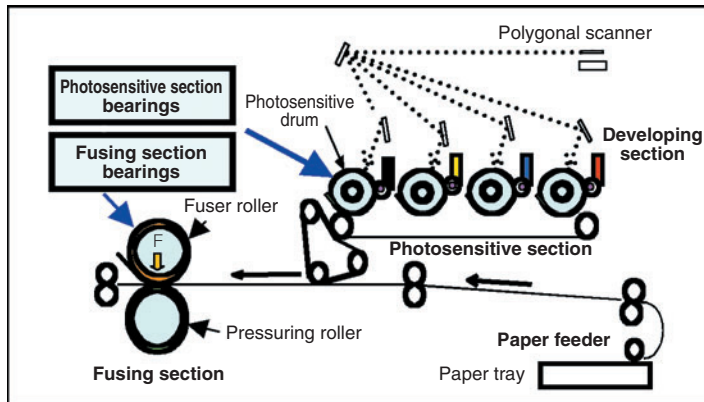


Fig. 1 Structure of color copy machine and LBP



Photo 1 Thin type deep groove ball bearing

3. Functions Required of Color Copying Machine and Color LBP Bearings

Photosensitive drum support bearings

- 1) Electrical conductivity
- 2) Resistance against chemical attack
- 3) Stable running accuracy

Fuser roller support bearings

- 1) Long life under high temperatures
- 2) Electrical conductivity
- 3) Prevention of frictional noise
- 4) Resistance against chemical attack

4. Bearing Technology

Explanations of bearing technologies related to conductivity (at ordinary and high temperatures), chemical attack resistance and frictional noise* elimination are presented below.

*Frictional noise is noise that occurs from interference between a bearing inner ring and a shaft resulting from a loose fit.

4.1 Conductive-bearing technologies

In the past, both grounding arrangements and conductive bearings were used in the photosensitive sections of color copying machines and color LBPs to eliminate triboelectricity. Recently, better conductivity for bearings used for this application is needed even more because grounding arrangements in photosensitive sections are being eliminated in order to simplify entire systems and to prevent the occurrence of electromagnetic noise. In addition, most recently, better conductivity for fuser roller support bearings has also become more necessary.

The following techniques have been used to provide electrical conductivity in rolling bearings:

- 1) Prefilling with conductive greases
- 2) Use of conductive contact rubber seals

- 3) Provision of metal bypasses between inner and outer rings

Recently, to meet the market price demands for color copying machines and color LBPs, the need has been mounting to minimize the costs of their internal mechanisms and associated components. Given this situation, the addition of new components and parts should be strictly avoided, so the most promising of the above measures seems to be the first, “prefilling with conductive greases.”

For this reason, NTN offers bearings prefilled with original greases, including types for use at room temperature and types for use at high temperature, that have been developed in cooperation with grease manufacturers. The performance data of these bearings are described below.

4.1.1 Conductive bearings for photosensitive drum support

The typical properties of the original NTN conductive greases for room temperature use, EP-2 Grease and EP-3 Grease, which is a variation of EP-2 with improved oil separation, are summarized in Table 1. A unique feature of these greases is the addition of carbon black, which is a conductive material, as a thickener.

Table 1 Typical properties of conductive grease for photosensitive drum

	NTN EP-2 Grease	NTN EP-3 Grease	Test method
Thickener	Carbon black	Carbon black Lithium soap	—
Base oil	Synthetic hydrocarbon	Synthetic hydrocarbon	—
Worked penetration	290	266	JIS K 2220
Oil separation mass %	3.2 (100°C, 24 hrs.)	1.6 (100°C, 24 hrs.)	JIS K 2220

The test rig used for measuring the resistance on conductive bearings is illustrated in Fig. 2, and the test conditions are summarized in Table 2.

Table 2 Test condition of bearing resistance

Test bearing	6806ZZ ϕ 30mm \times ϕ 42mm \times 7mm
Running speed (min ⁻¹)	100
Radial load (N)	4.9
Ambient temperature (°C)	Room temperature
Control resistance (k Ω)	300

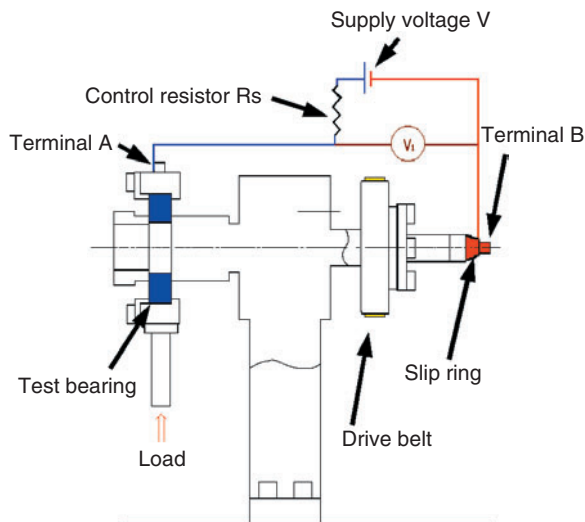


Fig. 2 Test rig of bearing resistance

The resistance values of bearings prefilled with EP-2 Grease, EP-3 Grease and a conventional grease are plotted in Fig. 3. The bearings prefilled with EP-2 and EP-3 exhibited resistance values that are maintained at lower levels. This means that EP-2 and EP-3 are relatively free from time-dependent deterioration.

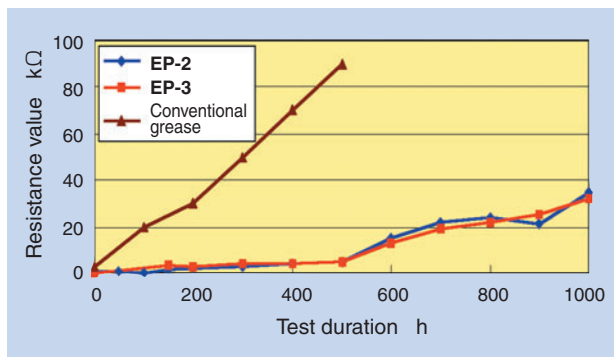


Fig. 3 Results of bearing resistance test

The amount of weight loss in the bearings used for the test described above are graphically plotted in Fig. 4. Compared with the bearing prefilled with EP-2 Grease, the bearing prefilled with EP-3 Grease features better base oil retention power and reduced loss of bearing weight. Thus, EP-3 was shown to be effective in preventing outward leakage of the base oil from running bearings.

Encouraged by the performance of the EP-3 Grease as described above, NTN will employ EP-3 Grease as a standard conductive grease for photosensitive drum support bearings.

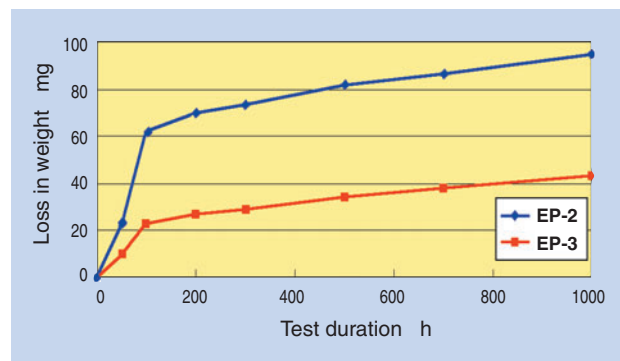


Fig. 4 Results of bearing weight loss test

4.1.2 Conductive bearings for fuser roller support

Unlike the photosensitive section, the fusing section gets very hot (max. 250°C). Therefore, since the fuser roller supporting conductive bearings must satisfy both high-temperature durability and conductivity, they are prefilled with fluorine grease. NTN high-temperature conductive greases have been developed from fluorine grease. The representative properties of NTN high-temperature conductive EF-5 Grease and EF-7 Grease, which is a variant of EF-5 with a longer life, are summarized in Table 3.

The electrical resistance of ordinary fluorine grease prefilled bearings are about 100 kΩ. In contrast, the resistance values of the bearings prefilled with EF-5 Grease and EF-7 Grease are lower, as shown in Fig. 5. In particular, the newly developed EF-7 Grease maintains low resistance for an extended period. As

Table 3 Typical properties of conductive grease for fuser roller

	NTN EF-5 Grease	NTN EF-7 Grease	Test method
Thickener	PTFE+graphite	PTFE+graphite	—
Base oil	Fluorine oil	Fluorine oil	—
Worked penetration	234	225	JIS K 2220
Oil separation mass %	5.0 (200°C, 24 hrs.)	3.9 (200°C, 24 hrs.)	JIS K 2220

can be seen in Fig. 6, EF-7 Grease boasts high-temperature life that is more than three times as long as that of EF-5 Grease. Therefore, NTN will employ EF-7 Grease as a standard conductive grease for fuser roller support bearings.

Table 4 Test condition of bearing resistance

	Operating conditions	Test conditions
Test bearing	2TS3-SC05B98ZZ $\phi 25\text{mm} \times \phi 32\text{mm} \times 7\text{mm}$	
Running speed (min^{-1})	130	
Radial load (N)	220	
Ambient temperature ($^{\circ}\text{C}$)	200	Room temperature
Control resistance ($\text{k}\Omega$)	—	300

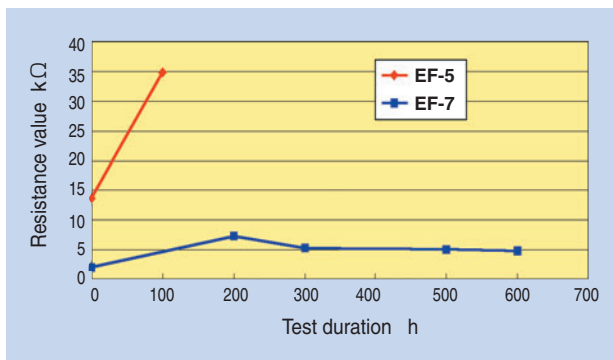


Fig. 5 Results of bearing resistance test

Table 5 Test condition of high temperature grease life

	Test conditions
Test bearing	2TS3-SC05B98ZZ $\phi 25\text{mm} \times \phi 32\text{mm} \times 7\text{mm}$
Ambient temperature ($^{\circ}\text{C}$)	200
Running speed (min^{-1})	130
Radial load (N)	220
Grease life judgment criteria	1) Temperature increase on the bearing ($+15^{\circ}\text{C}$) 2) Torque increase on the motor (1.5 times higher than that at the beginning of the test)

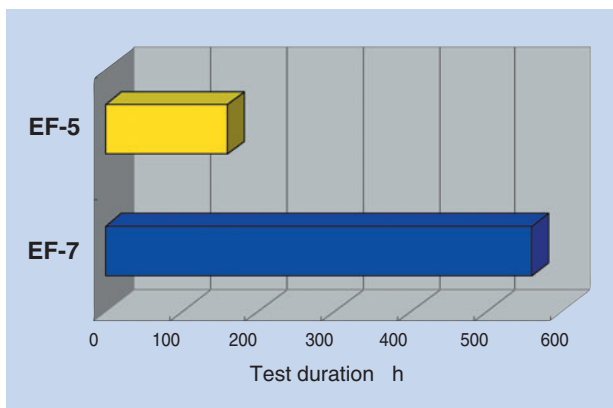


Fig. 6 Results of high temperature grease life test

4.2 Bearing technologies for chemical attack resistance

Many resin components (mainly those made of aromatic resins) are used in color copying machines and color LBPs. The bearings used in these machines are prefilled with grease as lubricant, and their outer faces are coated with rust-preventive oil. With particular combinations of oil and resin, cracking and/or crazing can occur on resin components.

4.2.1 Mechanism of chemical attack

Chemical attack (stress corrosion cracking) is a phenomenon where corrosion and static stress lead to cracking and embrittlement. Static stress is a stress occurring on an object when a given static load is applied to it. Corrosion occurs when compatibility between the resin and the solvent is high, as the solvent dissolves the resin or enters molecules in the resin and slackens its polymer chains and crystal structures, leading to the occurrence of cracking and/or crazing.

4.2.2 Chemical attack evaluation

As shown in Fig. 7, a resin test piece was bent by a particular amount, and the sample oil was applied to a face of the test piece where tensile stress was applied. The test piece was then left to stand under the test conditions summarized in Table 6.

Table 6 Test condition of solvent crack

Resin test piece (mm)	150 × 19 × 3 (length x width x thickness)
Deflection ratio (%)	5
Standing temperature ($^{\circ}\text{C}$)	70
Standing time (h)	72

(Deflection ratio = deflection/distance between supporting points)

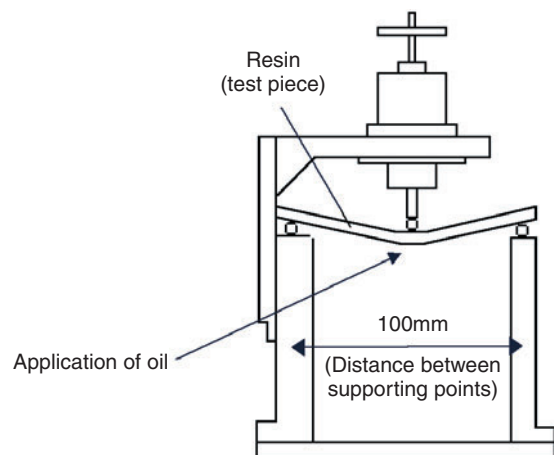
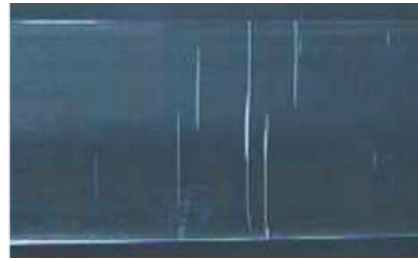


Fig. 7 Test rig of solvent crack



Photo 2 Example of test pieces after evaluation (occurred split and crack)



The result of evaluation for base oils used on bearings and typically used resin materials is summarized in **Table 7**.

Table 7 Results of chemical attack test

	Ester oil	Fluorine oil	Mineral oil	PAO
ABS	×	◎	○	◎
PC	×	◎	○	◎
POM	◎	◎	◎	◎
PA	◎	◎	◎	◎
PBT	○	◎	◎	◎
PEEK	◎	◎	◎	◎
PPS	◎	◎	◎	◎

◎ : The oil does not attack the resin much.
 ○ : In certain cases, the oil attacks the resin.
 × : The oil attacks the resin.

Color copying machines and color LBPs incorporate many components made of ABS (acrylonitrile-butadiene-styrene) and PC (polycarbonate). Therefore, the grease prefilled in bearings and the rust preventive oil must be oils that do not have chemical attack effects on resin materials.

Based on the chemical attack results of the evaluation described above, NTN is using greases and rust preventive oils that employ PAO and fluorine oils as their base oils. Additionally, the conductive greases previously described in Sec. 4.2 are also types that do not cause chemical attacks.

4.3 Fuser roller support bearings that prevent frictional noise

On the fuser roller support bearings, the fit between the inner ring and the shaft is loose to simplify the assembly work. Subjected to heat and load, the fuser roller is affected by both thermal expansion in the axial direction and bending. Due to the loose fit, the thermal expansion in the axial direction and the bending, the attitude of the roller is disturbed, the inner ring hits the shaft and, as a result, frictional noise occurs at a frequency of once per revolution. Previously, to control

this problem, grease or a resin sleeve (heat-insulating sleeve) was placed between the shaft and the inner ring.

Through a special lubricating surface treatment on the bore surface of the inner ring, NTN has succeeded in decreasing the friction coefficient on the bore surface of the inner ring by 40%. As a result, the attitude of the inner ring is not disturbed in spite of the thermal expansion and bending on the fuser roller, and the inner ring can follow the motion of the roller, thereby frictional noise that would occur otherwise is prevented.

The result of the durability evaluation of the special lubricating surface treatment on the bore surface of the inner ring is shown graphically in **Fig. 8**. After the elapse of 600 operating hours under the test conditions summarized in **Table 8**, there was virtually no change in the inner ring bore diameter, and it is apparent that wear did not occur on the treated surface.

Table 8 Test condition of wear test for special lubricant film

	Test conditions
Test bearing	2TS3-6804ZZ $\phi 20\text{mm} \times \phi 32\text{mm} \times 7\text{mm}$
Bearing temperature (°C)	200
Running speed (min ⁻¹)	120
Radial load (N)	294
Shaft material/ surface roughness	A5052/Ra0.5

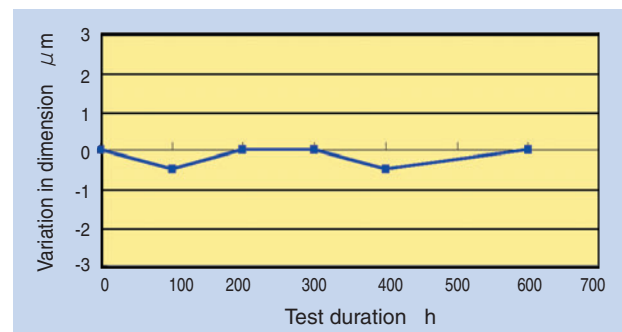


Fig. 8 Results of wear test for special lubricant film

5. Conclusion

As the functions of copying machines and printers have become increasingly diverse and sophisticated, the performance needs for the bearings in these machines has changed rapidly. **NTN** will further develop its bearing technology to help satisfy requirements for copying machines and printers and continue to contribute to achieving higher performance and energy conservation.

In closing this report, the author would like to encourage the readers to consult our General Catalog for Office Equipment Products (Catalog No. 8701/J), which presents **NTN's** products for office automation equipment, including rolling bearings, resin products, sintered products, torque limiter units, one-way clutch units and torque diodes.

Photo of author



Chikara KATAGIRI

Industrial Engineering Dept.
Industrial Sales headquarters

Unit Products for Office Equipment

Shoji ITOMI*
Atsushi MOROOKA*



The torque limiter and the torque diode are used for high-speed and medium-speed models of copiers and printers. NTN developed a new torque limiter and the torque diode that can be used also for a low-speed model.

1. Introduction of Ultra Compact Torque Limiter Units

1.1 Overview

Torque limiters are incorporated in the paper feeder sections of office automation equipment, such as photocopying machines and printers, to provide reliable paper stock separation. NTN has been supplying the NTS series of torque limiter units for many years, and they have been adopted by many customers.

Recently, needs have continued to increase for office automation equipment designs that use less space and are lighter weight. Given this, torque limiters and other paper feeder section components that are more compact are greatly needed.

Because of their sizes, the current NTS series products could force the designers of photocopiers and printers to make extra efforts to achieve space saving in their designs. To address these issues, NTN has developed the **NTB14 ultra-compact torque limiter unit**.

1.2 Optimization of internal structures

Each product of the current NTS series (hereafter referred to as the "old design") consists of an inner ring, a coil spring, an outer resin component and a lid.

The NTS series of products have a unique mechanism. When the torque working between the inner ring and the outer resin component is low, the inner ring rotates together with the outer resin component, but when the torque becomes greater, the inner ring rotates relative to the outer resin component while maintaining a certain torque remains between these members.

On the old design, the constricting force from the coil spring on the inner ring was utilized to control the rotary torque in the torque generation direction. In the inner structure of this old design, which is illustrated in **Fig. 1**, the coil spring consists of two sections that each has a unique diameter. The smaller diameter



Photo 1 Torque limiter

*Industrial Engineering Dept. Industrial Sales headquarters

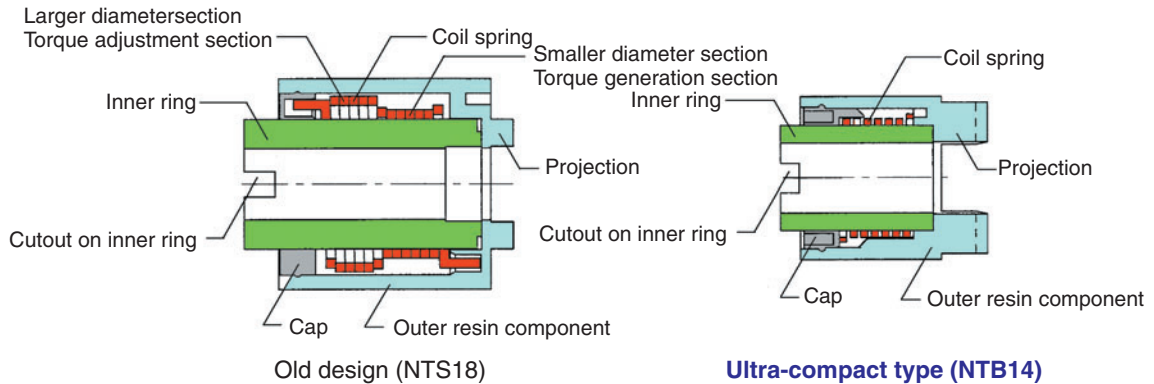


Fig. 1 Structure of current type (NTS18) and new type (NTB14)

section functions as a torque generation section, and the larger diameter section serves as a torque adjustment section. To set the torque, the lid is turned relative to the outer resin component to twist the larger diameter section, and the resultant constricting force causes the smaller diameter section of the coil spring to shrink to restrain the inner ring. On the old design, the end hooks of the coil spring are engaged with the outer resin component and the lid. Thus, the inner ring of the old design can rotate only in the torque generation direction.

The newly developed ultra-compact torque limiter unit (hereafter referred to as NTB14) does not have the large diameter section that is the torque adjustment section of the coil spring in the old design. Instead, the tightening allowance between the spring bore and the inner ring outer surface is responsible for control of the torque generated. As a result, the outer diameter and the length of the outer resin component on the NTB14 design are reduced. In addition, this novel structure has enabled the torque limiter to be capable of rotation in both directions.

1.3 Advantages of NTB14

1.3.1 Compact design

Old design (NTS18): 18 OD x 18 L (mm)

New design (NTB14): 14 OD x 12 L (mm)

Benefits of use

The torque limiter can be incorporated into the rubber rollers on the paper feeder section, so the sizes of the rubber rollers can be reduced in both diameter and length (**Fig. 2**). In addition, the number of parts associated with the rubber rollers may be decreased and the assembly procedure for the rubber rollers can be simplified.

1.3.2 Capability of rotation in both directions

The new design is capable of rotation in both directions.

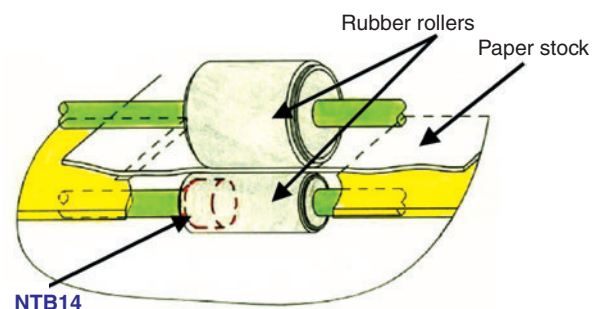


Fig. 2 Example of torque limiter and rubber roller all-in-one design

Benefits of use

Removal of jammed paper is easy.

1.3.3 Prevention of chemical attack

Like the old design, the new torque limiter has an inner ring made of an oilless sintered metal, in which the oil in the sintered metal does not pose risk of chemical attack to the resin components.

Benefits of use

- The new torque limiter does not pose problems to adjacent resin materials.
- Since the inner ring is made of an oilless sintered metal, there is no possibility of leaking lubricating oil, and no relubrication is necessary.

1.4 Durability

A typical result of a durability test is shown in **Fig. 3**.

The loss in torque with the new design is roughly equivalent to that with the old design. In other words, the durability of the new design is comparable to that of the old design.

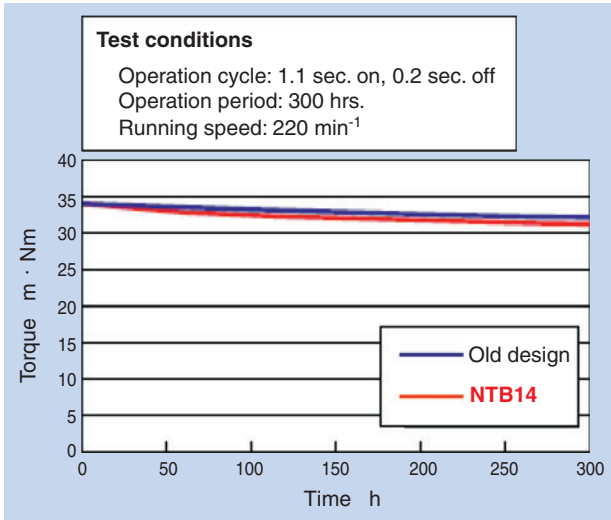


Fig. 3 Results of endurance test

1.5 Standard shape and materials used and torque setting

The standard shape of the NTB14 is illustrated in Fig. 4, and the materials used are listed in Table 1. Note NTN will supply non-standard shaped variants upon request.

Allowable torque setting range: 24.5–39.2 mN·cm {250–400 gf·cm}

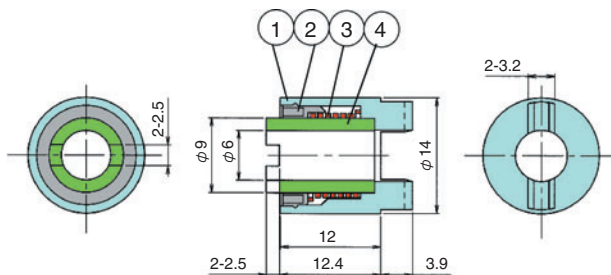


Fig. 4 Design of NTB14

Table 1 Composition and material of NTB14

Code	Component description	Material used
1	Outer resin component	Polyacetal resin (hue: black)
2	Lid	Polyacetal resin (hue: white)
3	Coil spring	Spring steel
4	Inner ring	Iron-based sintered material
—	Lubricant	Chemical attack-free oil (impregnated into the inner ring)

2. Introduction of the TDL16 Compact, Lightweight Torque Diode

2.1 Overview

To realize full-color capability, photocopying machines and printers are incorporating increasing numbers of components and movable parts. However, the floor space requirements of this equipment need to be roughly the same as with conventional monochromatic machines. Therefore, the need for more compact components is great. At the same time, demands are mounting for compliance with energy conservation and environmental regulations, as well as for satisfaction of requirements to acquire Blue Angel Mark certification. For these reasons, photocopying machine and printer manufacturers are making efforts to decrease power consumption for this type of equipment.

The lock-type torque diode can hold the drives for trays and other components in position with its reverse-input prevention function even when the equipment is powered off. For this reason, this type of torque diode is advantageous for saving energy compared to arrangements in which the drive is held in position by supplying power to the motor.

NTN has developed and continues to provide the TDL28 lock-type torque diode for office automation equipment. However, since its components are made of steel, it is heavy and structural limitations make development of a compact variant of this torque diode difficult. To address this challenge, NTN has developed the TDL16, a new torque diode that features both compact size and light weight.



Photo. 2 New type Torque Diode

2.2 Operating principle of lock-type torque diodes

A torque diode is essentially a reverse-input blocking clutch on which rotation on the input side is transmitted to the output side, but rotation on the output side is not transmitted to the input side. If the revolution on the output side is not transferred to the input side because the output shaft is locked, then the torque diode is defined as a lock type. If the revolution on the output side is not transferred to the input side because the output shaft rotates freely, then the torque diode is defined as a free type.

The operating principle of the lock-type torque diode is illustrated in Figs. 5 through 7.

When the input shaft is at a standstill, the rollers are forced by the spring to the wedge-shaped space between the inner ring cam surface, which is integrated with the output shaft, and the outer ring sliding surface. As a result, even when an attempt is made to turn the inner ring (integrated with the output shaft), the inner ring and outer ring are locked together and the inner ring does not turn (Fig. 5).

The input shaft and the cage rotate together, so when the input shaft rotates, the cage also rotates in the same direction. Then, the cage comes into contact with the roller to force the roller toward the larger side of the cam surface (toward the spring), releasing the lock (Fig. 6).

When the input shaft is further turned, the two surfaces on the input shaft come into contact with the two surfaces in the hole of the inner ring and force the inner ring (integrated with the output shaft) to rotate (Fig. 7).

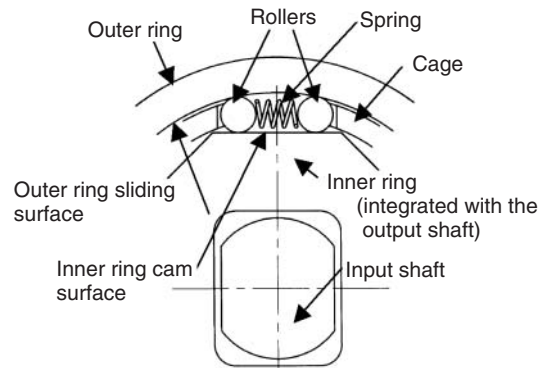


Fig. 5

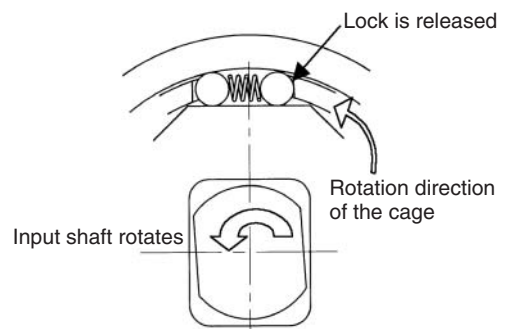


Fig. 6

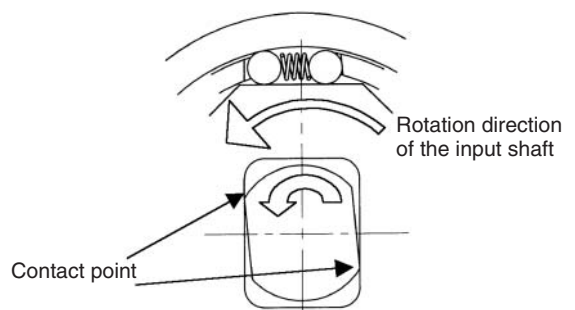
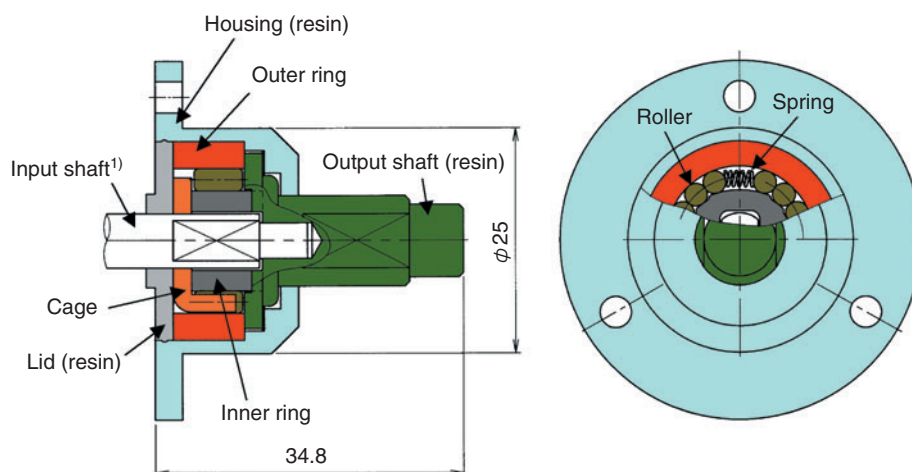


Fig. 7

2.3 Structure of the TDL16 compact, lightweight torque diode

The structure of the newly developed TDL16 compact, lightweight torque diode is illustrated in Fig. 8.



Note 1) The input shaft is not built into the torque diode.

Fig. 8 Structure of TDL16

2.3.1 Compact design

The structure of the old TDL28 is characterized in that the roller at each end of the spring is forced to the cam surface. In contrast, the TDL16 has a novel structure in which multiple rollers at each end of the spring are forced to the cam surface. Because of this arrangement, the outer diameter of the TDL16 is smaller than that of the TDL28 though both designs have the same number of rollers. Thus, the TDL16 has succeeded in minimizing the loss of load bearing capacity on the clutch.

In **Table 2**, the dimensions and limiting torque of the TDL16 are compared with those of the TDL28.

2.3.2 Lightweight design

By incorporating the resin components (output shaft, housing, lid) shown in **Fig. 8**, the authors' TDL16 compact, lightweight torque diode achieved weight reduction of 50% relative to the TDL28 (**Fig. 9**).

Table 2 Size and limiting torque of TDL16 and TDL28

	TDL16	TDL28
Shape	25 OD x 35.8 L (mm) (Note that the shape of the resin housing can be altered upon customer request.)	30 OD x 38.2 L (mm)
Limiting torque ²⁾	2.5N·m	4.9N·m

Note 2) These limiting torque values have been calculated based on the maximum surface pressures occurring on the cam surfaces. The useful operating life of a torque diode can vary depending on operating conditions.

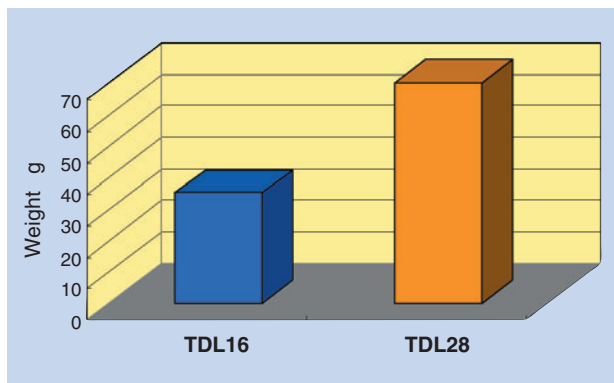


Fig. 9 Weight of TDL16 and TDL28

2.3.3 Durability

Under the test conditions summarized in **Table 3**, the TDL16 has successfully endured 300,000 cycles of load applications.

Table 3 Test condition of endurance test

Running speed	250min ⁻¹
Load torque	0.5 N·m (constant loading in one direction)
One cycle	Forward rotation for 2.5 sec.⇒standstill for 10 sec.⇒reverse rotation for 2.5 sec.⇒standstill for 10 sec.

3. Conclusion

NTN believes that their NTB14 ultra-compact torque limiter unit and TDL16 compact, lightweight torque diode positively contribute to space and energy conservation in photocopying machines and printers. NTN will further develop unit products to satisfy future market needs.

Photos of authors



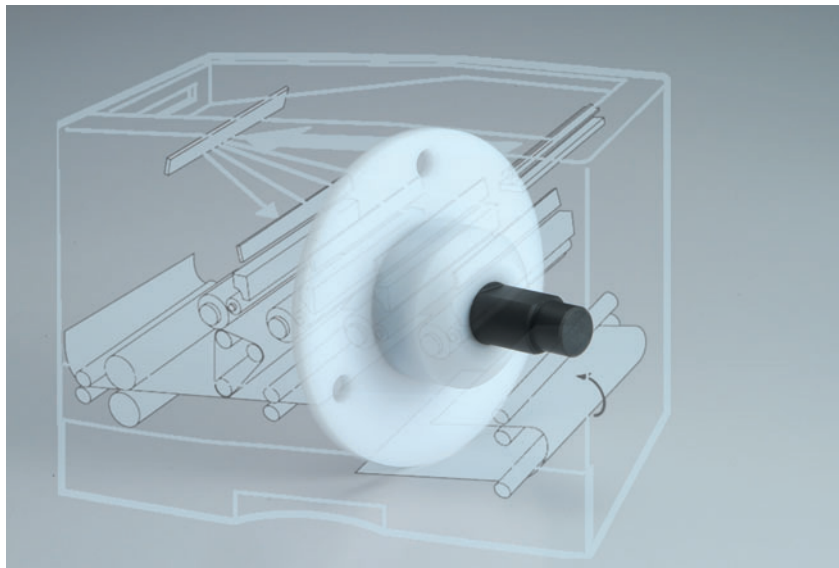
Shoji ITOMI

Industrial Engineering Dept.
Industrial Sales headquarters



Atsushi MOROOKA

Industrial Engineering Dept.
Industrial Sales headquarters



Honing Sludge and Electro Furnace Dust Briquetter

Shouzo GOTOH*
Kanji NAKAMURA*



Being an ISO14001-certified company, NTN is responsible for helping establish recycling technology to contribute to our recycling-oriented society. At first NTN started recycling grinding sludge with a grinding sludge briquetting machine, achieving Zero-emission with cost reduction. In 2002 NTN has established UNITOP, an environmental venture business based on briquetting technology. Honing sludge and electro furnace dust were picked up as the next targets. After testing, practical machines for honing sludge and electro furnace dust were developed. These machines will contribute to environmental load reduction.

1. Introduction

In 1998, the NTN Iwata Works became the first member of the NTN Group to acquire ISO 14001 certification. At that point, among NTN's waste, grinding sludge was the type that accounted for the largest environmental impact. In 1998, all of NTN produced approximately 8,000 tons of grinding sludge that was disposed of by industrial waste disposal agents. As a part of our efforts to acquire ISO 14001 certification, we began a commitment to recycling technologies with the aim of both recycling grinding sludge and reducing industrial waste disposal costs. Through the use of a solid-liquid separation technique for grinding sludge. We successfully established the recycling system that is illustrated schematically in Fig. 1. In 2000, we developed a grinding sludge recycling machine capable of commercial operation and began a full-scale grinding sludge recycling operation. Three years later, we succeeded in recycling nearly all the grinding sludge produced by the entire NTN Group. Consequently, we achieved "zero emissions" of waste, mitigating environmental impacts, which is the main objective of ISO 14001, as

well as cost reduction by eliminating industrial waste disposal expenses. To further promote our waste reduction efforts, in 2002, we founded UNI TOP, an environmental venture company that boasts a unique grinding sludge briquetting technique.

We have also succeeded in meeting the needs of our customers for technical assistance in their solid-liquid separation and solidifying efforts. We are now committed to the commercialization of a briquetter for honing sludge and electric-arc-furnace dust.

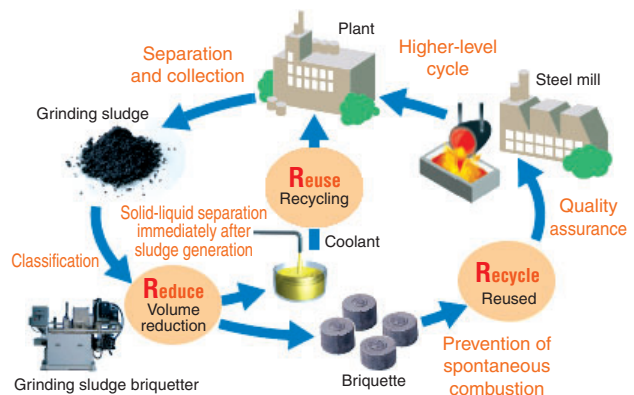


Fig. 1 3R recycling for grinding sludge

*Equipment Development Dept. Production Engineering R&D Center

2. Honing Sludge Briquetters

In 2004, NTN received a request from an automaker that wished for us to develop a briquetter that could solidify the sludge that results from the honing work on engine cylinder bores. We first attempted to meet this request with our grinding sludge briquetting technique. Regrettably, the sludge started to leak through the mechanical gaps between the die and the pressurizing shaft when pressurizing was begun. We investigated the cause of difficulty in solid-liquid separation and solidification, learning that the unique shape of the swarf (shavings) from the honing process is the cause. A microscopic photograph of honing swarf is shown in Fig. 2, while a microscopic photograph of grinding swarf is provided in Fig. 3. Through comparison of the two photos, it is apparent that grinding shavings are curled and can easily become entangled with each other, while honing shavings are rolled and cannot easily become entangled. To realize solid-liquid separation and solidification of honing sludge, the authors first tested a method, as shown in Fig. 4, in which the mechanical gaps are blocked with pieces of filter paper that allow only the coolant to drain away while retaining the honing swarf in the

honing sludge briquetting system. As a result, the authors verified that honing sludge could undergo solid-liquid separation and solidification through the use of this system.

Encouraged by this finding, the authors fabricated the prototype honing sludge briquetting system shown in Fig. 5. In the fall of 2005, this system was commissioned at a customer automaker's site and allowed to run continuously on a trial basis. The automaker was satisfied with the basic functions of this system. Fig. 6 illustrates the prototype machine schematically, and Fig. 7 shows the honing sludge used in the authors' test. Fig. 8 is a view of a briquette obtained from the authors' test, and Fig. 9 illustrates a view of the filtered and recovered coolant. For reference, a photographic view of the coolant in process is shown in Fig. 10. From a comparison of Fig. 9 and Fig. 10, the readers can see that the coolant is cleaned by filtration through solid-liquid separation and solidification using paper filters. The authors' newly developed honing sludge briquetter has the following advantages:

- 1) **Reliable solid-liquid separation and solidification: Labor time saving through stable operation**

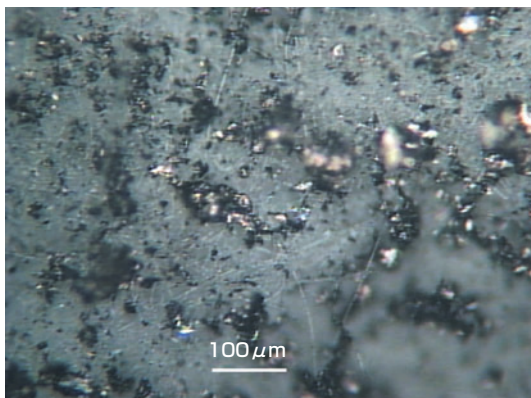


Fig. 2 Magnified honing swarf

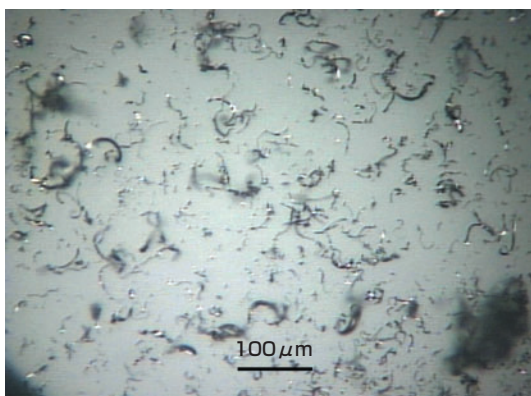


Fig. 3 Magnified grinding swarf

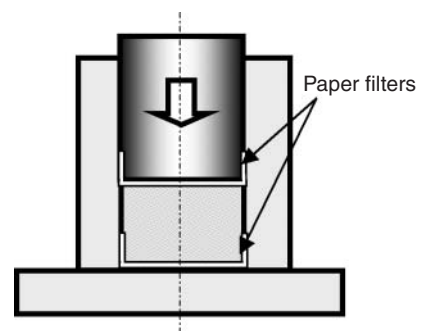


Fig. 4 Test method of honing sludge briquetting

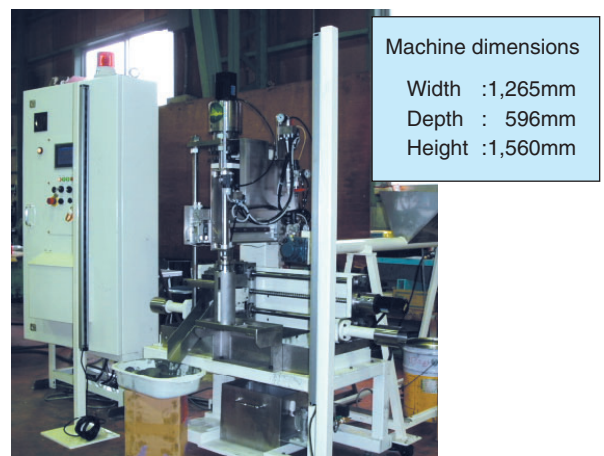


Fig. 5 Test machine for honing sludge briquetting

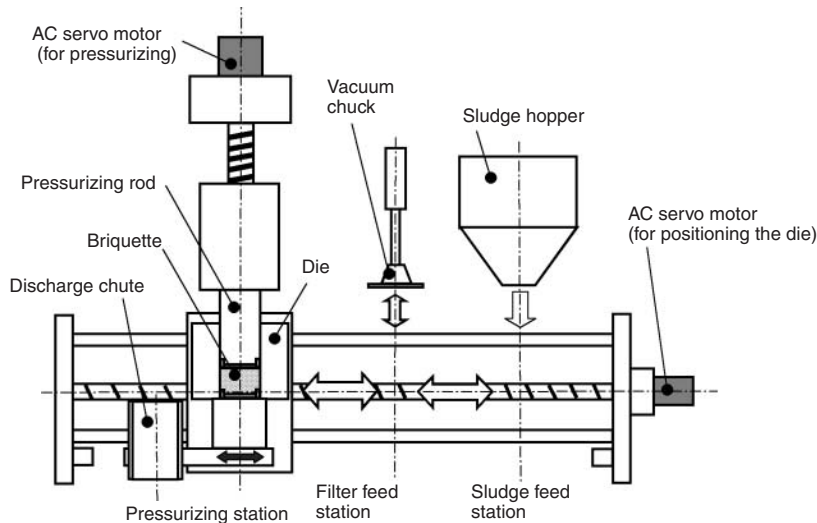


Fig. 6 Mechanism of horning sludge briquetter

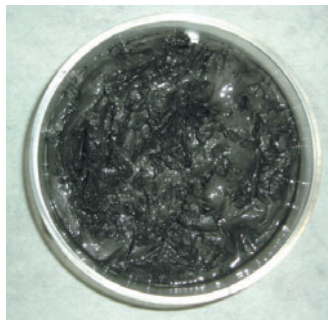


Fig. 7 Horning sludge



Fig. 8 Horning swarf briquette



Fig. 9 Recovered horning oil after paper filtration



Fig. 10 Horning oil in horning machine

- 2) **Separation into briquettes and clean coolant:**
Filtration is achieved in conjunction with solid-liquid separation
- 3) **Driven completely by electric power:** Energy saving, quiet running, optimal pressure control
- 4) **Compact design:** The briquetter can be installed onsite, so horning sludge can be processed immediately after generation

3. Electric Arc Furnace Dust Briquetter

In cooperation with Daiwa Steel Corporation, NTN has developed an electric arc furnace dust briquetter. By further advancing the technology that has been developed through its grinding sludge briquetters. This high-performance system is based on Daiwa's unique pelletizing technology and NTN's unique briquetting technology. In this system, electric arc furnace (EAF) dust and carbon are premixed and pelletized. The resultant pellets are loaded into the EAF dust briquetter without blending with a binder, which is often used in conventional EAF dust briquetters.

Incorporating a novel pelletizer, our EAF dust briquetter can produce briquettes of stable strength to help improve melting efficiency in the electric arc furnace. As a result, our EAF dust briquetter will lead to reductions in the amount of industrial wastes and electric power consumption for the furnace. In summary, our EAF dust briquetter can be defined as an eco-friendly system that will contribute to rapid recovery of investment.

3.1 EAF dust recycling

The concept for EAF dust recycling is shown in **Fig. 11**. The dust occurring in the electric arc furnace is captured with a filter. It is mixed with water and

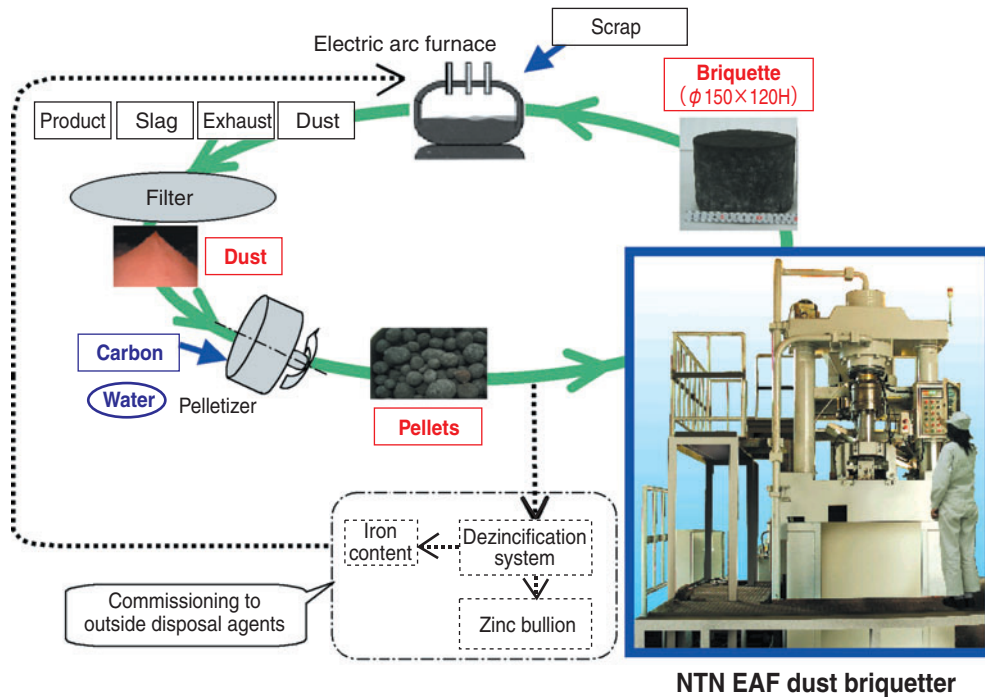


Fig. 11 Recycling of EAF (electric arc furnace) dust

carbon, which functions as a reducing agent and fuel, and the mixture is formed into pellets. The resultant pellets are not suitable for direct loading into an electric arc furnace due to their low mechanical strength and difficulty in handling. Therefore, the pellets are formed into briquettes with the authors' newly developed briquetter, and then the briquette is loaded into the electric arc furnace. Since EAF dust is repeatedly recycled, the concentration of zinc, which has a relatively low boiling point, in the EAF dust will increase and pose a problem in operating the electric arc furnace. Therefore, when the zinc concentration reaches a specific upper limit, the iron content is separated from the zinc content. The iron content is reloaded into the furnace while the zinc content is recycled as a valuable material.

Thanks to this recycling scheme, the disposal of EAF dust by landfill, no longer necessary. The number of zinc removal cycles can be decreased, thereby dramatically reducing the costs associated with industrial waste disposal.

3.2 Overview of the authors' briquetter

1) Formation principle

The principle of this briquette formation method is schematically illustrated in Fig. 12. The pellets are loaded into the die, and then the upper and lower punches apply force to the pellets in the die to convert the pellets into a briquette.

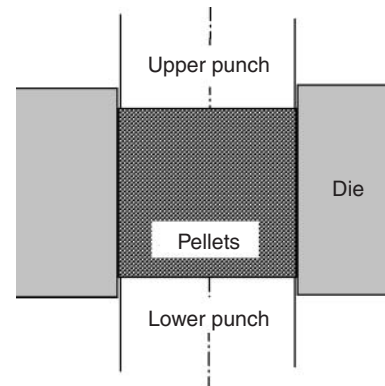


Fig. 12 Moulding method

2) Effects of various factors on the strength of briquettes

The authors investigated the effects of factors associated with materials and formation conditions on the mechanical strength of the briquettes obtained. The results of these investigations are shown in Figs. 13 through 16. The mechanical strength of the briquettes was translated into indexes by dropping each briquette from 1 meter above to a 5-cm thick layer of raw material powder and then counting the number of fractured pieces resulting. The greater the index is, the greater the mechanical strength of the briquette. By appropriately selecting the water and carbon content in the pellets and the formation

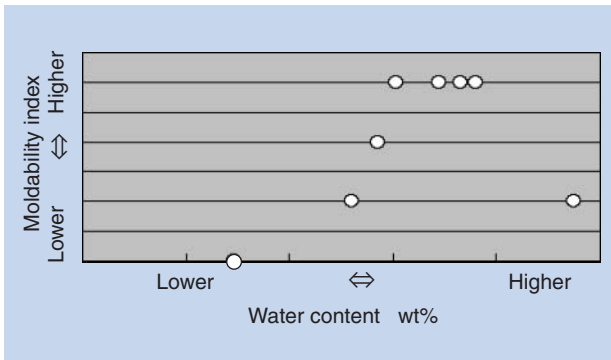


Fig. 13 Water content and briquette strength

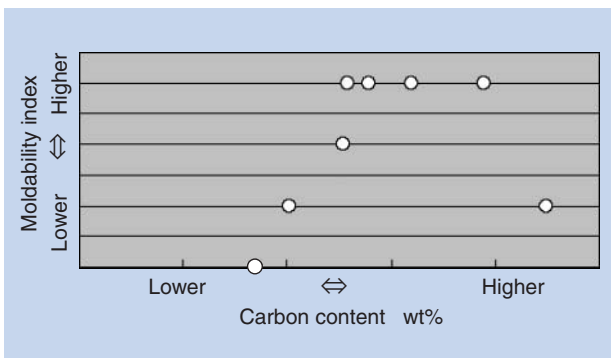


Fig. 14 Carbon content and briquette strength

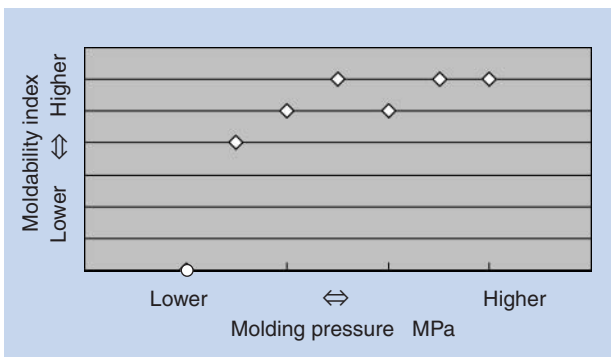


Fig. 15 Moulding pressure and briquette strength

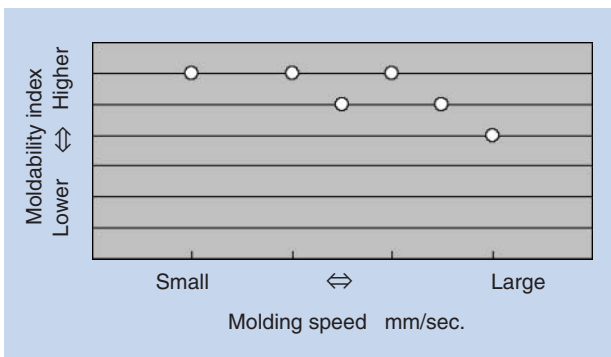


Fig. 16 Moulding speed and briquette strength

pressure for the briquette, the necessary formation strength can be obtained for the briquette. A lower formation speed is advantageous in attaining a higher briquette formation strength. However, the authors have selected an appropriate formation speed in consideration of the throughput of the briquetter.

3) Briquetter configuration

After the pellets are loaded into the inlet hopper, a cycle consisting of metering, water spraying, loading into the die, formation and discharge is executed automatically. Through setup for optimal briquetting conditions and rationalized machine design, stable briquette strength and higher productivity are attained. The major technical data for the authors' EAF dust briquetter are summarized in Table 1.

Table.1 Main specification of dust moulder

Model	HDM-150
Base materials	Pellets consisting of EAF dust, blended with carbon and water
Briquette size	Dia. 150 mm x 120 mm H, approx. 6.5 kg
Cycle time	17 sec
Machine size	3600 W x 5550 D x 4300 H (mm); weight: approx. 1500 tons
Throughput	800 tons/month (24 hours/day operation for 30 days)
Power supply	200 V, 3-phase, 50 kVA capacity

3.3 Advantages of the authors' technology

- 1) A pelletizing technology to produce pellets by adding a measured amount of carbon and water to the EAF dust, useful in obtaining briquettes of stable mechanical strength (patent pending).
- 2) This technology provides reliable briquetting of the pellets (patent pending).
- 3) The briquetter can be directly connected to the pelletizer to establish a fully automated briquetting system.
- 4) Non-processed EAF dust is not loaded into the furnace. This helps improve the working environment.

3.4 Benefits from adoption of the authors' briquetter

- 1) Prevention of EAF dust from being emitted as industrial waste and reuse of iron resources
⇒ Helps achieve zero emissions
- 2) Elimination of binder expenses, as well as the fees for commissioning briquetting work to an outside agent
⇒ First in the industry! Realization of briquetting without using a binder

- 3) Decrease electricity expenses through improvement of melting efficiency with electric arc furnaces (in comparison to conventional EAF dust recycling)
 - ⇒ Realization by mixing in carbon and use of heavier briquettes
- 4) By concentrating zinc, dramatic reduction in the amount of dezincification processing
 - ⇒ Improved melting efficiency leads to simpler dezincification process, which helps realize significant cost reductions
- 5) Significant cost-reduction for transportation to outside agents and improved logistics
 - ⇒ Significantly reduced burden of transportation to outside agents through improvements in dezincification process, etc.
- 6) Improved working environment, and simpler handling of briquettes
 - ⇒ No handling of powder is needed, greatly improving the working environment

4. Conclusion

Through further developments in these technologies as, described below, the authors strongly believe that NTN's unique honing sludge briquetting technology and EAF dust briquetting technology will contribute to the mitigation of environmental impacts.

Honing sludge briquetting technology

This technology will be applicable to various sludge types that cannot be solidified or briquetted with a grinding sludge briquetter. NTN is currently attempting to apply this unique technology to solid-liquid separation for ultrafinish-derived sludge so as to further mitigate environmental impacts from NTN's production activities.

EAF dust briquetting technology

The authors began the development work for this technology because it appeared to be advantageous in converting pellets into molded briquettes. Currently, we expect that our novel technology for directly converting powdered materials into briquettes will be commercialized and eventually adopted in various powder-solidification applications to realize the recycling of resources that were previously difficult to recover.

Photos of authors



Shouzo GOTOH

Equipment Development Dept.
Production Engineering R&D Center



Kanji NAKAMURA

Equipment Development Dept.
Production Engineering R&D Center

Ultra-Clean Bearing for Clean Environments

Ryouichi NAKAJIMA*
Masaaki HONDA*



NTN manufactures Ultra-Clean bearings for clean environments used for a semiconductor and LCD panel fabrication equipments, vacuum evaporation systems, etc.

NTN developed Ultra-Clean NC bearings and Ultra-Clean WB bearings to supply the demand for a long-life under high temperature and heavy load conditions.

1. Overview

Extremely low dust generation is needed for the bearings used in the systems and machines that manufacture semiconductor devices and liquid crystal display panels, as well as for those used in the vacuum evaporation systems for these products. Recently, demand has been mounting for longer maintenance intervals for these devices and systems. Given these demands, the bearings used in these situations must be capable of durable operation in high-temperature and high-load environments. To address these engineering challenges, NTN has developed a unique lubrication system, and with this, they have successfully developed unique Ultra-Clean NC bearings that feature long life in vacuums under high bearing pressure and unique Ultra-Clean WB bearings that boast long life in high-temperature environments. This report introduces these unique bearings.

Conventional oil-impregnated resin cages are made of sintered resin materials, and, consequently, their porosity, the ratio of pores to retain lubricating oil, was 20% at maximum. In contrast, NTN's newly developed



Fig. 1 Ultra-Clean NC bearing
NC : Network Cell

2. Introduction to NTN Ultra-Clean NC Bearings (Fig. 1)

For lubrication, the authors adopted a porous resin cage that was developed independently by NTN. This cage is impregnated with a low-vapor-pressure oil (Fig. 2).

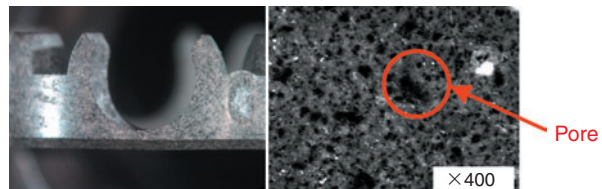


Fig. 2 Porous resin cage

*Industrial Engineering Dept. Industrial Sales headquarters

oil-impregnated porous resin cage features 35% or higher porosity thanks to a special manufacturing technique, allowing this cage to retain more lubricating oil. Compared to conventional ultra-clean bearings, NTN's new ultra-clean bearings are capable of longer life while maintaining low dust generation in high load applications.

2.1 Evaluation of various characteristics

2.1.1 Evaluation of dust generation characteristics

Under the test conditions summarized in **Table 1**, the test bearing was allowed to run for 150 hours, and the amount of resultant dust generated during the duration of the test was measured. As summarized in **Fig. 3**, the dust generated with the Ultra-Clean NC bearing was equivalent to the amount generated by bearing types usually used for clean applications (a low-dust-generating pre-filled-grease type for vacuum-use and a special PTFE-coated type).

2.1.2 Rotating torque

NTN evaluated the rotating torque for the Ultra-Clean NC bearing under the test conditions summarized in **Table 2**. As illustrated in **Fig. 4**, the Ultra-Clean NC bearing features a lower torque compared to the conventional bearing (special PTFE-coated type).

Table 1 Test conditions of dust generation

Test bearing	Deep groove ball bearing (#608) $\phi 8 \times \phi 22 \times 7$ mm
Degree of vacuum	10^{-5} Pa
Running speed	50 min ⁻¹
Size of particles being counted	0.2 μ m or greater
Thrust load	9.8N
Temperature	Ordinary temperature
Duration	150 hrs.

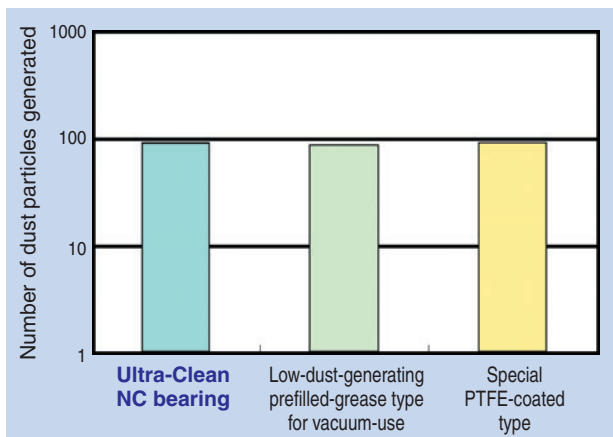


Fig. 3 Results of dust generation test

Table 2 Test conditions

Test bearing	Deep groove ball bearing (#608) $\phi 8 \times \phi 22 \times 7$ mm
Degree of vacuum	10^{-5} Pa
Running speed	500 min ⁻¹
Temperature	Ordinary temperature
Thrust load	196N

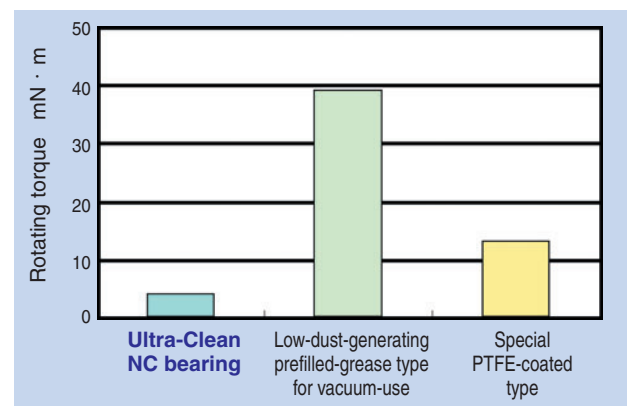


Fig. 4 Results of rotating torque

2.1.3 Endurance evaluation

Each bearing type was evaluated at each of the three thrust load levels specified in **Table 3**. As can be seen from the data in **Fig. 5**, the Ultra-Clean NC bearing boasts a longer life in all three loading

Table 3 Test conditions of endurance test

Test bearing	Deep groove ball bearing (#608) $\phi 8 \times \phi 22 \times 7$ mm
Degree of vacuum	10^{-5} Pa
Running speed	500 min ⁻¹
Temperature	Ordinary temperature
Thrust load	196N, 686N, 981N
End of life criterion	The point when a sudden increase in torque occurred

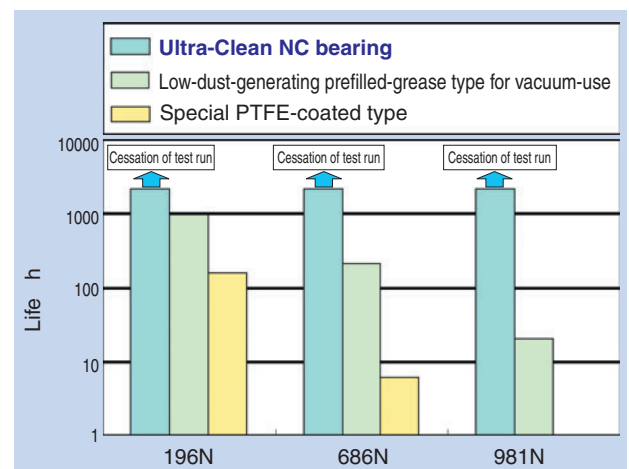


Fig. 5 Results of endurance test

conditions when compared to the conventional bearings. In particular, under a high-loading condition, the life of the authors' Ultra-Clean NC bearing is more than 10 times as long compared to the conventional bearings subjected to the same demanding conditions.

3. Introduction to NTN Ultra-Clean WB Bearings (Fig. 6)

Aware of the lubricating power of tungsten disulfide (hereafter, "WS₂"), NTN adopted one rolling element made of this material (Fig. 7) in the Ultra-Clean WB bearing. When the WS₂ rolling element rolls in the bearing, WS₂ is transferred onto the rolling surface and functions as a solid lubricant. Additionally, since WS₂ can withstand a maximum temperature of 400°C, which is much higher heat resistance compared to conventional special PTFE coating, the Ultra-Clean WB bearing is an ideal choice for vacuum and high-temperature environments such as those on vacuum evaporation systems and sputtering systems.



Fig. 6 Ultra-Clean WB bearing
WB : WS₂ Ball
Lubrication with tungsten disulfide ball

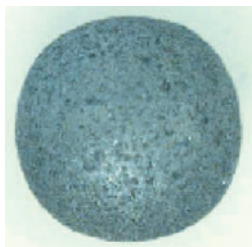


Fig. 7 WS₂ ball

3.1 Evaluation of various performance considerations

3.1.1 Rotating torque

Under the test conditions summarized in Table 4, the rotating torque of the Ultra-Clean WB bearing in a vacuum was evaluated. As can be seen from the

results in Fig. 8, the rotating torque with the Ultra-Clean WB bearing is much lower than that with the conventional bearing (special PTFE-coated type).

Table 4 Test conditions of rotating torque

Test bearing	Deep groove ball bearing (#608) φ8×φ22×7 mm
Degree of vacuum	10 ⁻⁵ Pa
Running speed	500 min ⁻¹
Temperature	Ordinary temperature
Thrust load	196N

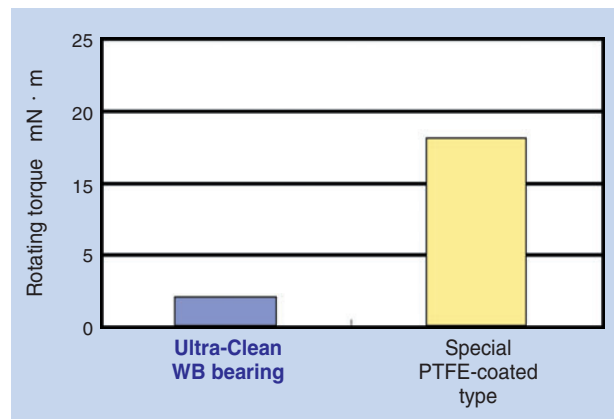


Fig. 8 Results of rotating torque

3.1.2 Endurance

1) High-temperature (300°C) endurance test

The applicable test conditions are summarized in Table 5, while the test results are illustrated in Fig. 9. The life of the Ultra-Clean WB bearing is more than five times as long as that of the conventional bearing (special PTFE-coated type).

2) High-load endurance test

The test conditions used are summarized in Table 6, while the test results obtained are illustrated in Fig. 10. The life of the Ultra-Clean WB bearing is more than nine times as long as that of the conventional bearing (special PTFE-coated type).

4. Conclusion

Products incorporating flat panel displays, such as personal computers and flat-panel TV sets, have become used more commonly, and demands are growing rapidly for bearings capable of use in the clean-environment manufacturing systems for these products. NTN believes that our Ultra-Clean NC bearings and Ultra-Clean WB bearings, which are enhanced variants of conventional Ultra-Clean

Table 5 Test conditions

Test bearing	Deep groove ball bearing (#608) $\phi 8 \times \phi 22 \times 7$ mm
Degree of vacuum	10^{-5} Pa
Running speed	$1,550 \text{ min}^{-1}$
Temperature	300°C
Thrust load	9.8N
End of life criterion	The point when a sudden increase in torque occurred

Table 6 Test conditions

Test bearing	Deep groove ball bearing (#608) $\phi 8 \times \phi 22 \times 7$ mm
Degree of vacuum	10^{-5} Pa
Running speed	500 min^{-1}
Temperature	Ordinary temperature
Thrust load	256 N
End of life criterion	The point when a sudden increase in torque occurred

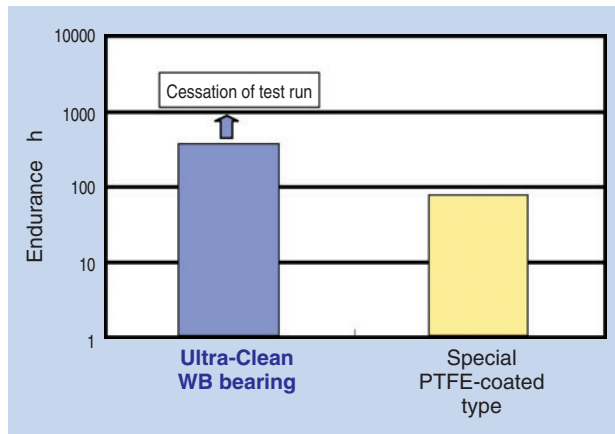


Fig. 9 Results of high temperature endurance test

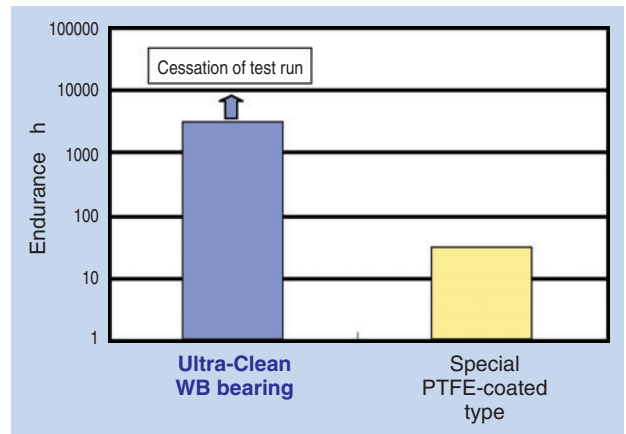


Fig. 10 Results of heavy load endurance test

Table 7 Performance of Ultra-Clean bearing series

	Ultra-Clean bearing	Ultra-Clean bearing	Ultra-Clean NC bearing	Ultra-Clean WB bearing
Lubrication system	Special PTFE-coating	Low dust-generating vacuum grease	Porous resin cage + low vapor pressure oil	Tungsten disulfide (WS ₂)
Temperature range tolerance (°C)	~+260	~+200	~+150	~+400
Degree of vacuum tolerance (Pa)	10^{-6} ~atm	10^{-5} ~atm	10^{-5} ~atm	10^{-5} ~atm
Load bearing capacity	△	◎	◎	◎
Low torque feature	○	△	◎	◎
Dust generation	◎	◎	◎	△
Corrosion resistance	△	△	△	△

◎ : Optimal ○ : Good △ : Acceptable

bearings, will satisfy the characteristics required of these manufacturing systems: low dust generation, tolerance of high vacuum conditions, and higher levels of endurance and heat resistance. NTN has already added new products to its Ultra-Clean bearing Series (see **Table 7**). We will continue to develop unique products that satisfy market needs, and we hope to contribute to improvements in various vacuum systems by helping extend their maintenance intervals and reduce their energy consumption.

Photos of authors



Ryouichi NAKAJIMA

Industrial Engineering Dept.
Industrial Sales headquarters



Masaaki HONDA

Industrial Engineering Dept.
Industrial Sales headquarters

Development of New RCT Bearing for Axleboxes and Insulated Bearing with Shields

Ryutaro OKA*



In recent years railroad carriages have been increasingly considered to be eco-friendly, energy efficient, and are viewed as a good means of transportation. Demand for railroad bearing business grows greatly in China and Europe.

High reliability is sought after in a bearing for railroad applications because of public visibility. There is also a strong demand from the railroad companies for longer time between maintenance periods.

Therefore the problems facing railroad bearings is how to effectively maintain reliability and extend the time between

maintenance periods. NTN has developed an Insulated Bearing with shields and the new RCT Bearing, which could solve these problems and satisfy the Chinese and European markets. This report discusses laboratory evaluation test results concerning the performance of Insulated Bearings with shields and the new RCT Bearing.

1. Introduction

Recently, the usefulness of rolling stock has been appreciated even more because trains are increasingly regarded as an eco-friendly means of transportation that excels in energy efficiency. In particular, there have been serious efforts for the construction of intercity railway infrastructure and the introduction of high-speed railway systems in China. Furthermore, in the European market, which accounts for 50% of the world's railway equipment demand, higher train speeds are needed to accommodate the recent expansion of the EU. Thus, in these markets, the demands for rolling stock bearings have been increasing dramatically.

The typical bearings for rolling stock include traction motor bearings for power transmission systems, drive system bearings used in the gearboxes (drives) that transmit the motor output to the axles, and axle bearings that support the weights of the train cars. Each of these bearings is a critical component whose performance directly affects the operation of railroads, and, therefore, they must all be highly reliable. At the same time, the end users who operate the trains are demanding longer maintenance intervals. Therefore,

the manufacturers of bearings for rolling stock now have to address the challenge of realizing longer maintenance intervals while maintaining high levels of bearing reliability.

Recently, we have developed unique bearing products to address these challenges and to fulfill the needs of the very promising Chinese and European markets. They are our new RCT bearings for axleboxes, which is a line of high performance axlebox bearings and our sealed insulated bearings for traction motors. This report describes the results of evaluation tests for our new RCT bearing for axleboxes and our sealed insulated bearings.

2. New RCT Bearings

In the European rolling stock axlebox bearing market, metric-series bearings have been used commonly, and such bearings are also often adopted in the Chinese rolling stock market. We have recently developed a new line of RCT bearings for axleboxes that satisfy the EN standards, which are commonly adopted in the European and Chinese rolling stock markets.

***RCT bearings: sealed double-row tapered roller bearings used on rolling stock axles.**

*Industrial Engineering Dept.

2.1 Development of the New RCT Bearing

We incorporated the three new technologies below in a conventional RCT bearing to develop our new RCT bearing, and we subjected this new product line to evaluation tests according to the relevant EN standards. The features of the new technologies and the test results are provided below:

- 1) Adoption of a resin cage
- 2) Adoption of an anti-fretting plate
- 3) Adoption of a light contact seal

2.2 Resin cage

The resin cage is made of a special resin material featuring impact resistance and is expected to provide longer lubrication life and boast better mechanical strength.

Verification of the benefits of adopting a resin cage

- 1) Inhibition of the occurrence of wear dust (iron dust)

The occurrence of iron dust from a steel cage in grease was compared with the occurrence from a resin cage. Consequently, we have verified that use of a resin cage can effectively inhibit the occurrence of iron dust on running bearings.

Test bearing

Double row tapered roller bearing (120 ID x 220 OD x 155/160mm)

Test conditions

Table 1 Condition of endurance test

Bearing speed (min ⁻¹)	Run pattern at 2125 min ⁻¹
Radial load (kN)	48.0±9.8
Axial load (kN)	0±14.7
Lubrication system	Grease lubrication
Run duration	Equivalent to 700,000 km of travel

Test results

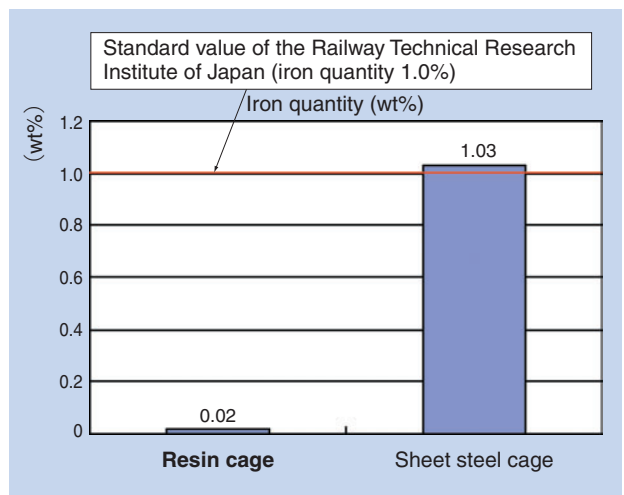


Fig. 2 Quantity of iron in grease after endurance test

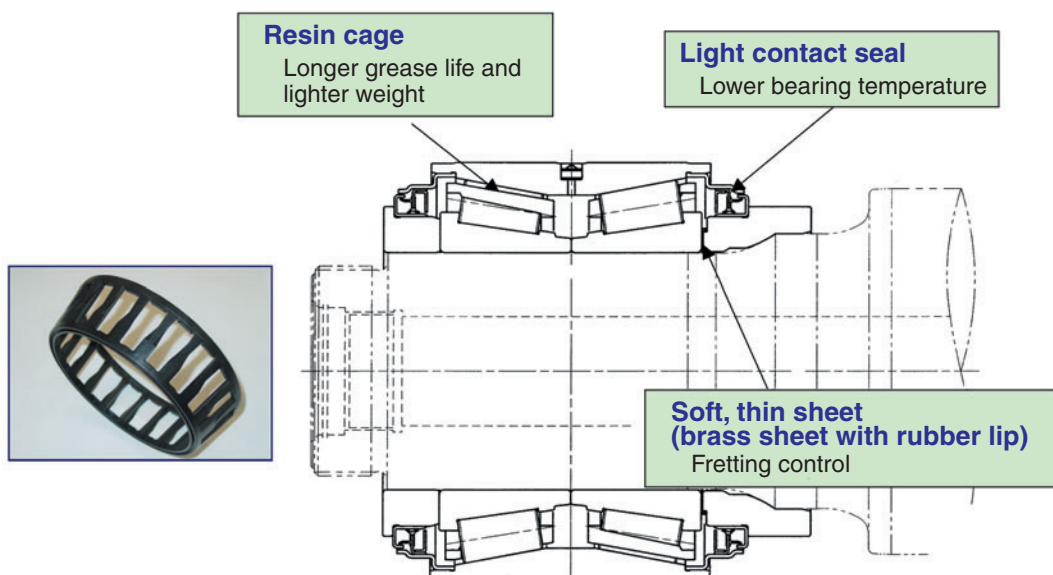


Fig. 1 New RCT Bearing

2) Cage with improved mechanical strength

A fall impact test was performed and determined that the resin cage excels in mechanical strength compared to the current NTN steel plate cage type, which has been performing well and has been accepted favorably in the bearing market.

Test conditions

Table 2 Condition of fall impact test

Vibration acceleration (m/s ²)	9800 (fall height: 80 mm)
Fall cycle frequency (cpm)	30

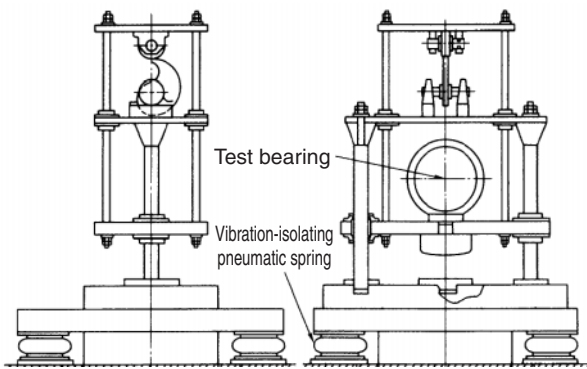


Fig. 3 Fall impact test machine

Test results

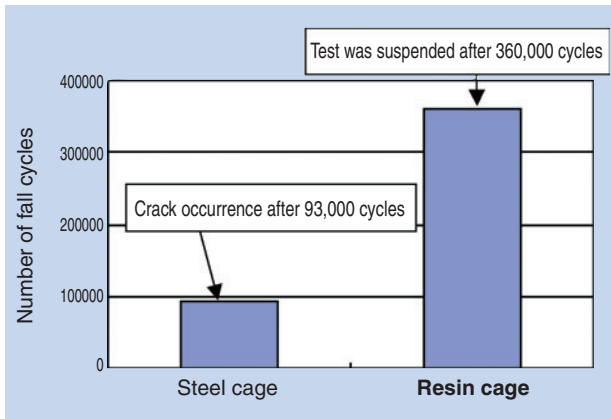


Fig. 4 Test result of fall impact test

2.3 Verification of the effectiveness of anti-fretting measures

The state of the backing rings after an endurance test was investigated. As a result, we learned that our anti-fretting measure is effective.

Test conditions

Table 3 Test condition of prevention of fretting test

Bearing speed (min ⁻¹)	2125 (equivalent to train operation at 330 km/h)
Radial load (kN)	54.9
Axial load (kN)	6.5
Run duration (h)	7273

Test results

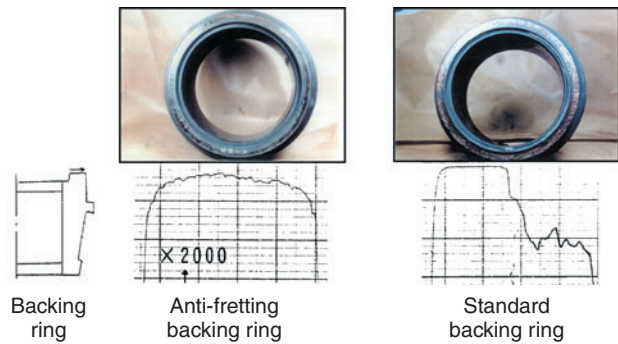


Fig. 5 Form of backing ring width after examination

2.4 Verification of the effectiveness of a light contact seal

Through rotation tests, the run temperature on the light contact seal was compared with that of a standard seal (with spring). As a result, it was discovered that compared with the standard seal, the lip temperature of the light contact seal is about 20°C lower. (The temperature measurement point was about 2 mm directly beneath the lip on the seal sliding section.)

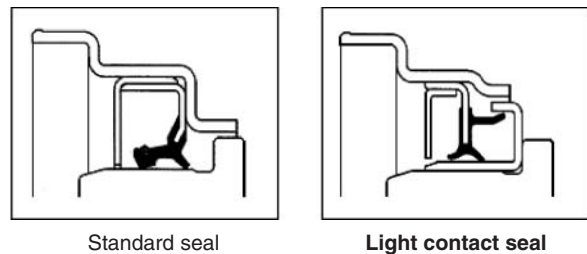


Fig. 6 Shape of oil seal

Test conditions

Table 4 Test condition of light contact seal

Radial load (kN)	68.3
Axial load (kN)	13.6
Bearing speed (min ⁻¹)	2216 (equivalent to train operation at 330 km/h)
Run pattern	Repeated forward/backward running cycles (according to EN standard)

Test results

Table 5 Test result of light contact seal

		Outer ring A row	Outer ring B row	Seal A row	Seal B row	Axlebox
Standard seal	Max	56.6	56.5	73.9	78.4	50.5
	Ave	50.3	49.9	65.2	69.6	45.2
Light contact seal	Max	44.2	46.4	45.9	52.8	41.5
	Ave	41.3	42.7	43.0	49.6	38.7

Note: data converted to equivalent value in a 20°C environment

2.5 Result of EN standard running test

The samples were subjected to a running test that conforms to the relevant EN standard. As a result, it has been verified that the new RCT bearing satisfies the EN standard.

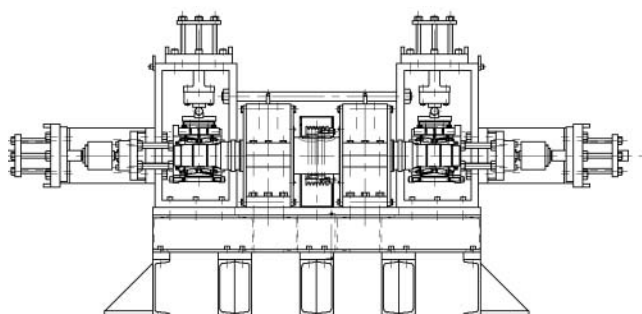


Fig. 7 Test machine for Journal bearing

Test conditions

Table 6 Test condition of EN standard

	Running-in operation				Endurance test
Bearing speed (rpm)	554	1108	1662	2216	2216
Train speed (km/h)	83	165	248	330	330
Radial load (kN)	68.3				
Axial load (kN)	3.4	6.8	10.2	13.6	13.6
Cooling air speed (m/s)	Approx. 10 (0 when no rotation is in progress)				
Run duration (h)	24 for each step				2910

Axial loading: One loading cycle consists of a 5-second loading period and a 5-second no-loading period (bi-directional)

Test results

Table 7 Test result of EN standard

			Bearing 1	Bearing 2	EN standard
Running-in operation	Peak value	Inner ring	97.9	98.8	—
		Outer ring	80.1	78.5	—
	Value at stable state	Inner ring	45.7	47.9	5°C or lower for 2 hours
		Outer ring	37.3	36.8	
Endurance test	Value at stable state (average value)	Inner ring	43.9		90 or lower
		Outer ring	34.1		
	Difference in outer ring temperature between Bearing 1 and Bearing 2		15 or lower		20 or lower
	Difference in outer ring temperature between adjacent cycles		10 or lower		20 or lower

2.6 Summary

By adopting a resin cage, a light contact seal and an anti-fretting measure, NTN has realized a journal bearing that satisfies the EN standard and is capable of extending maintenance intervals while ensuring a high degree of reliability.

3. Sealed Insulated Traction Motor Bearing

In order to realize higher train speeds as well as to promote increased use of LRVs, electric motors that are more compact are greatly needed to realize lighter trains. At the same time, railway companies are demanding extended maintenance intervals to decrease maintenance costs.

Currently, traction motor bearings are relubricated after every 600,000 to 900,000 km of operation. The maintenance intervals of traction motors are usually governed by the lubrication lives of the bearings, and can vary depending on whether or not the traction motor is a brushless design and whether or not the lubricant is an insulating type. Therefore, until now, long-life greases have been developed in an attempt to extend lubrication life. Since bearing life is extended only when the bearing is effectively lubricated for a long period, the importance of the structure around the bearing, including the grease pockets, has been attracting attention.

NTN has recently developed a sealed insulated bearing that allows compact design and does not need maintenance work for up to 1,200,000 operating km.

3.1 Features of sealed insulated bearings

The traction motors for rolling stock, such as those on Shinkansen high-speed trains, use insulated

bearings with outer rings that have insulation layers on their outer circumferential surfaces and side faces. The outer ring of the insulated bearing has an annular seal to provide grease pockets in order to extend the lubrication life of the bearing.

To ensure insulation performance, the annular seal is made of a resin, and its inner profile has a special form to prevent grease leakage even under demanding conditions of high temperature and severe vibration. Compared with the conventional design, the size of the new design is much more compact.

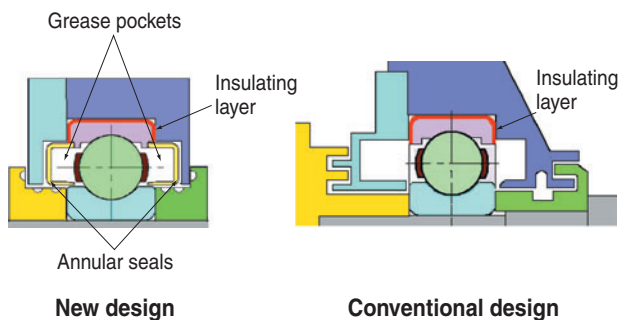


Fig. 8 Structure of sealed insulated bearing

3.2 Performance evaluation test

1) Insulation performance

The effect that the seal groove formed on the outer ring has on the insulation resistance performance was investigated. As a result, it has been verified that the insulation resistance with the new insulated bearing is 1000 MΩ or higher (relative to an applied voltage of 500 V), which is equivalent to that of current ceramic insulated bearings.

2) Rotation vibration test

The new insulated bearing was subjected to a rotation vibration test. As a result, it has been verified that under operation with vibration, the new bearing does not develop grease leakage or a loose seal.

Test bearings

NU214 and 6311

Test conditions

Table 8 Condition of rotation test with vibration

Bearing speed (min ⁻¹)	6500
Radial load (kN)	1.5
Ambient temperature (°C)	25±5
Axlebox vibration acceleration (m/s ²)	300
Vibration frequency (Hz)	(Sweep between the upper and lower frequencies in a 50-sec. period)

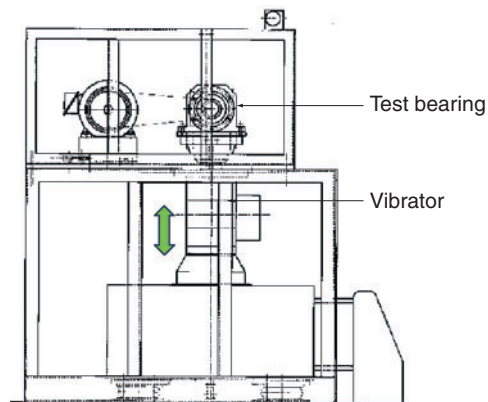


Fig. 9 Test machine with vibration

Test results

Neither NU214 nor 6311 developed grease leakage or loose seals.

3) Operation performance and endurance test

i) Rapid acceleration test

The temperature characteristics of the test bearings in rapid acceleration were determined. Consequently, it has been verified that each test bearing was capable of problem-free operation without developing rapid temperature rise or grease leakage.

Test bearings

NU214 and 6311

Test conditions

Table 9 Test condition of high speed

Bearing speed (run pattern) (min ⁻¹ × min)	1800 × 60 → 6180 × 30 → 8600 × 2 (The acceleration for all the run patterns was 242min ⁻¹ /s.)
Radial load (kN)	2.6

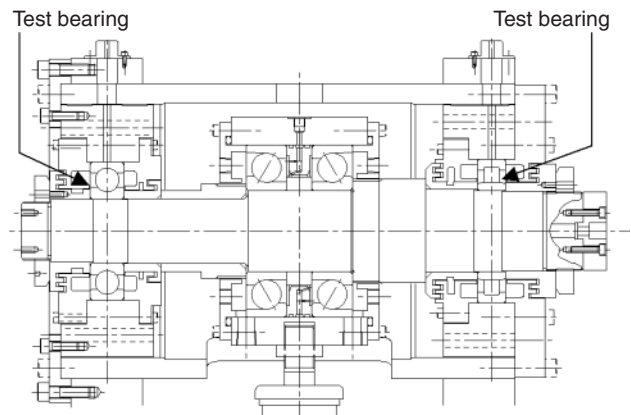


Fig. 10 Test machine for traction motor bearing

Test results

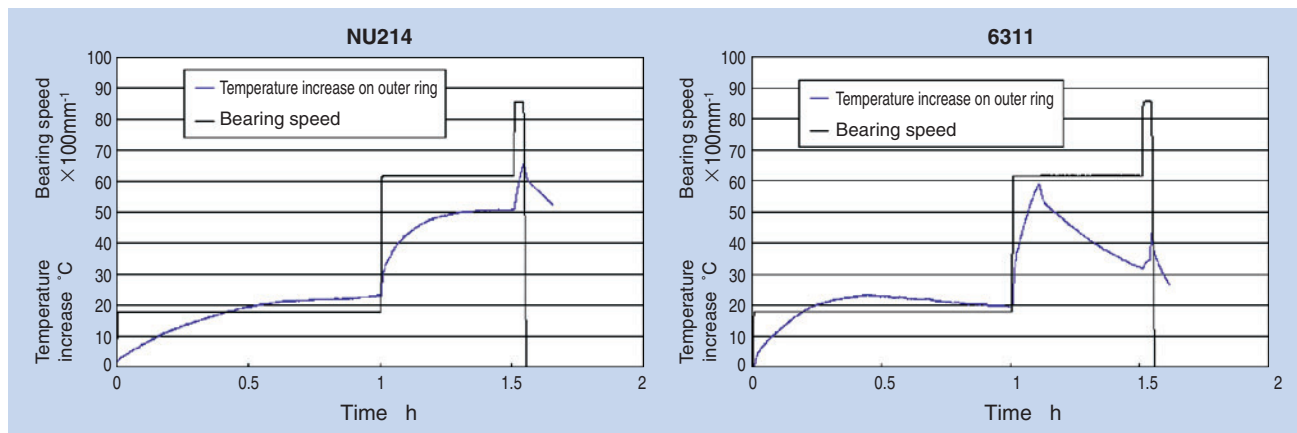


Fig. 11 Result of high speed test

ii) Endurance test

An endurance test simulating 2,400,000 km of travel was executed. The new insulated bearing did not develop grease leakages or experience rapid temperature increases. Deterioration of the bearing and grease after the endurance test was minor, and the bearing still remained fully operative.

Table 10 Result of Grease analysis after endurance test

Sample	X-ray fluorescence spectrometry (wt%)		Spreading consistency	Oil separation ratio (%)
	Fe	Cu		
NU214	0.03	0.02	200	6.2
6311	0.05	—	220	3.2
Fresh grease	0.00	0.00	250	—
Railway Technical Research Institute control value	0.5 or lower	0.3 or lower	150~350	30 or lower

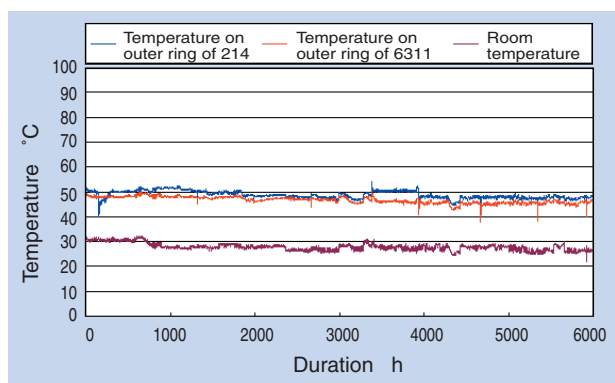


Fig. 12 Result of endurance test

3.3 Summary

NTN has successfully developed a novel traction motor bearing that boasts insulation resistance and high-speed running performance comparable to conventional ceramic insulated bearings and is capable of longer maintenance intervals due to its enclosed construction.

4. Conclusion

NTN's newly developed RCT bearings for axleboxes and sealed insulated bearings have been described and the results of tests with them have been presented.

The need for safer and more reliable rolling stock will continue to grow. At the same time, railway operators worldwide will further demand decreased maintenance costs for their rolling stock.

NTN's newly developed RCT bearings for axleboxes and sealed insulated bearings described above constitute useful means for extending the maintenance intervals and improving the reliability of the journal bearings that represent the most critical rolling stock components.

References

- 1) Suzuki M. et al.: Degradation of Lubricants Used in Electric Cars

Photo of author



Ryutaro OKA

Industrial Sales
headquarters

High Load Capacity Cylindrical Roller Bearings

Takuya OZU*



NTN has developed high load capacity cylindrical roller bearings appropriate for gearbox of wind turbines and other industrial machinery.

By using "Keystones" instead of the conventional cage, the new bearings have increased the load capacity without reducing speed performance.

As a result, the new bearings have 1.5 times or more the rating life of current caged bearings.

1. Introduction

The gearbox on wind turbines is located high off the ground and is therefore difficult to access for service. Therefore, the bearings in the gearbox must provide long life with a high degree of reliability. Even though the size of wind energy farms has been growing in recent years, demand for smaller, lighter nacelles have been on the rise in order to mitigate loads on towers. Given this, compact bearings for gearbox applications that boast greater load carrying capacity are greatly needed.

In response to these needs, NTN has developed a unique high load capacity cylindrical roller bearing product (Fig.1) that incorporates keystones in place of a cage. As a result, our new cylindrical roller bearing product boasts a greater load bearing capacity without loss in running performance. The rated life of the new product is more than 1.5 times longer than that of conventional caged cylindrical roller bearings.

2. Structure and Features

In the new NTN design, resin-made keystones are situated between the rollers to prevent roller-to-roller contact. Since these keystones are independent of each other, tensile stress otherwise resulting from roller-to-roller contact and separation does not affect them. As a result, the size and number of the rollers can be increased because the keystones can be thinner (Fig. 2).

In Table 1, the performance of the new design is compared with that of a conventional design.

• Longer life

The size and the number of the rollers are optimized to enhance the load carrying capacity of the bearing. As a result, a rated life that is more than 1.5 times as long as that of a conventional caged bearing design.

• Higher speed

Roller-to-roller contact occurring on full complement roller bearings is avoided by use of a unique keystone design. Through optimization of the shape and roller guiding scheme with the keystones, limiting speed and smearing resistance equivalent to a caged design have been achieved.

*Industrial Engineering Dept. Industrial Sales headquarters

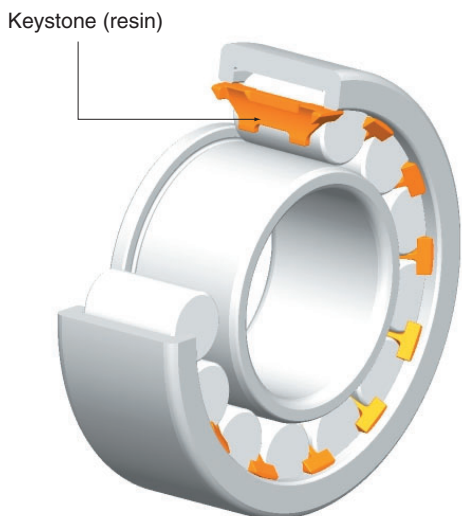


Fig. 1 High Load Capacity Cylindrical Roller Bearings

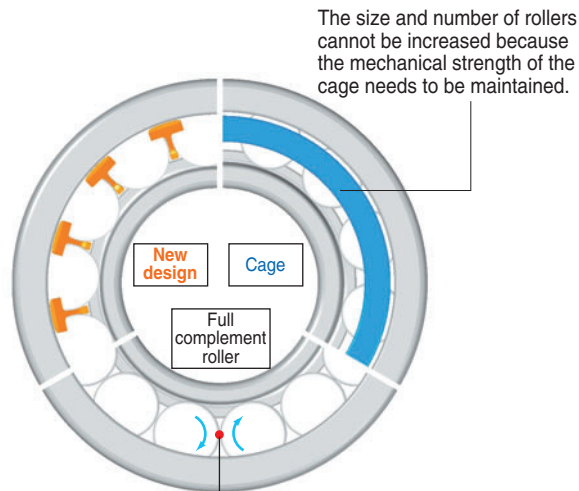


Fig. 2 Comparison of structure with conventional CRB

• Handling ease

Even when the inner ring is removed, the rollers on the keystone design do not disassemble. Thanks to this feature, the inner ring and outer ring sub-assembly can be handled independently, leading to easy bearing installation on machines.

Table 1 Comparison of performance with conventional CRB

Type	New design	Conventional design with cage	Full complement roller
Bearing size (mm)	$\phi 150 \times \phi 320 \times 108$ (equivalent to NJ2330E)		
Dynamic rating life (kN)	1330	1160	1410
Static rating life (kN)	1740	1600	1870
Rating life ratio	1.6	1	1.9
Allowable running speed (oil) min^{-1}	2000	2000	1000

3. Evaluation Test (1)



The following tests were performed by assuming that each test bearing was used on the output shaft of a gearbox for a wind turbine.

3.1 Test bearings

In general, the non-locating bearing on the output shaft is often an NU or NJ cylindrical roller bearing type, in the case the test bearings used were NJ2324E. The new design tested is a prototype identical to a conventional design, but that has an increased number of rollers compared to the conventional design.

In Table 2, the technical data for the conventional design (with a cage) is compared to that of the new design.

Table 2 Test bearings

Conventional design (machined cage)	Type	New design (rolling element separators)
	Appearance	
$\phi 120 \times \phi 260 \times 86$	Bearing size (mm)	←
$\phi 38 \times 62$	Roller size (mm)	←
13	Number of rollers	15

3.2 Temperature increase comparison test

The running performance of the new design was compared with that of the conventional design in terms of temperature increase.

As shown in Fig. 3, the temperature increase pattern with the keystone design closely matches that of the conventional design, and the new bearing was capable of trouble-free operation up to 3500 min⁻¹ (dn/dmn = 420,000/670,000).

3.3 Acceleration/deceleration test

To evaluate resistance to the smearing that can occur in non-load operation, the keystone bearing was subjected to an acceleration/deceleration test under a set of low-load conditions.

As can be seen from the test results plotted in Fig. 4, the temperature rise on the outer ring was limited to a stable level of approximately 15°C. (Additionally smearing did not occur during the test.)

3.4 Oil-resistance test with separator pieces

To determine oil resistance resin test pieces made of the same material as that used for the keystones were immersed in the lubricating oils that are used in wind turbine gearboxes. The tensile stress of the test pieces was taken and plotted in Fig. 5.

As can be seen from the data, the test pieces immersed in each of the two lubricating oils did not exhibit significant losses in mechanical strength.

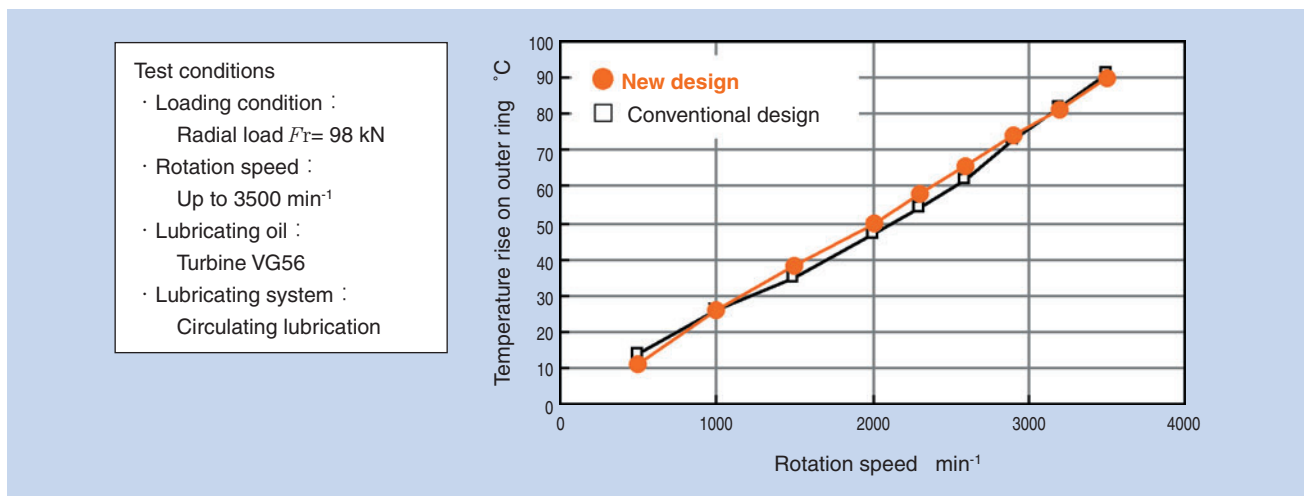


Fig. 3 Temperature rise

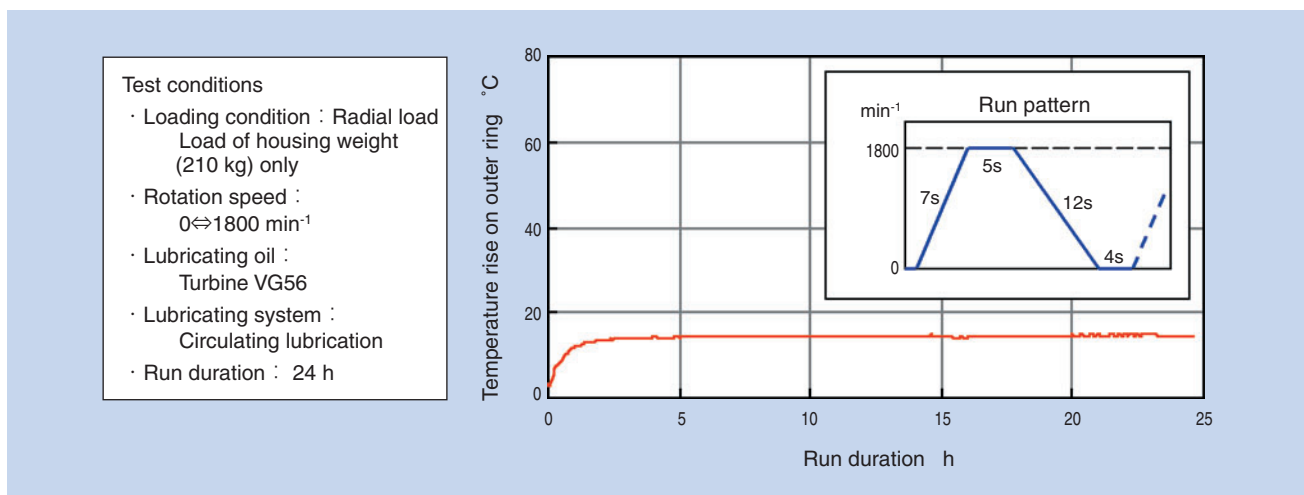


Fig. 4 Accelerated test result

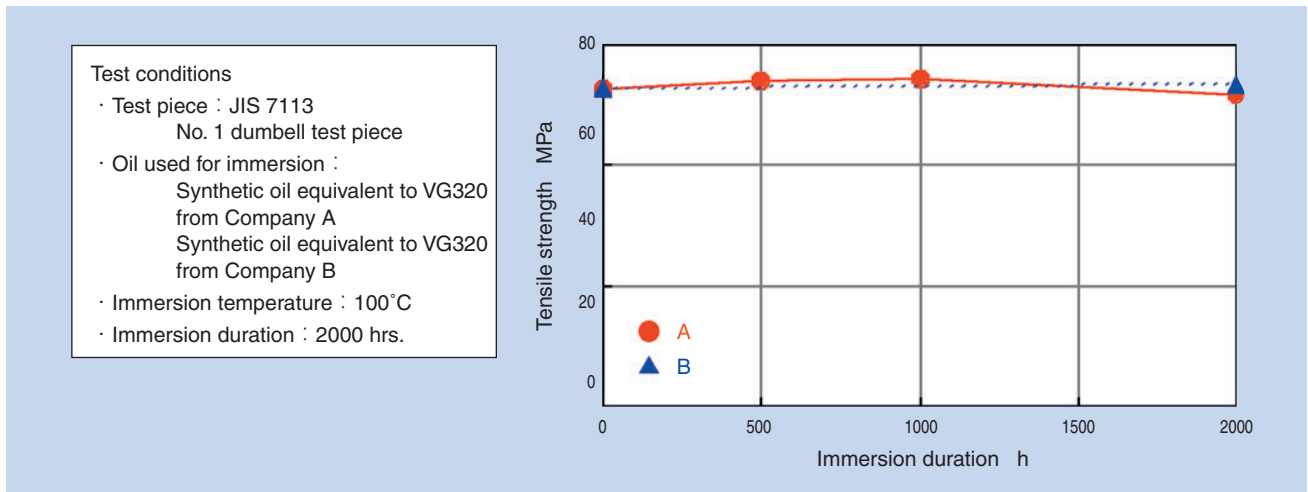


Fig. 5 Oil resistance of separator

4. Evaluation Test (2)

Additional tests were performed with an N-type cylindrical roller bearing (a type that has a double-ribbed inner ring). This type of bearing is often used in planetary gear applications.

On certain planetary gears, the bore surface of the gear may be used as a raceway surface for the outer ring. With this type of arrangement, an N-type cylindrical roller bearing that lacks an outer ring is often used (Fig. 6). Bearings for planetary gearing are usually used with their outer rings allowed to rotate. However, for these tests, the inner ring was allowed to rotate.

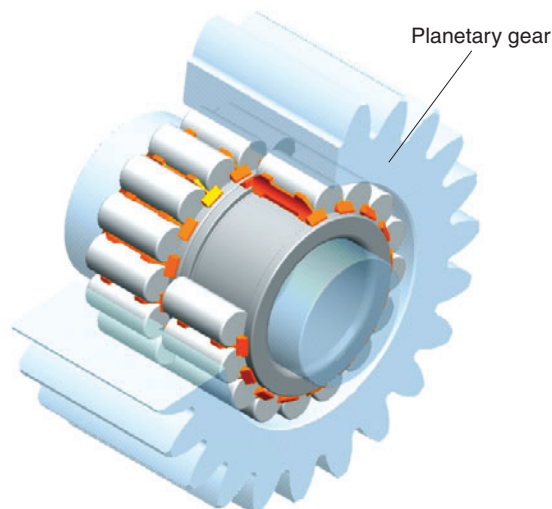


Fig. 6 Example of using N type

4.1 Test bearings

In Table 3, the technical data for the conventional design (full complement roller bearing) is compared with that for the new keystone design.

Table 3 Test bearings

Conventional design (full complement roller bearing)	Type	New design (complete with rolling element separator assembly)
	Appearance	
$\phi 101.6 \times \phi 190.2 \times 76.6$	Bearing size mm	←
$\phi 29.5 \times 60$	Roller size mm	←
17	Number of rollers	16

4.2 Temperature rise comparison test

To evaluate the running performance of the keystone design, the temperature increase characteristics were compared to those of the conventional design.

As shown in **Fig. 7**, the temperature increase of the keystone design was limited compared to the

conventional design. There was an approximately 10°C maximum difference in temperature increase between the new and conventional designs. In addition, after undergoing the test. The conventional design exhibited smearing, something not apparent in the keystone design (**Fig. 8**).

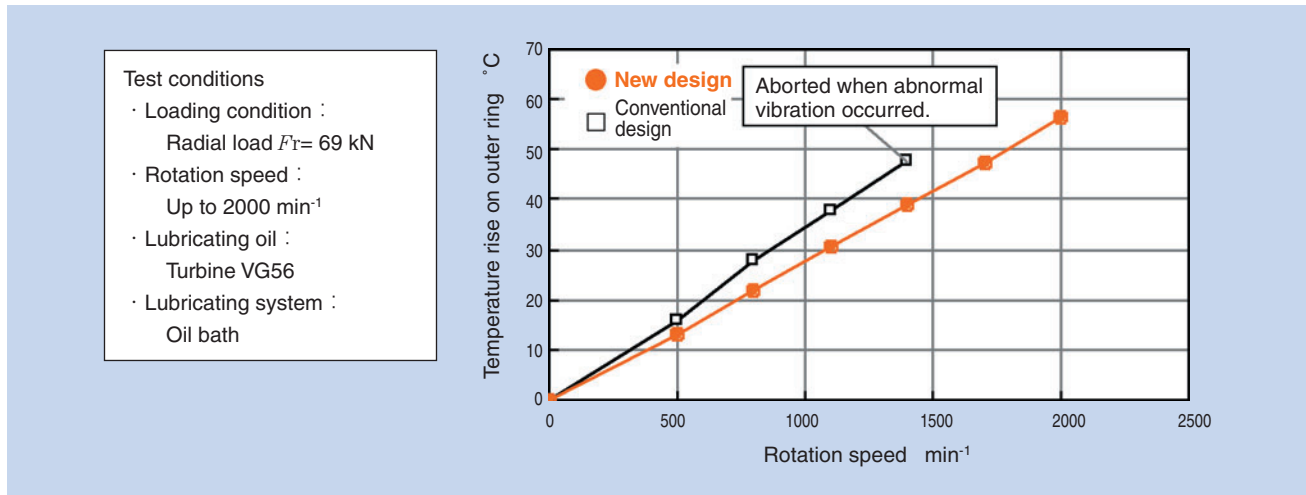


Fig. 7 Temperature rise



Fig. 8 Bearing condition after test

5. Conclusion

A unique high-load capacity cylindrical roller bearing design incorporating kestones has been described, and the results from evaluation tests with this new design have been discussed. The author believes that this new bearing design, which features the advantages not only of bearings with cages but also those of full complement roller bearings, will contribute significantly to longer bearing life and improved reliability for transmission systems.

The new high-load capacity cylindrical roller bearing design can be applied to systems other than gearboxes, so **NTN** will market this design as a high load capacity bearing product line.

Photo of author



Takuya OZU

Industrial Engineering Dept.
Industrial Sales headquarters

The Rust Guard Bearings of Highly Corrosion-resistant Bearings

Takashi YAGI*



The environment of bearings for steel mill machinery has recently become more severe. For example, the time intervals between machine maintenance has increased and the composition of the water used in the rolling process varies. Lastly, there is a growing demand for long-life bearings for the steel mill industry. To combat these tough conditions, NTN has developed the Rust Guard bearings of highly corrosion-resistant bearings. This publication describes the Rust Guard bearings in detail.

1. Introduction

The steelmaking industry worldwide has recently been undergoing a strong restructuring drive to ensure the availability of iron resources, including iron ores, and to prevent the oversupply of steel products in the future. To accomplish this, the production lines in present-day steel mills are being used to their full capacity, while extending maintenance intervals for steel mill machinery in order to improve productivity.

The durability of the bearings used in various applications in steel mills, such as the production and transportation machinery for raw materials and steel products, directly affects the productivity of such machinery. If a bearing failure occurs in an unexpectedly short time (hereafter referred to as “premature failure”), a long time is necessary for restoration and significant monetary loss results. NTN has developed the **RustGuard™** bearing line of highly corrosion-resistant roll neck bearing products for rolling lines where damaged bearings can greatly affect the operability of production lines. The goal in developing the RustGuard™ line is to prevent the premature failure of bearings.

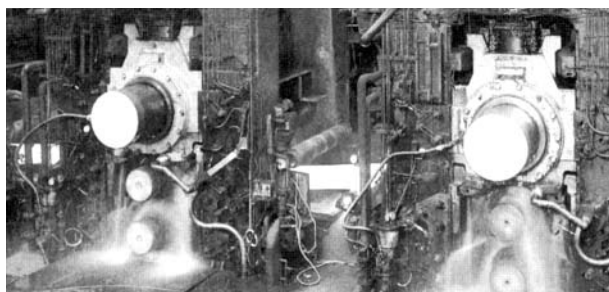


Photo 1 View of a Rolling Mill in the Rolling Process

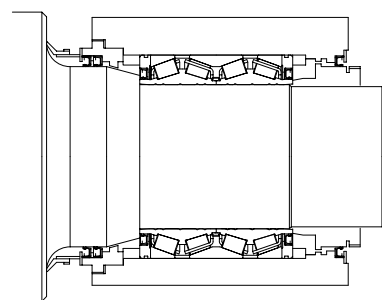


Fig. 1 Cross-sectional View of a Roll-neck Bearing on a Rolling Mill

2. Background for Developing RustGuard™

Flaking, which is a typical bearing failure, can be categorized into flaking that starts internally, in which fissures start inside immediately below the raceway

surface, and flaking that starts from the surface, in which flaking begins at damage on the outermost raceway surface. Many cases of premature bearing failures result from flaking that starts on the surface. Therefore, flaking that starts on bearing surfaces must be actively inhibited to ensure reliable operation of the rolling lines in steel mills.

*Industrial Engineering Dept. Industrial Sales headquarters

The initial efforts to realize longer life for roll neck bearings have included an attempt to achieve a higher bearing capacity by increasing the number of rollers through adoption of a pin-type cage and efforts to prevent failure that starts internally by adopting cleaner bearing materials. However, despite these efforts, premature failures still occur frequently because flaking that starts on the surface is unavoidable. A starting point for flaking could be a rusty spot or dent resulting from the ingress of water or foreign matter into the bearings, and the production sites in steel mills are usually contaminated with much water (rolling water and cooling water) and foreign matter (scale and the like). To address this problem, the lubricant and chock seal were improved, and sealed bearings have also been incorporated into components such as the work rolls in cold rolling machines. Despite these attempts, ingress of water and foreign matter has been unavoidable.

NTN has already marketed the EA Bearings, which are specially heat-treated products boasting limited loss in life even in contaminated conditions. This product line has attained a good reputation, and, when installed on a hot rolling machine, this bearing type has achieved L_{10} life three times as long compared with conventional bearings.

Incidentally, the problem known as “downtime-induced rust” (**Photo 2**) should be noted. This results from the ingress of water into the bearing and occurs when the bearing is at a standstill while the rolls are being polished or inspected. To address this type of rusting, NTN developed a special phosphating process (hereafter referred to as the “previous specification”) and has adopted this technique in conjunction with EA Bearings on actual steel mill machinery, verifying its effectiveness.

However, despite our efforts, the need to further improve the corrosion resistance of bearings has been mounting because much longer maintenance intervals are needed at the workplaces of steel manufacturers.

3. Features of RustGuard

The author’s newly developed RustGuard coating is a unique type of coating with improved corrosion resistance that was developed through further improvement of the previous special phosphate bearing coating (previous specification).

A phosphate coating is a type of a chemical conversion coating, in which chemical reactions with the compositions of the steel base material form crystals and an accumulation of these crystals creates the phosphate coating. Generally, phosphate coating is used to provide the initial sliding fit for sliding sections or to prepare a base for the application of paint. The purpose of phosphating on the bore surface of the inner ring of ordinary roll neck bearings is to provide initial sliding fit for sliding sections.

Capable of retaining lubricating oil between its crystals due to the capillary effect, the phosphate coating also provides corrosion resistance. However, because the base material is somewhat attacked during the initial coating formation process, the roughness of the base material surface (boundary with the coating) will deteriorate and can lead to loss in rolling life even though the oil retention capability of the base material will be improved. Therefore, the ordinary phosphate coating cannot be applied to the raceway surface of a bearing.

To address this problem, NTN has long been applying a special phosphate coating that does not lead to loss in rolling life by employing a special miniaturization technology. **Photo 3** shows rollers of the previous specification that underwent operation for a duration equivalent to five times as long as the calculated life L_{10} and new non-treated rollers. Both samples were partially submerged for 24 hours in tap water. From the state of rusting at the water surface of each sample, it can be seen that the rollers of the previous specification maintained corrosion resistance after use.

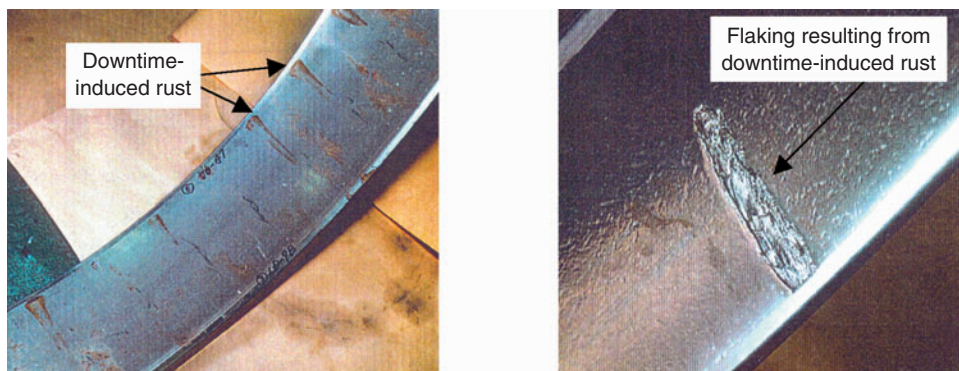


Photo 2 Examples of Downtime-Induced Rust

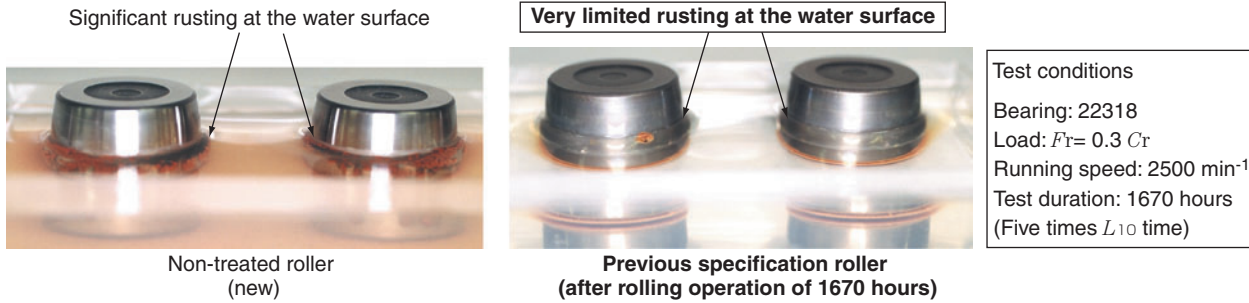


Photo 3 The rollers were soaked in water for 24hours

Incidentally, the previous specification was, in principle based on compatibility with bearing steel, and was not an optimal specification for the case hardening steel used for roll neck bearings. Therefore, we improved the previous specification, and determined the optimal crystal size through consideration of compatibility with components of case hardening steel. By using a special miniaturization technology, we successfully developed the RustGuard coating that boasts much improved corrosion resistance.

4. Corrosion Resistance Test

On actual steel mill machinery, each bearing goes through a repeated cycle of running and stopping. The

protective coating is worn down when the bearing is running, and rust occurs on the rollers when the bearing is at a standstill. The author's corrosion resistance test is intended to simulate use with actual steel mill machinery, so the test pieces were allowed to stand in a rust-promoting environment after operation, and then their rolling life was evaluated. The author has a wide range of experience with investigations into bearings that have been used in various actual steel mill machines. Based on this experience, the author set up a rust-promoting environment for simulation so that the severity of rust on the previous specification test pieces was equivalent to that on the samples from actual steel mill machines operated in rather severe operating conditions (Fig. 2).

As a result of the corrosion resistance test, the author's new design exhibited a smaller variation in life and boasted a longer life with an L10 that is 3.5 times greater than the previous specification.

Incidentally, in a clean environment, RustGuard samples have exhibited lifespans virtually equivalent to those of the previous specification samples.

5. Anti-Seizure Property Confirmation Test

Other than the downtime-induced rusting, the typical causes of premature bearing failure on actual steel mill machinery include lubrication failure and seizure caused by a failed lubrication system (for example, a clogged nozzle on an oil-mist lubrication system).

Boasting good oil retention and corrosion resistance quality, the RustGuard coating does not readily coagulate.

Fig. 3 summarizes the results of a

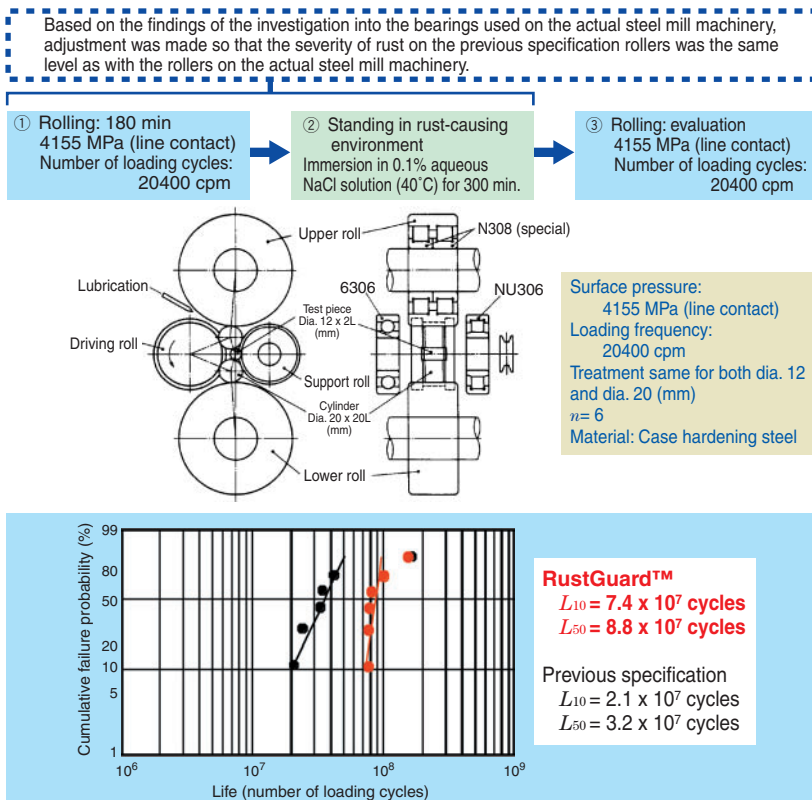


Fig. 2 Bearing failure mode simulation

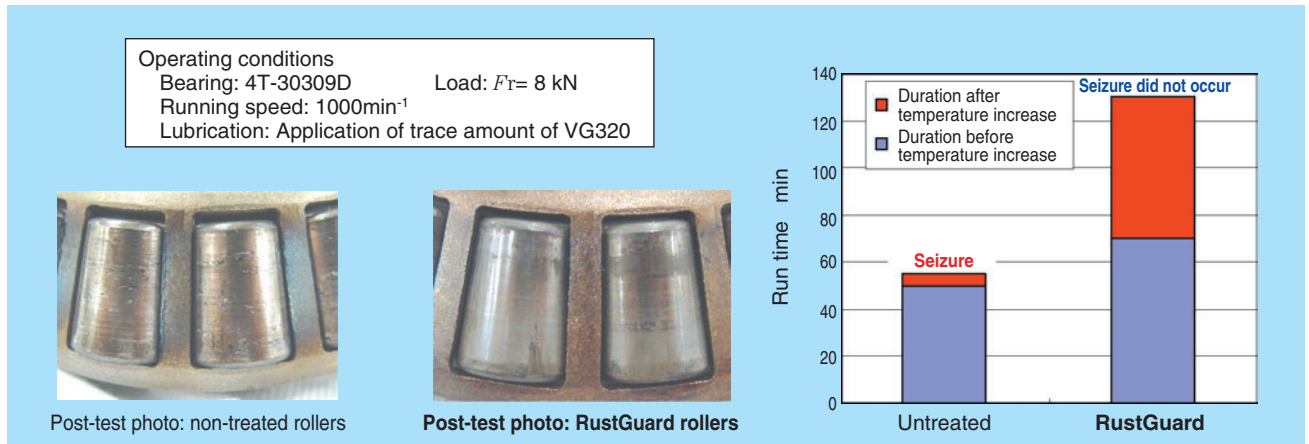


Fig. 3 Seizure resistance confirmation test

comparison test that simulated an underlubricated state. After the start of operation, the temperatures of the non-treated rollers and RustGuard rollers first stabilized and then increased. The non-treated rollers seized after 5 minutes of temperature increase. In contrast, the RustGuard rollers did not seize even after 60 minutes of temperature increase, showing their good anti-seizure qualities.

6. Examples of Applications in Actual Machinery

The major objectives of adopting the RustGuard coating, though varying somewhat between different steel manufacturer sites, include the extension of maintenance and replacement intervals, the simplification of maintenance works and the achievement of more reliable steel-making operations. Both in Japan and in other countries, RustGuard bearings are used on work rolls and backup rolls in cold rolling machines, in work rolls in hot rolling machines and in guide rolls in continuous casting machines.

The life (L_{10}) of the RustGuard bearings in the work rolls of actual cold rolling machines has been twice as long as that of the previous specification bearings. In addition, compared to the non-treated bearings from other bearing manufacturers, the bearing replacement intervals with the previous specification bearings have been increased to 1.3 times as long, while those with the RustGuard bearings have been extended to 1.7 times as long.

Incidentally, as with steel manufacturing works, papermaking plants using previous specification products (phosphate coating for bearing steel) have been experiencing problems of downtime-induced rust, particularly with the suction rolls used in the paper making process. Compared with the non-

treated bearing products, the average life of RustGuard bearing products used in this type of application is sometimes more than four times as long.

7. Conclusion

The operating conditions for the roll neck bearings on rolling machines in steel mill machinery are very demanding, and can lead to bearing failures that start from the surface. We have developed and commercialized the RustGuard product that actively resists the occurrence of “downtime-induced rust,” which is a typical cause of bearing failures that start from the surface. Furthermore, RustGuard also features good anti-seizure properties. In summary, the RustGuard line of products is highly suitable to the needs of steelmaking sites, including, for example, the stable operation of bearings in actual machinery.

NTN will remain committed to the development of products that satisfy customer worksite needs.

Photo of author

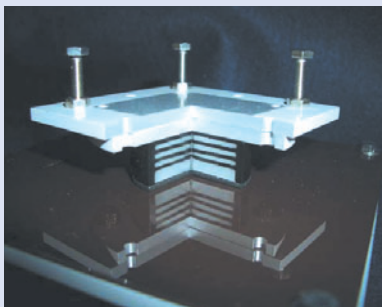


Takashi YAGI

Industrial Engineering Dept.
 Industrial Sales headquarters

“SSB” of Sliding Aseismic Isolation Unit Multi-ply Rubber

Norio ITOH*
Takuya ISHII*



SSB with multi-ply rubber is newly developed seismic isolation unit which has higher vertical rigidity and wider applicability than SSB with a single ply rubber, by arranging the number of rubber ply and thickness. New SSB is a low friction sliding seismic isolator with a friction coefficient of 0.024 that is equivalent to the current SSB. The expected applications are from low to high buildings such as condominiums, offices, factories, hospitals and schools, which are not only newly built but also retrofitting existing ones.

This article introduces the characteristic of multi-ply rubber SSB (Ministry of Land, Infrastructure and Transport authorization number MVBR-0304) and basic properties comparing with the current single layer rubber SSB which achieved business result.

1. Introduction

Most of the damage resulting from an earthquake is secondary damage caused by collapsing buildings and falling furniture. Since the Great Hanshin Earthquake in 1995, many seismically isolated apartment buildings and detached houses have been built. The probability of another large earthquake in the next 30 years, including powerful earthquakes near the Tokai or Tonankai regions, in particular, is approximately 60%. Given this, more seismically isolated apartment buildings and detached houses are expected to be built. The seismically isolating members used for these buildings can be categorized into multi-ply rubber isolators, sliding/rolling bearings and dampers. The sliding aseismic, multi-ply rubber Super Sliding Bearing (SSB) developed by NTN is a unique sliding bearing product that has overcome the technical challenges of conventional sliding bearings to provide stable performance for an extended period of time at a lower friction coefficient. This paper, through comparison with a conventional single-ply rubber SSB product already on the market, describes the features and basic characteristics of NTN's new multi-ply rubber SSB (Japanese Ministry of Land,

Infrastructure and Transport certification number MVBR-0304).

2. What are Seismically Isolated Structures?

A seismically isolated structure can be defined as a building that is made resistant to earthquakes by isolating it from the vibration of the ground rather than increasing the strength and rigidity of the building so that it can withstand severe seismic vibrations. As summarized in Fig. 1¹⁾, compared with earthquake resistant structures and vibration control structures,

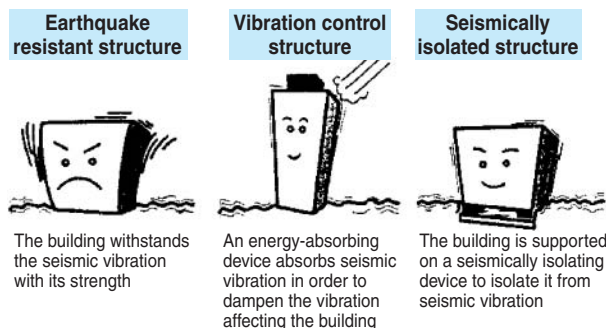


Fig.1 Concept of earthquake resistant structure, vibration control structure, and seismic isolated structure

*Engineering Dept. NTN Engineering Plastics Corp.

the severity of the seismic vibration is dampened by seismic isolation to prevent damage to the structures and maintain the functionality and habitability of the buildings.

3. Reasons Why Low-Friction Sliding Bearings Are Needed for Buildings

The time required for a building to vibrate once is called its natural period. For many seismic vibration modes, it is known that the severity of the vibration is greatest for periods of 1 second or less and that these seismic vibration periods are approximately the same as the natural periods of structures that are not seismically isolated. Thus, resonance vibration occurs in these structures and consequently they can be severely damaged. As schematically illustrated in Fig. 2¹⁾, SSBs can provide buildings with longer natural vibration periods because of their low friction coefficients. More specifically, compared to conventional sliding bearings made from a combination of PTFE sliding material and a non-coated stainless steel plate, our SSBs succeeded in reducing the vibrating force (seismic force) affecting the building to approximately 1/3 of its original value. As a result, since the sizes and numbers of pillars and beams can be decreased, building designers can create larger dwelling spaces.

4. Composition and Features of the Multi-Ply Rubber SSB

The composition of a multi-ply rubber SSB is

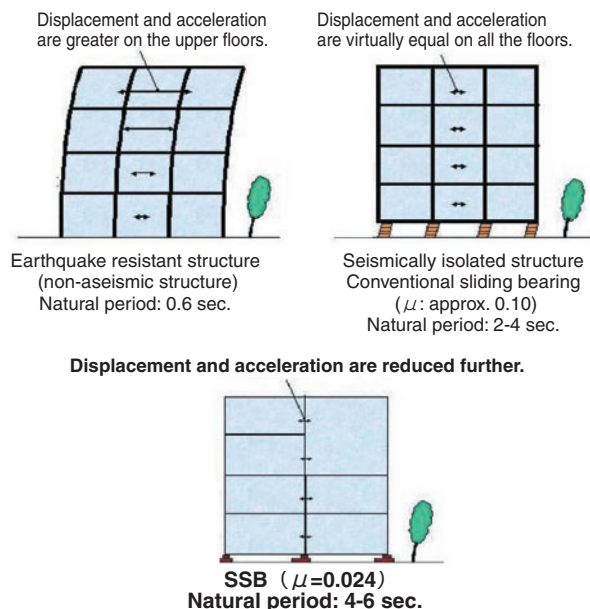


Fig. 2 Comparison of vibration strength of the building with seismic isolated structure

schematically illustrated in Fig. 3, and the materials in its major components are summarized in Table 1. The SSB is comprised of a multi-ply rubber integrated structure with laminated rubber and steel members, as well as sliding members arranged in series. The SSB has the following features.

Features of the multi-ply rubber SSB

- 1) Compared with a conventional single-ply rubber SSB, the authors' new design features a greater rubber component shape factor (= rubber diameter/4 x thickness of one ply of rubber). As a result, the new design boasts greater vertical rigidity and smaller rubber deformation.
- 2) Compared with a conventional single-ply rubber SSB, the NTN's new design features a long-term carrying load that is approximately twice as great. In addition, the combination of the thickness of each rubber ply and the total number of rubber plies can be altered arbitrarily. This feature allows greater freedom in designing aseismic structures.
- 3) NTN's new design involves a unique combination that is comprised of a sliding member made of PTFE and a corresponding sliding plate made of

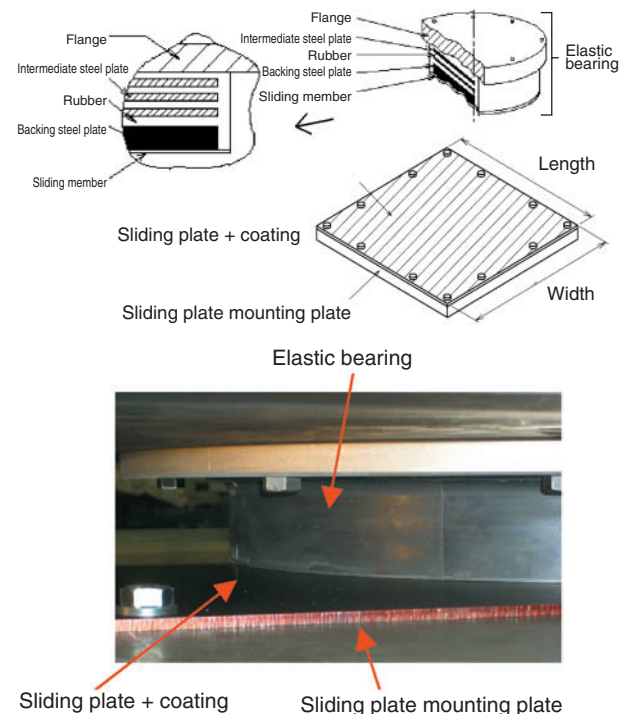


Fig. 3 Outlined structure of SSB

Table 1 Material of major parts of SSB

Member	NTN part designation	Composition
Multi-ply rubber member	BEAREE ER4080	Natural rubber
Sliding member	BEAREE FL3045	PTFE w/ filler
Coating member	BEAREE SP7001	Thermo-setting resin w/ filler

stainless steel (equivalent to JIS SUS-304). As a result, the authors' multi-ply rubber SSB has achieved a friction coefficient of 0.024 against a surface pressure of 15 N/mm². Consequently, the aseismic period of building structures with the authors' multi-ply SSBs can be made much longer (4 sec. or greater) and their response accelerations can be much lower.

- 4) The rotation generated on the sliding bearings by, for example, the bending of beams in response to an earthquake or deformation caused by construction error or the creeping of beams is mitigated by the multi-ply rubber. Furthermore, NTN's multi-ply rubber SSB is a seismically isolating member that smoothly changes mode from elastic deformation of the multi-ply rubber to sliding in the event of an earthquake.
- 5) When a minor earthquake occurs, sliding does not occur but elastic deformation of the multi-ply rubber occurs. In a medium or larger earthquake, sliding of the multi-ply rubber also occurs to dampen the seismic force.

5. Vertical Load Characteristics

The relationships between vertical displacement and vertical load (600-mm diameter rubber) for the multi-ply rubber SSB and a conventional single-ply rubber SSB are graphically plotted in Fig. 4. Since the shape factor for the multi-ply rubber SSB is approximately three times greater than with the single-ply rubber SSB, the vertical rigidity is approximately three times as great and the rubber displacement is approximately 1/3 with the multi-ply rubber SSB when compared with the single-ply rubber SSB.

When sliding bearings are used on a seismically isolated building structure, they are adopted in conjunction with multi-ply rubber isolators that restore the building to its original state. Since the vertical rigidity and rubber displacement of the multi-ply rubber

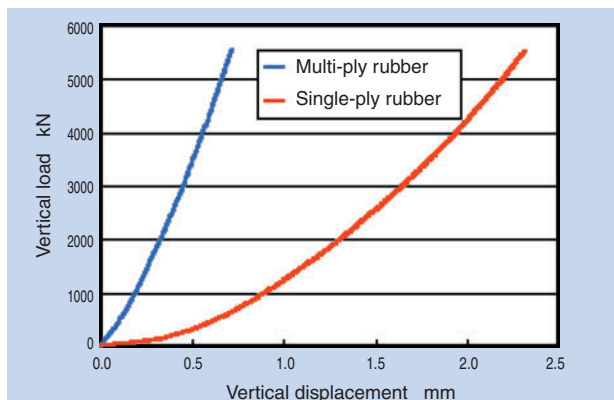


Fig. 4 Relation between vertical displacement and vertical load of a multi-ply rubber and a single ply rubber

SSBs are similar to those of multi-ply rubber isolators, the design of seismically isolated building structures can also be achieved more easily.

6. Dynamic Friction Coefficient

6.1 Comparison of a conventional sliding bearing and the NTN's multi-ply rubber SSB

The dynamic friction coefficient of a conventional sliding bearing that combines a PTFE sliding member with a non-coated stainless steel plate was compared with that of the multi-ply rubber SSB. The results obtained are plotted in Figs. 5 and 6. Even though the dynamic friction coefficients depend on surface pressure and velocity, the dynamic friction coefficients of NTN's multi-ply rubber SSB are less than 1/3 to 1/5 of those of the conventional sliding bearing.

As for the dynamic friction coefficients for the authors' multi-ply rubber SSBs, the authors have obtained the surface pressure dependency formula

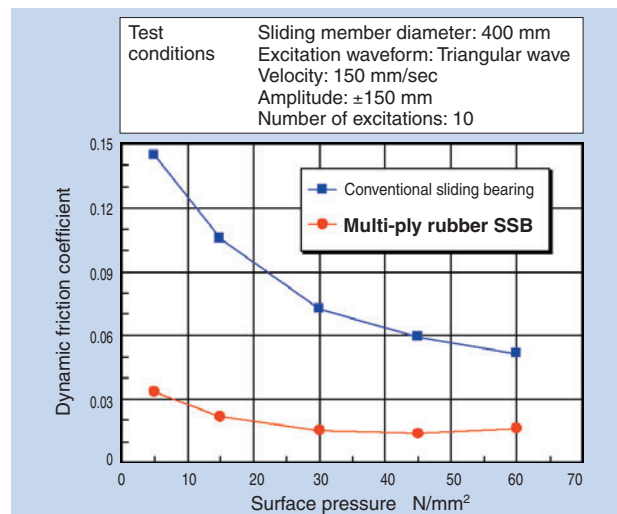


Fig. 5 Relation of the friction coefficient vs. pressure

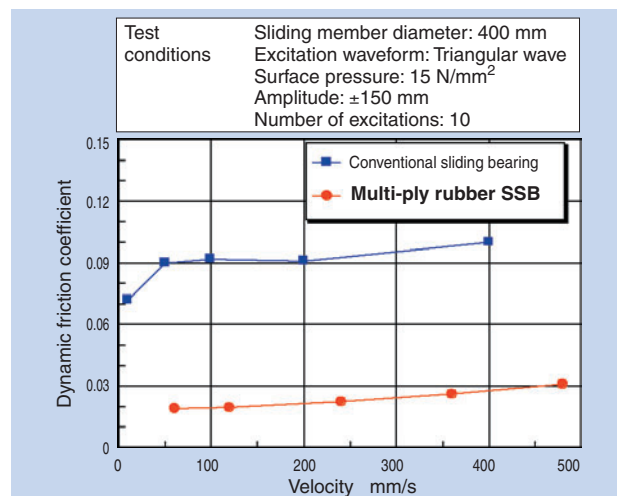


Fig. 6 Relation of the friction coefficient vs. velocity

and velocity dependency formula below based on the data from their experiments, and these are being considered in the structural design of seismically isolated building structures.

Surface pressure dependency formula (for velocity 15 mm/s)

$$\mu = 0.0618 \sigma^{-0.351}$$

where, σ : surface pressure (N/mm²)

Velocity dependency formula (for surface pressure 15 N/mm²)

$$\mu = 0.0173 (V/10)^{0.132} \quad \text{where, } V: \text{velocity (mm/s)}$$

6.2 Durability

The durability of the multi-ply rubber SSB is indicated in Fig. 7 in terms of the trend with the friction coefficients of the authors’ multi-ply rubber SSB. The grouping of the friction coefficient values is fairly stable. Therefore, a total sliding distance of 180 m for a seismically isolating device appears to be sufficient.

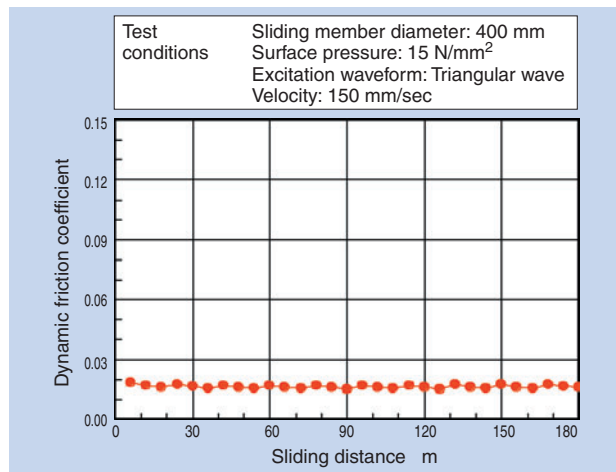


Fig. 7 Durability of the friction coefficient

7. Multi-Ply Rubber SSB Variations

Each building structure needs to cope with unique column loading considerations. Thus, NTN offers nine standard multi-ply rubber SSB types with bearing diameters ranging from 300 to 1300 mm.

Table 2 Specification of multi-ply rubber SSB standard series

Bearing diameter (mm)	300~1300
Long-term bearing load (kN)	1,060~19,910
Friction coefficient	0.024 (15N/mm ² standard surface pressure)
Variation in friction coefficients (%)	±30
Horizontal rigidity (kN/m)	4,712~22,122
Variation in horizontal rigidity (%)	±20
Vertical rigidity (MN/m)	4,607~30,222

8. Conclusion

The NTN R&D Center, which is shown in Photo 1, is a typical example of a seismically isolated building structure supported by the authors’ SSB, and Photo 2 is a view of an installed SSB. Capable of withstanding an earthquake as severe as the Hanshin Earthquake level, the NTN R&D Center is expected to function as a disaster relief center for the NTN Iwata Works. NTN remains committed to improving the reliability of our multi-ply rubber SSBs. We have been providing our customers with a full line of products that are capable of withstanding conditions in a variety of seismic load isolating applications. The NTN believes that their products can contribute to saving human lives and protecting property during seismic disasters.



Photo 1 Appearance of NTN R&D center

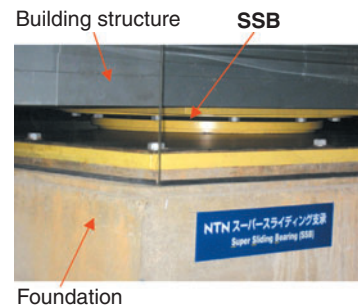


Photo 2 Installed SSB

References

- 1) Multi-ply Rubber for Seismic Isolation Editorial Committee: Handbook of Multi-ply Rubber for Seismic Isolation, Rikoh Toshoh. (In Japanese)

Photos of authors



Norio ITOH

Engineering Dept.
NTN Engineering Plastics Corp.



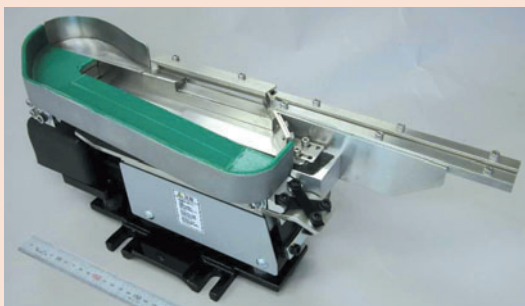
Takuya ISHII

Engineering Dept.
NTN Engineering Plastics Corp.

2005 Monozukuri Buhin Taisho Grand Prix Machine Component Award

Monodrive Two-Way Feeder

Toshio OGUSU*



The Monodrive Two-Way Feeder is a parts feeder where parts can be moved in two directions (the line supply side and the other side) by one driving unit. This reduces the driving unit and controller set from two pieces to only one piece. Therefore, the feeder becomes smaller and lighter, with reductions in power consumption, cost, and maintenance.

1. Introduction

NTN's Monodrive Two-Way Feeder is a unique compact vibratory parts feeder optimized for feeding many part types in smaller lots, and boasting greatly decreased floor space requirements compared with conventional bowl-type parts feeders.

As many bulk parts and components are now manufactured in plants outside Japan, automatic assembly lines in Japan are increasingly required to be capable of producing more product types in smaller lot sizes, thereby demands are growing for less expensive, more compact parts feeding devices. So far, the conventional parts feeder systems used for this purpose have generally consisted of a cylindrical bowl feeder type that aligns the parts by vibration and a linear feeder type that feeds the parts to the assemblers. In this arrangement, the floor space required for the bowl feeder section is often great. Therefore, believing that a unique driving unit capable of the entire process of parts alignment and feeding would dramatically raise user satisfaction, the author began his commitment to the development and commercial release of the Monodrive Two-Way Feeder™ product.

The design concept and novel operating principle of this product have been highly evaluated, and it even received the 2005 Monozukuri Buhin Taisho Machine Component Award sponsored by Nikkan Kogyo

Shimbun, Ltd., a leading Japanese industrial paper. This award was given to outstanding machine components among those developed or brought to market in the 2005 business year. In this report, the author would like to introduce this unique product to the readers.

2. Overview of the Monodrive Two-Way Feeder

Photo 1 shows the appearance of the author's monodrive two-way feeder.

In **Table 1**, the features of the author's monodrive two-way feeder design are compared with those of conventional compact vibratory parts feeder systems.

Various compact parts feeder designs that do not employ bowls have been available (Table 1). However, these products have drawbacks, including the need for two driving units and the difficulty of adjustment of the entire system.

Requiring multiple assemblies, conventional parts feeder systems that use two linear feeders do not satisfy the needs for less expensive, compact parts feeding systems. Therefore, the author tried various ideas for parts feeding systems in which one linear feeder unit could feed the parts. As a result of these attempts, the author has incorporated a vibration-direction switching leaf spring unit (**Photo 2**) into a conventional linear feeder. Thus, the author has

*Product Engineering Department Precision Equipment Division

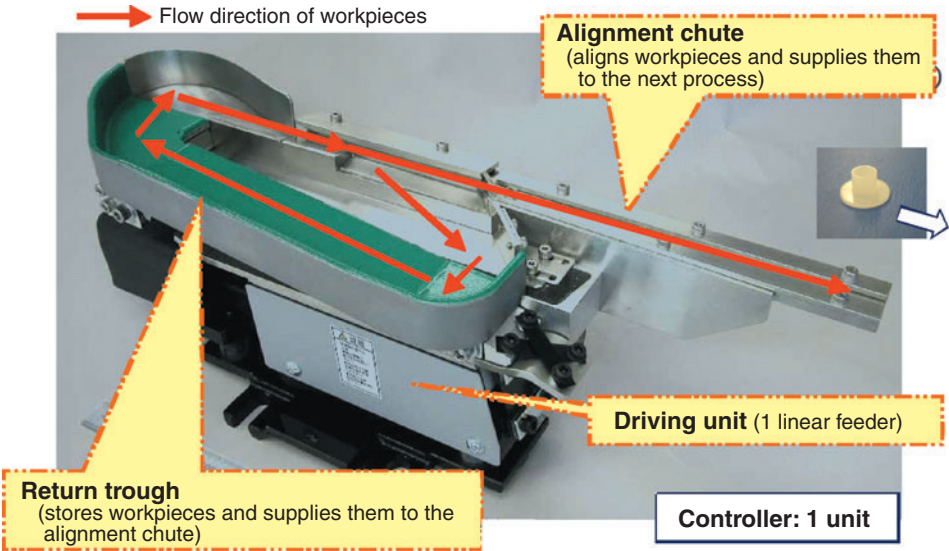


Photo 1 Monodrive Two-Way Feeder

Table 1 Space-saving parts feeding method (vibration type)

	Type	System	Advantages	Disadvantages
Conventional designs	Return feeder ①	Linear feeder x 2	Both feeders are controlled independently of the others	2 sets of drive units and controllers are necessary
	Return feeder ②	1 lower driving unit +2 chutes	1 drive unit and 1 controller	Difficulty of adjustment (for resonance point with 2 vibration systems) System-specific control is impossible
	Drum feeder	Rotary hopper + linear feeder	Storage of workpieces	Difficulty in supplying workpieces 2 sets of drive units and controllers are necessary
Monodrive two-way feeder		Linear feeder + return chute	1 drive unit and 1 controller Easy adjustment and maintenance Easy storage and input of workpieces	System-specific control is impossible

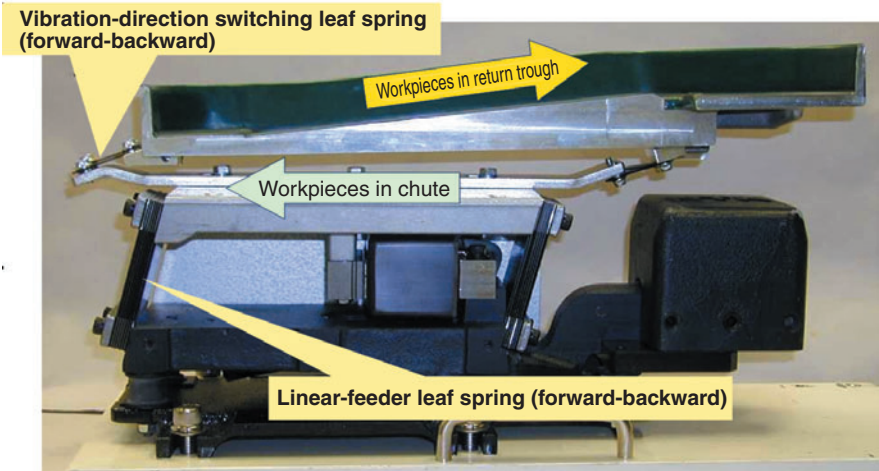


Photo 2 Composition of leaf spring (Monodrive Two-Way Feeder)

succeeded in generating vibration of not only the alignment and feeding section but also of the return section with just one driving unit and one controller. Furthermore, the vibration direction of the alignment and feeding section is opposite the vibration direction of the return section.

The author has adopted a vibration-direction switching leaf spring with rigidity in the leaf thickness direction that is lower than the leaf spring rigidity of the linear feeder. Consequently, the vibration in the leaf spring thickness is dampened while only the longitudinal vibration is utilized so that the vibrating angle with the linear feeder (alignment feeder) is converted to the opposite direction, which is necessary for the driving motion on the return side.

2.1 Advantages

The author’s monodrive two-way feeder boasts the following advantages.

1) One linear feeder propels transfer chutes in two directions—the alignment/supply side and the return side (patent pending)

The completely new operation principle combines the resonance phenomenon, which has been used commonly, with forced vibration movement.

2) Reduction of installation space

The greatest advantage of the author’s parts feeder is the reduction of installation space. Compared with the combination of a conventional bowl feeder and a linear feeder, the floor space requirement for the author’s design is approximately 1/2 or less (Fig. 1).

3) Energy conservation and lighter weight

The author’s linear feeder system is capable of parts storage, alignment and supply, and therefore

is a lighter parts feeding system that contributes to reduced energy consumption. Compared with the combination of a conventional bowl feeder and a linear feeder, both the weight and energy consumption of the author’s system are less than 1/3 (data by NTN).

4) Simple construction makes it an optimal choice for multiple product type and small-lot production

The author’s feeder arrangement is very simple. It essentially consists of an ordinary linear parts feeder with the addition of a vibration direction switching leaf spring unit, and it boasts excellent maintainability. The author’s system is capable of handling a variety of workpiece types just by mounting the relevant chutes.

5) Possibility of CAD design for the tooling (alignment section)

Three-dimensional tooling efforts such as those needed for conventional bowl feeder systems are usually not necessary with the author’s system. Thus, the tooling on the author’s feeder system can be readily designed using a CAD system.

2.2 Technical data

The main technical specifications of the monodrive two-way feeder are given below.

- **Models:** Three models—MD10, MD20 and MD30

- **Size**

MD10: 366L x 120W x 189H (mm)

MD20: 458L x 166W x 229H (mm)

MD30: 663L x 205W x 342H (mm)

*The size of the alignment chute is not included.

- **Mass of feeder**

MD10: 9 kg (The chute is not included.)

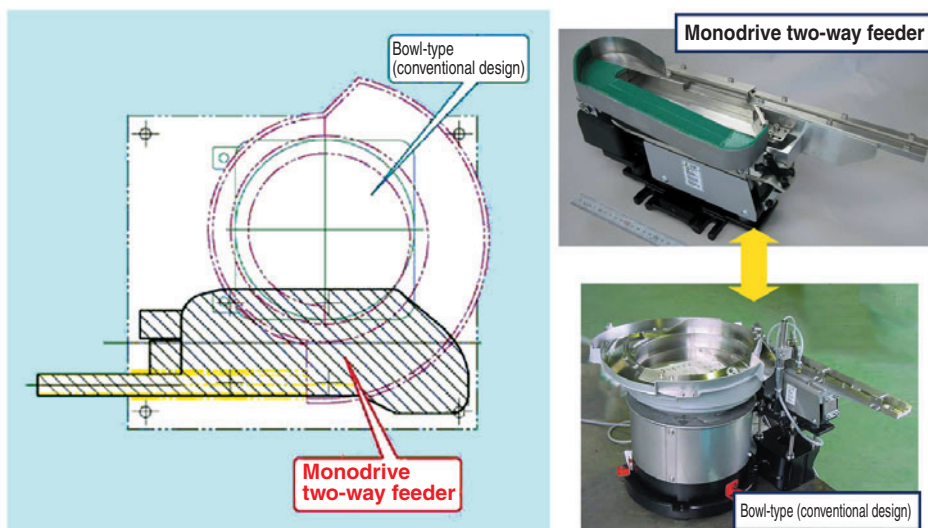


Fig. 1 Comparison of space-saving

MD20: 17.5 kg (The chute is not included.)

MD30: 49 kg (The chute is not included.)

- **Return trough inclination angle:**

5° as standard (variable in a range of 4° to 7.5°)

- **Length of the chute mounted (additional mass)**

MD10: 450-600 mm (1.1 kg)

MD20: 550-800 mm (2.0 kg)

MD30: 850-1100 mm (7.0 kg)

- **Applicable controller:** K-ECA46 (or K-ECA49)

- **Suitable workpiece types:**

Small/medium-sized parts (for machines, electronics and plastics)

Bolts, pins, lightweight parts

Moderately oily parts and various other workpiece types

3. Conclusion

The author's monodrive two-way feeder described above features a very simple construction comprised of one driving unit and one controller, and is still capable of the functions of storage, alignment and supply necessary for any parts feeder. In summary,

the author's monodrive two-way feeder fulfills user needs for reduced floor space requirements, lighter weight, economy in energy consumption and resource conservation.

Each component of the author's feeder, including the tooling, is very simple. Consequently, unlike conventional "handmade" parts feeders, the author's parts feeder boasts unprecedented quality and stability. As a result, the author's novel parts feeder has been highly evaluated for new applications and in new industrial fields.

So far, we have brought three medium and large linear feeder product models to market. In the future, we would like to expand the range of this unique product by adding, small-sized models and special-purpose feeders to best meet different user requirements.

References

- 1) T. Ogusu: Automation Advancement, Vol. 35, No. 1, (2006). (In Japanese)

Photo of author



Toshio OGUSU

Product Engineering Department
Precision Equipment Division

2005 Technology Prize of the Japanese Society of Tribologists

"Hybrid Bearphite" a Sintered Metal Sliding Bearing Inserted with Plastic

Masaki EGAMI*



This report introduces the new "Hybrid Bearphite" sintered metal sliding bearing with a plastic sliding material on its inner surface. Because the plastic layer is only 0.25 mm thick, temperature changes give minimal dimension changes. This assures a higher precision over a wide temperature range (10-60°C). Furthermore, combining the plastic with a special filler gives an extremely low friction coefficient of 0.05 (1/2 the friction coefficient of conventional plastic sliding bearings), resulting in low rotational torque.

This new sliding bearing "Hybrid Bearphite" received the Japanese Society of Tribologists technology prize.

1. Introduction

Our Hybrid Bearphite is a unique high-precision low-friction sliding bearing that consists of a sintered metal backing, and a bore surface of thinly formed resin sliding material. ¹⁾ The features of the Hybrid Bearphite are described below.

1) Excellent running accuracy that is comparable to sintered oil-impregnated bearings

This feature is accomplished with a thin insert molding of resin on the bore surface of a sintered metal sliding bearing.

2) Lower friction (friction coefficient $\mu = 0.05$)

A high-performance sliding resin is used as a coating on the inner bore surface of the bearing. This unique resin features a friction coefficient half that of conventional resin materials.

2) Our Hybrid Bearphite sintered metal sliding bearing can be used in conjunction with soft shaft materials such as aluminum.

Hybrid Bearphite products can readily be used to replace rolling bearings due to their low prices. In addition, they offer an ideal choice for a compact sliding bearing design.

The Hybrid Bearphite line of products has achieved the above-mentioned accuracy and lower running torque at a decreased cost. The Japanese Society of Tribologists has evaluated this achievement and awarded their 2005 technology prize to NTN's Hybrid Bearphite.

2. Development background

Rotary mechanisms on photocopying machines and printers (Fig. 1) employ a variety of bearing types. In this field of application, rolling bearings excel over usual sliding bearings in terms of running accuracy, rotational torque and durability, but they are more expensive. Furthermore, sintered oil-impregnated bearings are less expensive compared to rolling bearings and excel over resin bearings in terms of running accuracy and rotational torque. On the other hand, they accelerate the wear of the soft shafts (aluminum shafts, Ni-plated shafts, etc.) typically used in printers and photocopying machines because they are lubricated in boundary lubrication mode. Incidentally, resin bearings are the least expensive, and allow soft metal materials, including aluminum, to be used as a shaft material. However, the materials

*Elemental Technological R&D Center

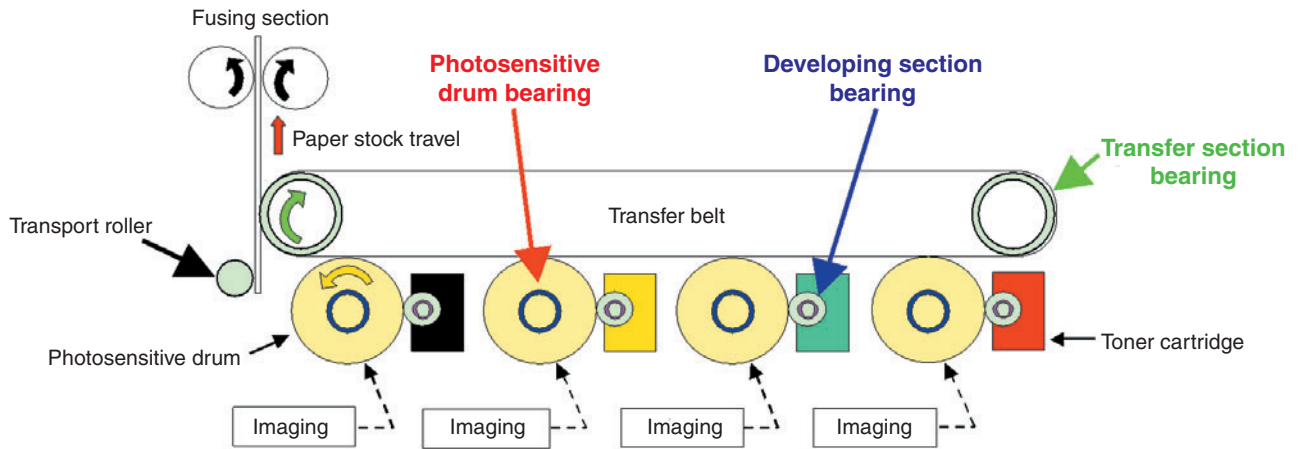


Fig. 1 Schematic of copying machines and printers

for resin bearings, used in this type of application, can have disadvantages. During the molding process, their shrinkage rate and coefficient of linear thermal expansion are large and, as a result, their dimensional accuracy and stability are poor.

Mechanisms, such as the photosensitive drum whose running accuracy greatly affects print quality, incorporate rolling bearings because rolling bearings boast better functionality even though they are relatively expensive. Consequently, there has been a growing need for a bearing suitable for this application that are both less expensive and more accurate.

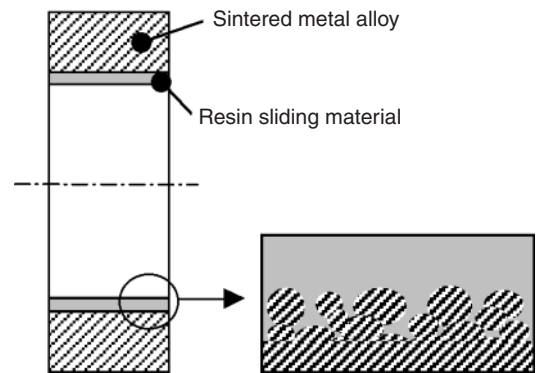


Fig. 2 Concept of HYBRID BEARPHITE

3. Development of Hybrid Bearphite

3.1 Concept for the newly developed bearing

To satisfy the needs described in Section 2, we developed the Hybrid Bearphite, based on a concept that consists of the following parts. 1) An insert molding technique is used to form a thin resin layer on the inner bore surface of a metal backing to achieve better dimensional accuracy. 2) The metal backing is made of sintered metal alloy to ensure effective bonding to the resin layer due to its anchoring effect. 3) The resin layer is made of a low friction sliding material so that the rotational torque with the bearing is low. The newly developed Hybrid Bearphite bearing is schematically illustrated in Fig. 2.

A resin layer formed inside the bore surface of a metal member will usually develop peeling on the metal-resin interface due to shrinkage occurring from molding operation with the resin.

With our Hybrid Bearphite sliding bearing, however, the resin material is allowed to fill the pores in the sintered metal so that the resultant anchoring effect helps prevent the resin layer from peeling off the metal

backing. At the same time, through improvement of the insert molding process, the thickness of the resin layer is regulated to 0.25 mm so that the resin layer features good dimensional accuracy and the dimensional stability of the resin layer is high relative to temperature variation. If the end faces are each provided with a resin layer, then the sliding bearing can bear not only a radial load but also an axial load.

3.2 Development of resin sliding material

Since the main purpose of the Hybrid Bearphite sliding bearing is the replacement of rolling bearings, the friction on its sliding surface needs to be low. However, the friction coefficient of any conventional resin sliding material is 0.1 or higher,²⁾ so such a material would not serve for this sliding bearing. To address this problem, we attempted to develop a new resin sliding material with a friction coefficient half that of conventional resin sliding materials.

The friction-wear characteristics of a resin are usually improved by blending in oil or a solid lubricant such as polytetrafluoroethylene (PTFE) or graphite.

Use of oil is effective to decrease the friction coefficient. Until now, NTN had been attempting to lower the friction coefficient for sliding bearings by using an oil dispersion technique with a polymer alloy, for example.³⁾

However, conventional techniques had limitations because the addition of an excessive amount of oil can lead to deterioration in the mechanical strength and formability of a sliding material. Therefore, we developed a technique that adopted porous silica as an oil retaining material (oil-impregnated silica). Thereby, we attempted to increase the content of oil included in the resin while maintaining good mechanical characteristics and formability of the resultant sliding resin material.⁴⁾

Compositions and frictional characteristics of materials prepared by blending different proportions of oil-impregnated silica into ultrahigh-molecular-weight polyethylene (UHMWPE) are summarized in **Table 1** and **Fig. 3**. Compared with the material blended with oil alone ②, the material blended with oil-impregnated silica ③ exhibited a lower dynamic friction coefficient though its oil content was equal to that of material ②.

With an increase in the amount of oil-impregnated silica (material ④), the dynamic friction coefficient further decreased, reaching a level lower than a third the level obtained with a PTFE-based sliding material.

Having undergone the test, the sliding surface of material ④ was inspected, and the oil-impregnated

Table. 1 Composition of test specimens for sliding tests

Material	Composition (vol%)
①	UHMWPE (100)
②	UHMWPE (85)/Silicone oil (15)
③	UHMWPE (82)/Oil-impregnated silica*(18)
④	UHMWPE (70)/Oil-impregnated silica*(30)

* 1:5 porous silica to silicone oil ratio

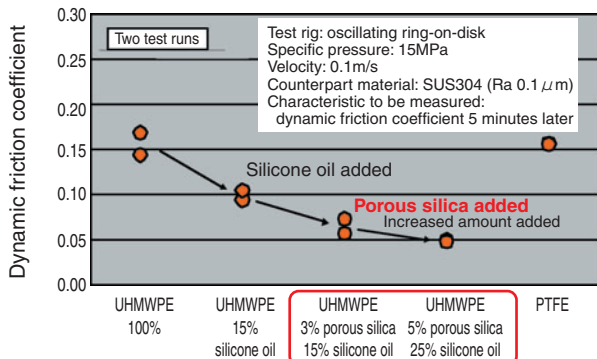


Fig. 3 Friction properties of the materials filled with oil-impregnated-silica

silica exposed on the sliding surface was found as a result (**Fig. 4**). In addition, the static oil seepage from material ④ at room temperature and 15 MPa conditions was measured. As shown in **Fig. 5**, the oil seepage increased as the time elapsed and reached 6% in 100 hours. Assuming that only the oil near the surface layer seeped out this level of leakage is too great.

From these findings, we estimated the low friction mechanism of this material as shown in **Fig. 6**. In other words, we believe the following theory about the mechanism. Since the oil-impregnated silica serves as the load bearing point, solid-to-solid contact is inhibited, making it easier for an oil film to form.

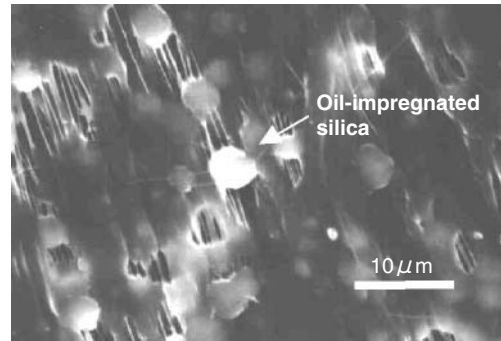


Fig. 4 Surface of the material ④ after sliding test

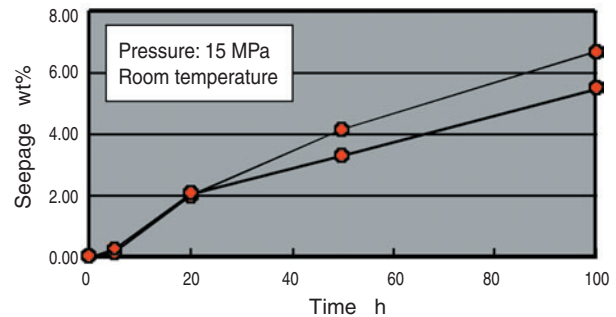


Fig. 5 Relationship between loading time and oozed oil amount from the material ④

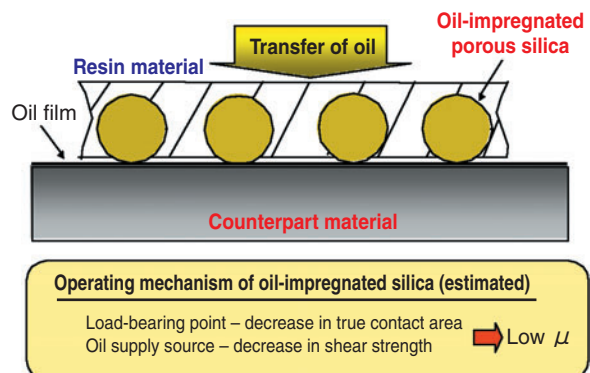


Fig. 6 Estimated mechanism of low friction of the developed material

Furthermore, the oil-impregnated silica particles link with each other and function as passages for the oil. Through these passages, the oil inside the material is continuously supplied to the sliding surface, thereby giving the material a stable low friction coefficient.

The resin sliding material ④ was modified so that its melted viscosity was suitable for injection molding and was adopted for the resin layer on the Hybrid Bearphite.

3.3 Insert injection molding to sintered metal backing

The factors that help ensure high accuracy with the Hybrid Bearphite sliding bearing are summarized in Fig. 7. As already mentioned, if a resin layer is formed on the bore surface of a conventional metal member, peeling will unavoidably occur on the metal-resin interface due to molding-induced shrinking with the resin material. For our Hybrid Bearphite sliding bearing design, a resin material is allowed to fill the pores on the sintered metal so that, due to the

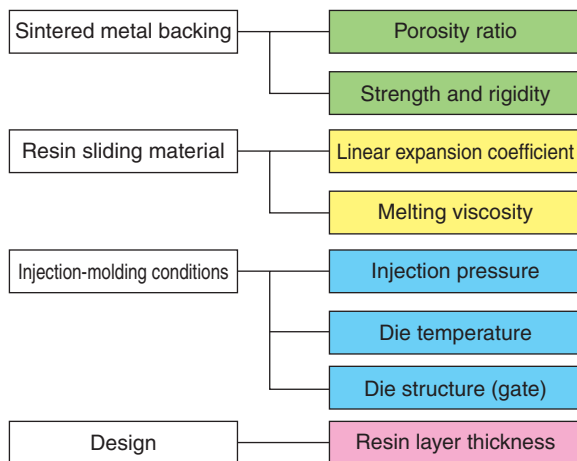


Fig. 7 Factors to achieve high precision

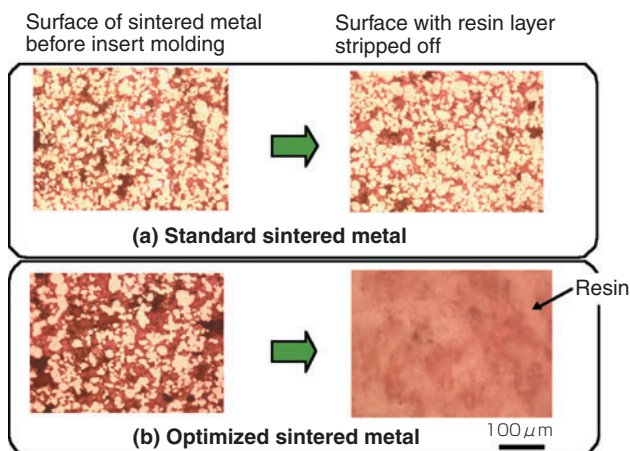


Fig. 8 Inner surface of sintered back metal

resultant anchoring effect, the resin layer does not come off the metal backing. Therefore, we attempted to optimize the porosity ratio of the surface of the sintered metal as well as the injection molding conditions.

Fig. 8 shows an example of optimization of the surface porosity ratio with a sintered metal backing. Fig. 8(a) illustrates a standard sintered metal for an oil-impregnated sliding bearing. Fig. 8(b) provides an example of optimization of the surface porosity ratio through adjustment for grain size of the starting metal powder and molding pressures. Both Fig. 8(a) and Fig. 8(b) show the surfaces of the sintered metal prior to insert-molding with a resin material (black areas denote pores) as well as a view of the surfaces of the sintered metal after the resin layer formed by insert-molding had been stripped off by force. The surface shown in Fig. 8(a) where the resin layer was stripped off does not show traces of the previously deposited resin, suggesting that the resin did not fill the pores.

In contrast, with the example in Fig. 8(b), the resin layer itself was split, and this suggests that the bonding of the resin layer to the sintered metal was very strong. As can be understood from this fact, the bonding strength of the sintered metal backing and resin layer is very high with our Hybrid Bearphite.

4. Performance of Hybrid Bearphite

Fig. 9 shows the appearance of our Hybrid Bearphite, which is essentially a sintered metal sliding bearing with a resin insert. The example in this photo has a resin layer on its side faces in order to be able to bear not only a radial load but also an axial load. The thickness of the resin layers on the bore surface and end faces is 0.25 mm. The performance of our Hybrid Bearphite is described below.



Fig. 9 Appearance of HYBRID BEARPHITE

4.1 Friction-wear characteristics

The Hybrid Bearphite, which is provided with the insert-molded resin sliding material in its bore surface was combined with an Ni-plated shaft and was run under a radial load of 29.6 N and a running speed of 240 min⁻¹. The resultant friction coefficient is graphically plotted in Fig. 10. For comparison, the characteristics of a sintered oil-impregnated bearing (mineral oil-impregnated copper sintered bearing) are also plotted in the same diagram.

The friction coefficient of the sintered metal oil-impregnated bearing was high during the earliest stage of operation, but eventually decreased as running-in proceeded, and finally became stable at 0.06. In contrast, the friction coefficient with the Hybrid Bearphite always remained stable at about 0.06 even at the earliest stage of operation. The wear with the sintered metal oil-impregnated bearing after 500 hours of operation reached 10 μm while the Hybrid Bearphite was as small as 6 μm. This means that the friction-wear quality of the Hybrid Bearphite sliding bearing is better than that of the sintered metal oil-impregnated bearing.

In a test with aluminum shafts, the sintered metal oil-impregnated bearing caused the aluminum shaft to be worn rapidly. In contrast, our Hybrid Bearphite exhibited performance equivalent to that shown in Fig. 10.

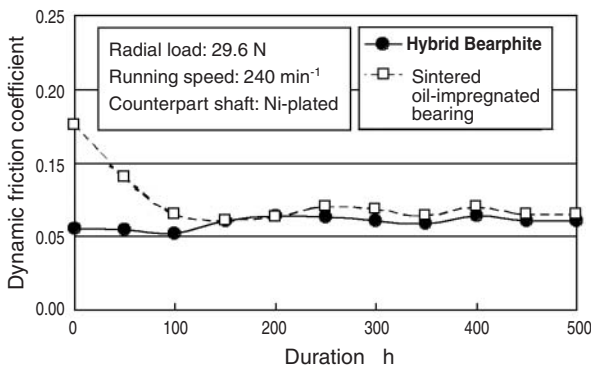


Fig. 10 Friction property of HYBRID BEARPHITE

4.2 Dimensional accuracy

The dimensional accuracy data and features of our Hybrid Bearphite are summarized in Table 2. The Hybrid Bearphite boasts dimensional accuracy comparable to that of a sintered oil-impregnated bearing. Furthermore, since the resin sliding layer on the Hybrid Bearphite expands and shrinks relative to the reference surface, it features extremely small dimensional variation due to temperature variations (Fig. 11). Note that greater dimensional variation with a bearing leads to larger shaft clearance, resulting in greater variation in running accuracy.

For the Hybrid Bearphite with a bore diameter of 7.5 mm, the resin layer thickness was adjusted to 0.25 mm and the linear expansion coefficient of the resin layer was assumed to be 14 x 10⁻⁵/°C. Thus, the temperature-dependent variation in the bore diameter of the Hybrid Bearphite was calculated (reference temperature: 25°C) and was compared (Fig. 12), with that obtained from an ordinary resin sliding bearing comprised solely of resin material. This diagram also includes the actual measurement data at 60°C. The steepness of the straight line representing the

Table. 2 Dimensional properties and characteristics of sliding bearings

Characteristic	Hybrid Bearphite	Resin sliding bearing	Sintered metal oil-impregnated bearing
Bore diameter	±5 μm	±15 μm	±5 μm
Outside diameter	±15 μm	±15 μm	±15 μm
Bore roundness	10 μm max.	50 μm max.	10 μm max.
Concentricity	15 μm max.	30 μm max.	15 μm max.
Cylindricity	10 μm max.	40 μm max.	10 μm max.
Dimensional variation	○	×	○
Sliding relative to aluminum	○	○	×
Sliding relative to SUM + Ni-plating	○	○	△

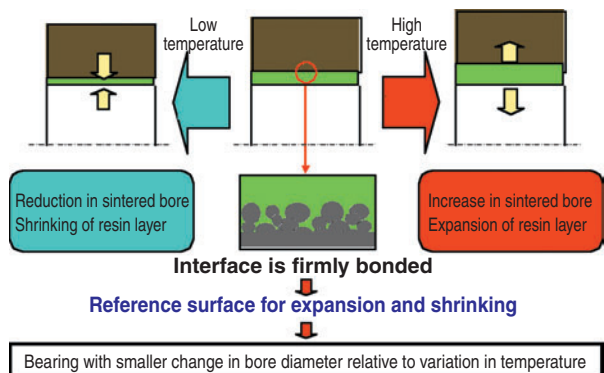


Fig. 11 Dimensional change of HYBRID BEARPHITE against temperature change

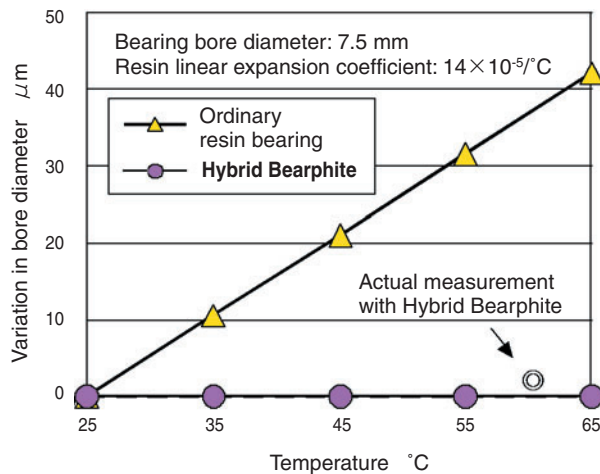


Fig. 12 Dimensional stability of HYBRID BEARPHITE

dimensional variation is governed by the design of the resin layer thickness. In other words, if the thickness of a resin layer is determined through consideration of the dimensional variation of the shaft, and the clearance between the shaft and the bearing can be maintained at a constant dimension for a wider temperature range. This is a revolutionary new feature for resin bearings. Consequently, our Hybrid Bearphite can realize higher running accuracy at a wider temperature range, an achievement not previously attained with conventional resin bearing technologies.

4.3 Bonding strength of the resin layer

The resin layer must be firmly bonded to the sintered metal in order to maintain a high level of dimensional accuracy in a sintered metal sliding bearing. The results of a heat shock test are summarized in Table 3 to provide data about the bonding strength of the resin layer. In this test, the Hybrid Bearphite sliding bearing was subjected to 100 heating-cooling cycles, with each cycle consisting of 1 hour at -20°C followed by 1 hour +60°C. Through this, the dimensions before and after the heat shock test and the bonding strengths between the sintered metals and the resin layers were inspected.

The dimensional variation occurring on our Hybrid Bearphite sliding bearing after undergoing the test

Table 3 Inner diameter change of HYBRID BEARPHITE after 100 cycles of heat shock test

TP	Before test mm	After test mm	Variation μm	State of bonding
1	7.501	7.500	1	No peeling
2	7.510	7.508	2	No peeling
3	7.508	7.504	3	No peeling

was very small. This means that the bonding is very firm between the sintered metal and the resin material of our Hybrid Bearphite.

4.4 Chemical attack resistance

Resin materials have been used increasingly on bearing housings in products such as office automation equipment. Because of the requirements for satisfying dimensional accuracy and impact strength, the resins often used on housings are amorphous resins that are not sufficiently oil-resistant. Examples of such resins include polycarbonate (PC) and acrylonitrile-butadiene-styrene copolymer (ABS). If an operating resin housing comes into contact with an inappropriate oil, it can develop cracks. This problem is known as solvent cracking, and it occurs when the compatibility of a resin with an oil is high. This allows the oil to penetrate and disentangle the polymer molecules that constitute the resin, causing the resin to develop cracks and/or crazing.

Polycarbonate test pieces measuring 152 mm in length, 12.5 mm in width and 6.35 mm in thickness were prepared. Each oil was applied to the area of the test piece where the maximum tensile stress occurs, and a bending load was exerted for a specific duration (Fig. 13). Thus, the chemical attack quality of each oil was evaluated.

The support distance adopted was 100 mm and the test temperature was 75°C. As can be seen in Table 4, silicone oil, which is included in the resin layer of

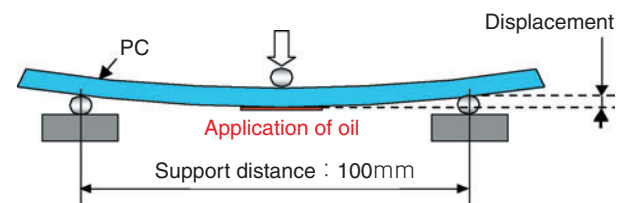


Fig. 13 Test rig for chemical attack

Table 4 Chemical attack of oils for polycarbonate

Condition / Oil type	Displacement (mm)	1.5	3.0	3.5	3.5
	Time (h)	3	3	3	196
No oil				○○○○○	
Polyethylene glycol		×××××			
Polyol ester oil		×××××			
Ether oil (ADE oil)			○○×××		
Mineral oil			○○○○○	○○×××	
PAO*			○○○○○	×××××	
Silicone oil**			○○○○○	○○○○○	○○○○○

* : poly α olefin oil
 ** : Oil blended in Hybrid Bearphite
 Symbols in the table: ○: no crack occurrence, ×: crack occurrence

the Hybrid Bearphite, does not damage the polycarbonate by chemical attack.

4.5 Electrically conductive Hybrid Bearphite EC

Electrophotographic printers and copying machines utilize static electricity to form an image and transfer the toner to paper stocks. For this reason, if the bearings on the photosensitive drum are triboelectrically charged, the static electricity and toner on the photosensitive drum (Fig. 1) will be adversely affected and the latent image on the photosensitive drum will be disturbed. The static charge on certain bearings other than those on the photosensitive drum needs to be eliminated. This is achieved with a grounding mechanism, but provision of the grounding mechanism causes the number of associated parts to increase. Therefore, such bearings are sometimes required to be electrically conductive.

Any ordinary resin material is electrically nonconductive and does not satisfy this requirement. Therefore, to address this challenge, we developed the electrically conductive Hybrid Bearphite EC by adding nanometer-sized carbon particles into the resin sliding material. The volume resistivity of this resin is $3 \times 10^3 \Omega \text{ cm}$, and this performance value is sufficient for elimination of static charge from the bearing. Its friction characteristics for sliding action with a Ni-plated shaft are summarized in Fig. 14. Addition of carbon particles caused the friction coefficient to increase to approximately 0.1. However, this level is half or less compared with that of other electrically conductive resin sliding materials available on the market. Incidentally, the physical properties of the Hybrid Bearphite EC, including chemical attack resistance, are equivalent to those of the electrically insulating Hybrid Bearphite.

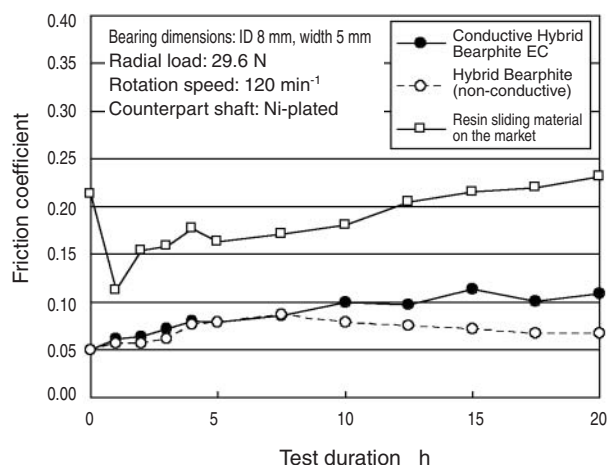


Fig. 14 Friction property of electrically conductive "HYBRID BEARPHITE EC"

5. Conclusion

Our Hybrid Bearphite, a sintered metal sliding bearing with a resin insert, boasts higher accuracy and lower torque at a decreased cost. This sliding bearing will be used in a diverse variety of industrial fields other than office automation equipment, and its applications include the replacement of rolling bearings as well as provision of improved functionality for sliding bearings. We will remain committed to improving the physical properties, including the heat resistance, of Hybrid Bearphite in order to contribute actively to the development of compacter and lighter designs that allow lower energy consumption and reduced costs for a variety of equipment.

References

- 1) Egami, Shimizu, Ohira: Tribology Meeting Draft Proceedings 2006-5 Tokyo (2006) p. 313. (In Japanese)
- 2) Egami, Hirose: Development of Plastic Sliding Materials for OA Equipment, NTN Technical Review, No.67 (1998) p.98. (In Japanese)
- 3) Shimazu, Egami, Shimokusuzono: Tribology Meeting Draft Proceedings 1998-10 Nagoya (1998) p. 379. (In Japanese)
- 4) Tsutsui, Egami, Ishii: Tribology Meeting Draft Proceedings 2003-5 Tokyo (2003) p. 77. (In Japanese)

Photo of author



Masaki EGAMI

Elemental Technological
R&D Center

DOJ Compact High-Angle Constant Velocity Joint

Lightweight and compact with a maximum operating angle of 30°DOJ



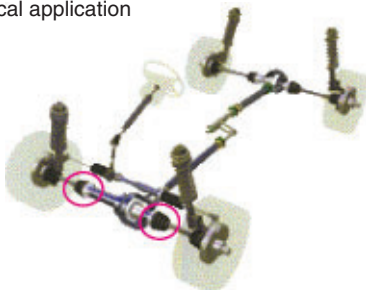
Features

- **External dimensions:** one size more compact (approximately 4%) compared to the current 30° DOJ
- **Weight:** approximately 6% lighter
- **Strength and durability:** improved actual strength and durability through optimization of track contact angle/contact ratio, and cage offset

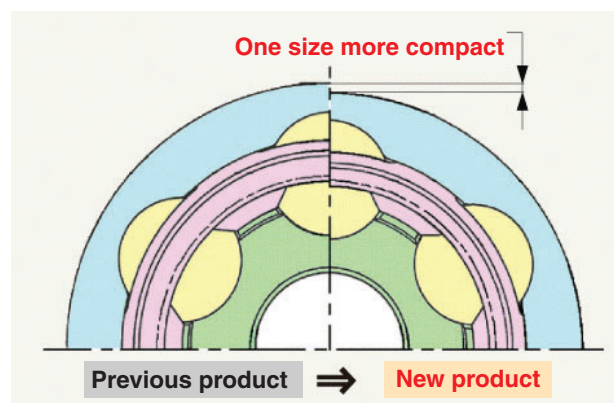
Applications

- SUVs and other vehicles that require greater operating angles

Typical application



Structure



PTJ High-Angle Low-Vibration Constant Velocity Joint

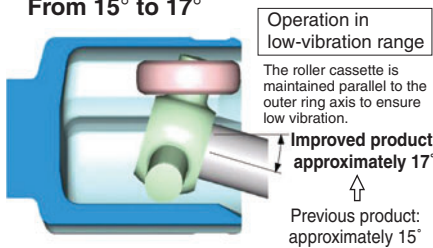
The PTJ low-vibration constant velocity joint boasts the world's highest level of NVH performance^{※1} and achieves a maximum operating angle of 30° for the first time in the world^{※2}



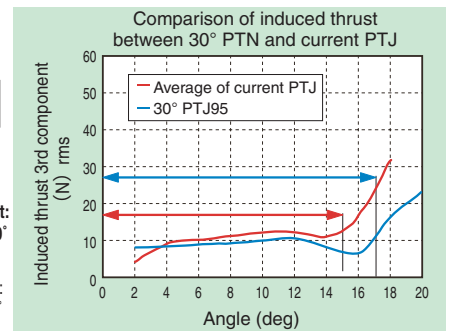
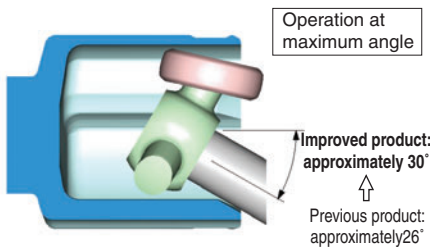
※1 Performance associated with vehicle noise and vibration. ※2 In the low-vibration tripod CVJ category

Features

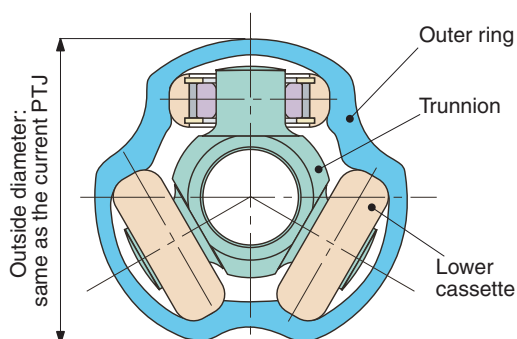
- **Extended operating angle range that ensures low vibration**
From 15° to 17°



- **Enlarged operating angle range**
Operation possible up to 30°

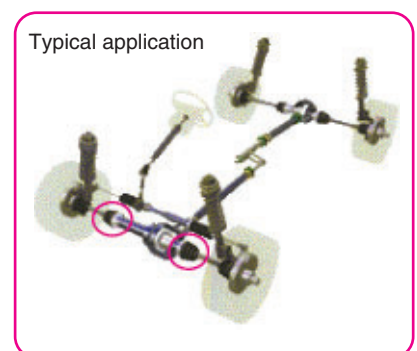


Structure



Applications

- **Crossover SUVs and other vehicle types that require greater operating angle and lower vibration**
Example of application



Super-Wide Operating Angle (54°) Fixed CVJ (TUJ)

The world's first fixed CVJ capable of a super-wide operating angle (θ max. = 54°)

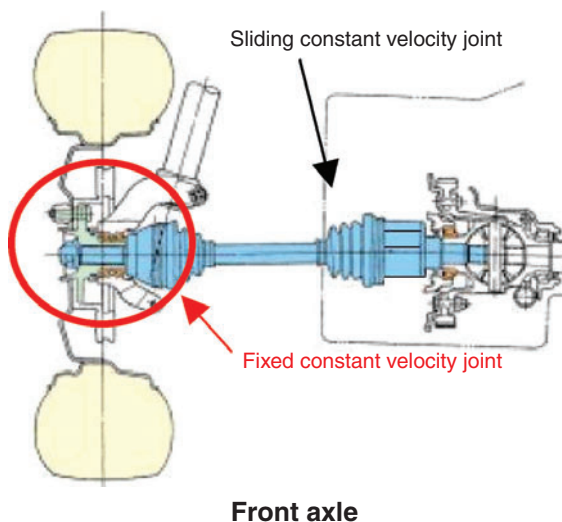
Results of a case study that assumes a 4° increase in the operating angle with a fixed joint on an ordinary medium-sized FF vehicle

Approximately 70 cm (13%) decrease in the minimum turning radius of the vehicle
(when the wheelbase is the same as a conventional CVJ)

Approximately 40 cm (15%) increase in the wheelbase
(when the minimum turning radius is the same as a conventional CVJ)



Example of use



Features

- Maximum operating angle (θ max): 54° (current UJ: 50°)
- Outer ring outside dia.: Same as with UJ
- Mechanical strength, durability: Equivalent to those with UJ

Applications

- Large-sized and medium-sized FF and 4WD vehicles boasting smaller minimum turning radius

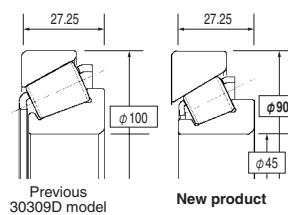
Ultra-Low Torque Tapered Roller Bearing

Significantly lower running torque
(1/2 that of previous tapered roller bearing in the same class),
without loss in bearing life and rigidity



Features

- Realization of lower torque: 1/2 that of previous bearing
- Compact bearing size: 10% or greater reduction of outside bearing diameter (same life and rigidity compared to previous bearing)



Engineering challenges and solutions

Challenge 1: Realization of lower torque

Means for realization: Implementation of optimization in design

Adoption of a new cage form with reduced oil stirring resistance

Challenge 2: Maintain bearing life comparable to that of the previous bearing

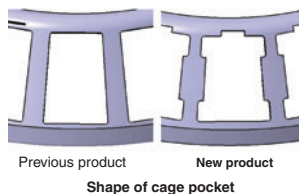
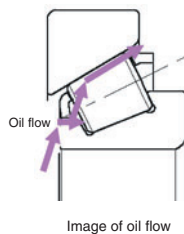
Means for realization: Adoption of FA heat treatment

When lubricated with clean oil, the new product boasts a bearing life 2.8 times as long as that of the 4T product.

Challenge 3: Maintain rigidity comparable to that of the previous bearing

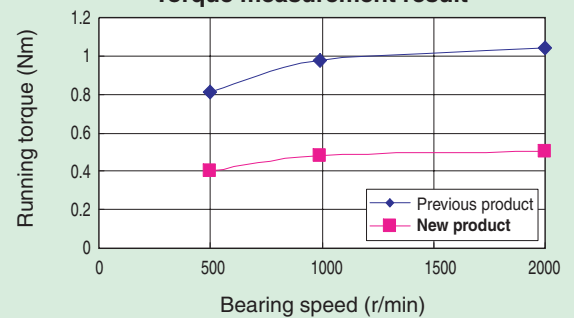
Means for realization: Adoption of a high load capacity design

The cage is situated near the outer ring and a maximum possible number of rollers are incorporated.



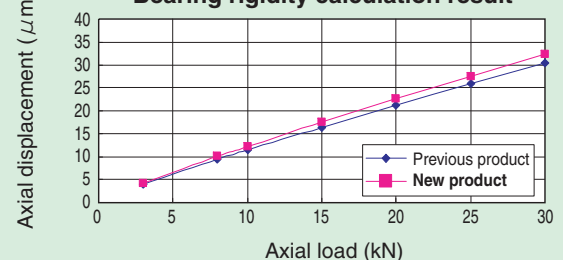
Performance

Torque measurement result



Running torque is 1/2 as low as the previous product at a practical speed range of 500–2000 r/min.

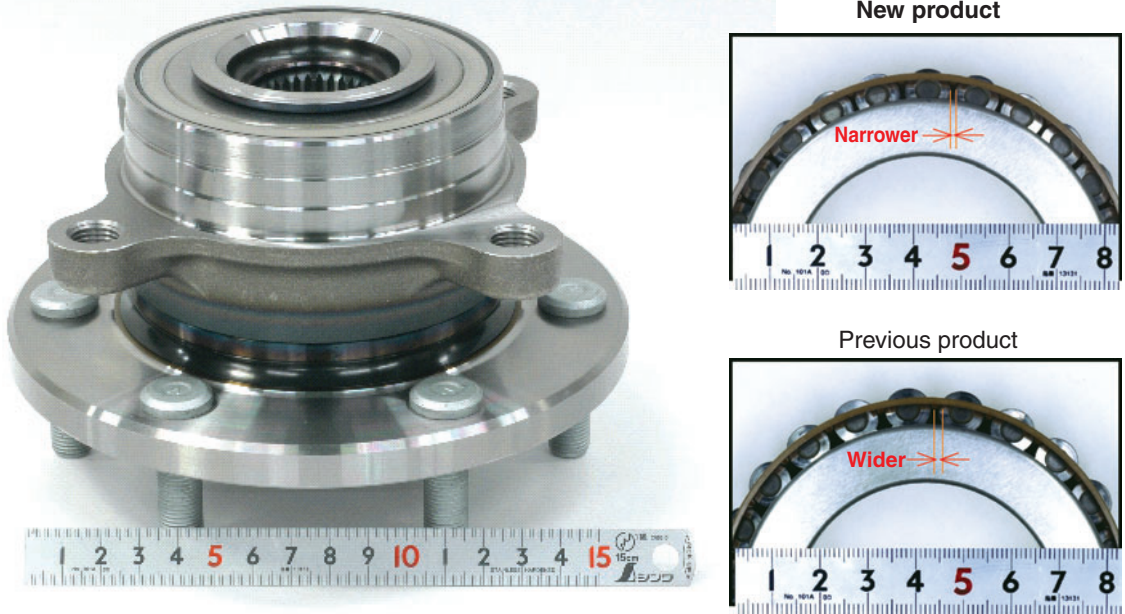
Bearing rigidity calculation result



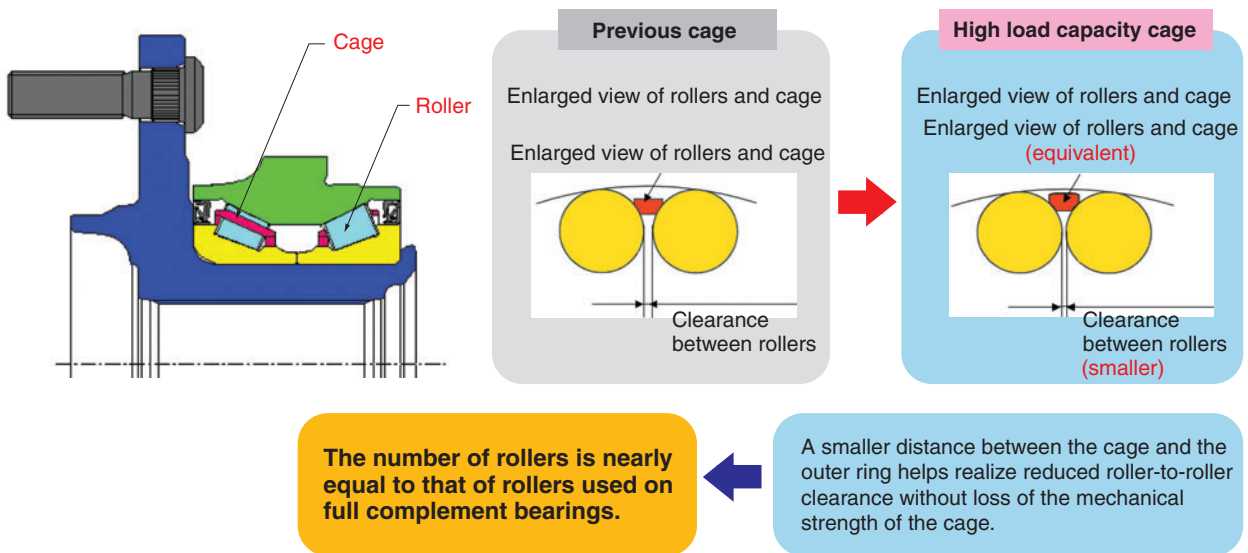
The new product has rigidity nearly equivalent to that of the previous product

High Load Capacity Tapered Hub Bearing for SUVs

Realization of 20% longer bearing life and 7% higher rigidity in the same amount of space



Structure



Features

- 20% increase in bearing life (calculated life)
- 7% increase in bearing rigidity

Features

- Wheel bearings for SUVs

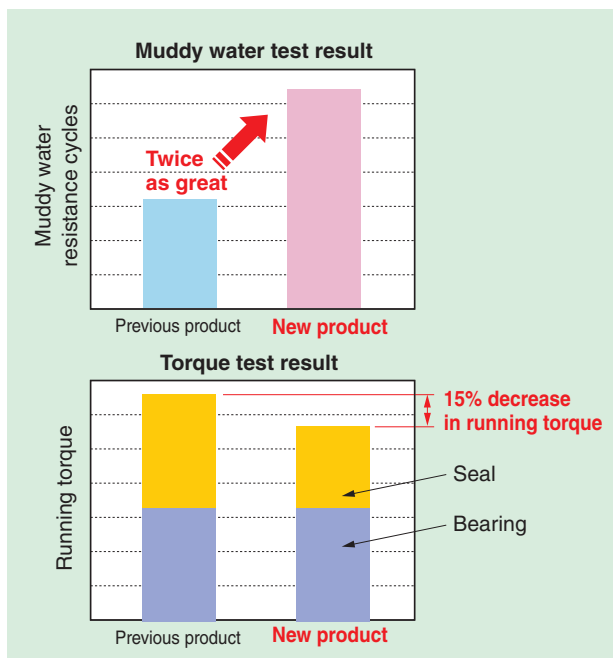
Hub Bearing with Built-In Low-Torque Hermetic Seal

Twice the sealing performance and a 15% reduction in running torque in the same seal space through optimization of structure, form and rubber material

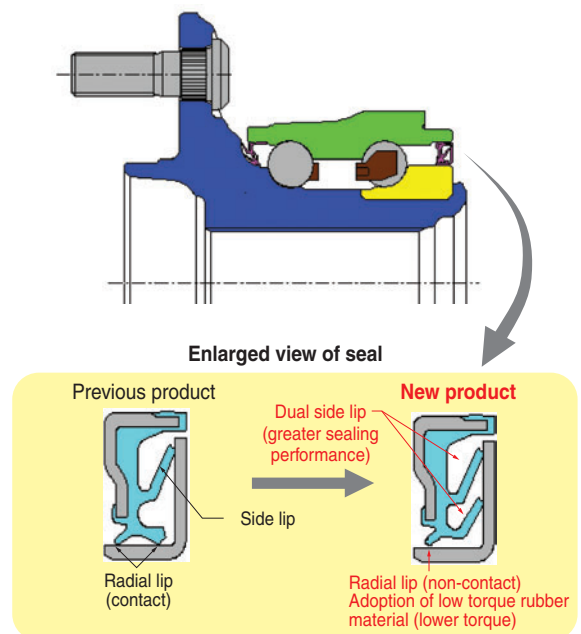


Features

- Sealing performance: twice the resistance to muddy water
- Lower torque: 15% decrease in running torque (30% decrease with seal alone)



Structure



Applications

- Wheel bearings for passenger cars

Hub Bearing with Built-In Active Sensor

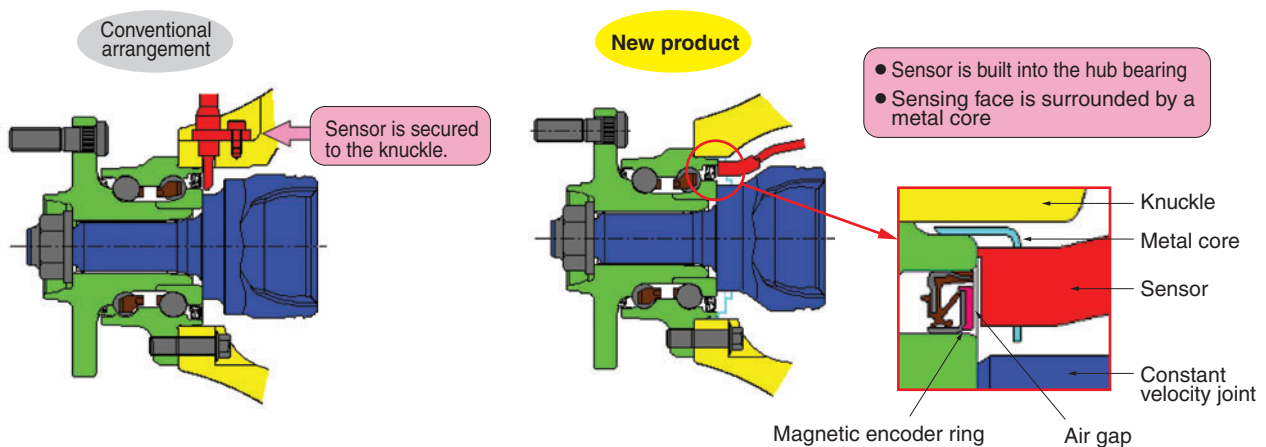
No need for adjustment of sensor air gap or machining of knuckle



Features

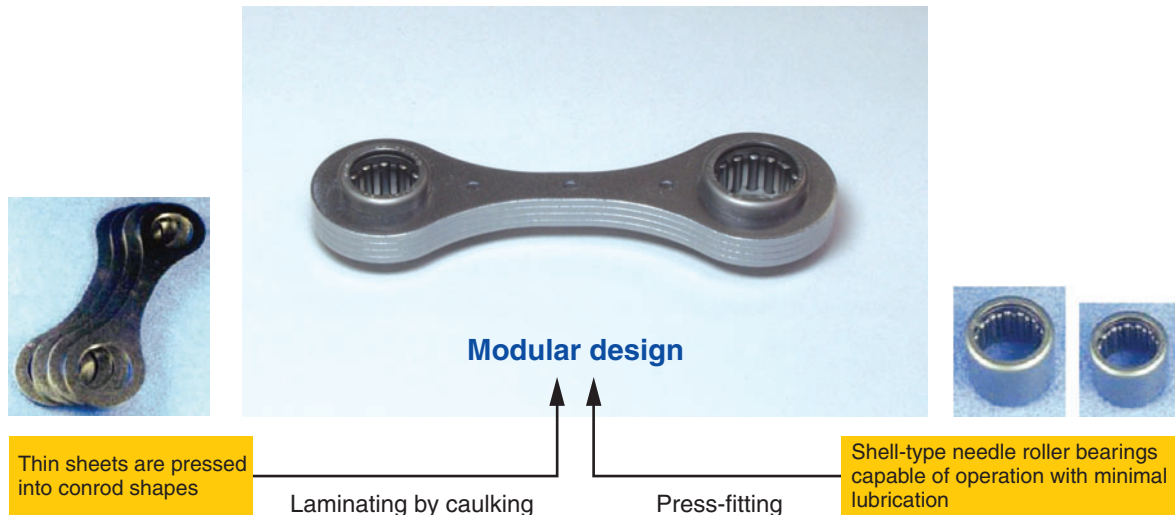
- No need for adjustment of sensor air gap
- No need for machining work or assembly to secure the sensor to the knuckle
- Protection against flying rocks and prevention of jamming by foreign objects

Means for realization



Low-Emission Capable Laminated Conrod Module

- Shell-type needle roller bearing that can operate under minimal lubrication conditions to help comply with emission control
- Realization of compact size with NTN's unique laminated conrod
- Proposal of total VA/VE with modular design involving conrod that incorporates the shell-type needle roller bearings described above

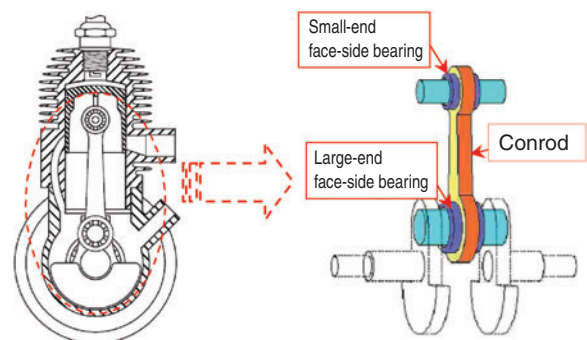


Features

- Through optimized design of the cage used on shell-type needle roller bearings and the higher precision of the outer ring, this conrod boasts excellent anti-seizure performance even under a severely reduced lubrication condition that is four times as demanding as conventional lubrication conditions (75% reduction in the amount of mixed oil).
- This conrod product features a unique laminated construction prepared by pressing thin sheets. As a result, it is very compact, with a minimum width that is 17% (6% in terms of outside dimensions) more compact than conventional conrod products formed by fine blanking techniques.
- NTN offers a modular conrod product that is capable of operation with minimal lubrication. This is prepared by press-fitting shell-type needle roller bearings into its unique laminated conrod component. Being highly functional and compact, this product also serves for VA/VE applications.

Applications

- 2-cycle engines for agricultural machinery (pruning machines, spraying machines, chainsaws, etc.)



Cross-sectional view of a 2-cycle engine for agricultural machinery

High-Speed, High-Quality Color Filter Repair System

Capable of coping with large-sized substrates, the system features multi-functionality and advanced functions



Features

1) Realization of quick repair

- A dedicated high-speed drive mechanism is provided for repair fluid application
- A combination of a dedicated applicator needle and a repair fluid container is provided for each repair fluid
- No need to rinse the applicator needle; simpler color switching
- The tip of the applicator needle is refilled by repair fluid during application
- No need for separate repair fluid filling

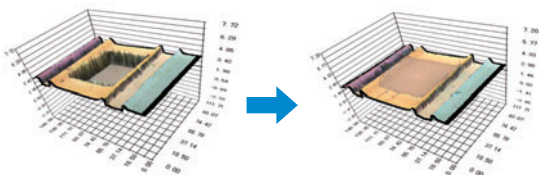
70% reduction in repair time compared to previous repair systems

2) Realization of high-quality repair

- Each applicator needle has a specially treated tip. The amount of the repair fluid applied is adjusted precisely based on the time of contact between the color filter substrate and the applicator needle
- Prevention of overflow of repair fluid to defect-free areas

Improvement in repair quality

Example of repair



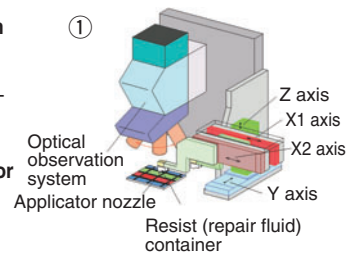
Coating is removed by lasers

Repair fluid is applied

Advantages of the NTN's unique applicator mechanism

① High-speed mechanism specialized for application (for X1, X2, Y, and Z axes)

The time needed for repair is reduced by the high-speed, high-precision drive motion of ultra-compact linear motors.

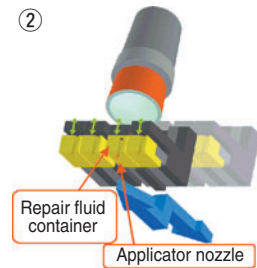


② Provision of four applicator needles

Color switching without rinsing and reduced repair time are realized.

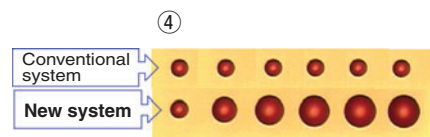
③ Unified support structure for applicator needles and repair fluid containers

Filling of applicator needles with repair fluid is not necessary.



④ Filler-applicator needle

The amount of liquid applied is adjusted in a range from a few picoliters (one trillionth of liter) to tens of picoliters. Repair quality is improved because any defect can be filled with a very small amount of the repair fluid.



Advanced Functionality Controller for Parts Feeder

Power consumption by parts feeders can be reduced by 30% compared with previous controllers

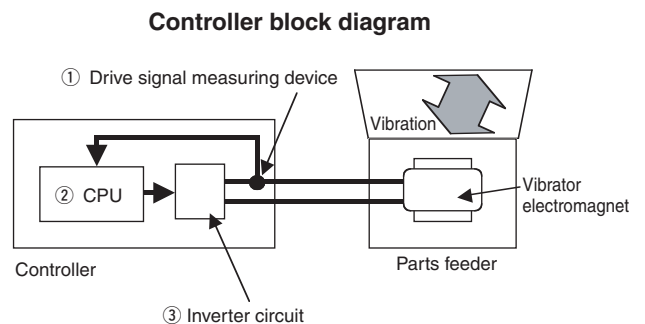
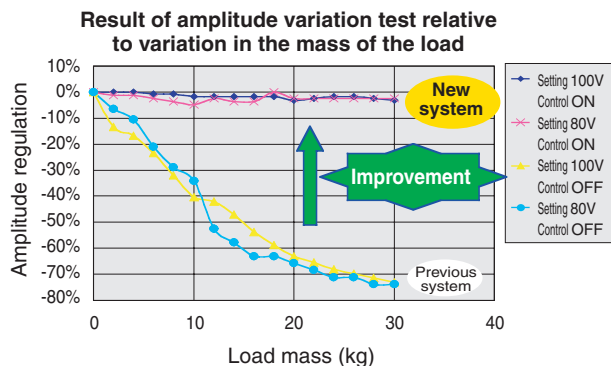


Features

- 1) **Optimal vibration frequency automatic adjustment function**
 - Automatic adjustment to the most efficient frequency
→ Approximately 30% energy conservation
- 2) **Constant amplitude function allows parts to be transported in an optimal state.**
 - Amplitude regulation: within 3% (under conditions that result in amplitude variation of 10% or greater with previous controllers)
- 3) **No need for a vibration sensor**
 - Work to mount a vibration sensor and lay wires is not necessary
→ The new controller can be easily installed to replace an older controller
 - No problems such as broken vibration sensor leads
→ Reduction of malfunctions

Means for realization

- 1) The drive signal (voltage, current) to the vibrator electromagnet is accurately measured [drive signal measuring device]
- 2) Based on the measured values, (i) deviation from the optimal vibration frequency and (ii) the amount of transportation (vibration amplitude) are estimated [CPU]
- 3) The electromagnet is energized based on the vibration frequency and amplitude ordered by the CPU [inverter]
→ Automatic adjustment of optimal frequency and constant amplitude functions are realized without use of an external vibration sensor



HEADQUARTERS

NTN CORP. URL <http://www.ntn.co.jp>

Head Office / 3-17, 1-chome, Kyomachibori, Nishi-ku, Osaka 550-0003 Japan
Phone: 81-6-6443-5001 Telex: J63750, NTN CORP. Fax: 81-6-6445-8581
Tokyo Headquarters / TOC Building, 6th Floor, 22-17, 7-chome, Nishi-Gotanda,
Shinagawa-ku, Tokyo 141-0031 Japan Phone: 81-3-5487-2815

NTN USA CORP.

1600 E. Bishop Court, P.O. Box 7604, Mount Prospect, IL 60056-7604, U.S.A.
Phone: +1-847-298-7500 Fax: +1-847-294-1209

SALES NETWORK

NTN BEARING CORP. OF AMERICA

Head Office / 1600 E. Bishop Court, P.O. Box 7604, Mount Prospect, IL 60056-7604,
U.S.A.
Phone: +1-847-298-7500 Fax: +1-847-699-9744
Central Sales Office / 111 West Washington Street Suite 310, East Peoria, IL 61611 U.S.A.
Phone: +1-309-699-8600 Fax: +1-309-699-8670
Eastern Sales Office / 191 Sheree Blvd., Suite 101, Exton, PA 19341, U.S.A.
Phone: +1-610-524-1477 Fax: +1-610-524-157
South Eastern Sales Office / 5475 Peachtree Industrial Blvd., Norcross, GA 30092,
U.S.A.
Phone: +1-770-448-4710 Fax: +1-770-448-6969
Western Sales Office / 2251 SW Grapevine Parkway, Grapevine, TX 76051, U.S.A.
Phone: +1-817-329-1818 Fax: +1-817-329-4711
NTN Automotive Center / 39255 W. 12 Mile Road, Farmington Hills, MI 48331-2975,
U.S.A.
Phone: +1-248-324-4700 Fax: +1-248-324-1103

NTN BEARING CORP. OF CANADA LTD.

Head Office / 305 Courtneypark Drive West, Mississauga, Ontario, L5W 1Y2, Canada
Phone: +1-905-564-2700 Fax: +1-905-564-7749
Vancouver Branch / 201-669 Ridley Place Annacis Island Delta, B.C., V3M 2Y9 Canada
Phone: +1-604-517-1777 Fax: +1-604-517-1794
Edmonton Branch / 4608-97th Street, Edmonton, Alberta T6E 5N9, Canada
Phone: +1-780-435-6200 Fax: +1-780-435-3600
Winnipeg Branch / 220-530 Century Street, Winnipeg, Manitoba, R3H 0Y4, Canada
Phone: +1-204-633-8045 Fax: +1-204-694-9701
Montreal Branch / 4973 Levy Street, Ville, St-Laurent, Quebec, H4R 2N9, Canada
Phone: +1-514-333-8054 Fax: +1-514-333-1078
Moncton Branch / 55 Halifax Street, Moncton, New Brunswick, E1C 9R5, Canada
Phone: +1-506-858-9954 Fax: +1-506-858-9168

NTN WÄLZLAGER (EUROPA) G.m.b.H.

Head Office / Nordrhein-Westfalen Branch /
Max-Planck-Strasse 23, 40699 Erkrath, F.R.Germany
Phone: +49-211-2508-0 Fax: +49-211-2508400
Stuttgart Branch / Schurwaldstrasse 13, 73765 Neuhausen, F.R.Germany
Phone: +49-7158-17040 Fax: +49-7158-170460
München Branch / Geretsrieder Strasse 10A, 81379 Munchen, F.R. Germany
Phone: +49-89-7488630 Fax: +49-89-786382
Hamburg Branch / Barkhausenweg 7, 22339 Hamburg, F.R. Germany
Phone: +49-40-536962-0 Fax: +49-40-53696215
Italy Branch / Via Maestri del Lavoro, 3, 40138 Bologna, Italy
Phone: +39-051-535174 Fax: +39-051-538492

NTN BEARINGS (UK) LTD.

Wellington Crescent, Fradley Park, Lichfield, Staffordshire, WS13 8RZ, U.K.
Phone: +44-1543-445000 Fax: +44-1543-445035

NTN FRANCE S.A.

Head Office / Z.I.Sablrière BP 338 Schweighouse Sur Moder 67507 Haguenau Cedex, France
Phone: +33-3-88-53-22-22 Fax: +33-3-88-73-46-95
Lyon Branch / Parc Technologique 2 Pace Berthe Morisot 69792 Saint-Priest
cedex, France
Phone: +33-4-72-04-0044 Fax: +33-4-72-04-4456
Paris Branch / Boulevard De Beaubourg B.P. 27 Emerainviller, 77313 Marne-la-
vallee Cedex 2, France
Phone: +33-1-64-80-4747 Fax: +33-1-64-80-4778

NTN BEARING-SINGAPORE (PTE) LTD.

Head Office / No.9 Clementi Loop Singapore 129812
Phone: +65-64698066 Fax: +65-64695400
Philippine Representative Office / Unit 1002 Philippine Axa Life Centre Condominium
Corporation
Sen. Gil Puyat Ave Corner Tindalo Street Makati City, Philippines
Phone: +63-2-759-4407 Fax: +63-2-759-4409
India Representative Office / 805, International Trade Tower, Nehru Place, New Delhi
110019, India
Phone: +91-11-51513234 Fax: +91-11-51513236

NTN CHINA LTD.

Head Office / Rm. 1914-1915, Park-in Commercial Centre, 56, Dundas Street,
Mongkok, Kowloon, Hong Kong
Phone: 852-2385-5097 Fax: +852-2385-2138
Guangzhou Liaison Office / Room 7306, CITIC Plaza, No.233 Tian He North Road,
Guangzhou, China. 510613
Phone: +86-20-8626-6766 Fax: +86-20-8626-6630
Shanghai Liaison Office / Unit 2212, Shanghai Maxdo Centre, 8 Xing Yi Road,
Changning District Shanghai, 200336, China
Phone: +86-21-5208-1006 Fax: +86-21-5208-1016

NTN BEARING-THAILAND CO., LTD.

Head Office / 12th Floor, Panjathani Tower, 127/15 Nonsee Road, Chongnonsee
Yannawa, Bangkok 10120, Thailand
Phone: +66-2-681-0401 Fax: +66-2-681-0408
Khon Kaen Branch / 189-191 Ruen Rom Road Tambon Nai-Muang, Amphur
Muang, Kohn Kaen, 40000, Thailand
Phone: +66-43-223679 Fax: +66-43-223061
Haad Yai Branch / 198-198/1 Nipat U-Thid 2 Road, Amphur Haad Yai, Songkhla,
90110, Thailand
Phone: +66-74-236568 Fax: +66-74-231520
Bangna Sales Office / 35/35 Bangna-Trad Road, KM11 Bangplee, Samutprakarn,
10540, Thailand
Phone: +66-2-7501732 Fax: +66-2-7501731
Chiangmai Sales Office / 94. 94/1 Chayapoom Road, Tumbolsripoom, Amphur
Muang, Chiang Mai 50200, Thailand
Phone: +66-53-874328 Fax: +66-53-874330

NTN BEARING-MALAYSIA SDN. BHD.

Head Office / No.2, Jalan Arkitek U 1/22, Hicom Glenmarie Industrial
Park, 40150 Shah Alam, Selangor, Malaysia
Phone: +60-3-55696088 Fax: +60-3-55690200
Butterworth Branch / 4700, Jalan Permatang Pauh, 13400 Butterworth, Malaysia
Phone: +60-4-3328312 Fax: +60-4-3324407
Ipoh Branch Office / 65, Medan Kidd, Kinta Mansion, 30200 Ipoh, Malaysia
Phone: +60-5-2547743 Fax: +60-5-2538077
Kuantan Branch / B-72, Ground Floor, Jalan Beserah 25300 Kuantan, Malaysia
Phone: +60-9-5141132 Fax: +60-9-5141164
Johor Bahru Branch / 51 Jalan, Sri Bahagia 5, Taman Sri Bahagia, Tampoi, 81200
Johor Bahru, Malaysia
Phone: +60-7-2364929 Fax: +60-7-2370897

NTN-CBC (AUSTRALIA) PTY. LTD.

3, The Crescent, Kingsgrove, NSW 2008, LOCKED BAG 1800, Kingsgrove 1480.
NSW Australia
Phone: +61-2-9502-1833 Fax: +62-2-9502-4013

NTN DE MEXICO, S.A.

Guadalajara Office / Calle 22 No.2465, Esq. Calle 3, Zona Industrial, C.P. 44940
Guadalajara, Jalisco, México
Phone: +52-33-3145-1490 Fax: +52-33-3145-1594
México Office / Calle Emilio Cardenas No.158, Fracc.Industrial San Nicolas
C.P.54030 Tlalnepantla, Estado De Mexico
Phone: +52-55-5565-5562 Fax: +52-55-5565-8638

NTN SUDAMERICANA, S.A.

World Trade Center Panama
Calle 53 Este, Urbanización Marbella Piso NO.16, Oficina 1601
Apartado Postal 832-0487, Panamá, Rep.de Panamá
Phone: +507-269-4777 Fax: +507-264-5592

NTN DO BRASIL LTDA.

Av. Moema, 94-9º Andar-conj, 92a94 CEP 04077-020-Indianópolis-São Paulo-SP,
-Brasil
Phone: +55-11-5051-0600 Fax: +55-11-5051-2807

NTN KOREA CO., LTD.

Head Office / 10th Floor, Press Center, 25, Taepyeong-Ro 1-GA, Jung-Gu, Seoul
100-745, Korea
Phone: +82-2-720-3665 Fax: +82-2-720-3669
Pusan Branch / Rm.707, 7th Floor, Daerim Bldg., 341-5 Bujeon 1-Dong, Busanjin-
Gu, Busan, Korea, 614-843
Phone: +82-51-811-1351 Fax: +82-51-811-1353

NOTE : The appearance and specifications may be changed without prior notice
if required to improve performance. Although care has been taken to
assure the accuracy of the data compiled in this catalog, NTN does not
assume any liability to any company or person for errors or omissions.

NTN TECHNICAL REVIEW No.74

Printed and published in November 1, 2006

Editor **Kenji Okada**

Publisher **Hitoshi Takai**

Published by NTN Corporation
3-17, 1-chome, kyomachibori, Nishi-ku, Osaka, J apan

Printed by
NISSHA Co., Ltd

**No part of this publication may be reprinted or reproduced
without the prior permission of the copyright owner.**